Fakultät für Medizin
Institut für Virologie

Generation and characterization of MHC class II-restricted T-cell receptors for T-cell therapy of chronic hepatitis B

Sophia Schreiber

Vollständiger Abdruck der von der Fakultät für Medizin der Technischen Universität München zur Erlangung des akademischen Grades eines

Doktors der Naturwissenschaften (Dr. rer. nat.)

genehmigten Dissertation.

Vorsitz: Prof. Dr. Dirk Busch

Prüfer*innen der Dissertation:

1. Prof. Dr. Ulrike Protzer
2. Prof. Dr. Aphrodite Kapurniotu
3. Prof. Dr. Carolin Daniel

Die Dissertation wurde am 09.11.2021 bei der Technischen Universität München eingereicht und durch die Fakultät für Medizin am 12.07.2022 angenommen.

Table of Contents

Abstract

Hepatitis B virus (HBV) infection remains a severe global health problem with current treatment options being unable to achieve viral clearance. Whereas chronic HBV infection is generally accompanied by a dysfunctional T-cell response, a hallmark of the acute, self-limiting course of disease is a strong, curative T-cell response. Restoring T-cell immunity via adoptive T-cell therapy thus represents a promising therapeutic approach. $CD8^+$ T cells engrafted with MHC class I-restricted T-cell receptors (TCRs) were already shown to have the potential to cure HBV infection *in vitro* and *in vivo*. Nevertheless, also $CD4^+$ T cells are considered essential in resolving HBV infection and may benefit T-cell therapy. The aim of this thesis was therefore to identify and characterize MHC class II-restricted TCRs from HBV-specific $CD4^+$ T cell clones for further use in adoptive T-cell therapy of HBV infection. To this end, peripheral blood mononuclear cells from donors with resolved HBV infection were stimulated with a selection of HBV peptides. *In vitro e*xpanded samples were then sorted by flow cytometry on CD4 expression and activation-induced cytokine secretion and clonally expanded from a single-cell level. TCR α- and β-chain sequences of HBV-specific clones were identified, codon-optimized and cloned into a retroviral vector for subsequent in-depth characterization. In total, 23 TCRs specific for eight different epitopes from the HBV core, envelope or polymerase protein were identified and characterized throughout this thesis. By using potent retroviral supernatant for the transduction of primary human T cells, high levels of transgenic TCR expression were achieved, with transduction rates typically ranging from 65-85%. Ten different MHC class II restrictions were identified, i.e. HLA-DRB1*01:01, DRB1*07:01, DRB1*11:04, DRB1*13:01, DRB3*02:02, DPA1*01:03/DPB1*02:01, DPA1*01:03/DPB1*04:01, DPA1*01:03/DPB1*15:01, DQA1*01:01/DQB1*05:01 and DQA1*01:01/DQB1*06:03. 17 TCRs recognized either three or four HBV genotype variants and 19 TCRs demonstrated high functional avidity in a low nanomolar range. All TCRs were capable of activating both $CD4^+$ and $CD8^+$ T cells independently of their coreceptor. Notably, 15 TCRs enabled both $CD8^+$ and $CD4^+$ T cells to kill peptide-pulsed HLA-matched target cells. Finally, in a proof of concept experiment, TCR-transduced $CD4^+$ T cells were able to provide help to $CD8^+$ T cells via cross-talk at the dendritic cell. Taken together, a diverse set of MHC class II-restricted HBV-specific TCRs was generated, which provides a valuable resource for the adoptive T-cell therapy of chronic HBV infection and HBV-related hepatocellular carcinoma as well as an important research tool to study the role of $CD4^+$ T cells in HBV infection and cure.

Zusammenfassung

Die Infektion mit dem Hepatitis B Virus stellt nach wie vor ein globales Gesundheitsproblem dar, da es mit aktuellen Behandlungsmethoden nicht möglich ist, die Infektion auszuheilen. Da die chronische HBV Infektion meist von einer dysfunktionalen T-Zell-Antwort begleitet wird, ein selbst-limitierender Verlauf jedoch durch eine starke und kurative T-Zell-Antwort geprägt ist, stellt die Wiederherstellung der Immunantwort durch adoptive T-Zell-Therapie einen vielversprechenden therapeutischen Ansatz dar. Es wurde bereits gezeigt, dass $CD8^+$ T-Zellen, die mit einem MHC Klasse I-restringierten Rezeptor versehen wurden, das Potential haben, eine HBV Infektion *in vitro* und *in vivo* zu heilen. Nichtsdestotrotz sind auch $CD4^+$ T-Zellen bekanntermaßen essentiell für die spontane Ausheilung einer HBV Infektion, ihr Einsatz könnte sich folglich positiv auf eine adoptive T-Zell-Therapie auswirken. Das Ziel der vorliegenden Arbeit war es daher, MHC II-restringierte Rezeptoren aus HBV-spezifischen $CD4^+$ T-Zell-Klonen zu identifizieren und zu charakterisieren. Zu diesem Zweck wurden periphere mononukleäre Blut-Zellen von Spendern mit ausgeheilter HBV Infektion mit einer Auswahl von HBV Peptiden stimuliert. Die *in vitro* expandierten Proben wurden dann mit Hilfe von Durchflusszytometrie basierend auf CD4 Expression und aktivierungsabhängiger Zytokinsekretion sortiert, sowie monoklonal expandiert. Die Sequenzen der jeweiligen TCR α- und β-Ketten von HBV-spezifischen Klonen wurden identifiziert, codonoptimiert und in einen retroviralen Vektor kloniert zur anschließenden Charakterisierung. Insgesamt wurden auf diese Weise 23 T-Zell-Rezeptoren spezifisch für acht verschiedene Epitope des HBV Kapsid-, Hüll- oder Polymerase-Proteins identifiziert und characterisiert. Durch retrovirale Transduktion mit hoch-potentem viralen Überstand konnten hohe transgene Expressionsraten in typischerweise 65 bis 85% der primären humanen T-Zellen erreicht werden. Zehn MHC Restriktionen wurden identifiziert: HLA-DRB1*01:01, DRB1*07:01, DRB1*11:04, DRB1*13:01, DRB3*02:02, DPA1*01:03/DPB1*02:01, DPA1*01:03/DPB1*04:01, DPA1*01:03/DPB1*15:01, DQA1*01:01/DQB1*05:01 und DQA1*01:01/DQB1*06:03. 17 Rezeptoren erkannten drei oder vier HBV Genotypen und 19 Rezeptoren demonstrierten eine hohe funktionale Avidität in einem niedrig-nanomolaren Bereich. Alle T-Zell-Rezeptoren waren in der Lage, sowohl $CD4^+$ als auch $CD8^+$ T-Zellen zu aktivieren, unabhängig vom jeweiligen Korezeptor. Insbesondere ermöglichten es 15 Rezeptoren sowohl $CD8^+$ als auch $CD4^+$ T-Zellen, HLA-kompatible Zielzellen zu lysieren. In einem abschließenden Proof-of-Concept Experiment wurde gezeigt, dass TCR-transduzierte $CD4^+$ T-Zellen in der Lage sind, $CD8^+$ T-Zellen via Interkation an einer

dendritischen Zelle Hilfestellung zu leisten. Zusammenfassend wurde ein diverses Set von MHC Klasse II-restringierten HBV-spezifischen Rezeptoren erzeugt, das eine wertvolle Ressource für die adoptive T-Zell-Therapie der chronischen HBV Infektion und des HBV-bedingten hepatozellulären Karzinoms sowie ein wichtiges Instrument für die Erforschung der Rolle von $CD4^+$ T-Zell-Antworten in HBV Infektion und Ausheilung darstellt.

Abbreviations

AAV	adeno-associated virus
ACT	adoptive T-cell therapy
ALT	alanine amino transferase
APC	antigen presenting cell
β2M	beta 2-microglobulin
B-ALL	acute lymphoblastic B-cell lymphoma
BFA	Brefeldin A
B-LCL	B-lymphoblastoid cell line
C gene segment/-GENE	constant gene segment
CAR	chimeric antigen receptor
cccDNA	covalently closed circular DNA
CD	cluster of differentiation
CDR	complementarity-determining region
CHB	chronic hepatitis B virus infection
CMV	cytomegalovirus
cpm	counts per minute
CRISPR	clustered regularly interspaced short palindromic repeats
CRTAM	class I-restricted T cell-associated molecule
CTL	cytotoxic T lymphocyte
CTLA4	cytotoxic T-lymphocyte-associated protein 4
D gene segment/-GENE	diversity gene segment
DNA	deoxyribonucleic acid
E:T	effector to target ratio
EBV	Eppstein-Barr virus
EC_{50}	half maximal effective concentration
ELISA	enzyme-linked immunosorbent assay
ER	endoplasmatic reticulum
FDA	Food and Drug Administration
GALV	gibbon ape leukaemia virus
GM-CSF	granulocyte–macrophage colony-stimulating factor
GrzB	Granzyme B
GvHD	graft-versus-host disease
HBeAg	hepatitis B e-antigen
HBsAg	hepatitis B surface antigen
HBV	hepatitis B virus
HBV-HCC	HBV-related HCC
HBx	hepatitis B X protein
HCC	hepatocellular carcinoma
HCV	hepatitis C virus
HDV	hepatitis D virus
HIV	human immunodeficiency virus

HLA	human leukocyte antigen
HPV	human papillomavirus
HS	human serum
HSV-TK	herpes simplex virus thymidine kinase
hTCM	human T cell medium
IC_{50}	half maximal inhibitory concentration
iCasp9	inducible caspase 9
IFN	interferon
IgG1	immunoglobulin 1
IL	interleukin
ITAM	immunoreceptor tyrosine-based activation motif
IVT	in vitro transcribed
J gene segment/-GENE	joining gene segment
k.o.	knockout
L protein	large envelope protein
LB	lysogeny broth
LCMV	lymphocytic choriomeningitis virus
M protein	medium envelope protein
MAGE-A3	melanoma antigen A3
mTRBC	murine TCR β constant
mCD3	murine CD3 δγεζ-chains
MFI	mean fluorescence intensity
MHC	major histocompatibility complex
miRNA	micro RNA
MLV	murine leukemia virus
MoDCs	monocyte-derived dendritic cells
mRNA	messenger RNA
NCBI	National Center for Biotechnology Information
NFAT	nuclear factor of activated T cells
NTCP	sodium taurocholate co-transporting polypeptide
NUC	nucleos(t)ide analogue
NY-ESO-1	New York esophageal squamous cell carcinoma-1
ON	overnight
ORF	open reading frame
PBMC	peripheral blood mononuclear cells
PCR	polymerase chain reaction
PD-1	programmed cell death protein 1
pgRNA	pregenomic RNA
pMHC	peptide-MHC complex
rapid amplification of cDNA ends PCR	RACE-PCR
rcDNA	relaxed circular DNA
RNA	ribonucleic acid
S protein	small envelope protein
S-CAR	HBsAg-specific chimeric antigen receptor

scFv	single-chain variable fragment
SI	stimulation index
SNP	single nucleotide polymorphism
TALEN	transcription activator-like effector nucleases
TAP	transporter associated with antigen processing
T_{CM}	central memory T cells
TCR	T-cell receptor
tEGFR	truncated epidermal growth factor receptor
T_{EM}	effector memory T cells
T_{fh}	follicular helper T cells
TGF	transforming growth factor
TIL	tumor-infiltrating lymphocyte
Tim-3	T-cell immunoglobulin and mucin-domain containing-3
TME	tumor microenvironment
T_N	naive T cells
TNF	tumor necrosis factor
TRAC	T-cell receptor α-chain
T_{regs}	regulatory T cells
V gene segment/-GENE	variable gene segment
WHO	World Health Organization
WPRE	woodchuck hepatitis virus posttranscriptional regulatory element

1 Introduction

1.1 Hepatitis B virus

Infection with the hepatotropic hepatitis B virus is most commonly resolved through an acute, self-limiting course of disease, mediated by an intact immune response. Chronic infection, however, develops in approximately 5-90% of all patients correlating inversely with age[1], and carries severe health-related consequences, such as an increased risk of liver fibrosis, cirrhosis and ultimately hepatocellular carcinoma (HCC)[2]. Chronic HBV infection remains a serious global health problem with roughly 296 million chronic carriers in 2019[2]. Whereas death rates associated with other infectious diseases such as malaria, human immunodeficiency virus infection and tuberculosis are declining[3], chronic hepatitis B-related deaths are forecasted to rise from approximately 714'000 in 2016 to 1.3 million in 2040[4], unless appropriate counter-measures were to be developed. This underlines the urgent need to keep investigating into novel treatment methods for chronic hepatitis B (CHB) and associated liver diseases. The following chapter will address the molecular structure and replication cycle of HBV, describe HBV-associated diseases such as CHB and HBV-related HCC (HBV-HCC), and illustrate current treatment options and their limitations. Further below, potential immunotherapeutic strategies will be outlined.

1.1.1 Structure and replication of the hepatitis B virus

1.1.1.1 *Viral structure and genome*

The hepatitis B virus is a member of the *Hepadnaviridae* family; as such, it shows a narrow host specificity as well as a strong tropism for hepatocytes. Infectious virions, named Dane particles after their discoverer, were first identified by electron microscopy in 1970[5]. They measure 42 nm in diameter and consist of an outer lipid bilayer containing small (S), medium (M) and large (L) envelope proteins, as well as an icosahedral nucleocapsid composed of core (C) protein subunits. Inside the capsid, a partially double-stranded deoxyribonucleic acid (DNA) genome, the so-called relaxed circular DNA (rcDNA), is associated with the viral DNA polymerase (P)[6]. In addition, HBV-infected cells can form smaller, subviral particles of spherical or filamentous shape which do not contain viral DNA and are therefore non-infectious[7]. They exceed Dane particles in numbers by a factor of 10^3-10^4 [8] and include larger amounts of S and M protein compared to L protein and lipids[6].

The viral genome measures only 3.2 kb in size and is highly organized with four overlapping open reading frames (ORF). It encodes seven viral proteins, namely preCore, core, polymerase and hepatitis B X protein (HBx) as well as the three envelope proteins S, M and L. The envelope proteins are isoforms, which are translated from one ORF via differential initiation sites, with S being the smallest (24 kD), most abundant protein and common denominator sequence among the three. The translation of the M protein initiates further upstream with the additional N-terminal sequence preS2, whereas the L protein, being the largest of the three, is translated from the furthest upstream start codon and includes both preS1 and preS2[6,8]. The envelope proteins S, M and L are collectively referred to as hepatitis B surface antigen (HBsAg) in diagnostic terminology[6]. The 22 kD core protein is the basic subunit of the nucleocapsid, which is composed of 120 core dimers[9]. Translation of its complete ORF starting further upstream once again yields a protein variant, the preCore protein, which is translated directly into the endoplasmatic reticulum (ER) via a signaling peptide, proteolytically processed in the Golgi apparatus and ultimately secreted as a 16 kD cleavage product[6]. This so-called hepatitis B e-antigen (HBeAg) is commonly used as a serologic marker in HBV infection[2] and is thought to have an immunoregulatory effect by causing T-cell tolerance towards the nucleocapsid[10]. The 90 kD polymerase protein mediates the synthesis of viral rcDNA through reverse transcriptase activity and subsequent degradation of the viral ribonucleic acid (RNA) template (see section 1.1.1.2). While HBx is not known to have a structural function, it is has been found to be essential for HBV replication[11] and seems to target the Smc5/6 complex, thereby ultimately enhancing viral transcription[12]. In addition, it is believed to play a role in the oncogenesis of HBV-HCC[13].

1.1.1.2 *Replication cycle*

The hepatitis B virus initially attaches to the hepatocyte surface through interaction of the preS1 domain of the large envelope protein and the antigenic loop of the S domain with glycosaminoglycan side chains of heparan sulfate proteoglycans[14,15]. This is followed by specific binding to the sodium taurocholate co-transporting polypeptide (NTCP), a human bile acid transporter that is expressend on hepatocytes and was found to be essential for HBV entry[16]. The virus then enters the cell via clathrin-mediated endocytosis[17] and releases its nucleocapsid into the cytoplasm through fusion of the envelope with the endosomal membrane – a process known as uncoating. The capsid further translocates to the nucleus, where the rcDNA genome is released through a nuclear pore. On the inside, host cell enzymes are hijacked to

convert the partially double-stranded genome into covalently closed circular DNA (cccDNA)[18]. This episomal structure is a crucial element for viral persistence, since it serves as transcription template for viral RNAs and is not only extremely stable, but also seems to be partially transmitted to daughter cells after cell division[19]. Following transcription, viral RNA transcripts, including both mRNA for viral proteins as well as the full length pregenomic RNA (pgRNA), are transported into the cytoplasm and translated to viral proteins[18]. The pgRNA associates with the viral polymerase and core protein. This complex then self-assembles into RNA-containing nucleocapsids, followed by viral polymerase-mediated reverse transcription within the capsid to yield dsDNA. The mature nucleocapsid is either reimported into the nucleus to maintain a cccDNA pool or follows a secretion pathway via the ER. Since S, M and L proteins are integrated in the ER membrane during co-translation, the mature nucleocapsids are enveloped through budding into the lipid bilayer and ultimately released through multivesicular bodies[20]. An overview of the HBV replication cycle is given in Figure 1.

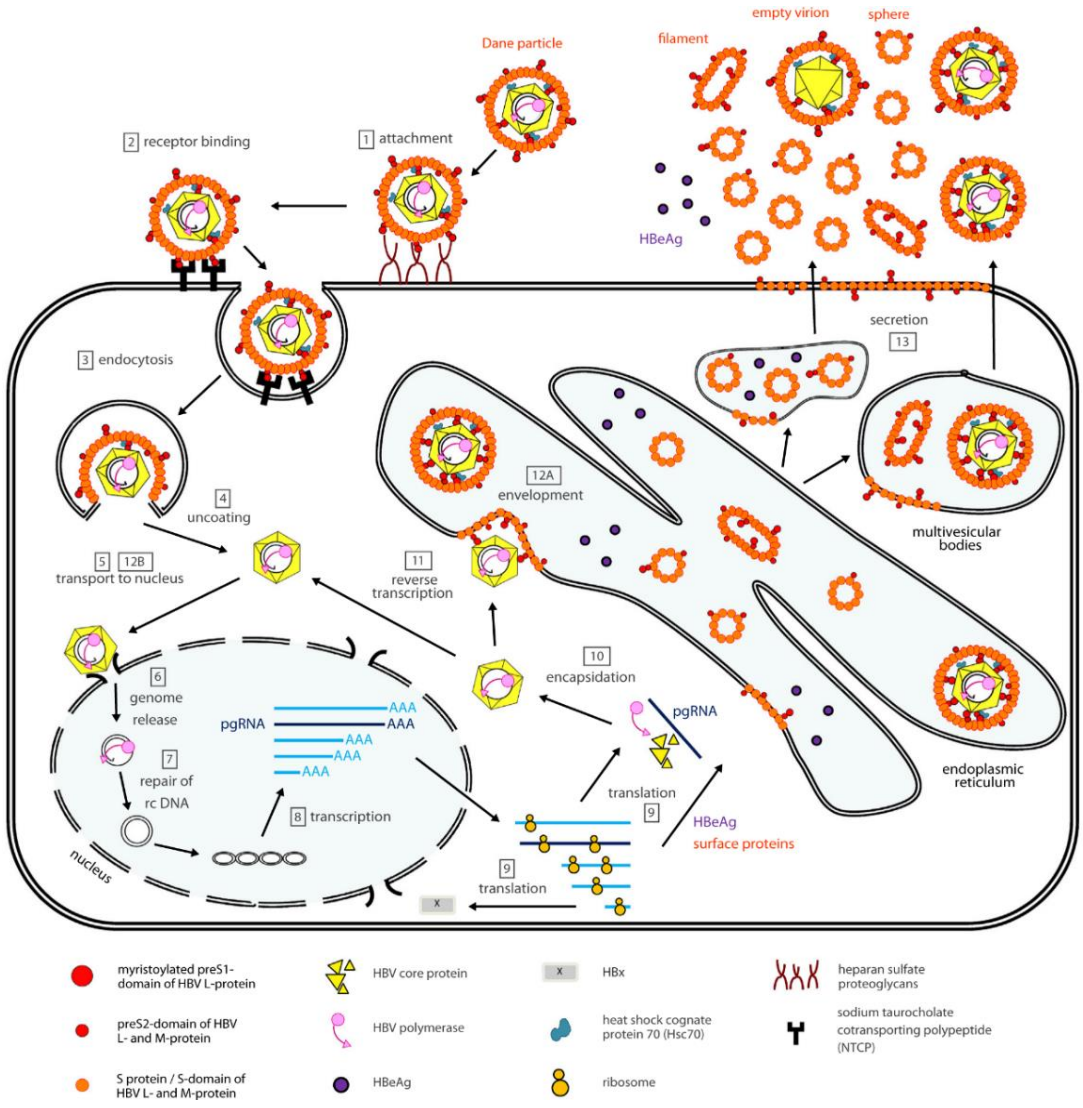

Figure 1: HBV replication cycle[19]. Description see text in section 1.1.1.2.

1.1.2 Epidemiology and HBV genotypes

While there are approximately 296 million chronically HBV infected individuals globally, the regional distribution of hepatitis B varies greatly on a worldwide scale. Areas where hepatitis B is highly prevalent, meaning >8% of the population are HBsAg positive, include East Asia, in particular China, the Asian Pacific states as well as sub-Saharan Africa. Intermediate prevalence of HBV (2-7%) is observed in regions such as North Africa, the Middle East, parts of Eastern and Southern Europe, parts of Latin America, and South Asia. And lastly, low prevalence areas (<2%) include Australia, Western Europe, North America, Japan and some countries in South America[21]. Infection in high prevalence areas often occurs through vertical transmission at childbirth. This is thought to correlate to some extent with the predominance of certain HBV genotypes that are linked to higher infectivity in women of child-bearing age[21].

The hepatitis B virus comes in nine genotypes, A to I, of which genotypes A to E are estimated to account for 96% of all chronic HBV infections worldwide[22]. Areas of low and intermediate HBV prevalence mostly vary in terms of genotype distribution, with the exception of Europe, Northern Africa and Russia, where genotype D is dominant. In Eastern Asia and the Asian Pacific States, however, genotypes B and C are most commonly found, whereas sub-Saharan Africa can be roughly divided into an Eastern region with higher prevalence of genotype A and a Western region where genotype E is most frequently present[21,22]. Of note, certain genotypes have been associated with virological, immunological and clinical differences, for instance serum levels of HBV DNA and HBeAg, differential tendencies towards chronic infection, cirrhosis and liver carcinoma, seroconversion rates, modes of transmission as well as responses to therapy[23].

Based on the antigenic properties of the HBsAg S domain, HBV can also be classified into four serotypes: *adw*, *adr*, *ayw* and *ayr*[24]. Common to all serotypes is a highly immunogenic 24 amino acid structure known to induce a protective humoral immune respone, the so-called *a* determinant[25]. Although the causal relationship between serotypes and genotypes is not clearly known, the following correlation with the most common genotypes can be observed: serotype *adw* is usually present in genotypes A, B and C; *ayw* is found in genotypes B, D and E; *adr* and *ayr*, however, are only associated with genotype C[23].

1.1.3 HBV-associated liver diseases

As mentioned above, infection with the hepatitis B virus can be either self-limiting or persistent, with CHB patients facing a high risk of developing liver cirrhosis and hepatocellular carcinoma. These HBV-associated liver diseases will be described below.

1.1.3.1 *Acute HBV infection*

Clinical symptoms occurring in the majority of patients with acute HBV infection include icteric skin and sclera, gastrointestinal manifestations, liver pain on percussion and fatigue[26]. While supportive symptomatic treatment is usually given to diagnosed patients[26], more than 95% of infected individuals with a competent immune system are able to clear the infection effectively without further therapeutic requirements[27]. Fulminant hepatitis occurs only in a minor fraction of patients, therefore mortality rates associated with acute HBV infection are below 1%[27]. The virological status of patients with resolved infection is termed “functional cure” and is defined by undetectable serum levels of HBV-DNA, nonexistent liver damage indicated by normal serological levels of alanine amino transferase (ALT) and seroconversion to HBsAg-specific antibodies[28]. Yet, HBV may still persist in a minority of hepatocytes in the form of cccDNA where it is kept under tight translational repression by the immune system[29].

1.1.3.2 *Chronic HBV infection*

Only 2-6% of adults develop chronic hepatitis B as a result from HBV infection. The risk, however, is much higher in children under five years of age, where 30-90% fail to clear the infection[27]. Chronic HBV infection is diagnostically defined by the persistence of HBsAg in blood or serum for at least six months[2]. Its clinical manifestation varies greatly among patients[27]. While it is mostly asymptomatic with no major liver damage, there is an increased risk of fibrosis, cirrhosis and hepatocellular carcinoma. Progression towards these conditions is associated with a number of risk factors such as co-infection with the human immunodeficiency virus (HIV), the hepatitis C virus (HCV) or the hepatitis D virus (HDV) as well as alcohol abuse[27].

According to the guidelines of the World Health Organization, chronic HBV infection can be categorized into the following phases: During the “immune tolerant” phase, mostly seen in children and young adults, serum HBV-DNA levels are frequently

above 200.000 IU/ml with normal or slightly increased ALT levels. This phase may last 10-30 years after initial infection with HBV and the progression to more severe liver conditions is uncommon. The “immune active” phase, on the other hand, is marked by liver inflammation with abnormal ALT levels and high or fluctuating levels of HBV replication. Liver damage and fibrosis are more common and can be substantial. The “immune control” phase is characterized by seroconversion to HBeAg antibodies, HBeAg clearance, reduction of liver damage, normal ALT levels and undetectable or low HBV-DNA serum levels <2000 IU/ml. Last but not least, both the “immune escape” phase, which is related to the occurrence of viral escape mutants, and the “reactivation” phase correlate with abnormal ALT levels and moderate to high HBV replication. Patients in these states are at higher risk for disease progression towards fibrosis and cirrhosis. HBV “reactivation” can occur spontaneously or can be triggered e.g. by immunosuppressive therapy[27,30,31].

1.1.3.3 *HBV-related hepatocellular carcinoma*

Chronic HBV infection is considered to be the most common cause for hepatocellular carcinoma on a global level, with chronically infected patients facing an elevated risk of developing HCC during their lifetime[32]. Accordingly, HCC incidence is especially high in regions where CHB is considered endemic[33]. HBV-related carcinogenesis is believed to be linked to one of the following molecular mechanisms: First, the expression of HBx is known to modulate the host cell on many levels, e.g. through interference with cellular pathways or DNA repair mechanisms and induction of epigenetic changes, with several of these alterations being tumorigenic[13]. Also, HCC has been associated with various mutated forms of HBx and in particular with the presence of truncated HBx[13], which was shown to induce hepatocarcinogenesis through increased cellular proliferation and lower apoptosis[34]. Second, it has been shown that in HCC the viral genome frequently integrates into the host cell genome[35,36]. These integrations can deregulate gene expression and cause genomic instability with potentially carcinogenic consequences[37,38]. Third, on-going inflammation and liver damage as well as increased hepatocyte proliferation compensating for the loss of infected hepatocytes results in the accumulation of genetic modifications[37]. While the viral genome often rearranges after integration, the preS2 and HBx sequences seem to remain rather unaffected, hinting at an additional importance of these two proteins for the development of HCC[39]. In addition, micro ribonucleic acids (miRNAs) seem to be involved in the establishment of HCC; for example, miR-221 and miRNAs expressed by the miR-17-92 and the miR-106b-25

cluster, have been shown to be upregulated in aggressive HCC[40,41]. The average survival rate of patients with HCC is between six and 20 months[42]. With this in mind, primary liver cancer, of which 75-85% of cases are HCC, is the fourth leading cause of cancer death worldwide[43].

1.1.4 Prophylaxis and current treatment options

1.1.4.1 *Hepatitis B vaccination*

Since the early 1980s, a prophylactic HBV vaccine based on HBsAg has been available and has greatly decreased HBV incidence and morbidity rates[44]. The World Health Organization (WHO) recommends vaccinating infants as soon as possible after birth, especially in regions of high endemicity[45]. Delivery of the vaccine within 24 hours of birth, when followed up by at least two additional doses, has proven 90-95% effective in preventing HBV infection through vertical transmission[30]. A three dose application scheme is equally recommended for delayed vaccination in children, adolescents and adults[45]. The presence of >10 IU/l anti-HBs antibodies 1-2 months after administration of the last dose of the primary vaccination series, is considered a reliable serological measure of long-term protection[46].

The conventional HBV vaccine contains recombinantly produced S protein from yeast, which forms spherical HBsAg particles exposing the *a* determinant. A glycosylated vaccine alternative, composed of S, M and L protein produced in mammalian cells, is administered to non-responders and is licensed in Israel and some countries in East Asia[44]. A potential limitation of the currently marketed vaccines is their genotype: they consist of genotype A2 adw2, which is mostly prevalent in the USA and Northern Europe, whereas over 99% of all HBV carriers worldwide are infected with other genotypes[44]. Cross-protection among different genotypes was observed both in chimpanzees[47] and in humans[48,49]. However, the extent of cross-protection may vary depending on genotype and serotype, as evidenced by a shifting distribution in infant HBV infection from genotype B adw2 to genotype C adr in Taiwan following the implementation of a universal perinatal vaccination with the standard A2 adw2 yeast-derived formulation[50]. Similar observations were made in China 25 years after the implementation of an HBV vaccination plan[51].

Overall, vaccination against hepatitis B has proven to be highly successful. For example, since vaccination was first introduced in Taiwan in 1984, HCC incidence has dropped by 60%, mortality due to fulminant hepatitis by 76% and mortality due to chronic liver disease by 92%[52]. Similarly, HBV prevalence in the Western Pacific

Region before and after implementation of the vaccine decreased from >8% to <1% in most countries[53]. With global coverage of the three-dose vaccination schedule during infancy reaching 84% in 2015[54], major advances in the worldwide response to HBV are evident.

1.1.4.2 *Current treatment options*

Despite the availability of a prophylactic vaccine, there is a large number of chronic HBV carriers and many of them require therapy. Treatment is indicated for patients with signs of liver cirrhosis or individuals >30 years of age with persistently elevated ALT levels and HBV-DNA >20.000 IU/ml. While these clinical symptoms typically occur during the “reactivation” phase of chronic infection, patients in other phases may also require treatment. Therefore, close monitoring is recommended for all chronic carriers[30]. Clinically approved treatments include pegylated interferon (IFN)-α and nucleos(t)ide analogues (NUCs)[55]. IFN-α is known to directly target HBV on a transcriptional, post-transcriptional and epigenetic level[56-60]. For example, it has been shown to mediate APOBEC3A-induced degradation of cccDNA[61]. In addition, IFN-α exerts an influence on the host immune system, e.g. through enhancing the antiviral activity of natural killer (NK) cells[62]. The complete mechanism of action of IFN-α, however, remains to be fully understood. Pegylated IFN-α achieves viral suppression in 10-40% of all $HBeAg^+$ patients, with HBsAg loss occurring in only 2-17% of patients, depending on genotype and patient ethnicity[63-65]. This overall modest therapeutic efficacy is accompanied by substantial side effects, including neutropenia and/or thrombopenia, depression and auto-immune manifestations, among others[63,66,67]. NUCs, on the other hand, are generally better tolerated than IFN-α and function through the inhibition of the viral polymerase, i.e. the reverse transcriptase. The currently available, orally administered compounds include lamivudine, adefovir, entecavir, tenofovir disoproxil and tenofovir alafenamide, with entecavir and tenofovir being the recommended first-line therapy, since development of resistance is less frequently observed to date[55]. In terms of efficacy, the application of tenofovir disoproxil achieves viral suppression in 90% of all patients, although HBsAg loss only occurres in <1% of patients despite long-term treatment[68]. Since cessation of therapy is mainly indicated upon loss of HBsAg, the majority of patients is required to take NUCs as a life-long measure[55]. One idea that emerged during recent years, though, is the calculated withdrawal of NUC treatment. It was shown that the sudden withdrawal of NUCs causes a relapse of HBV DNA. The subsequent re-exposure to viral antigens can trigger immune control in some patients, followed by HBsAg loss in

approximately 20%. This is why certain patients without severe conditions may opt for stopping NUC therapy under controlled circumstances[69]. Overall, current treatment options rarely achieve functional cure; therefore the goal of presently available antiviral therapy for chronic HBV carriers is to improve survival by delaying the onset of liver cirrhosis and HCC[63].

Effective treatment of HCC is currently limited to the early stages of disease. This is where surgical therapy, such as resection or liver transplantation, is generally recommended, with the latter achieving survival rates of 60-80% after 5 years. Tumor ablation, in turn, is only advised for candidates not suitable for surgery[70]. For patients with advanced disease, transarterial and systemic treatment is indicated. The multi-kinase inhibitor Sorafenib was the first systemic compound to be approved by the US Food and Drug Administration (FDA) and remains standard of care for first-line therapy to date[70], despite its rather moderate survival advantage of 2.8 months compared to placebo[71]. What is more, up to 91% of all Sorafenib-treated patients have been reported to encounter side effects, with 45% suffering from grade 3 to 4 adverse events[72]. Lenvatinib, a small molecule inhibitor of receptor tyrosine kinases, was approved in 2018 as an alternative first-line treatment of patients with unresectable HCC, as it showed a non-inferior efficacy in terms of overall survival compared to Sorafenib in clinical trials and superiority regarding objective response rate and progression-free survival, among others[73]. Recently, immunotherapy with checkpoint inhibitors has emerged as a treatment option with promising outlook[74]. As such, treatment with the programmed cell death protein 1 (PD-1) inhibitor nivolumab achieved an objective response rate of 20% in patients with adavanced hepatocellular carcinoma[75]. Nevertheless, the occurrence of grade 3 to 4 adverse events remains high and the overall patient survival is limited[74]. Taken together, the limitations of currently available treatment methods underline the necessity for research into novel therapeutic options.

1.2 Basics of T-cell immunology

The immune system is composed of innate and adaptive immunity, with the latter being further divided into a humoral and a cellular immune response[76]. Key players of the cellular immune response are T cells, which are named after their development in the thymus and are divided into two major subsets, cytotoxic cluster of differentiation(CD)8^+ T cells and $CD4^+$ T cells with a helper function. T-cell activation is based on the recognition of products from intracellular proteolysis, which are presented by target cells on major histocompatibility complex (MHC) molecules.

These T-cell epitopes are detected with the help of membrane-bound T-cell receptors on the T cell side. The basis of MHC molecules, TCRs and their interaction process will be described in the following section. Additionally, the role of $CD4^+$ T cells will be elaborated in more detail.

1.2.1 Major histocompatibility complexes and presentation pathways

In humans, the major histocompatibility complex is also referred to as the human leukocyte antigen (HLA) complex. It is a large multigenic region on chromosome 6 of the human genome and encodes mainly for the human MHC class I and class II molecules. Different MHC molecules can have varying roles and present antigen to a number of immune receptors. The so-called “classical” MHC molecules, which refer to HLA-A, -B, -C for MHC class I and HLA-DR, -DQ, -DP for MHC class II, are the ones recognized by T-cell receptors from either $CD8^+$ or $CD4^+$ T cells, respectively. The differentiation between class I and class II is based on pathways of antigen processing and peptide loading.

For the MHC class I pathway, intracellular proteins, e.g. from pathogen infection, are typically cleaved by the cytosolic protease complex. The resulting peptides are translocated into the ER via the transporter associated with antigen processing (TAP). The peptides are then loaded onto MHC class I molecules, consisting of an α1-α3 polymorphic heavy chain in conjunction with the invariant soluble beta 2-microglobulin (β2M) (Figure 2). The loaded complex is trafficked via the Golgi apparatus to the plasma membrane. In contrast, MHC class II presentation results largely from extracellular proteins or pathogens that enter the cell via endocytosis or phagocytosis and are degraded through lysosomal proteolysis. MHC class II molecules, which are composed of an α- and β-chain (Figure 2), are assembled in the ER and transported to the endosomal compartments for peptide loading. The fully loaded MHC class II complex is then trafficked to the plasma membrane. While the described pathways represent the most common mechanisms for antigen presentation, both MHC class I and MHC class II molecules can access peptides from the respective other system. This is particular relevant for MHC class I molecules loaded with peptides from an extracellular origin, a process that is known as cross-presentation and is critical for the priming of naïve $CD8^+$ T cells by dendritic cells[77].

Whereas MHC class I molecules are expressed on all body cells with the exception of erythrocytes, the MHC class II pathway is a unique feature of antigen presenting cells (APCs), such as dendritic cells, macrophages or B cells. The MHC α- and β-

chain are encoded in the classical HLA class II gene loci, DR, DQ and DP. The DR locus comprises a practically constant α-chain gene as well as a different DR β-chain variant, encoded by the DRB1 allele and usually one or two of any DRB3, DRB4 or DRB5 alleles. This means that an individual typically expresses the HLA-DR molecules based on the α/β-chain combination from DRB1, as well as one or more HLA-DR isoforms resulting from the DRB3, DRB4 or DRB5 alleles, depending on the respective allele composition. In contrast, for HLA-DQ and HLA-DP, both chains can have allelic variants. Unlike MHC class I, the peptide binding grove of MHC class II molecules is open at both ends, which allows for binding of peptides with variable lengths, typically 13-25 amino acids[78] (Figure 2). The main interaction between peptide and MHC grove takes place via the so-called peptide binding core, which is usually nine amino acids long with anchor residues at positions 1, 4, 6 and 9[79]. Nevertheless, it has been shown that the peptide flanking regions on either side of the binding core also influence MHC-peptide affinity and therefore ultimately epitope immunogenicity[80].

MHC molecules can be highly polymorphic, since most HLA gene loci consist of many different allelic variants. These variants are named with a unique number: the first number corresponds to the main HLA type, followed by a colon and a second number designating the subtype, e.g. HLA-DRB1*01:01[81]. The corresponding protein is often abbreviated to HLA-DR1, which stands for the DR1 molecule and its most common subtype. A variety of HLA alleles, both MHC class I and MHC class II, have been associated with susceptibility or resistance to HBV infection or vaccination, HBV clearance, course of disease and treatment outcome[82]. Given the interaction of the T-cell receptor with the classical MHC molecules, the HLA type as well as the respective epitopes are closely related to an individual's T-cell response to infection.

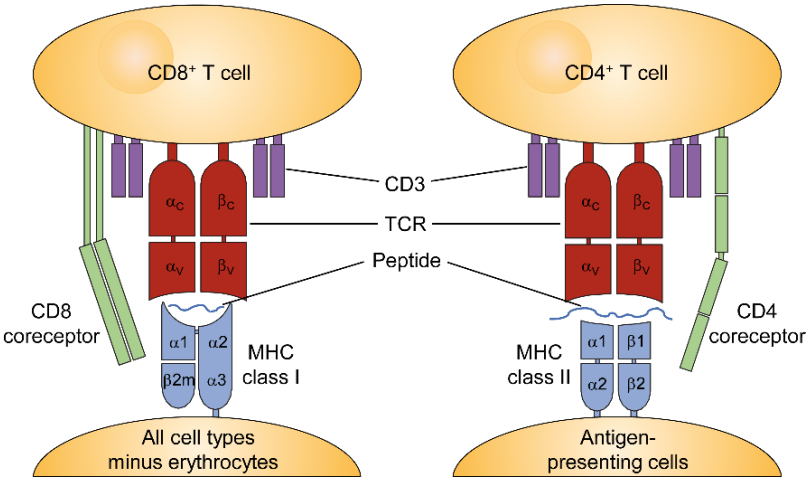

Figure 2: T-cell interaction with MHC class I and class II molecules.
Description see text in sections 1.2.1 and 1.2.2.

1.2.2 T cells and T-cell receptors

The two main T cell subsets are $CD8^+$ and $CD4^+$ T cells. The former are also called cytotoxic T lymphocytes (CTLs) due to their main purpose, the killing of infected or cancerous cells. They are activated based on the interaction between their T-cell receptor and an MHC class I-peptide complex on the target cell. This is supported by the CD8 glycoprotein, a disulfide-linked heterodimer which serves as a coreceptor through binding with the interacting MHC molecule. $CD4^+$ T cells, on the other hand, are named after their CD4 coreceptor, which is composed of four domains with two domains each being joined by a flexible hinge and sustains the activation process initiated by the T-cell receptor interaction with MHC class II.

The vast majority of T cells express a T-cell receptor composed of an α-chain and a β-chain with an N-terminal variable and a C-terminal constant region each. The TCR is embedded in the plasma membrane via a transmembrane domain within the constant region, which allows interaction with CD3, a complex crucial for the generation of a TCR-induced activation signal. While the α-chain is encoded by a variable (V), joining (J) and constant (C) gene segment on chromosome 14, the β-chain locus is located on chromosome 7 and contains an additional diversity (D) element in between the V and J segments. The diversity of the T-cell receptor variable domains, in particular within the complementarity-determining regions (CDR) 1-3 that form the antigen-binding sites of both the α- and the β-chain, is given by the random recombination of V(D)J segments and the addition or deletion of nucleotides during T-cell clonal development[76]. The structural composition of the T-cell receptor as well as their interaction with MHC molecules class I or II as described above is illustrated in Figure 2.

1.2.3 $CD4^+$ T cells

$CD4^+$ T cells are initially activated in secondary lymphoid organs such as the spleen or the lymphnodes, where antigen-presenting cells present peptides on MHC class II molecules and deliver necessary co-stimulatory signals and pro-inflammatory cytokines. Activated $CD4^+$ T cells differentiate into a variety of $CD4^+$ T cell subsets, including Th1, Th2, follicular helper T cells (T_{fh}), Th17 and regulatory T cells (T_{regs}) - accordingly, the role of $CD4^+$ T cells is much more diverse than that of $CD8^+$ T cells. T_{fh} cells, for example, are essential to the development of a functional and long-lived B-cell response. Following viral infection, they drive the formation of germinal centers through expression of SLAM-associated protein[83,84]. B-cell activation, differentiation

and antibody production crucially depend on IL-21 secretion by T_{fh} cells[85] as well as interaction between CD40 and CD40L[86]. This same interaction is also relevant for licensing of dendritic cells by $CD4^+$ T cells: TCR-based recognition of antigen by $CD4^+$ T cells increases CD40-CD40L signaling by dendritic cells, resulting in their activation, production of IL-12 and IL-15 and upregulation of CD80, CD86 and CD70. The latter are important costimulatory molecules and interact with CD28 and CD27 on $CD8^+$ T cells, leading to clonal expansion and the generation of a fully functional CTL response[87]. CD70-CD27 signaling, in particular, promotes the differentiation of $CD8^+$ T cells into effector and memory cells[88]. In this regard, Janssen et al. showed that whereas $CD4^+$ T cells may be dispensable for a primary $CD8^+$ T cell response, secondary CTL expansion, i.e. following antigen re-exposure, is fully dependent on $CD4^+$ T cell help being present during the $CD8^+$ T cell priming stage[89]. One molecular explanation of this observation appears to be the downregulation of TNF-related apoptosis-inducing ligand (TRAIL) in helped $CD8^+$ T cells, ultimately making them less prone to TRAIL-mediated apoptosis[90]. Interestingly, regarding their role in $CD8^+$ T cell priming, the importance of APCs activated by $CD4^+$ T cells versus APCs activated through pathogen interaction remains unclear, with most experimental evidence pointing towards a complimentary role[87]. In addition to APC-mediated help, $CD4^+$ T cells also have a more direct impact on $CD8^+$ T cells: IL-2 and IFN-γ secretion, for example, promote effector CTL differentiation[91,92] and IL-21 seems to contribute to the maintenance of a functional $CD8^+$ T cell effector response[93]. Last but not least, $CD4^+$ T cells also exert direct effector functions. As such, antiviral activity was observed in several different infection models, through both the production of cytokines, mostly IFN-γ and TNF-α, as well as direct cytolytic activicty[86].

1.3 Immune response in hepatitis B virus infection

In contrast to the innate immune response, adaptive immunity is generally considered to be the key player in self-limited HBV infection[94]. To this end, T-cell immunity has been heavily investigated in the context of HBV and will be described below. The humoral immune response, on the other hand, is less well described, despite the fact that anti-HBV antibodies were found capable of neutralizing free virus particles and preventing HBV reinfection decades ago[95].

1.3.1 Innate immunity

A major characteristic of HBV infection is the poor activation of innate immunity[94]. In patient samples of acute hepatitis B, type I interferons such as IFN-α, i.e. typical

markers of the innate immune response, are hardly detectable during the first month of infection[96] or delayed when compared to patients with HIV infection[97]. In line with these findings, a limited induction of interferon-related genes is observed both in chimpanzees after HBV infection[98] and in a woodchuck model of chronic viral hepatitis[99], which is why HBV has been termed a “stealth virus”[100].

NK cells are key players of innate immunity and can be directly activated by type I interferons upon viral infection[101]. Their role in HBV infection is, however, poorly understood. Some patient studies report an elevated number of NK cells at an early time point after infection[102,103], other findings indicate reduced NK cell activation at the peak of viremia compared to healthy donors[96]. In chronic HBV infection, their functionality appears to be impaired by immunosuppressive cytokines such as interleukin (IL)-10 or transforming growth factor (TGF)-β[104]. Hepatic NK cells have also been suggested to correlate with increased cytolytic activity and liver injury[105]. In any case, NK cells have been decidedly linked to the treatment with IFN-α, since a rapid increase in NK cell activation and proliferation has been repeatedly encountered in patients with CHB upon therapy initiation[62,106].

1.3.2 Humoral adaptive immune response

The importance of humoral immunity for HBV immune surveillance is evidenced by clinical data demonstrating that B-cell depletion in lymphoma patients with previously controlled infection poses a major risk for viral reactivation[107]. Furthermore, the transplantation of hematopoietic stem cells from vaccinated donors to chronically HBV infected individuals has frequently resulted in the loss of HBsAg, which could be partially attributed to the transfer of a functional B-cell response[108]. The role of B cells for HBV infection may even reach beyond the production of HBV-specific antibodies, e.g. they could positively influence T-cell immunity in their capacity as antigen-presenting cells[109] and were shown to exert regulatory functions in the pathogenesis of CHB[110]. A recent *ex vivo* study analyzing both circulating and liver-resident B cells in chronic HBV carriers, moreover, revealed cellular defects in antibody production and atypical memory B cells with high expression of inhibitory receptors and significantly altered cellular properties[111].

In terms of clinical application, the administration of Hepatitis B immunoglobulin (HBIG), i.e. antibodies isolated from donors with high titers of anti-HBsAg antibodies, can confer temporary immunity and is indicated as post-exposure prophylaxis and to prevent perinatally transmitted HBV infection[45,112]. Similarly, recombinantly produced

HBsAg-specific antibodies were able to reduce the HBsAg load repeatedly after administration, even though the response was not durable[113]. Design improvements have since been made for a murine HBV-specific antibody with promising therapeutic outcome in mice and cynomolgus monkeys[114].

1.3.3 Cellular adaptive immune response

As mentioned above, T-cell responses in HBV infection have been extensively investigated and are known to play a crucial role for viral clearance during the self-limited course of infection. Strong evidence of this has been gathered in chimpanzees: The transient depletion of $CD8^+$ T cells six weeks after HBV infection leads to a severely prolonged disease in comparison to the healthy control animal[115]. In the liver of infected animals, the expression of a large number of T cell-associated IFN-γ-responsive genes appeared to be upregulated during HBV clearance, underlining the impact of an effective T-cell response[98]. The HBV-specific T-cell response has also been studied at length in humans. As such, samples of patients with acute HBV consistently show evidence of a functional, polyclonal $CD8^+$ and $CD4^+$ T-cell response[103,116-118]. A large number of HBV-specific $CD8^+$ T cells with an activated phenotype is observed during the acute phase of infection[96,116]. A non-cytolytic mechanism based on IFN-γ and tumor necrosis factor (TNF)-α seems to play a role, since $CD8^+$ T cells were able to abolish HBV replication in a transgenic mouse model with only minor hepatocyte killing[119]. This is further emphasized by studies in chimpanzees, where a rapid decline of HBV DNA was seen long before liver damage reached its maximum[120,121]. Nevertheless, cytolytic activity has also been reported for $CD8^+$ T cells infiltrating the liver, linked to the secretion of chemokines such as CXCL-10 and platelet activation[122-125]. Despite the initial rise in $CD8^+$ T-cell numbers in patients with acute infection, a functional impairment of $CD8^+$ T cells was observed at the peak of viremia[96,126], possibly linked to increased levels of IL-10[96] and arginase[127].

Compared with $CD8^+$ T cells, the characteristics of $CD4^+$ T cells in HBV infection have been studied to a lesser extent. Notably, their presence seems equally critical for a curative response, since their depletion prior to infection with HBV inevitably lead to chronic disease in the complete absence of virus-specific $CD8^+$ T cells in chimpanzees[128]. In addtion, their existence was similarly imperative for the induction of a functional $CD8^+$ T-cell response in a murine model[129]. In patients with self-limited hepatitis B, they were shown to exhibit a Th1 phenotype[130,131]. In a recent study, larger numbers of IFN-γ-producing $CD4^+$ T cells were correlated with increased levels of viral clearance in chronic HBV carriers, whereas TNF-α-secretion by $CD4^+$ T cells was

rather associated with elevated ALT levels in patients with hepatitis B flares[132]. More extensive research is clearly needed to clarify the role of $CD4^+$ T cells in resolving HBV infection. Ultimately, successful control of HBV infections is associated with the formation of a mature T-cell memory compartment[133,134] and HBV-specific $CD4^+$ and $CD8^+$ T cells remain detectable for years[29,135,136].

Virus-specific T cells in patients with chronic HBV infection are generally scarce and mostly dysfunctional[117,137-141], possibly as a consequence of exhaustion given the continued exposure to viral antigens. They typically express inhibitory molecules such as PD-1, cytotoxic T-lymphocyte-associated protein 4 (CTLA4) and T-cell immunoglobulin and mucin-domain containing-3 (Tim-3) on $CD8^+$ T cells[140,142-146], are defective in proliferation and cytokine production[140,142,147,148], and show metabolic alterations[149,150]. The severity of T-cell dysfunction has been correlated with high viremia[138,140,141] and liver-resident T cells have been found to be more affected compared to those in the periphery[147].

1.4 Principles of adoptive T-cell therapy and application to HBV

The general idea of adoptive T-cell therapy (ACT) is to generate a robust anti-target immune response by infusing *ex vivo* enriched and/or engineered T cells. This concept was first introduced through the isolation of naturally occurring tumor-infiltrating lymphocytes (TILs) from a tumor biopsy and subsequent transplant into the patient, a therapeutic approach known as TIL therapy. Initial clinical results were obtained in 1988 for the treatment of metastatic melanoma[151], however real breakthrough in terms of efficacy came in 2002, when an immunodepleting chemotherapy prior to adoptive transfer was shown to enable clonal repopulation by transferred lymphocytes[152]. To this day, TIL therapy remains a viable tool for melanoma[153] and other cancers; yet, with the rapid advance of molecular engineering technologies, alternative approaches using genetically modified T cells have emerged. The so-called autologous adoptive T-cell therapy involves the isolation of the patient's own T cells, activation *in vitro* to facilitate proliferation and gene transfer, redirection by introduction of a target-specific transgenic receptor, expansion, formulation of the final product followed by quality control measures, and finally, reinfusion into the patient (Figure 3).

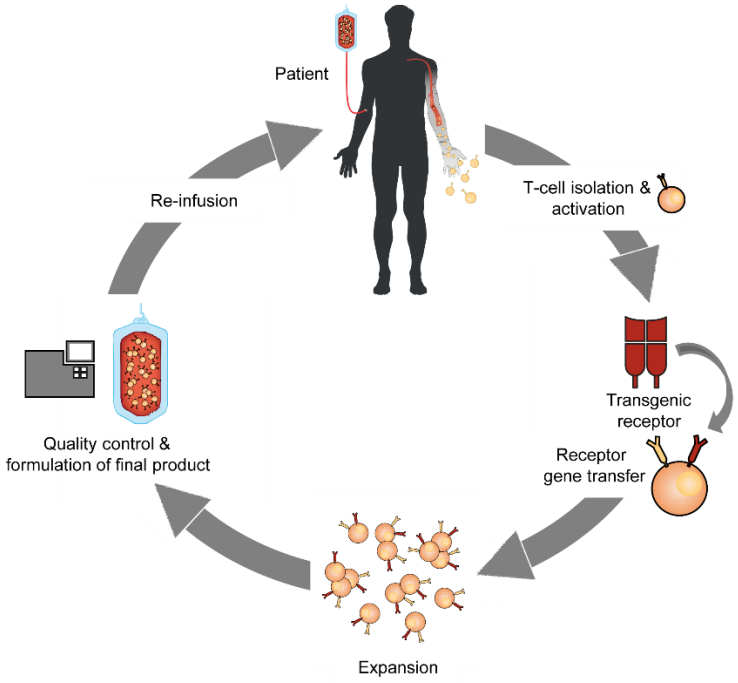

Figure 3: Schematic representation of adoptive T-cell therapy for chronic hepatitis B or HBV-HCC. T cells are obtained from the patient's blood and activated *in vitro* to enable proliferation and gene transfer of an HBV-specific receptor, e.g. a T-cell receptor of known target specificity. The T cells are expanded *in vitro,* the cell product is then submitted to quality control measures, e.g. sterility testing, and the final formulation is reinfused into the patient. Adapted from Tan, A. and Schreiber, S., Antiviral Research (2020).

The first successful clinical trial that resulted in tumor regression based on this method was reported in 2006 for the treatment of melanoma[154]. In general terms, genetically modifying T cells with pre-existing, well-characterized target-specific receptors, allows a wider applicability of adoptive T-cell therapy to a larger patient group with various cancer types or infectious diseases. The rationale for treating chronic HBV infection and HBV-related hepatocellular carcinoma with ACT is based on the idea of restoring the dysfunctional T-cell immunity commonly observed in patients with CHB. The design of transgenic receptors for adoptive T-cell therapy and clinical application for HBV will be described below.

1.4.1 Transgenic receptors in adoptive T-cell therapy

Transgenic receptors used for redirecting autologous T cells in adoptive T-cell therapy are typically either TCRs or chimeric antigen receptors (CARs). The former usually refers to a naturally occurring, mostly human TCR with few modifications. The latter is a synthetic construct which consists of an antibody-derived binding domain combined with an intracellular signaling domain and is commonly expressed as a single polypeptide chain. Both come with a distinct set of advantages and limitations, which will be outlined below.

1.4.1.1 *Chimeric antigen receptors*

A modular receptor with CAR-like features, capable of T-cell activation upon target engagement, was first developed by Zelig Eshhar in 1989 and termed "T-body" or

"immunoreceptor" at the time[155]. CAR design has since been optimized over the years and today typically contains a single-chain variable fragment (scFv) for target recognition, followed by a spacer domain of variable length and an intracellular signaling domain with CD3ζ as primary T-cell activation signal and CD28 or 4-1BB as co-stimulatory signals[156]. The main advantage of CARs consists in their antibody-like binding moiety, which recognizes surface-bound target independent from presentation on MHC molecules. Not only can CAR therapy address a broader patient range independent of their HLA type, it is particularly relevant, given that MHC molecules are down-regulated in a number of cancers[157-160]. On the downside, CAR-T cells can only target approximately 30% of all known proteins, since they have to be expressed on the cell surface. In addition, they are susceptible to interference by soluble forms of the target in the periphery, which could either capture CAR-T cells and prevent them from reaching their target site, or even worse, cause off-target activation resulting in adverse events.

1.4.1.2 *T-cell receptors*

In contrast to CARs, TCRs recognize intracellularly processed antigen presented on MHC molecules in the form of linear epitopes, therefore covering a much larger number of possible targets. The redirection of T cells using a transgenic TCR α- and β-chain followed by successful target recognition was first shown in 1995. However, the potential of mispairing with α- and β-subunits of the endogenous TCR was also revealed, leading to a lower expression of the correctly paired transgene on the cell surface[161]. More importantly, it was observed to potentially result in TCRs with novel or even autoimmune reactivity[162,163], and such events have caused severe graft-versus-host disease in murine models[164]. Still, a study cohort of 106 patients transplanted with TCR-redirected T cells showed no signs of graft-versus-host disease[165], therefore somewhat alleviating this concern for humans. To further mitigate the risk by reducing the amount of mispairing events, TCRs with murine constant regions were introduced leading to an overall improved expression, stability and functionality of the transgenic receptor[166]. Further modifications resulting in higher expression levels and better functionality include the addition of cysteine residues to create disulfide bonds between the α- and β-chain[167] as well as codon-optimization of the open reading frame which improves translational efficiency[168-170]. More recently, novel techniques have been developed, completely abolishing the possibility of mispairing. As such, the targeted integration of a T-cell receptor into the endogenous TCR α-chain (TRAC) locus with simultaneous knock-out of the endogenous β-chain

through clustered regularly interspaced short palindromic repeats (CRISPR)-Cas9 technology has shown promising results with the additional benefit of the transgenic TCR being under control of the physiological promotor[171].

1.4.2 Clinical application of adoptive T-cell therapy

Following several decades of research, adoptive T-cell therapy encountered a real clinical breakthrough with CAR-T therapy of B cell lymphomas. As such, autologous anti-CD19 CAR-T cells were approved by the FDA in 2017 for the treatment of acute lymphoblastic B-cell lymphoma (B-ALL) in children and young adults (Kymriah™ by Novartis) and adult large B cell lymphoma (Yescarta™ by Gilead)[156]. A recent global multi-center phase 2 CAR-T study reported on 75 patients with refractory or relapsed B-ALL with a median of three previous therapies; after receiving Kymriah, 81% of all patients went into complete remission[172]. In view of the overwhelming clinical success of anti-CD19 CAR-T cells, numerous ACT trials for many different indications have emerged. However, many challenges remain, in particular for the application of ACT to solid tumors[173]. For example, the identification of suitable tumor antigens that are truly unique to the tumor site has been difficult and low expression of tumor antigens on healthy tissue has led to severe or even fatal side effects in case studies of renal cell cancer[174] and colon cancer[175,176]. Further difficulties arising from solid tumors include the tumor microenvironment with physical obstacles such as a dense extracellular matrix and immunological barriers, for instance an accumulation of immunosuppressive cells and cytokines[173].

In HBV-associated HCC, carcinogenesis is closely associated with HBV integration into the host genome (see 1.1.3.3). This is why targeting viral antigens through adoptive T-cell therapy is beneficial, since their expression is limited to the liver with the exception of circulating HBsAg and HBeAg. The tumor microenvironment is composed mostly of hepatic stellate cells, fibroblasts, immune cells such as $CD4^+$ $CD25^+$ T_{regs} and Kupffer cells, as well as endothelial cells, which have been implicated in different ways in hepatocarcinogenesis[177]. In addition, non-cellular components like TGF-1β, matrix metalloproteinases and inflammatory cytokines e.g. IL-6, TNF-α and IL-1, have been linked to the stroma of HCC[177]. An immunosuppressive environment is generally a characteristic feature of the liver, which has been described in detail regarding its effect on viral hepatitis[178,179].

1.4.3 $CD4^+$ T cells in adoptive T-cell therapy

To date, most research efforts have focused on the use of $CD8^+$ T cells with TCRs restricted against MHC class I molecules. Nevertheless, given the importance of $CD4^+$ T cells for a systemic immune response, for example concerning the induction and maintenance of a functional $CD8^+$ T cells and a long-lived B-cell response, their benefit for immunotherapy of cancer and viral infection is evident[180,181]. Ample evidence as to the potential of adoptively transferred $CD4^+$ T cells has been gathered in mice: Early on, their efficacy was shown in a model of leukemia in combination with chemotherapy[182] as well as in a model of metastasizing melanoma, where their effect was attributed to the activation of tumoricidal macrophages[183]. Further confirmation was gained from mice with bladder carcinoma, where tumor rejection was partially linked to the induction of tumor-specific NK cells through transferred T helper cells[184]. Meanwhile, in a hematopoietic tumor model the transfer of specific subsets of both $CD4^+$ and $CD8^+$ T cells lead to a superior anti-tumor effect than $CD8^+$ T cells only[185]. More recently, in a model of mouse sarcoma treated with immune checkpoint inhibitors, an effective anti-tumor immune response was shown to require the presence of MHC class II-restricted tumor antigens[186]. On the clinical side, a case study of a patient with metastatic melanoma who received autologous New York esophageal squamous cell carcinoma-1 (NY-ESO-1)-specific $CD4^+$ T-cell clones reported complete remission mediated by an endogenous multi-specific T-cell response[187]. Despite this encouraging data, only few MHC class II-restricted T-cell receptors have been generated so far[188-194]. Of note, the addition of $CD4^+$ T cells engrafted with an NY-ESO-1-specific MHC II-restricted TCR strongly increased tumor regression in a murine xenograft model compared to the transfer of redirected $CD8^+$ T cells only[194]. So far only the HLA-DPB1*0401-restricted TCR targeting the melanoma antigen A3 (MAGE-A3) has been clinically tested regarding safety and efficacy[195]. This strongly emphasizes the current research deficit in terms of MHC class II-restricted T-cell receptors and their use in adoptive T-cell therapy of cancer or viral infection.

1.4.4 Current approaches for the treatment of CHB and HBV-HCC

Based on the importance of HBV-specific T cells during the self-limiting course of infection outlined above, the idea of adoptively transferring HBV-specific immunity to patients with chronic infection or HBV-HCC emerged. This rationale was backed by clinical reports on chronically HBV infected patients who cleared the infection after

receiving an otherwise indicated bone marrow transplant from donors who had undergone vaccination or self-limited HBV infection[196,197].

The idea of using a transgenic receptor for adoptive T-cell therapy of HBV was first introduced in 2008 through the development of an HBV-specific chimeric antigen receptor[198]. This so-called S-CAR is composed of an HBsAg-specific scFv, the Fc spacer domain of human immunoglobulin 1 (IgG1) as wells as CD28 and CD3ζ signaling domains[198]. S-CAR-grafted $CD8^+$ T cells were shown to efficiently control HBV replication in a transgenic mouse model with only limited liver damage[199]. Since a murine immune response against the human scFv and the IgG1 spacer domain was observed, a fully immunocompetent CAR-tolerant mouse model was later developed to study the effect of transferred T cells over an extended period of time. In this adeno-associated virus (AAV)-based model of HBV infection, the S-CAR-redirected T cells persisted for more than three months until the end of the experiment and were able to decrease HBsAg by 2 log and HBV-DNA by 60% compared to the controls[200].

The development of the S-CAR was followed by a number of MHC class I-restricted HBV-specific TCRs. After having been thoroughly characterized *in vitro*[193,201,202], they have since shown promising *in vivo* and clinical results. Two methods of transgene delivery have been used to date to redirect T cells with HBV-specific TCRs: electroporation of *in vitro* transcribed (IVT) messenger RNA (mRNA) and γ-retroviral transduction, leading to either transient or stable transgene expression. Transiently redirected T cells were able to prevent tumor seeding and suppress tumor growth in a xenograft model of HCC upon repeated administration[203]. As for CHB, a chimeric mouse repopulated with human hepatocytes has proven to be a useful *in vivo* model for HBV infection. Multiple injections of transiently redirected HBV-specific T cells caused a 1 log reduction of viremia within 12 days accompanied by a slight decrease of HBeAg serum levels[204]. In the same mouse model, a single transfer of stably TCR-transduced T cells lead to a 4 log reduction of viremia within three weeks, with HBsAg and HBeAg being undetectable in most cases[205]. Most importantly, combining the transfer of TCR-redirected T cells with the application of HBV entry inhibitor myrcludex B lead to sustained control of HBV infection[205]. Both transiently and stably transduced HBV-specific T cells caused only limited and transient liver injury[204,205].

In a clinical setting, stably transduced HBV-specific T cells were first applied in a proof-of-concept study for the treatment of a patient with metastatic HCC following liver transplantation in 2015[206]. The transferred T cells efficiently expanded *in vivo* and were activated upon engagement with metastatic tumor cells, leading to a reduction

of HBsAg serum levels upon day 30. However, clinical efficacy after six weeks was limited as volumes of metastases remained constant[206]. In a second clinical trial including two liver-transplanted patients with metastatic HCC, transiently redirected T cells were then administered over a period of five and twelve months respectively, resulting in a minor but notable anti-tumor effect in one patient. Interestingly, HCC cells of these patients only expressed partial HBV antigens; yet, this was sufficient to provide a target epitope for the therapeutic TCR used in this trial. Liver damage and adverse events were minor[207].

In summary, adoptive T-cell therapy of HBV infection and HBV-related HCC has achieved promising results over the last few years using both an HBsAg-specific CAR and MHC class I-restricted TCRs with different transgene delivery techniques. However, the generation of MHC class II-restricted TCRs and their therapeutic implementation in the context of HBV has not yet been attempted.

1.5 Aim of this thesis

Since a strong, functional and polyclonal T-cell response is characteristic of the self-limiting course of HBV infection, adoptive T-cell therapy with the objective of restoring T-cell immunity represents a promising therapeutic approach for the treatment of HBV-related HCC and chronic HBV infection. While an HBV-specific CAR and several MHC class I-restricted T-cell receptors have been generated and extensively characterized to date, no MHC class II-restricted TCRs have been available so far. Given the importance of $CD4^+$ T cells for the induction of a functional HBV-specific T-cell response and ultimately for resolving HBV infection, the aim of this thesis was therefore to identify, clone and characterize HBV-specific T-cell receptors for adoptive T-cell therapy of chronic HBV infection or HBV-HCC.

The first part of this work should begin with the isolation of HBV-specific $CD4^+$ T cells and the identification of their TCRs. To this end, peripheral blood mononuclear cells (PBMC) from donors with resolved HBV infection were to be stimulated with peptides from HBV core, envelope and polymerase proteins in order to isolate HBV-specific $CD4^+$ T-cell clones and identify their respective TCRs. The second part of this thesis aimed at optimizing the recombinant expression of the identified TCRs in human T cells through retroviral transduction. TCR-transduced T cells from healthy donors were to be used to thoroughly characterize and compare the generated TCRs *in vitro*, concerning their expression levels in primary human T cells, their MHC restriction, their physiological target recognition and therapeutic applicability, as well as their

binding affinity and functionality in terms of cytokine secretion and cytotoxicity. Finally, this thesis aimed to evaluate the overall applicability of the generated TCRs for adoptive T-cell therapy of HBV infection. Therefore, the suitability of *in vitro* and *in vivo* models was to be explored, followed by an initial proof-of-concept experiment of $CD4^+$ T-cell help with an exemplary TCR.

2 Results

2.1 Identification of T-cell receptors from HBV-specific CD4⁺ T-cell clones

MHC class II-restricted HBV-specific T-cell receptors were identified as illustrated in Figure 4 and detailed in the following chapter. In Brief, PBMC from donors who had cleared HBV infection were stimulated with a selection of HBV peptides derived from surface, core or polymerase antigens. Following *in vitro* expansion, HBV-specific CD4⁺ T cells secreting TNF-α were sorted by flow cytometry and expanded from a single-cell level. Subsequently, clones were screened for HBV specificity and TCR α- and β-chains of selected clones were identified through Sanger sequencing. Variable α- and β-TCR chains were codon-optimized and cloned into a retroviral vector. TCRs were then functionally characterized as described further below in chapter 2.3.

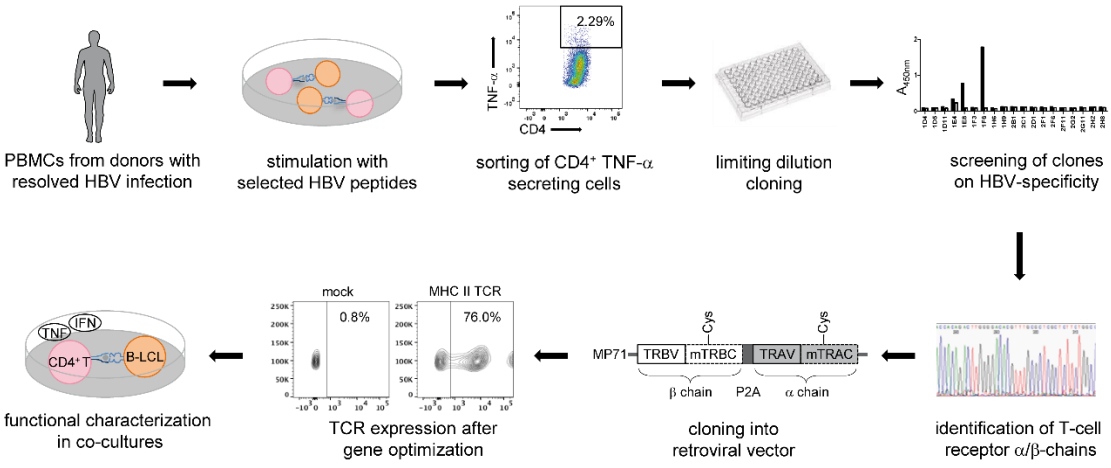

Figure 4: Procedure for identification and optimization of T-cell receptors from HBV-specific CD4⁺ T-cell clones. PBMCs from donors with resolved HBV infection were stimulated with HBV peptides derived from surface, core or polymerase antigens at 1 µM peptide concentration for 13-15 days. Following *in vitro* expansion, HBV-specific TNF-α- secreting CD4⁺ T cells were sorted by flow cytometry upon antigen re-stimulation and expanded from a single-cell level through limiting dilution cloning. Clones were then screened for HBV specificity and TCR α- and β-chains were identified by sequencing. Variable α- and β-domains (TRAV and TRBV) were codon-optimized and cloned into the retroviral vector MP71, combined with murine constant domains (mTRAC and mTRBC) and additional cysteine residues (Cys). TCRs were then functionally characterized in co-cultures with peptide-pulsed B-LCLs.

2.1.1 Choice of donors with resolved HBV infection

Donors with resolved HBV infection were chosen based on their availability and HLA type. MHC class II allele DRB1*01:01 was considered favorable, since TCRs with this restriction could be potentially tested in a mouse model transgenic for the human HLA-DR1. TCRs from two donors were generated throughout this thesis (Table 1).

Table 1: MHC class II alleles of donors with resolved HBV infection. n.d.= none determined; hz = homozygous.

Donor	Age	Sex	HBV infection status	DRB1*	DQB1*	DPB1*	DQA1*	DPA1*	DRB3*	DRB4*	DRB5*
1	52	M	resolved	01:01, 13:01	05:01, 06:03	02:01, 04:01	01, 01	01:03 hz	02:02	n.d.	n.d.
2	33	F	resolved	01:01, 07:01	02:02, 05:01	03:01, 11:01	01, 02:01	01:03, 02:01	n.d.	01:01	n.d.

2.1.2 Selection of HBV peptides

HBV peptides used for *in vitro* stimulation were chosen based on a literature review of published HBV epitopes presented on MHC class II, as well as *in silico* binding prediction of HBV peptides with HLA-DR1 and HLA-DR13. Epitopes found on MHC class II molecules commonly consist of up to 18 residues. In addition, the MHC class II molecule is not restricted to a certain epitope length due to its morphology, i.e. a groove open at both ends. Therefore, 18-mers were considered adequate for prediction and stimulation.

Since HBV infection in donor 1 was diagnosed as genotype A (personal communication with the physician in charge) and the HBV infection of donor 2 had not been genotyped, the *in silico* binding prediction was performed using the HBV genotype A consensus sequence. Table 2 shows the final selection of peptides that was used for stimulation of PBMCs from resolved donors. IC_{50} refers to the half maximal inhibitory concentration, which describes a measure of potency of a substance to inhibit or exert a particular biological function, in this case the binding to an MHC molecule or the inhibition of binding of a standard reference peptide. IC_{50} binding values of all peptides to HLA-DR1 or HLA-DR13 were predicted by algorithms SMM-align[208] and/or NetMHCIIpan 3.2[209] and cross-referenced with literature. Peptides with IC_{50} values below 50 nM are considered strong binders and peptides with IC_{50} values below 500 nM are estimated weak binders[209]. From experimental confirmation with MHC binding assays, it has been estimated that >80% of all known HLA class II T-cell epitopes bind their corresponding restriction element with IC_{50} values below 1000 nM[210-212].

Of this selection, TCRs were ultimately generated for seven epitopes (Table 2, peptides marked in bold), five of which had been previously described in the literature. Two epitopes were newly identified to be immunogenic, preS9 and C91. However, the preS9-specific TCR isolated during this thesis proved to be restricted against a different HLA-molecule than the predicted HLA-DR1 or HLA-DR13 (see 2.3.2). Taken together, these results underline the difficulty of accurate *in silico* prediction of MHC class II epitopes.

Table 2: Selection of 18-mer peptides from HBV core (C), envelope (preS/S) and polymerase (P) proteins used for stimulation of PBMCs from donors with resolved HBV infection. The subsequent number refers to the peptide starting residue within the respective antigen. IC_{50} binding values of all peptides to HLA-DR1 or HLA-DR13 were predicted by algorithms NetMHCIIpan 3.2 and/or SMM-align (accessed via http://tools.iedb.org/mhcii/). Peptide specifities of TCRs generated in this thesis are marked in bold. Literature review with therein published epitopes, corresponding HLA alleles and references are indicated. Literature references of therein published epitopes are indicated[213-222]. Amino acid overlaps with peptides from this study are double underlined. n.d.= none determined.

HBV protein	Peptide name	Amino acid sequence	HLA-DR1		HLA-DR13	Literature review		
			NetMHCIIpan IC_{50} (nM)	SMM-align IC_{50} (nM)	NetMHCIIpan IC_{50} (nM)	Published peptide (overlap with peptides from this study)	HLA	Reference
Core	C7	KEFGATVELLSFLPSDFF	493	274	1855	MDIDPYKEFGATVELLSFLP	DR	213
	C28	RDLLDTASALYREALESP	530	341	964			
	C61	WGELMTLATWVGNNLEDP	696	238	2048	LCWGELMTLATWVGVN	DR1	214
	C84	LVVNYVNTNMGLKIRQLL	156	447	65			
	C91	TNMGLKIRQLLWFHISCL	387	349	193			
	C113	ETVLEYLVSFGVWIRTPP	205	78	884	GRETVLEYLVSFGVW EYLVSFGVWIRTPPA	DR1 DRw52/DR6	215 213
	C119	LVSFGVWIRTPPAYRPPN	104	430	277	VSFGVWIRTPPAYRPPNAPI	DR1	213
	C133	RPPNAPILSTLPETTVVR	801	168	2446			
Envelope	**preS9**	RKGMGTNLSVPNPLGFFP	704	528	2025			
	preS83	GILTTVSTIPPPASTNRQ	786	216	2276			
	preS116	HPQAMQWNSTAFHQALQD	573	1827	780	MQWNSTTFHQTLQDPRVRGLYFPAGG MQWNSTALHQALQDP	DR1 DR2	216 217
	preS134	PRVRGLYFPAGGSSSGTV	149	153	4167			
	S8	FLGPLLVLQAGFFLLTRI	502	52	1574			
	S17	AGFFLLTRILTIPQSLDS	130	72	395	FFLLTRILTIPQSLD FFLLTRILTIPQSLD QAGFFLLTRILTIPQS	DR2 DR7 DR1	218 219 217
	S36	WTSLNFLGGSPVCLGQNS	77	41	2344	TSLNFLGGSPVCLGQ	DR1	217
	S69	CPGYRWMCLRRFIIFLFI	363	300	242	PICPGYRWMCLRRFIIFL	DR12	219
	S93	FLLVLLDYQGMLPVCPLI	144	155	1106	FLLVLLDYQGMLP	DP4	220
	S158	FAKYLWEWASVRFSWLSL	117	419	450	WEWASARFSWLSL WASVRFSW	DP4 DR11/14	220 221
	S165	WASVRFSWLSLLVPFVQW	165	63	656	SVRFSWLSLLVPFVQWF	DP2	219
	S179	FVQWFVGLSPTVWLSAIW	68	67	813	SLLVPFVQWFVGLSPTVWLSV VGLSPTVWLSVI	DR1 DP4	217 220
	S199	WYWGPSLYSIVSPFIPLL	161	92	1164	YWGPSLYSIVSPFIPL	DR3	219
	S209	VSPFIPLLPIFFCLWVYI	410	68	2029			
Polymerase	P104	NEKRRLKLIMPARFYPTH	40	73	33			
	P412	PNLQSLTNLLSSNLSWLS	80	35	488	LQSLTNLLSSNLSWL	n.d.	222
	P454	SGLSRYVARLSSNSRIFN	61	124	92			
	P524	SPFLLAQFTSAICSVVRR	62	89	569			
	P573	TNFLLSLGIHLNPNKTKR	63	35	157			
	P636	QRIVGLLGFAAPFTQCGY	151	35	1112			
	P650	QCGYPALMPLYACIQSKQ	250	137	1532			
	P774	LRGTSFVYVPSALNPADD	22	22	908	AANWLRGTSFVYVP	n.d.	222
	P827	HLPVRVHFASPLHVAWRP	47	225	109			

2.1.3 Fluorescence activated cell sorting of HBV-specific T cells

Based on the selection above, PBMC were stimulated with 1 µM of the respective peptide and expanded *in vitro* for 14 days with restimulation on day 7. One day prior to cell sorting, typically on day 12-14, PBMC were selected regarding their activation upon restimulation with 1 µM of their respective peptide, measured by intracellular cytokine staining (ICS) of TNF-α and IFN-γ (data not shown). Only samples with cytokine secretion above a threshold equivalent to double the negative control values were included in the subsequent fluorescent activated cell sorting (FACS) procedure. $CD4^+$ TNF-α^+ cells were sorted with a stringent gating strategy given the high background of unspecifically activated cells in the negative control (Figure 5A-C). Flow cytometry plots showed cells stimulated with the previously published C61 epitope[214] to be particularly highly activated. Cells stimulated with C113, S17, P454, P774 and P827 also showed a higher TNF-α secretion compared to their respective negative control. Absolute numbers of cells gained from each sorting procedure (Figure 5D) were largely consistent with gating frequencies observed before (Figure 5A-C).

To increase specificity of cell sorting, the experimental measures were adapted to analyze both TNF-α^+ and IFN-γ^+-secretion in $CD4^+$ T cells. For donor 1, stimulation with C61, C91 and C113 resulted in percentages of $CD4^+$ TNF-α^+ IFN-γ^+ double positive cells ranging from 0.26-0.63% (Figure 6). In donor 2, samples stimulated with C61, C113, S17 and S36 were more strongly activated ranging from 0.26-0.96% (Figure 7A). Up to 35238 cells were sorted in total for C113-stimulated PBMC from donor 2 (Figure 7B).

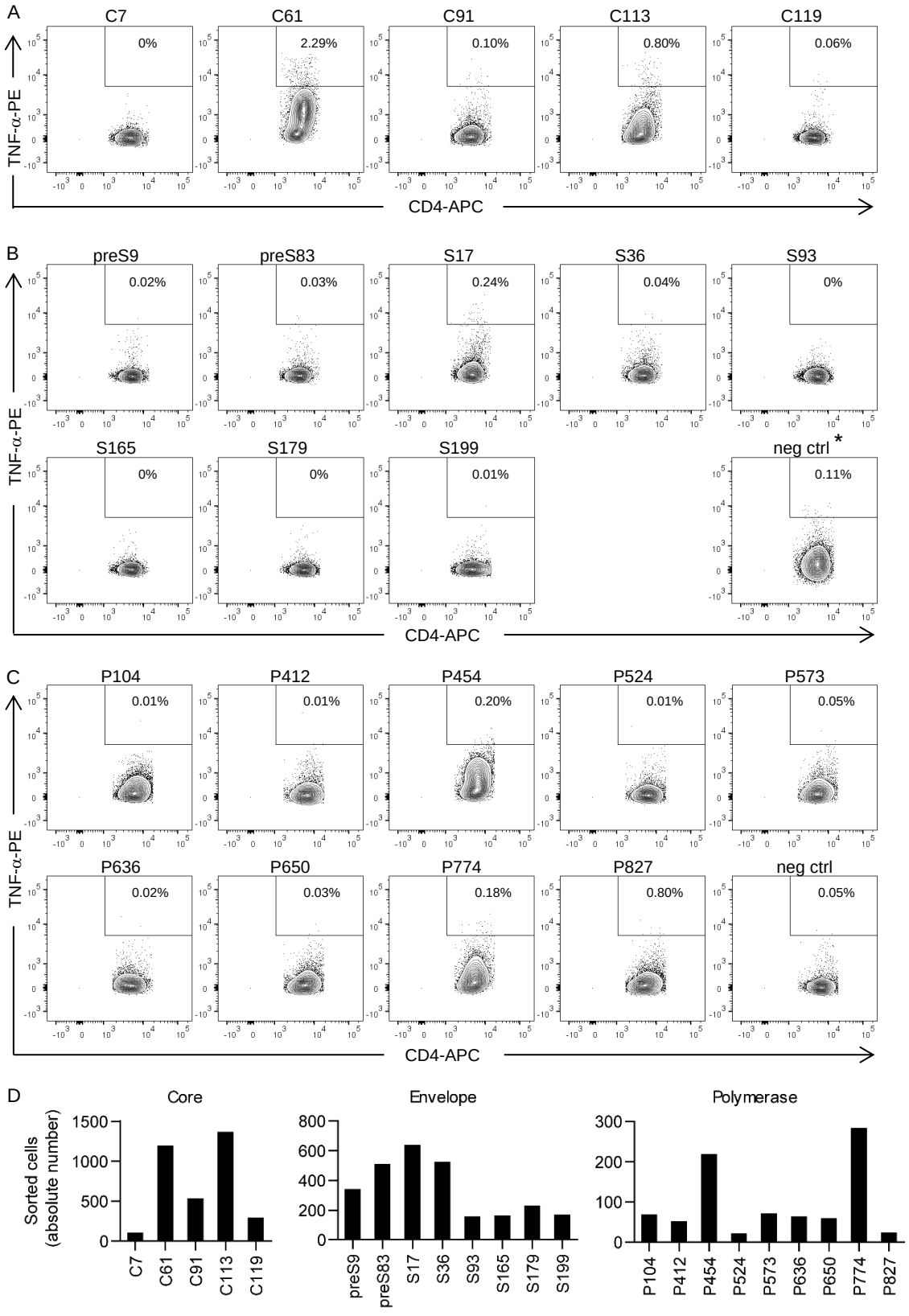

Figure 5: Fluorescence activated cell sorting of PBMC from donor 1. For cell sorting, PBMC were restimulated for 3 h at 37 °C with 1 µM of their respective peptide. Acivated cells were stained with a TNF-α secretion assay based on TNF-α capture at the cell surface. Flow cytometry plots show CD4 and TNF-α staining of samples stimulated with core (A), envelope (B) or polymerase (C) peptides. Absolute number of sorted $CD4^+$ $TNF\text{-}\alpha^+$ cells gained from each sorting procedure (D). Cell sorting was performed on a FACSAria II (BD) device. *negative control was recorded with higher PE-voltage.

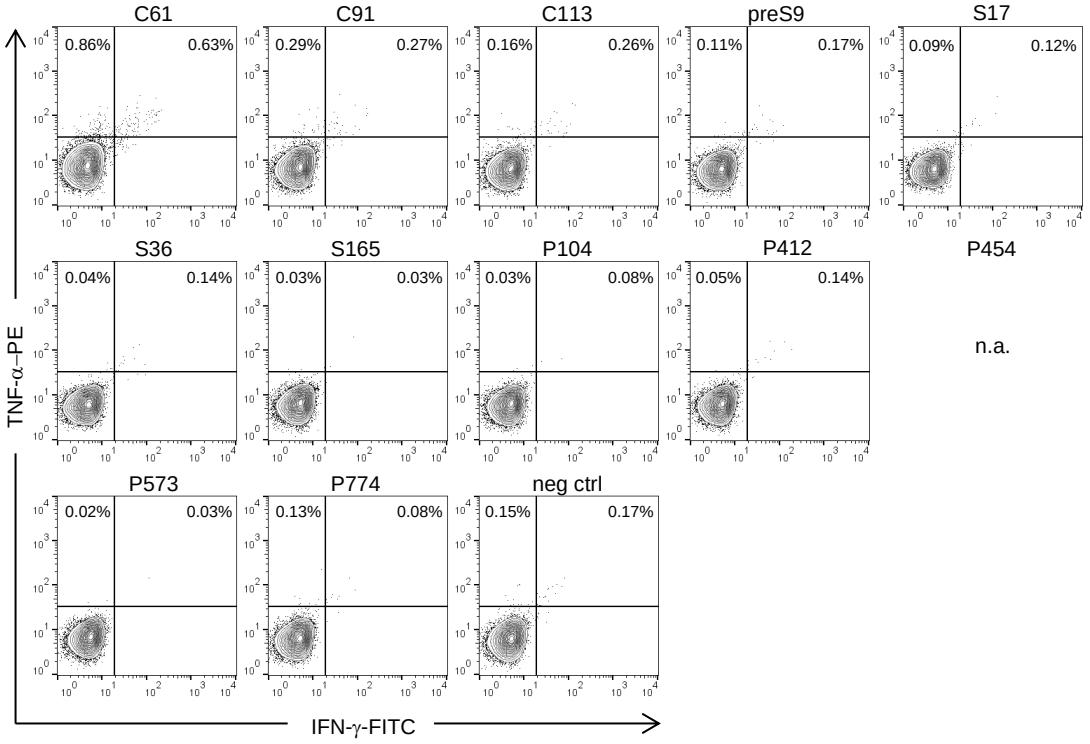

Figure 6: Fluorescence activated cell sorting of PBMC from donor 1. For cell sorting, PBMC were restimulated for 3 h at 37 °C with 1 µM of their respective peptide. Flow cytometry plots show TNF-α and IFN-γ staining of $CD4^+$ T cells. Activated cells were stained with a secretion assay based on cytokine capture at the cell surface. Cell sorting was performed on a MoFlo II (Beckman Coulter) device. Data for P454 and sorted cell numbers were not recorded.

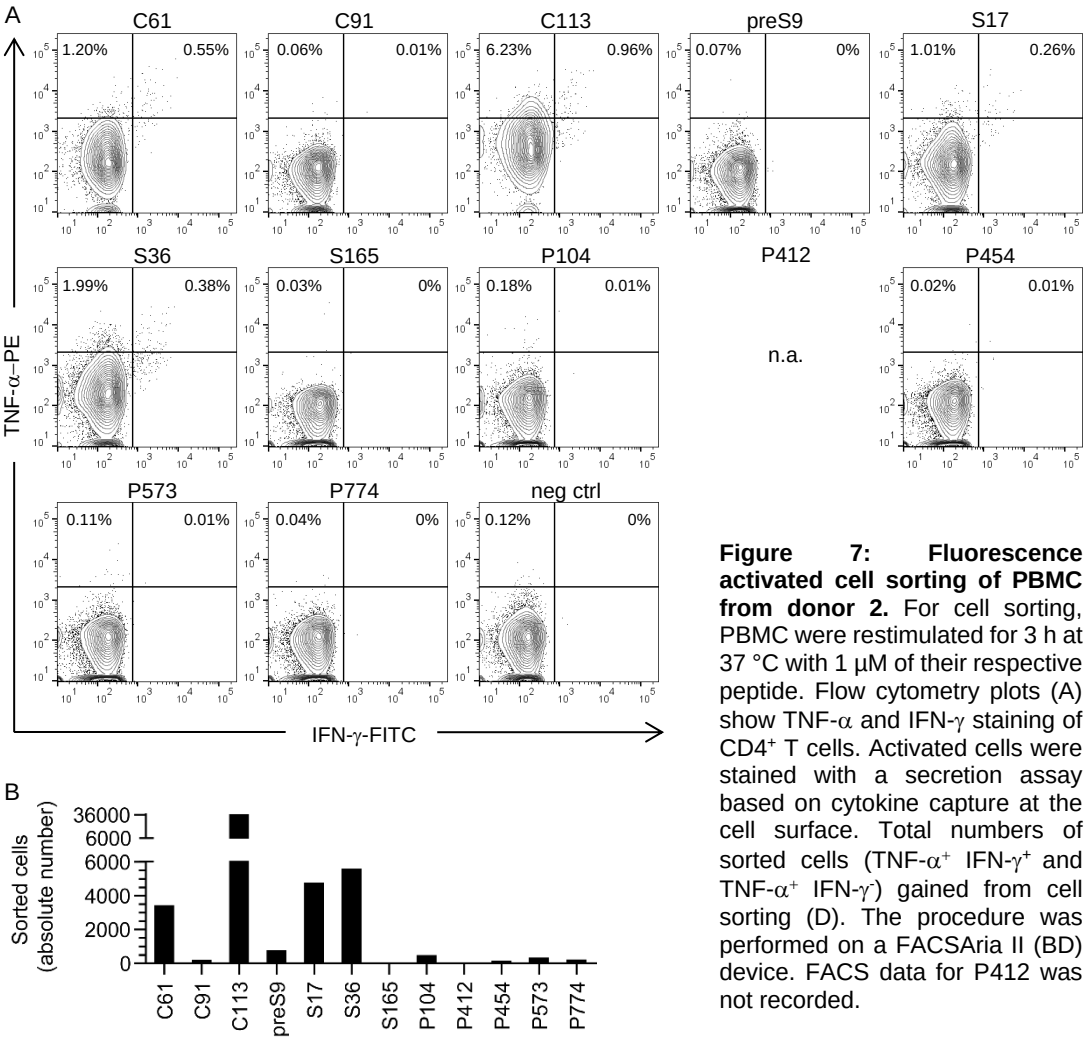

Figure 7: Fluorescence activated cell sorting of PBMC from donor 2. For cell sorting, PBMC were restimulated for 3 h at 37 °C with 1 µM of their respective peptide. Flow cytometry plots (A) show TNF-α and IFN-γ staining of $CD4^+$ T cells. Activated cells were stained with a secretion assay based on cytokine capture at the cell surface. Total numbers of sorted cells (TNF-α^+ IFN-γ^+ and TNF-α^+ IFN-γ^-) gained from cell sorting (D). The procedure was performed on a FACSAria II (BD) device. FACS data for P412 was not recorded.

2.1.4 Screening of clones for HBV specificity

The sorted cells were then expanded based on limiting dilution cloning, i.e. with seeding densities of 0.3-0.5 clones per well to ensure the expansion of single clones and the addition of irradiated feeder cells, IL-2 and CD3 stimulation. After approximately two weeks, visually outgrown clones were restimulated with HLA-matched B-LCLs loaded with the respective peptide. Detection of cytokine secretion via enzyme-linked immunosorbent assay (ELISA) after 24 hours of co-culture suggested HBV specificity. In total, 542 clones were screened and exemplary results for clones from donor 1 stimulated with core, envelope or polymerase peptides are shown (Figure 8). Clones that secreted higher amounts of IFN-γ upon restimulation with peptide compared to the negative control, indicated by black arrows, were chosen for further expansion and analysis. Interestingly, all ten clones restimulated with peptide C61 (Figure 8A) seemed to be specific, whereas the rate of specific clones was much lower for other peptides. This is in line with the respective cell sort, where C61-stimulated cells also showed a superior activation profile in flow cytometry compared to other samples (Figure 5). During subsequent screening rounds, TNF-α secretion was found to be a more specific measure than IFN-γ secretion to distinguish between clones restimulated with peptide and their respective negative control, as illustrated by exemplary clones from cell sort of donor 1 (Figure 9).

All clones chosen during initial screening were further expanded for approximately two more weeks and then resubmitted to restimulation and screening. In general, the second screening after a total of four weeks of expansion typically yielded clearer results with a larger signal to noise ratio in positive clones, since background cytokine secretion was reduced (data not shown). 60 of 542 clones were confirmed to be specific after the second screening, this amounts to a relative specificity rate of 11%.

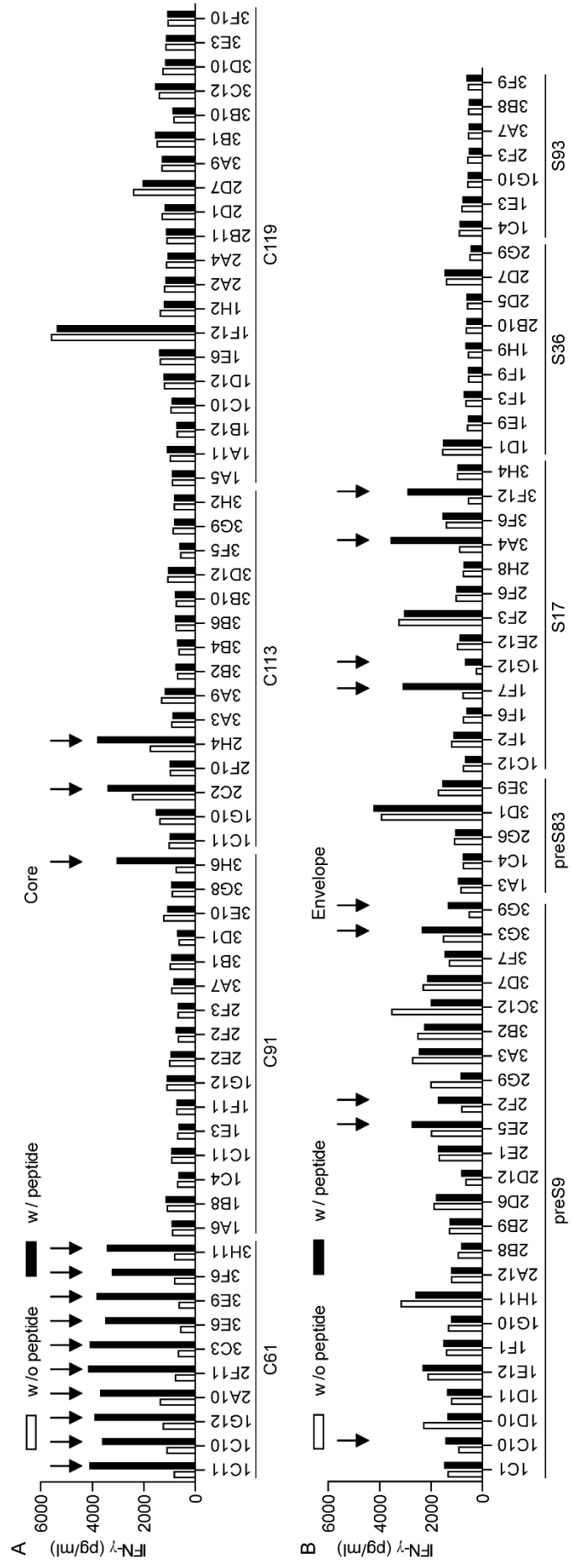

Figure 8: HBV-specificity assay of visually outgrown clones from cell sort of donor 1 (Figure 5). 20 µl of each clone was co-cultured with $5x10^4$ B-LCLs, pulsed with 1 µM of their respective peptide from core (A), envelope (B) or polymerase (C) protein (black bars) or without peptide (white bars). IFN-γ secretion in pg/ml was determined after 16 hours of co-culture via ELISA. Black arrows indicate clones chosen for further analysis. Cell sorts for peptides C119, preS83, S36, S93, P104, P412, P454, P573, P636 and P650 did not yield any specific clones in this experiment.

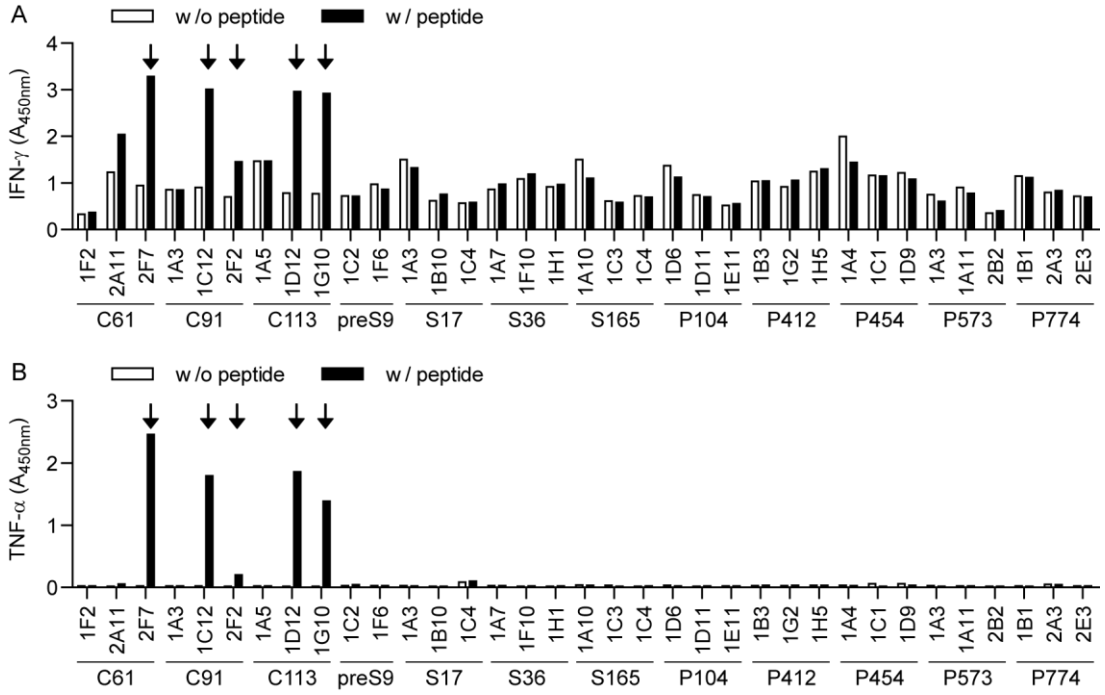

Figure 9: HBV-specificity assay of visually outgrown clones for exemplary clones from cell sort of donor 1 (Figure 6). Clones were co-cultured with B-LCLs pulsed with the respective peptide (black bars) or without peptide (white bars). IFN-γ (A) and TNF-α (B) secretion were measured via ELISA; A_{450nm} represents absorption at 450 nm wavelength. Specific clones chosen for further analysis are indicated by black arrows.

2.1.5 Identification of functional T-cell receptor sequences

HBV-specific T-cell clones were then subjected to RNA extraction and subsequent reverse transcription. The resulting complementary DNA (cDNA) was used for polymerase chain reaction (PCR) to identify the T-cell receptor α- and β-chain sequences by Sanger sequencing. This method yielded excellent results for the TCR β-chain, with an expected DNA amplification of ~500bp length and reliable β-chain identification based on the sequencing results (data not shown). Regarding the TCR α-chain, however, degenerate primer PCR rarely produced bands of the right size. Since different annealing temperatures improved PCR product yield for certain clones, a selection of degenerate α-chain PCRs was performed at 55°C, 57°C or 59°C, which is shown for clones $1B9_{S36}$, $2H12_{S36}$ and $2F9_{P104}$ (Figure 10A). The subscript epitope abbreviation, i.e. S36 and P104, refers to the respective specificity of a T-cell clone or T-cell receptor, this annotation will be applied throughout the remaining part of this thesis. Whereas the PCR product improved slightly for clone $1B9_{S36}$ at 55°C annealing temperature (indicated by a black arrow), the degenerate primer PCR for clones $2H12_{S36}$ and $2F9_{P104}$ remained unproductive. All clones with an unproductive result during degenerate primer PCR were subjected to PCR with specific primer pairs covering the most common TCR α- or β-chains. This procedure

is exemplified for clone $S36_{2H12}$ with primer pairs covering 32 different variable α-chains (Figure 10B). Black arrows (a, b, c) indicate PCR products of the right size. Sequencing of the purified PCR products lead to the identification of two different α-chains for this clone: TRAV34*01/TRAJ53*01 and TRAV29/TRAJ54*01, where TRAV represents the V gene segment and TRAJ the J gene segment of the variable α-chain (Figure 10C). PCR products a and c, which were amplified with different primers, yielded the same result, i.e. TRAV34*01/TRAJ53*01, indicating a potential cross-reactivity between primers and TCR chains. Unless otherwise indicated, TCR α- and β-chains are named after the international ImMunoGeneTics information system (IMGT) nomenclature[223].

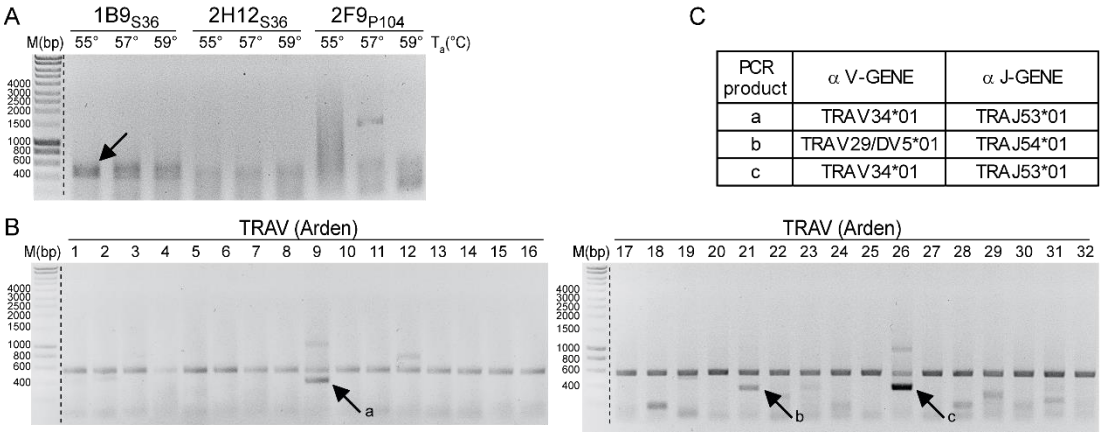

PCR product	α V-GENE	α J-GENE
a	TRAV34*01	TRAJ53*01
b	TRAV29/DV5*01	TRAJ54*01
c	TRAV34*01	TRAJ53*01

Figure 10: TCR α-chain identification by PCR and sequencing for exemplary clones. (A) Degenerate primer PCR was performed with a wobble forward primer in combination with a constant reverse primer for either the TCR α- or β-chain with varying annealing temperatures (T_a). The black arrow indicates a slight improvement regarding PCR product yield for clone $1B9_{S36}$ at 55°C. (B) TCR α-chain identification for clone $2H12_{S36}$ by PCR with specific primer pairs for TRAV 1 to 32 (specific primers are numbered according to Arden nomenclature[224]). Black arrows (a, b, c) indicate PCR products of the right length. (C) Sanger sequencing results of PCR products a, b and c. TRAV29/TRAJ54*01 equals TRAV 21 and TRAV34*01/TRAJ53*01 equals TRAV 26 in Arden[224] nomenclature. M=DNA marker; bp=base pairs.

Notably, several T-cell clones of the same specificity revealed to carry an identical T-cell receptor, defined by an identical CDR3 region (data not shown). In case at least one α- and one β-chain were successfully identified for a particular clone or set of redundant clones, those were amplified from the respective cDNA and cloned separately into a γ-retroviral vector. The α- and β-chain were then co-transfected into γ-retroviral producer cells and the resulting supernatant was used to transduce Jurkat cells, a T-cell line which lacks the endogenous TCR. By staining for the human TCR and CD3 with mock transduced cells as negative control, the transduction rate was determined in flow cytometry (Figure 11). A successful transduction was indicated by a double positive population, where CD3 seemed to stain slightly stronger than the human TCR. A number of TCRs, e.g. $3A6_{C61}$, $1F1_{S17}$, $1B3_{S36}$, $2F9_{P104}$, $1H9_{P412}$, could

not be transduced. In some cases, e.g. $3H6_{C91}$, two different α-chains (indicated as a and b) had been identified and were each combined with the same β-chain. Both combinations were successfully transduced into Jurkat cells.

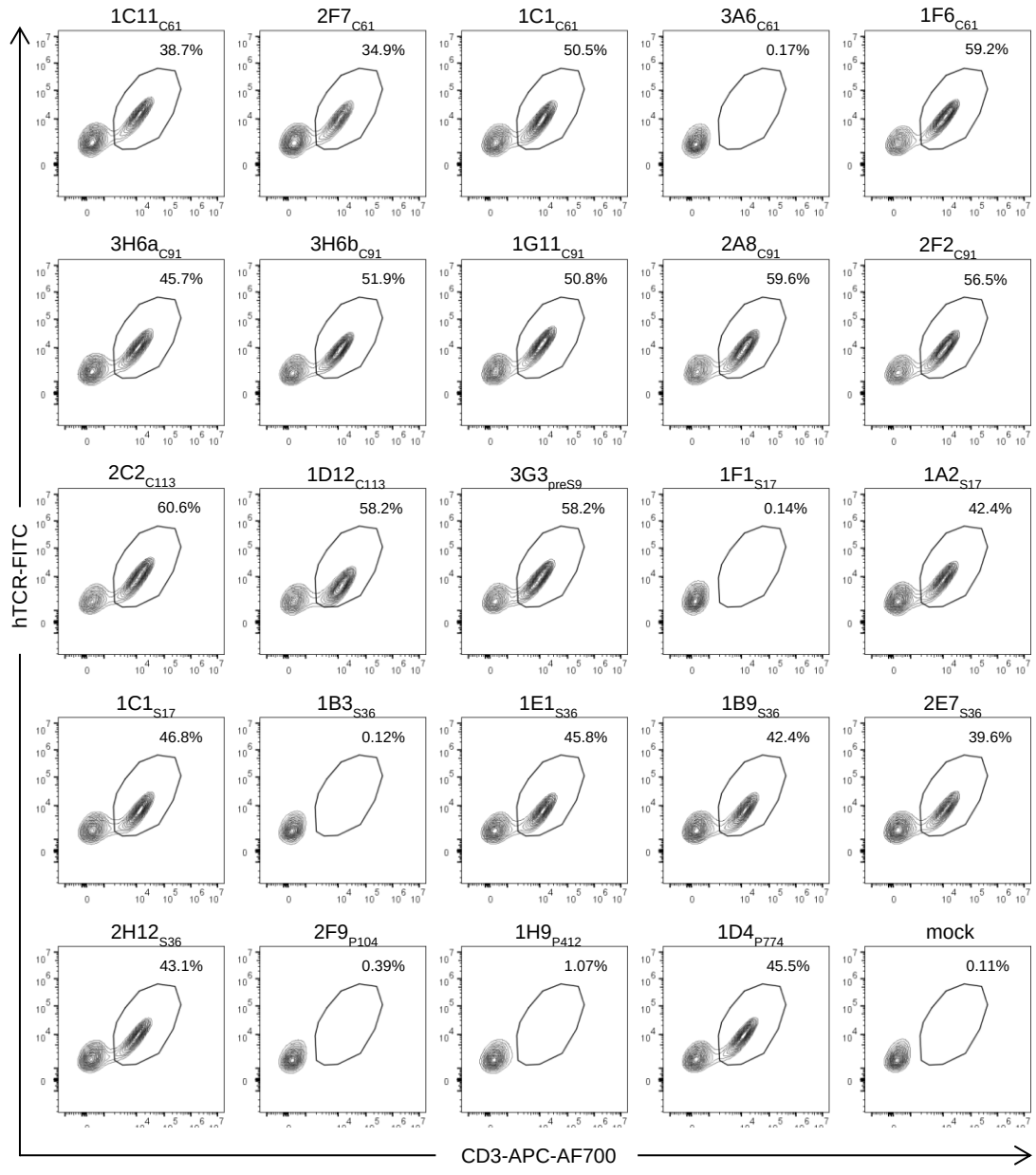

Figure 11: Retroviral transduction of Jurkat cells with fully identified TCR α- and β-chains. The transduction rate was measured via staining of the human TCR and CD3 in flow cytometry.

Primary human T cells from a healthy donor, which had been transduced in parallel to Jurkat cells, were then used to conduct a functional test through co-culture with peptide-pulsed HLA-matched B-LCLs. Since an anti-human TCR antibody would have stained both the transgenic and the endogenous TCR in primary T cells, transduction rates could not be determined and were assumed to be equal to those measured in Jurkat cells. Cytokine secretion was measured through ELISA (Figure

12A) as well as intracellular cytokine staining and flow cytometry (Figure 12B). A TCR α/β-chain combination was considered functional when cytokine secretion was positive compared to the negative control in both assays.

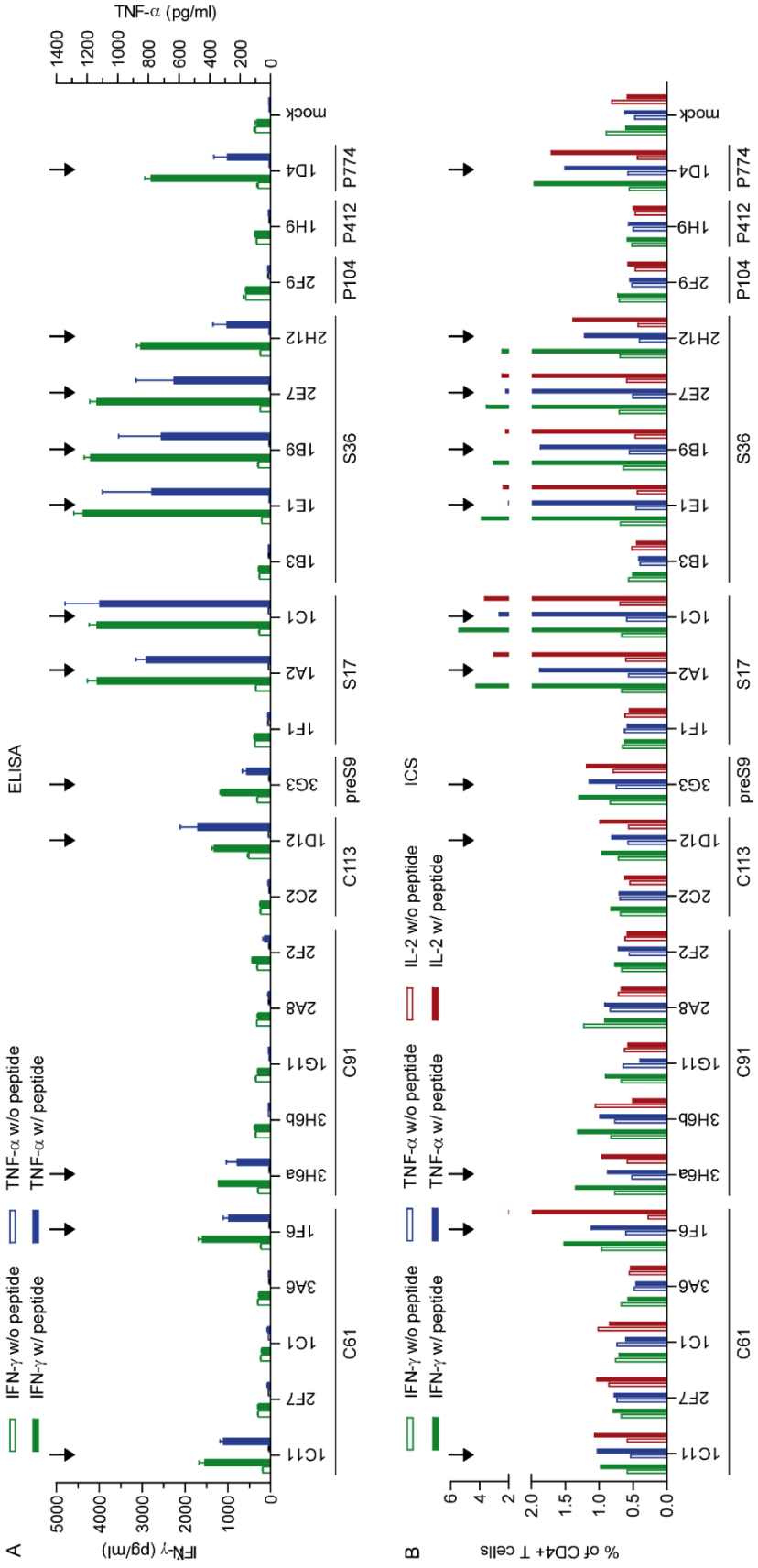

Figure 12: Functional test of identified TCR α/β-chain combinations. TCR-transduced T cells were co-cultured at an effector-to-target ratio of 2:1 with B-LCLs pulsed with 1 µM of the respective peptides (colored bars) or without peptide (white bars). (A) IFN-γ and TNF-α secretion was measured after 16 h via ELISA. Data points represent mean values ± SD from triplicates. (B) Brefeldin A was added one hour after co-culture start and IFN-γ, TNF-α and IL-2 were determined after 16 hours of co-culture via intracellular cytokine staining and flow cytometry. Black arrows indicate functional TCR α/β-chain combinations that were subsequently codon optimized.

A number of TCRs, for which either the transduction (Figure 11) or the functional test (Figure 12) had been unsuccessful, were resubmitted to the step of α-chain identification. For TCRs $2F7_{C61}$, $3A6_{C61}$, $1G11_{C91}$ or $1F1_{S17}$, combining the original β-chain with a different α-chain ultimately resulted in a functional TCR as confirmed by ELISA, whereas others, e.g. $2F9_{P104}$ and $1H9_{P412}$, remained unfunctional (Figure 13).

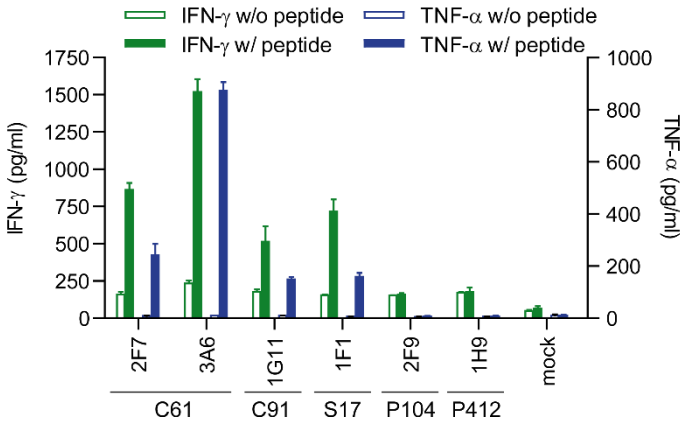

Figure 13: Functional test of new TCR α/β-chain combinations after secondary α-chain identification for exemplary clones. TCR-transduced T cells were co-cultured at an effector-to-target ratio of 2:1 with B-LCLs pulsed with 1 µM of the respective peptides (colored bars) or without peptide (white bars). IFN-γ (green) and TNF-α (blue) secretion were measured after 16 h via ELISA. Data points represent mean values ± SD from triplicates.

2.1.6 Final panel of TCRs

17 TCRs were successfully identified from donor 1 and 2 during this thesis. In addition, six TCRs had been identified from donor 3-6 during previous work by Melanie Honz and were included in the final panel for further characterization (Table 3).

Table 3: Final panel of T-cell receptors. TCRs are indicated with their respective peptide specificity, donor, and α- or β-chain gene segments. n.d. = not determined. * = TCRs identified by Melanie Honz.

Peptide	TCR	Donor	β V-GENE	β J-GENE	β D-GENE	α V-GENE	α J-GENE
C61	1C11	1	TRBV9*01	TRBJ1-1*01	TRBD1*01	TRAV9-2*01	TRAJ37*01
	2F7	1	TRBV3-1*01	TRBJ2-5*01	TRBD1*01	TRAV8-1*01	TRAJ5*01
	3A6	2	TRBV20-1*01	TRBJ2-1*01	TRBD2*02	TRAV9-2*02	TRAJ32*02
	1F6	1	TRBV5-5*01	TRBJ1-1*01	TRBD1*01	TRAV5*01	TRAJ13*01
	P74*	3	TRBV9*01	TRBJ1-2*01	TRBD2*01	TRAV5*01	n.d.
C91	3H6	1	TRBV7-2*01	TRBJ1-2*01	TRBD1*01	TRAV35*02	TRAJ4*01
	1G11	1	TRBV10-3*01	TRBJ1-1*01	TRBD1*01	TRAV13-1*02	TRAJ45*01
	2F2	1	TRBV5-1*01	TRBJ1-6*02	TRBD1*01	TRAV2*01	TRAJ42*01
C113	1D12	1	TRBV7-9*01	TRBJ1-3*01	TRBD1*01	TRAV12-1*01	TRAJ9*01
	CP11*	5	TRBV6-1*01	TRBJ2-7*01	TRBD2*01	TRAV12-3*01	TRAJ11*01
preS9	3G3	1	TRBV29-1*01	TRBJ2-3*01	TRBD1*01	TRAV21*02	TRAJ9*01
S17	1F1	1	TRBV2*01	TRBJ1-2*01	TRBD2*02	TRAV8-4*03	TRAJ37*01
	1A2	2	TRBV7-6*01	TRBJ1-3*01	TRBD1*01	TRAV9-2*02	TRAJ48*01
	1C1	2	TRBV6-2*01	TRBJ2-3*01	TRBD1*01	TRAV21*02	TRAJ50*01
	SP1*	4	TRBV6-6*02	TRBJ2-6*01	TRBD1*01	TRAV8-3*02	n.d.
	S125*	4	TRBV6-6*02	TRBJ2-6*01 F	TRBD1*01	TRAV8-3*02	n.d.
	S113*	4	TRBV19*01	TRBJ1-5*01	n.d.	TRAV17*01	n.d.
S21	S123*	6	TRBV30	TRBV30*01	TRBJ1-3*01	TRBD1*01	n.d.
S36	1E1	2	TRBV19*01	TRBJ1-6*01	TRBD1*01	TRAV38-2/DV8*01	TRAJ40*01
	1B9	2	TRBV19*01	TRBJ2-3*01	TRBD1*01	TRAV12-2*02	TRAJ6*01
	2E7	2	TRBV6-1*01	TRBJ1-5*01	n.d.	TRAV12-2*02	TRAJ20*01
	2H12	2	TRBV11-2*01	TRBJ2-2*01	TRBD2*01	TRAV34*01	TRAJ53*01
P774	1D4	1	TRBV7-2*01	TRBJ2-7*01	TRBD2*01	TRAV39*01	TRAJ44*01

2.2 Optimization of recombinanty expressed TCRs

To optimize the expression of the transgenic TCR and the transduction of engineered primary human T cells, each TCR from the final panel was codon-optimized and cloned into a retroviral vector. Retroviral transduction was optimized through the generation of stable producer cell lines.

2.2.1 Codon optimization and cloning of retroviral constructs

TCR α- and β-chain variable domains were synthesized as codon-optimized sequences (by Thermo Fisher Scientific GeneArt Gene Synthesis) and cloned onto the γ-retroviral vector MP71[225], along with murine constant domains containing additional cysteine residues and separated by a P2A site to ensure equimolar expression of both chains (Figure 14A). The final constructs were transduced into primary human T cells and the transduction rate was determined by staining the murine constant domain of the β-chain in flow cytometry (mTRBC) (shown for exemplary TCRs in Figure 14B).

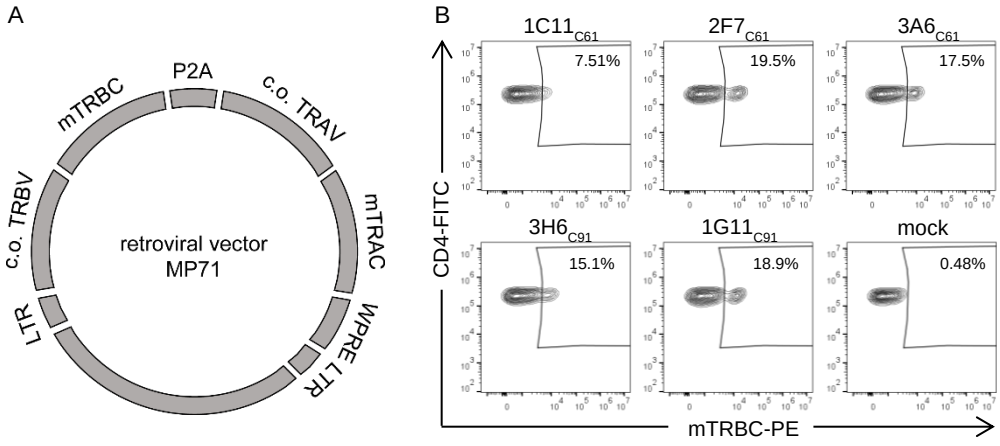

Figure 14: Optimization of recombinant TCR constructs. (A) Overview of the retroviral vector MP71: The β-chain codon-optimized variable (c.o. TRBV) and murine constant domain (mTRBC) are linked to the α-chain codon-optimized variable (c.o. TRAV) and murine constant domain (mTRAC) by a P2A element to ensure equimolar expression. The TCR elements are followed by a woodchuck hepatitis virus posttranscriptional regulatory element (WPRE) and flanked by myeloproliferative sarcoma virus long terminal repeats (LTR). (B) Flow cytometry plots of exemplary TCR-transduced primary human T cells. Transduction rates are shown as a percentage of $mTRBC^+$ $CD4^+$ T cells.

2.2.2 Establishing producer cell lines for potent retroviral supernatant

To increase transduction rates by using a potent and highly effective retroviral supernatant for each TCR, stable producer cell lines were generated. To this end, the retroviral supernatant from transiently transfected gibbon ape leukaemia virus (GALV) producer cells was used to transduce RD114 producer cells, thereby resulting in a stable genomic integration of the TCR coding sequence. The TCR expression in RD114 cells was analyzed through flow cytometry by staining the mTRBC either on the surface of RD114 cells or intracellularly. Overall, TCR^+ populations were not clearly separable from untransduced cells, in particular for surface staining (exemplary TCRs in Figure 15A). Intracellular staining showed intermediate to high intracellular levels of all TCRs, whereas surface expression was variable, with some cells showing little or no surface expression at all, i.e. $1C11_{C61}$, $1D12_{C113}$, $1A2_{S17}$ and $1D4_{P774}$ (Figure 15B).

TCR surface expression was required for enrichment of producer cells by flow cytometry; therefore, a strategy was devised to increase and stabilize TCR expression in cells for which surface staining had previously not been possible. Since the CD3 complex has been attributed a stabilizing role in T-cell receptor expression[226], TCR-transduced RD114 cells were transiently transfected with a plasmid containing the murine CD3 δγεζ-chains (mCD3) (shown for exemplary TCRs in Figure 15C). Whereas this improved the surface levels of "weakly" expressing TCRs, e.g. $1C11_{C61}$, $1D12_{C113}$ and $1A2_{S17}$, to approximately 2-5%, no additional benefit was observed for TCRs which had been "strongly" expressed in the first place, e.g. TCRs $2F7_{C61}$ and $2F2_{C91}$.

The producer cell lines were subsequently enriched via fluorescence activated bulk cell sorting based on TCR surface staining, with or without prior mCD3 transfection depending on the respective necessity for surface expression. The undiluted retroviral supernatant from thereby obtained enriched producer cells was then used for transduction of primary human T cells. As a result, transduction rates on day 6 after stimulation were mostly above 95% (Figure 15D). Notably, the transduction rate of several TCRs, e.g. $3A6_{C61}$, $1G11_{C91}$ and $1B9_{S36}$, substantially decreased upon day 15, indicating a potential apoptotic effect of transduction with a high MOI.

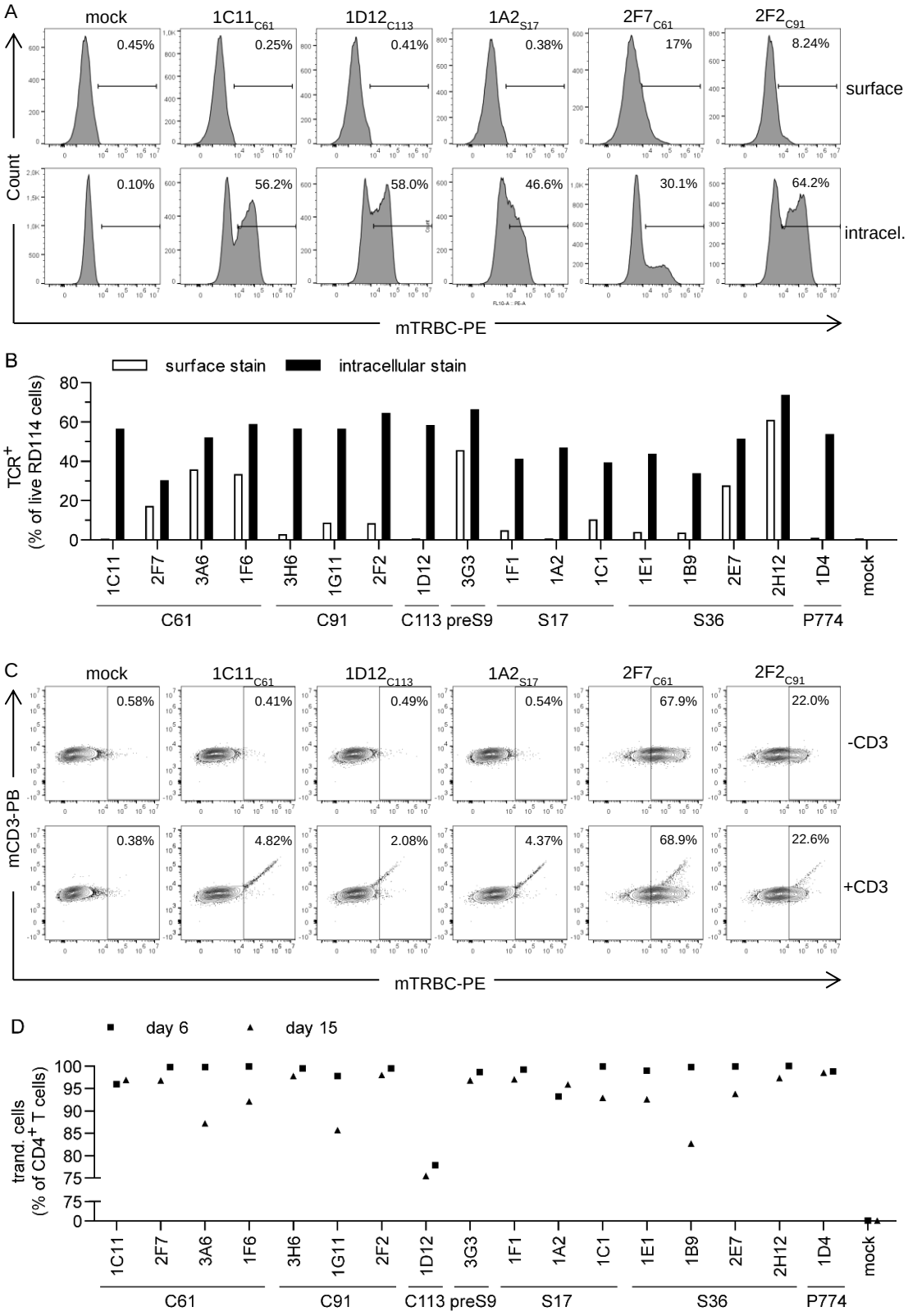

Figure 15: Establishing producer cell lines to generate potent recombinant TCR supernatant. (A)/(B) TCR expression in TCR-transduced RD114 cells was analyzed through flow cytometry by staining the mTRBC either on the surface (surface/white bars) or intracellularly (intracel./black bars). (A) Exemplary histograms of "weakly" expressing TCRs 1C11$_{C61}$, 1D12$_{C113}$, 1A2$_{S17}$ and "strongly" expressing TCRs 2F7$_{C61}$ and 2F2$_{C91}$. (B) TCR$^+$ cells (as % of live RD114 cells) for all 17 TCRs identified in this thesis. (C) Flow cytometry plots of RD114 cells transduced with "weakly" expressing TCRs 1C11$_{C61}$, 1D12$_{C113}$, 1A2$_{S17}$ and "strongly" expressing TCRs 2F7$_{C61}$ and 2F2$_{C91}$, with or without transient transfection of murine CD3 δγεζ-chains (mCD3). (D) TCR surface expression on primary human T cells transduced with undiluted supernatant from retroviral producer cell lines on day 6 (squares) and day 15 (triangles).

In order to achieve high, but non-toxic transduction rates for all TCRs, the supernatant from retroviral producer cells was titrated on Jurkat cells. An exemplary titration using supernatant from TCR $P74_{C61}$ showed Jurkat cells and primary T cells to be in a similar dimension in terms of transduction efficiency (Figure 16A). The retroviral supernatant was subsequently titrated on Jurkat cells for all TCRs with dilution factors ranging from 1:10 to 1:80 (Figure 16B). Differences in potencies became clearly apparent, with retroviral supernatants from TCRs $P74_{C61}$, $1F1_{S17}$ and $1A2_{S17}$ displaying the highest transduction efficiencies and supernatant from TCR $1D4_{P774}$ being the least potent. Transduction efficiency and supernatant dilution appeared to correlate linearly below a transduction rate of approximately 50%. For future experiments, a transduction rate of approximately 70% was considered suitably high and retroviral supernatant dilution factors for each TCR were estimated accordingly for subsequent transduction experiments.

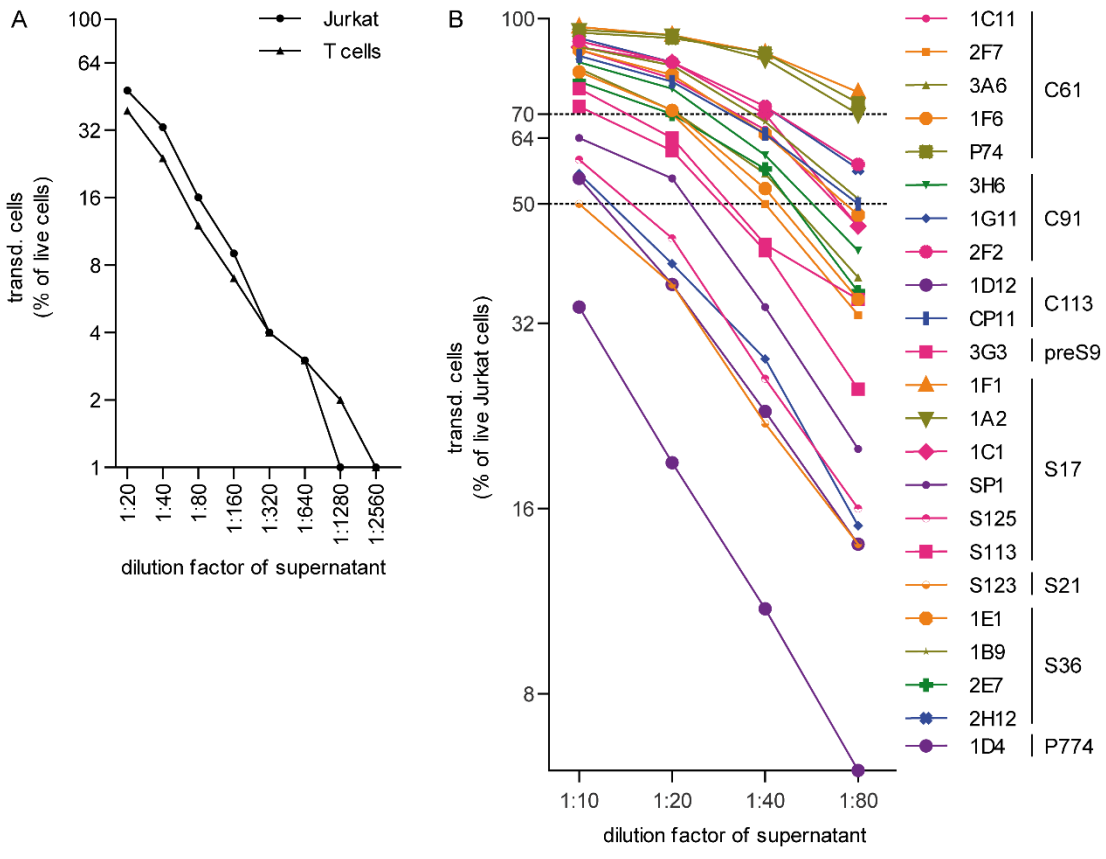

Figure 16: Titration of supernatant from retroviral producer cells. (A) Retroviral superntant of TCR $P74_{C61}$ was titrated on $1x10^6$ Jurkat cells (circles) and $1x10^6$ primary human T cells (triangles) with dilution factors ranging from 1:20 to 1:2560. (B) Titration of retroviral supernatant for all TCRs on $1x10^6$ Jurkat cells with dilution factors ranging from 1:10 to 1:80. Transduction rates were measured by surface staining of the mTRBC on day 5 after transduction.

2.3 Characterization of TCRs

After having generated stable γ-retroviral producer cell lines for each TCR, large amounts of T cells were transduced in one batch. All TCRs were then characterized in depth regarding cellular expression, MHC class II restriction, recognition of processed antigen, recognition of different HBV genotypes, T-cell receptor functional avidity and cytokine secretion as well as cytotoxic activity of both $CD4^+$ and $CD8^+$ T cells.

2.3.1 Expression of TCRs

T-cell receptor expression can be described by several measures. For example, the percentage of TCR^+ T cells in flow cytometry compared to the mock control represents the transduction rate; however, surface staining also results in a distinct mean fluorescence intensity (MFI) for the TCR^+ population of each sample. Whereas the transduction rate seemed to correlate with the amount of retrovirus used for transduction, i.e. the dilution of retroviral supernatant as shown in Figure 16, the mean fluorescence intensity appeared to be characteristic for each TCR. This was observed when comparing normalized MFIs of four independent transduction experiments for a large number of TCRs (Figure 17). Interestingly, TCR $1D12_{C113}$, which had shown a "weak" surface expression on RD114 cells (see section 2.2.2), also presented with a very low MFI.

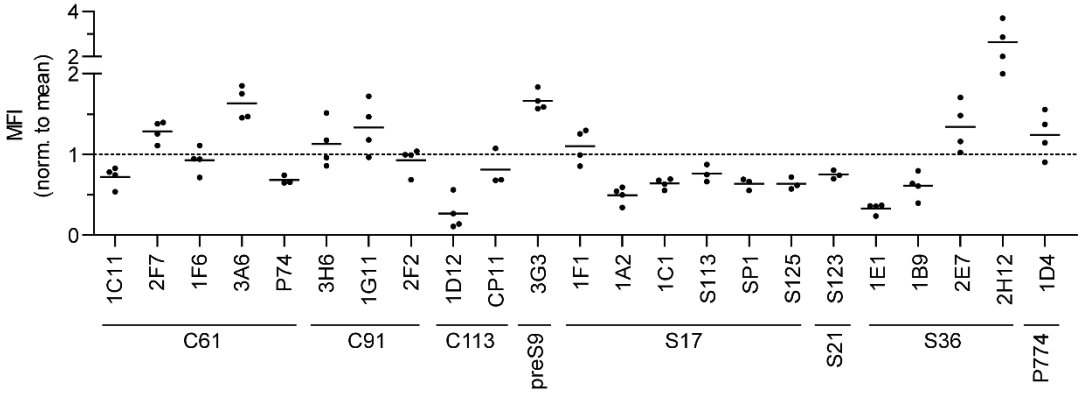

Figure 17: TCR expression as mean fluorescence intensity of surface staining on transduced T cells in flow cytometry. Mean fluorescence intensities of TCR^+ populations from four independent transductions are normalized to mean of each experiment.

In addition, the expression of each TCR depends on the number of genome integrations resulting from transduction. The average number of integrates per bulk cell population, i.e. including both transduced and non-transduced cells, was determined by quantitative PCR (qPCR). A linear correlation between the average number of integrates and the transduction rate below 50% was shown exemplary for

TCR $P74_{C61}$ (Figure 18A). The transgenic expression of TCR $P74_{C61}$ was highly efficient with an average integrate number of 1 being sufficient for a transduction rate of approximately 50%. Assuming the non-transduced population to be integrate free, one can conclude that each transduced cell of the 50%-transduced population must contain on average two integrates. The cell batch used for the majority of characterization experiments featured an average number of integrates below 5 with transduction rates ranging from approximately 60-90% (Figure 18B). “Weakly” expressing TCR $1D12_{C113}$ presented with a relatively high number of integrates despite a transduction rate of only 59%.

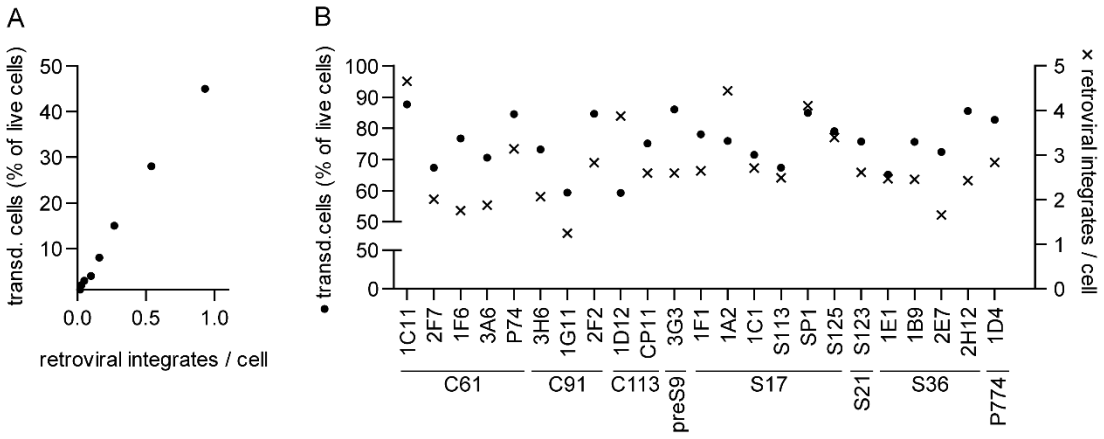

Figure 18: Average number of retroviral genome integrates and transduction rates. The average number of retroviral integrates per bulk cell population, i.e. including both transduced and non-transduced cells, was measured in a multiplex quantitative PCR of viral woodchuck hepatitis virus postregulatory element relative to the genomic single-copy gene PTBP2. (A) Average number of integrates for $P74_{C61}$-transduced T cells with transduction rates below 50%. (B) Transduction rate (in % of live cells) as determined by mTRBC staining of TCR-transduced T cells and average number of integrates for a representative cell batch that was used for the majority of characterization experiments.

2.3.2 MHC class II restriction

Next, the panel of TCRs was characterized with regards to MHC restriction, since the TCRs could potentially be restricted against any of the donor’s MHC class II molecules (see donor 1-6 HLA types in section 4.1.7). To narrow down the possibilities, the affinity between peptide and MHC class II molecule was predicted *in silico* by the NetMHCIIpan algorithm. In addition, the peptide-MHC interaction was measured via a radioactivity-based peptide-inhibition assay, combining each peptide with every MHC class II molecule of all donors. *In silico* predicted and measured values were within the same $\log_{10}$ range in 70% of all cases with values below 10000 nM (Table 4, marked in grey). Approximately 80% of all known MHC class II T-cell epitopes are typically found to have peptide-MHC binding values below 1000 nM[210-212] and peptides with an IC_{50} <50 nm are generally considered high affinity binders. The C61 peptide displayed a high affinity towards the HLA-DR1 molecule which was expected

since C61 represents a published HLA-DR1-restricted epitope[214]. However, some peptides, e.g. S17 or P774, showed a high measured binding affinity for several MHC molecules, making it impossible to draw conclusions regarding the MHC restriction of the respective TCRs. Hence, additional cell culture assays were required to determine the MHC restriction.

The MHC restriction was further determined by co-culturing TCR-transduced T cells with MHC class II knockout (k.o.) target cells, which had been stably transfected with a single MHC class II molecule, i.e. α- and β-chain. Each TCR was matched with a set of single MHC class II transfectants, resembling the MHC type of its respective donor. Cytokine secretion was determined via ELISA and is shown relative to values from co-culture with the respective HLA-matched peptide-loaded B-LCLs (Figure 19). The MHC class II restriction was conclusive for 18 TCRs. All four S36-specific and four C61-specific TCRs were HLA-DRB1*01:01 restricted. The latter observation is in line with the published DRB1*01:01-restriction of the C61 epitope[214]. For TCR $1C11_{C61}$, a promiscuous though specific binding behavior towards DRB3*02:02 in the presence of the target antigen was noticed. All C91-specific TCRs were HLA-DRB1*13:01-restricted. $1D12_{C113}$ was both DRB1*01:01 and DQA1*01:01/DQ*05:01-restricted, whereas $CP11_{C113}$ was DRB3*02:02-restricted. Most S17-specific TCRs were either DRB1*07:01 or DRB1*11:04-restricted, depending on the original donor. The MHC class II restriction of $1F6_{C61}$, $3G3_{preS9}$, $1F1_{S17}$, $S123_{S21}$ and $1D4_{P774}$ could not be determined by this method, since no cytokine secretion was detected upon co-culture with the available single MHC class II transfectant target cells.

Table 4: IC50 affinity values of each peptide with every MHC class II molecule of donors 1-6. IC50 values (in nM) were determined through in silico prediction by the NetMHCIIpan algorithm and measured in a binding assay based on their ability to inhibit the binding of a radiolabeled probe peptide to the purified MHC molecule. Color code: In silico predicted and measured values within the same log10 range (grey); >log10 difference (blue); either in silico predicted or measured value >10000 nM, not available (n.a.) or none determined (n.d.) (white).

Peptide	IC_{50} (nM) determination	DRB1*							DQA1*/DQB1*								DPA1*/DPB1*						DRB3*		DRB4*	
		01:01	03:01	04:03	07:01	11:04	13:01	14:54	05:01/ 02:01	02:01/ 02:02	03:01/ 03:01	05:05/ 03:01	03:01/ 03:02	01:01/ 05:01	01:04/ 05:03	01:03/ 06:03	01:03/ 02:01	01:03/ 03:01	01:03/ 04:01	01:03/ 04:02	11:01	15:01	01:01	02:02	01:03	01:01
C61	*in silico* prediction	32	≥10000	1577	1071	3514	2048	2736	465	2870	1260	488	2141	748	390	232	1415	257	2626	1381	1418	194	≥10000	4880	1607	2188
	binding assay	7.8	≥10000	102	76	304	1230	n.a.	285	644	n.a.	≥10000	1750	69	855	382	984	≥10000	614	40	n.a.	n.a.	≥10000	3700	n.a.	1.1
C91	*in silico* prediction	32	651	727	12	360	193	64	3258	4431	3108	1753	8059	89	393	162	76	13	34	26	18	3.5	1972	643	65	23
	binding assay	957	n.d.	631	422	4530	3067	n.a.	n.d.	n.d.	≥10000	2010	n.d.	n.d.	4340	n.d.	521	92	167	71	n.a.	n.a.	396	8860	n.a.	120
C113	*in silico* prediction	12	2892	768	24	1232	884	643	1421	2615	1014	330	712	274	581	311	200	28	129	77	70	11	666	1566	802	542
	binding assay	28	≥10000	7140	123	≥10000	3222	n.a.	17	423	≥10000	680	792	18	13	8020	181	1570	137	18	n.a.	n.a.	451	3030	n.a.	4930
preS9	*in silico* prediction	58	2981	1882	138	5769	2025	1562	2584	9274	1332	256	≥10000	≥10000	4861	391	3497	1282	8263	4570	5552	1930	1189	1075	1206	3982
	binding assay	925	n.d.	3540	291	≥10000	≥10000	n.a.	977	≥10000	3030	1000	≥10000	1050	436	3240	5190	920	3290	516	n.a.	n.a.	≥10000	85	n.a.	1310
S17	*in silico* prediction	40	1165	105	44	441	395	117	308	1939	1345	626	504	444	446	110	2.2	3.7	5.2	4.9	4.3	2.1	1515	304	51	132
	binding assay	6.0	7780	55	1.3	23	2558	n.a.	68	956	n.d.	1390	1610	10	7.3	84	1.0	36	0.05	0.02	n.a.	n.a.	26	4050	n.a.	41
S21	*in silico* prediction	48	1195	192	256	771	234	183	259	2717	1592	1441	958	3360	977	160	2176	72	1038	462	384	71	9490	581	58	67
	binding assay	453	1910	107	14	2010	846	n.a.	137	1590	≥10000	6010	8980	1410	18	519	571	47	100	83	n.a.	n.a.	≥10000	≥10000	n.a.	10
S36	*in silico* prediction	5.7	1983	617	11	4580	2344	810	2748	6294	241	26	4236	2911	1427	165	729	122	1170	598	959	191	5406	494	626	438
	binding assay	3.1	n.d.	2140	109	≥10000	n.d.	n.a.	184	≥10000	575	130	n.d.	n.d.	≥10000	316	≥10000	n.d.	≥10000	73	n.a.	n.a.	n.d.	n.d.	n.a.	532
P774	*in silico* prediction	6.2	3810	63	14	966	908	192	531	3850	389	79	2272	2842	1062	182	139	37	382	167	268	42	714	103	414	1712
	binding assay	5.1	≥10000	225	15	≥10000	≥10000	n.a.	113	2890	≥10000	69	391	744	88	164	4.5	4.9	0.9	1.0	n.a.	n.a.	457	51	n.a.	1150

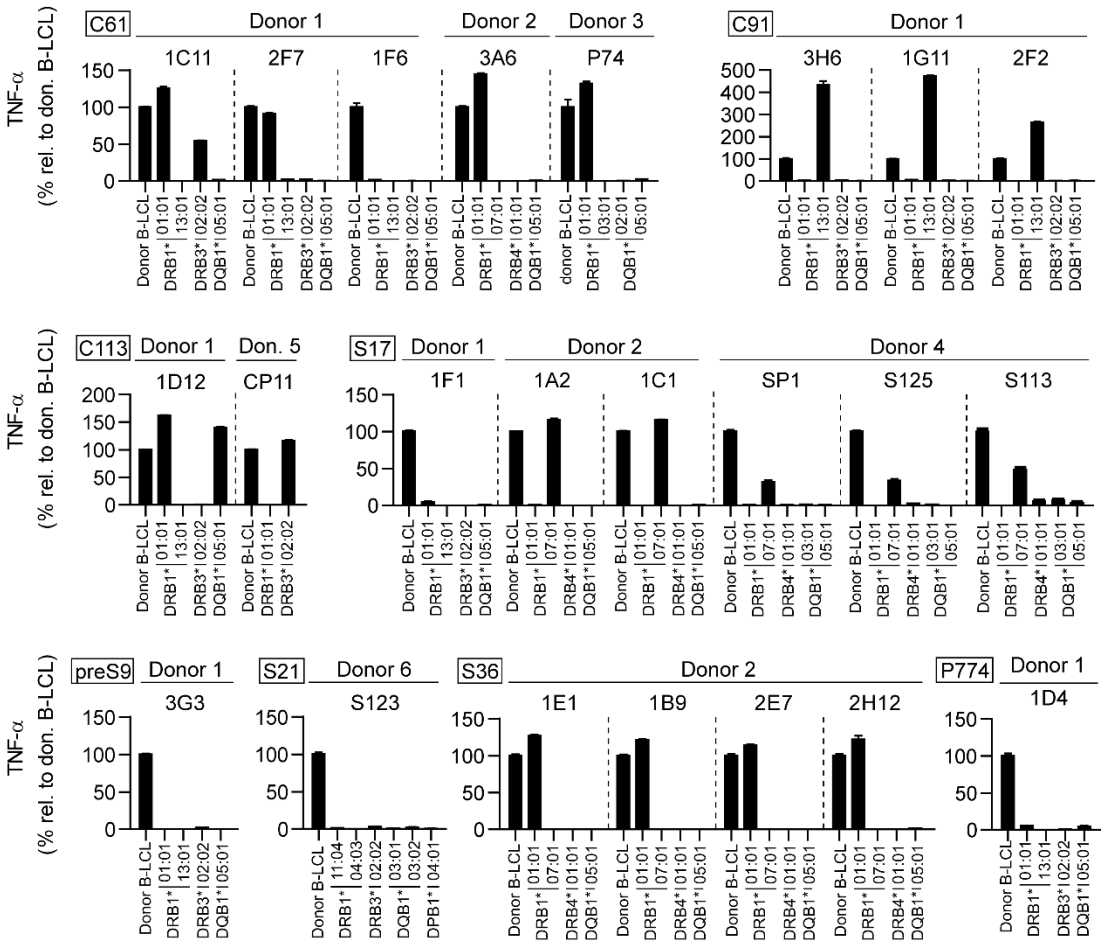

Figure 19: Restriction assay with single MHC class II transfectant target cells. TCR-transduced CD4$^+$ T cells were co-cultured at an effector-to-target ratio of 2:1 with MHC class II k.o. fibroblasts or Raji-derived B-LCLs, stably transfected with a single MHC class II molecule, i.e. α- and β-chain according to the donor's HLA type (limited to availability), and pulsed with 1 µM of target peptide. MHC class II single transfectants are named after their respective β-chain. TNF-α secretion was determined via ELISA after 16 h of co-culture and is shown relative to values from co-culture with B-LCLs. Data points represent mean values ± SD from triplicates. Controls without peptide were consistently below 5% with the exception of TCR 2F2$_{C91}$, which showed similarly high TNF-α secretion during co-culture with HLA-DRB1*13:01 target cells with or without peptide (data not shown). Square boxes at the top left of each graph indicate peptide specificities.

TCR-transduced T cells for which the MHC restriction remained unclear were subsequently co-cultured with a panel of partially HLA-matched B-LCLs (Figure 20). The MHC class II type of the respective donor was then compared with the MHC class II types of the panel of partially HLA-matched B-LCLs in order to identify MHC molecules tha are shared among the donor and other specifically cytokine-inducing B-LCLs but absent in all other B-LCLs (Table 5, shared MHC molecules are highlighted in grey). By this, TCR $1F6_{C61}$ and $3G3_{preS9}$ were shown to be DQA1*01:01/DQ*06:03-restricted. TCR $3G3_{preS9}$, however, showed additional unspecific cytokine secretion, i.e. both with or without loaded peptide, for a number of B-LCLs that shared the molecule HLA-DRB1*11 with subtypes 01, 02 and 04. To confirm this cross-reactivity, further experiments, e.g. with single MHC class II transfectant target cells, would be needed.

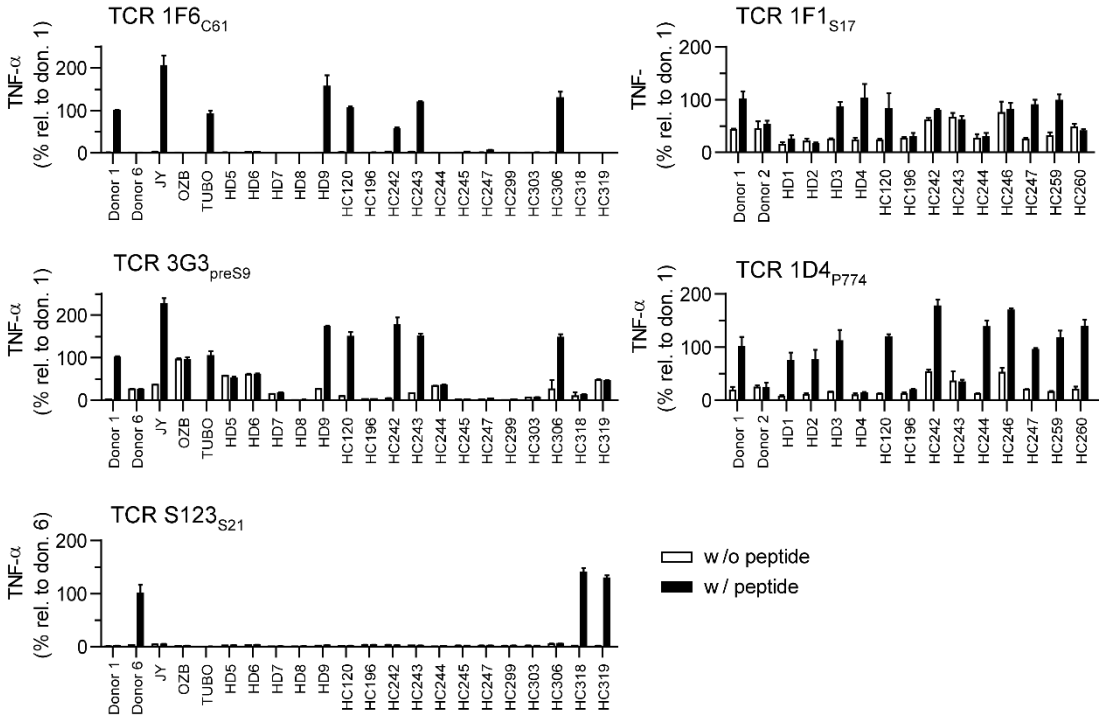

Figure 20: Co-culture of TCR-transduced T cells with partially HLA-matched B-LCLs. T cells were transduced with TCRs $1F6_{C61}$, $3G3_{preS9}$, $1F1_{S17}$, $S123_{S21}$ and $1D4_{P774}$ and co-cultured with partially HLA-matched B-LCLs (x-axis), pulsed with 1 µM of the respective peptide (w/ peptide, black bars) or without peptide (w/o peptide, white bars). TNF-α secretion was determined via ELISA after 16 h of co-culture and is shown relative to values from co-culture with donor B-LCLs (donor 1 for TCRs $1F6_{C61}$, $3G3_{preS9}$, $1F1_{S17}$ and $1D4_{P774}$ or donor 6 for TCR $S123_{S21}$). Data points represent mean values ± SD from triplicates. TCR clone names are indicated at the top left of each graph.

Table 5: Overview of MHC class II types of B-LCLs used for MHC restriction studies. B-LCLs which induced cytokine secretion in TCR-transduced T cells solely in the presence of the corresponding peptide are labeled “specific”. B-LCLs which induced cytokine secretion both in the presence and absence of peptide are labeled “unspecific”. No cytokine secretion in the presence or absence of peptide is labeled “negative”. MHC molecules shared exclusively among “specific” B-LCLs are marked in grey for each TCR.

TCR $1F6_{C61}$															
	B-LCL	DRB1		DRB3		DRB4	DRB5	DQB1		DPB1		DQA1		DPA1	
Specific	donor 1	01:01	13:01	02:02				05:01	06:03	02:01	04:01	01	01	01:03	
	JY	04:04	13:01	01:01		01:03		03:02	06:03	02:01	04:01	01:03	03:01	01:03	
	TUBO	01:01	13:01	02:02				05:01	06:03	02:01	04:01	01:01	01:03	01:03	01:03
	HD9	01:01	11:04	02:02				03:01	05:01	04:01	04:02	01:01	05:05	01:03	
	HC120	13:01	13:02	01:01	03:01			06:03	06:04	03:01		01:02	01:03	01:03	
	HC242	15:01					01:01	06:02	06:03	04:01		01:02		01:03	02:02
	HC243	13:01	13:02	01:01	03:01			06:03	06:04	03:01	11:01	01:02	01:03	01:03	02:01
	HC306	11:01	13:01	02:02				03:01	06:03	04:01	13:01	01:03	05:05	01:03	02:01
Negative	donor 6	04:03	11:04	02:02		01:03		03:01	03:02	04:01	15:01	03:01	05:05	01:03	
	OZB	11:04		02:02				03:01		04:02	10:01	05:05		01:03	02:01
	HD5	11:04	16:01	02:02			02:02	03:01	05:02	04:01	10:01	01:02	05:05	01:03	02:01
	HD6	04:02	11:01	02:02		01:03		03:01	03:02	02:01		03:01	05:05	01:03	
	HD7	03:01	04:01	01:01		01:03		02:01	03:01	01:01	16:01	03:03	05:01	01:03	02:01
	HD8	03:01	04:03	02:02		01:03		02:01	03:05	04:01	26:01	03:01	05:01	01:03	02:01
	HC196	04:04				01:03		03:02	04:02	03:01	06:01	03:01	03:03	01:03	
	HC244	03:01	07:01	01:01		01:03		02:01	02:02	04:01	10:01	02:01	05:01	01:03	02:01
	HC245	13:02	15:01	03:01			01:01	06:02	06:04	02:01	04:01	01:02		01:03	
	HC247	15:01					01:01	06:02		02:01	04:02	01:02		01:03	
	HC299	04:03	09:01			01:03		03:02	03:03	05:01	13:01	03:01	03:02	02:06	04:01
	HC303	04:04	13:03	01:01		01:03		03:01	03:02	04:01		03:01	05:05	01:03	01:03
	HC318	04:01	11:02	02:02		01:03		03:01		04:01	15:01	03:03	05:05	01:03	01:03
	HC319	03:01	11:04	02:02				02:01	03:01	04:01	15:01	05:01	05:05	01:03	01:04
TCR $3G3_{preS9}$															
	B-LCL	DRB1		DRB3		DRB4	DRB5	DQB1		DPB1		DQA1		DPA1	
Specific	Donor 1	01:01	13:01	02:02				05:01	06:03	02:01	04:01	01	01	01:03	
	JY	04:04	13:01	01:01		01:03		03:02	06:03	02:01	04:01	01:03	03:01	01:03	
	TUBO	01:01	13:01	02:02				05:01	06:03	02:01	04:01	01:01	01:03	01:03	01:03
	HD9	01:01	11:04	02:02				03:01	05:01	04:01	04:02	01:01	05:05	01:03	
	HC120	13:01	13:02	01:01	03:01			06:03	06:04	03:01		01:02	01:03	01:03	
	HC242	15:01					01:01	06:02	06:03	04:01		01:02		01:03	02:02
	HC243	13:01	13:02	01:01	03:01			06:03	06:04	03:01	11:01	01:02	01:03	01:03	02:01
	HC306	11:01	13:01	02:02				03:01	06:03	04:01	13:01	01:03	05:05	01:03	02:01
Unspecific	Donor 6	04:03	11:04	02:02		01:03		03:01	03:02	04:01	15:01	03:01	05:05	01:03	
	OZB	11:04		02:02				03:01		04:02	10:01	05:05		01:03	02:01
	HD5	11:04	16:01	02:02			02:02	03:01	05:02	04:01	10:01	01:02	05:05	01:03	02:01
	HD6	04:02	11:01	02:02		01:03		03:01	03:02	02:01		03:01	05:05	01:03	
	HD7	03:01	04:01	01:01		01:03		02:01	03:01	01:01	16:01	03:03	05:01	01:03	02:01
	HC244	03:01	07:01	01:01		01:03		02:01	02:02	04:01	10:01	02:01	05:01	01:03	02:01
	HC318	04:01	11:02	02:02		01:03		03:01		04:01	15:01	03:03	05:05	01:03	01:03
	HC319	03:01	11:04	02:02				02:01	03:01	04:01	15:01	05:01	05:05	01:03	01:04
Negative	HD8	03:01	04:03	02:02		01:03		02:01	03:05	04:01	26:01	03:01	05:01	01:03	02:01
	HC196	04:04				01:03		03:02	04:02	03:01	06:01	03:01	03:03	01:03	
	HC245	13:02	15:01	03:01			01:01	06:02	06:04	02:01	04:01	01:02		01:03	
	HC247	15:01					01:01	06:02		02:01	04:02	01:02		01:03	
	HC299	04:03	09:01			01:03		03:02	03:03	05:01	13:01	03:01	03:02	02:06	04:01
	HC303	04:04	13:03	01:01		01:03		03:01	03:02	04:01		03:01	05:05	01:03	01:03
TCR $S123_{S21}$															
	B-LCL	DRB1		DRB3		DRB4	DRB5	DQB1		DPB1		DQA1		DPA1	
Specific	Donor 6	04:03	11:04	02:02		01:03		03:01	03:02	04:01	15:01	03:01	05:05	01:03	01:04
	HC318	04:01	11:02	02:02		01:03		03:01		04:01	15:01	03:03	05:05	01:03	01:03
	HC319	03:01	11:04	02:02				02:01	03:01	04:01	15:01	05:01	05:05	01:03	01:04
Negative	Donor 1	01:01	13:01	02:02				05:01	06:03	02:01	04:01	01	01	01:03	
	JY	04:04	13:01	01:01		01:03		03:02	06:03	02:01	04:01	01:03	03:01	01:03	
	OZB	11:04		02:02				03:01		04:02	10:01	05:05		01:03	02:01
	TUBO	01:01	13:01	02:02				05:01	06:03	02:01	04:01	01:01	01:03	01:03	01:03
	HD5	11:04	16:01	02:02			02:02	03:01	05:02	04:01	10:01	01:02	05:05	01:03	02:01
	HD6	04:02	11:01	02:02		01:03		03:01	03:02	02:01		03:01	05:05	01:03	
	HD7	03:01	04:01	01:01		01:03		02:01	03:01	01:01	16:01	03:03	05:01	01:03	02:01
	HD8	03:01	04:03	02:02		01:03		02:01	03:05	04:01	26:01	03:01	05:01	01:03	02:01
	HD9	01:01	11:04	02:02				03:01	05:01	04:01	04:02	01:01	05:05	01:03	
	HC120	13:01	13:02	01:01	03:01			06:03	06:04	03:01		01:02	01:03	01:03	
	HC196	04:04				01:03		03:02	04:02	03:01	06:01	03:01	03:03	01:03	
	HC242	15:01					01:01	06:02	06:03	04:01		01:02		01:03	02:02
	HC243	13:01	13:02	01:01	03:01			06:03	06:04	03:01	11:01	01:02	01:03	01:03	02:01
	HC244	03:01	07:01	01:01		01:03		02:01	02:02	04:01	10:01	02:01	05:01	01:03	02:01
	HC245	13:02	15:01	03:01			01:01	06:02	06:04	02:01	04:01	01:02		01:03	
	HC247	15:01					01:01	06:02		02:01	04:02	01:02		01:03	
	HC299	04:03	09:01			01:03		03:02	03:03	05:01	13:01	03:01	03:02	02:06	04:01
	HC303	04:04	13:03	01:01		01:03		03:01	03:02	04:01		03:01	05:05	01:03	01:03
	HC306	11:01	13:01	02:02				03:01	06:03	04:01	13:01	01:03	05:05	01:03	02:01

Table 5 continued.

TCR $1F1_{S17}$															
	B-LCL	DRB1		DRB3		DRB4	DRB5	DQB1		DPB1		DQA1		DPA1	
Specific	Donor 1	01:01	13:01	02:02				05:01	06:03	02:01	04:01	01	01	01:03	
	HD3	07:01	15:01			01:03	01:01	02:02	05:01	02:01	04:01	01:02	02:01	01:03	
	HD4	07:01				01:03		03:03		02:01		02:01		01:03	
	HC120	13:01	13:02	01:01	03:01			06:03	06:04	03:01		01:02	01:03	01:03	
	HC247	15:01					01:01	06:02		02:01	04:02	01:02		01:03	
	HC259	04:01	08:02			01:03		03:02	04:02	02:01	04:01	03:01	04:01	01:03	
Unspecific	HD1	07:01				01:03		02:02		04:01	13:01	02:01		01:03	
	HD2	01:01	08:01					04:02	05:01	04:01	04:02	01:01	04:01	01:03	
	HC242	15:01					01:01	06:02	06:03	04:01		01:02		01:03	02:02
	HC244	03:01	07:01	01:01		01:03		02:01	02:02	04:01	10:01	02:01	01:03	01:03	02:01
	HC246	08:01						04:02		03:01	04:01	04:01	04:02	01:03	
	HC260	01:01	04:01			01:03		03:02	05:01	04:01	04:02	01:01	03:01	01:03	
	Donor 2	01:01	07:01			01:01		02:02	05:01	03:01	11:02	01	02:01	01:03	02:01
	HC243	13:01	13:02	01:01	03:01			06:03	06:04	03:01	11:01	01:02	01:03	01:03	02:01
	HC196	04:04				01:03		03:02	04:02	03:01	06:01	03:01	03:03	01:03	
TCR $1D4_{P774}$															
	B-LCL	DRB1		DRB3		DRB4	DRB5	DQB1		DPB1		DQA1		DPA1	
Specific	Donor 1	01:01	13:01	02:02				05:01	06:03	02:01	04:01	01	01	01:03	
	HD1	07:01				01:03		02:02		04:01	13:01	02:01		01:03	
	HD2	01:01	08:01					04:02	05:01	04:01	04:02	01:01	04:01	01:03	
	HD3	07:01	15:01			01:03	01:01	02:02	05:01	02:01	04:01	01:02	02:01	01:03	
	HC120	13:01	13:02	01:01	03:01			06:03	06:04	03:01		01:02	01:03	01:03	
	HC242	15:01					01:01	06:02	06:03	04:01		01:02		01:03	02:02
	HC244	03:01	07:01	01:01		01:03		02:01	02:02	04:01	10:01	02:01	01:03	01:03	02:01
	HC246	08:01						04:02		03:01	04:01	04:01	04:02	01:03	
	HC247	15:01					01:01	06:02		02:01	04:02	01:02		01:03	
	HC259	04:01	08:02			01:03		03:02	04:02	02:01	04:01	03:01	04:01	01:03	
	HC260	01:01	04:01			01:03		03:02	05:01	04:01	04:02	01:01	03:01	01:03	
Unspecific	Donor 2	01:01	07:01			01:01		02:02	05:01	03:01	11:02	01	02:01	01:03	02:01
	HC243	13:01	13:02	01:01	03:01			06:03	06:04	03:01	11:01	01:02	01:03	01:03	02:01
Negative	HD4	07:01				01:03		03:03		02:01		02:01		01:03	
	HC196	04:04				01:03		03:02	04:02	03:01	06:01	03:01	03:03	01:03	

To further investigate the cross-reactivity of TCR $1C11_{C61}$ that was initially observed towards DRB3*02:02 (Figure 19), $1C11_{C61}$-transduced T cells were co-cultured with partially HLA-matched B-LCLs (data not shown). Based on this, an additional reactivity towards non-self HLA molecules DRB1*04:01, DRB1*04:04, DRB1*11:01 and DRB1*11:04 was hypothesized. Co-culture with single MHC class II transfectant target cell lines indeed confirmed this promiscuous yet specific binding behavior of TCR $1C11_{C61}$ (Figure 21).

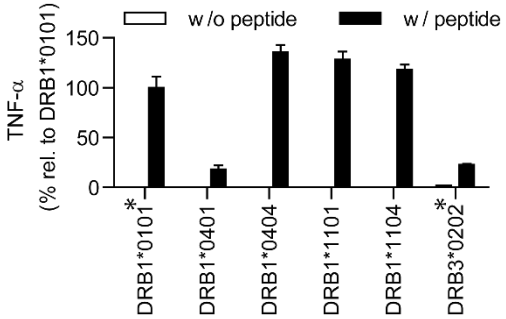

Figure 21: Promiscuous binding of TCR $1C11_{C61}$. TCR-transduced T cells were co-cultured at an effector-to-target ratio of 2:1 with single MHC class II transfectant target cells with peptide (w/ peptide, black bars) or without peptide (w/o peptide, white bars). TNF-α secretion was determined via ELISA after 16 h of co-culture and is shown relative to values from DRB1*01:01 single MHC transfectant. Data points represent mean values ± SD from triplicates. Self HLA molecules are marked with *.

In conclusion, thirteen MHC class II restrictions could be identified for all TCRs and are depicted in Table 6. To assess their therapeutic relevance, allele frequencies of representative populations in Germany and China were extracted from the Allele Frequency Net Database[227] (Figure 22A). In addition, allele frequencies of all promiscuously bound MHC molecules for TCR $1C11_{C61}$ as well as their cumulative frequencies were plotted (Figure 22B, DRB3*02:02 not available).

Table 6: MHC class II restrictions identified for all TCRs.

TCR	Peptide	Restricting MHC molecule	
		α-chain	β-chain
1C11	C61	DRA	DRB1*04:01
		DRA	DRB1*04:04
		DRA	DRB1*11:01
		DRA	DRB1*11:04
		DRA	DRB3*02:02
2F7		DRA	DRB1*01:01
3A6			
P74			
1F6		DQA1*01:01	DQB1*06:03
3H6	C91	DRA	DRB1*13:01
1G11			
2F2			
1D12	C113	DRA	DRB1*01:01
		DQA1*01:01	DQB1*05:01
CP11		DRA	DRB3*02:02
3G3	preS9	DQA1*01:01	DQB1*06:03
1F1	S17	DPA1*01:03	DPB1*02:01
1A2		DRA	DRB1*07:01
1C1			
SP1		DRA	DRB1*11:04
S125			
S113			
S123	S21	DPA1*01:03	DPB1*15:01
1E1	S36		DRB1*01:01
1B9			
2E7			
2H12			
1D4	P774	DPA1*01:03	DPB1*04:01

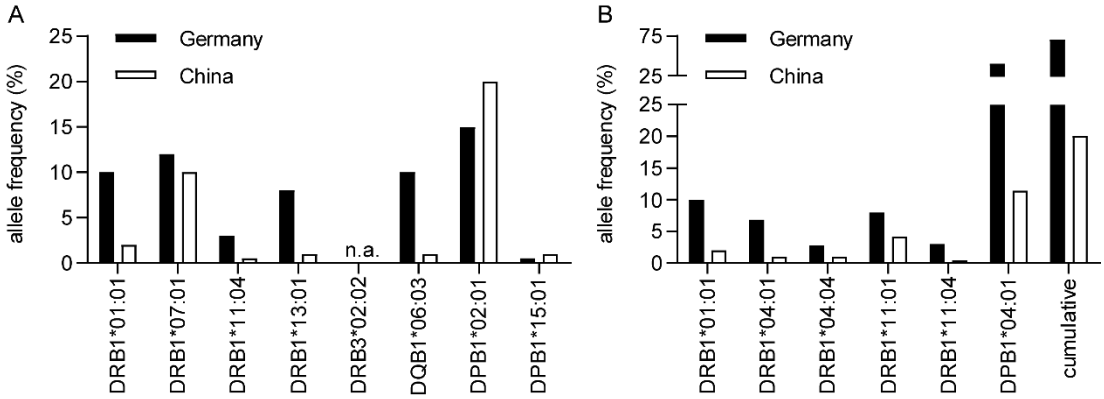

Figure 22: MHC class II allele frequencies extracted from the Allele Frequency Net Database. The allele frequency represents the total number of copies of a given allele in the population sample, i.e. alleles/2n. If only phenotype frequencies were traced, the allele frequency was calculated assuming Hardy-Weinberg proportions[228] by the following formula: phenotype frequency=1-(1-allele frequency)*2. I.e., the phenotype frequency equals roughly double the allele frequency. (A) Allele frequencies of all main MHC restrictions identified for the 23 TCRs throughout this thesis. (B) Allele frequencies of all promiscuously bound MHC molecules for TCR 1C11$_{C61}$ as well as their cumulative frequency in Germany (black bars) and China (white bars). HLA-DRB3*02:02 was not available. All frequencies were extracted from the Allele Frequency Net Database[227].

2.3.3 Recognition of processed antigen

For HBV-specific MHC II-restricted TCRs to be used in a therapeutic context, they need to recognize physiological epitopes presented on MHC class II as a result from intracellular processing of HBV proteins. To this end, it was assessed whether the TCRs reacted not only to externally loaded peptides but also to antigen that had been taken up, processed and presented via the MHC class II pathway. TCR-transduced T cells were co-cultured with HLA-matched B-LCLs, preincubated with the respective antigen (Figure 23). A concentration-dependent recognition of all tested epitopes was confirmed. TNF-α secretion of T cells transduced with C61- and S21-specific TCRs was consistently ten-fold lower than for other core- or S protein-specific TCRs, possibly indicating less efficient intracellular processing of these two epitopes. Due to a lack of availability of the large envelope and polymerase protein, TCRs $3G3_{preS9}$ and $1D4_{P774}$ were not included in this assay. Since all TCRs were selected from a repertoire primed by HBV infection, it seems plausible that TCRs $3G3_{preS9}$ and $1D4_{P774}$ would also recognize processed antigen. Taken together, all tested TCRs recognized physiologically processed and presented antigen, thereby making them suitable candidates for further studies with HBV proteins or viral particles.

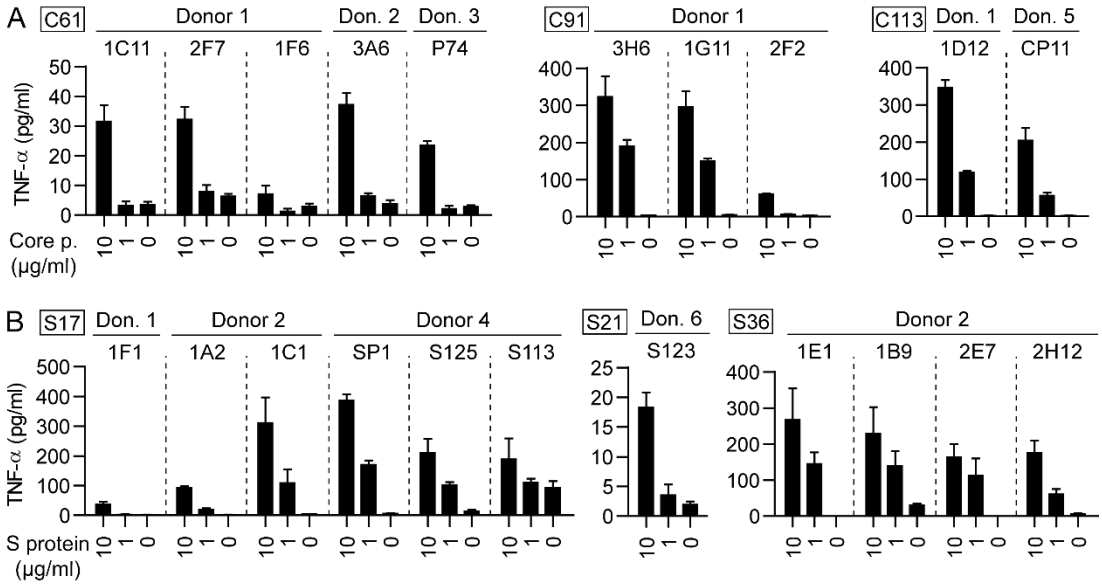

Figure 23: Recognition of physiologically processed HBV epitopes. TCR-transduced $CD4^+$ T cells were co-cultured at an effector-to-target ratio of 2:1 with HLA-matched B-LCLs which had been preincubated for 4 h with 10 or 1 µg/ml of core protein (A) or small envelope (S) protein (B). TNF-α secretion in pg/ml was determined after 16 h of co-culture via ELISA. Data points represent mean values ± SD from triplicates. Square boxes at the top left of each graph indicate peptide specificities.

2.3.4 Recognition of different HBV genotypes

The recognition of different HBV genotypes gives TCRs a broader range of therapeutic applicability and is therefore considered favorable. The peptides which were used initially for stimulation of PBMCs from donors with cured HBV infection were derived from the HBV genotype A sequence, since donor 1 had been formerly diagnosed with HBV genotype A. The amino acid sequences of all eight epitopes, for which HBV-specific TCRs were ultimately generated, are given in Table 7 for HBV genotypes A, B, C and D.

Table 7: Amino acid sequences of core, envelope and polymerase protein epitopes for HBV genotypes A, B, C and D. Genotype A peptides were used for isolation of TCRs. Amino acid differences with regards to genotype A are highlighted in red. Deletions are indicated with - .

Genotype / Peptide	A	B	C	D
C61	WGELMTLATWVGNNLEDP	WGELMNLATWVGSNLEDP		WGELMTLATWVGGNLEDP
C91	TNMGLKIRQLLWFHISCL	VNMGLKIRQLLWFHISCL		TNMGLKFRQLLWFHISCL
C113	ETVLEYLVSFGVWIRTPP			ETVIEYLVSFGVWIRTPP
preS9	RKGMGTNLSVPNPLGFFP		RQGMGTNLSVPNPLGFFP	- - - MGQNLSTSNPLGFFP
S17	AGFFLLTRILTIPQSLDS	AGFFLLTKILTIPQSLDS	AGFFLLTRILTIPQSLDS	
S21	LLTRILTIPQSLDSW	LLTKILTIPQSLDSW	LLTRILTIPQSLDSW	
S36	WTSLNFLGGSPVCLGQNS	WTSLNFLGGTPVCLGQNS	WTSLNFLGGAPTCPGQNS	WTSLNFLGGTTVCLGQNS
P774	LRGTSFVYVPSALNPADD			

To evaluate the additional recognition of HBV genotype B, C and D peptides, TCR-transduced T cells were co-cultured with HLA-matched B-LCLs pulsed with the respective peptides from Table 7 (Figure 24). All DRB1*01:01-restricted C61-specific TCRs recognized all HBV genotypes, represented by three different C61 variants. Interestingly, the DQA1*01:01/DQ*06:03-restricted TCR $1F6_{C61}$ was only activated upon interaction with the genotype A peptide. C91-specific TCRs 3H6 and 1G11 detected both the A and B/C variant, whereas TCR $2F2_{C91}$ additionally bound to the genotype D peptide. The C113-specific TCRs recognized both epitope variants, covering all four genotypes. The preS9-specific TCR $3G3_{preS9}$ was unable to recognize the genotype D peptide, which seems plausible given the major amino acid deletion in comparison to genotype A. S17-specific TCRs SP1, S125 and S113 and S21-specific TCR S123 recognized all four genotypes with A, C and D being sequence identical and B differing by one amino acid exchange. Interestingly, this amino acid exchange seemed relevant for TCRs $1F1_{S17}$, $1A2_{S17}$ and $1C1_{S17}$, which only bound the A/C/D epitope variant. S36-specific TCRs interacted mostly with the genotype A peptide; however $1B9_{S36}$ and $2H12_{S36}$ displayed minor binding towards genotypes B and C, respectively.

Those TCRs specific for a highly conserved epitope, such as 1D4$_{P774}$, are of particular interest for therapeutic application. Similarly, TCRs recognizing different genotypes despite their sequence varieties can be considered favorable. Taken together, nine core-specific, seven envelope-specific TCRs and one polymerase-specific TCR recognized several HBV genotypes and can therefore be attributed a higher therapeutic range than TCRs that only recognize a single genotype variant.

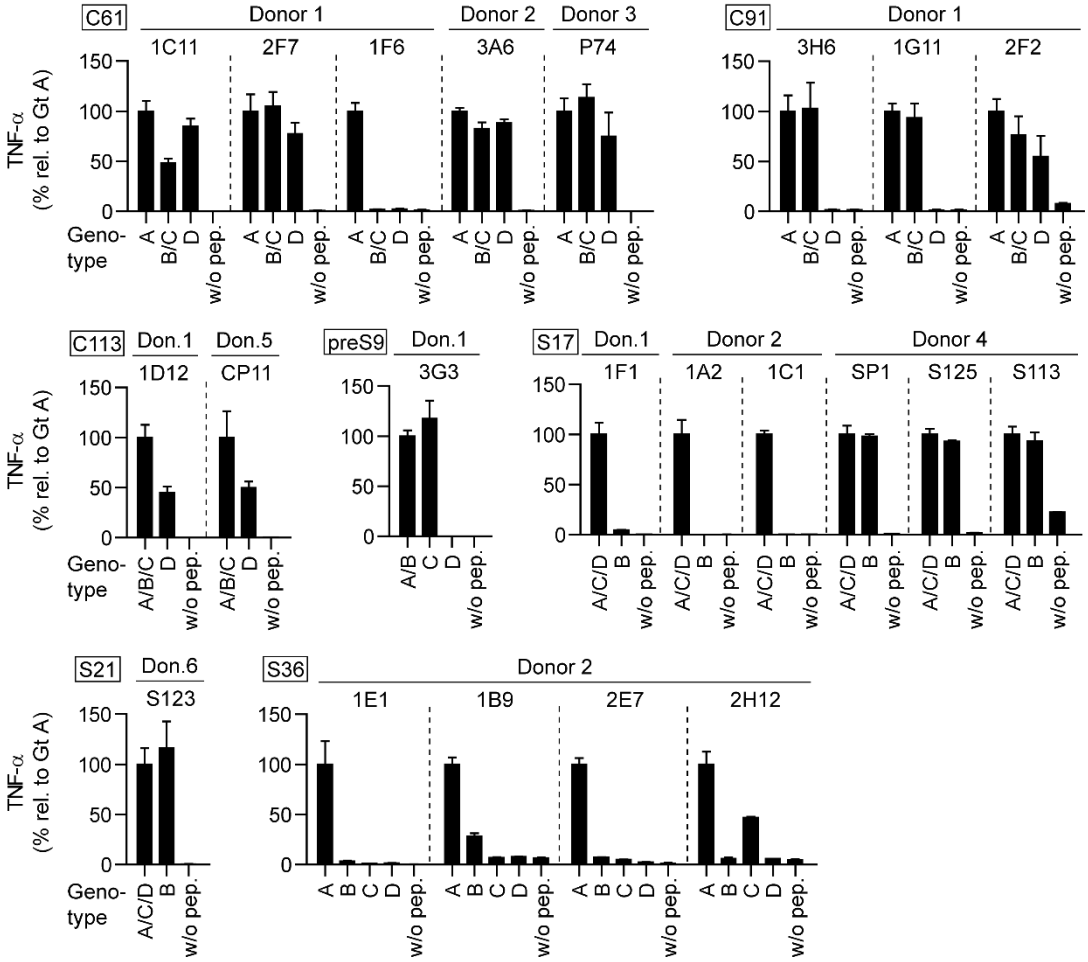

Figure 24: Recognition of a variety of HBV genotype variants. TCR-transduced CD4$^+$ T cells were co-cultured at an effector-to-target ratio of 2:1 with HLA-matched B-LCLs pulsed with 1 µM of peptide from HBV genotypes A, B, C and D or without peptide (w/o pep.). TNF-α secretion was determined after 16 h of co-culture via ELISA and is shown relative to values from co-culture with genotype A. Data points represent mean values ± SD from triplicates. Square boxes at the top left of each graph indicate peptide specificities. TCR 1D4$_{P774}$ was not included in this assay, since the P774 peptide is conserved across all four genotypes.

2.3.5 Comparison of T-cell receptor functional avidities

TCRs with higher affinity are potentially more suitable for therapeutic application. The affinity of the HBV-specific MHC II-restricted TCRs was measured indirectly via the proliferative capacity upon co-culture with HLA-matched B-LCLs and titration of the target peptide, it is therefore referred to as “functional avidity”. Incorporation of radioactive thymidine as a measure of proliferation is expressed as stimulation index, representing the ratio of mean counts per minute (cpm) obtained in the presence or absence of antigen (Figure 25). EC_{50} refers to the half maximal effective concentration (EC), a measure of potency of a substance to exert a certain biological function, in this case the induction of proliferation. EC_{50} values for most TCRs were determined based on a non-linear log(dose) vs. response fit. All TCRs specific for epitopes C61, pres9, S17, S21, S36 and P774 showed EC_{50} values in a one- or two-digit nanomolar range. EC_{50} values of C91- and C113-specific specific TCRs could not be determined, since the peptide titration did not cover an adequate response range. Based on the given data, a lower functional avidity of these TCRs seems likely. Notably, this matched the rather low peptide-MHC binding affinity that was measured between the C91 peptide and the restricting MHC molecule HLA-DR13 (Table 4). In summary, 18 TCRs displayed high functional avidity values that are typical for TCRs recognizing virus, i.e. foreign antigen[229].

Since the stimulation index is defined as counts per minute divided by the negative control without peptide, the maximum stimulation index for each TCR (i.e. the plateau values in Figure 25) varied depending on the background proliferation. In a relative comparison, TCRs with a higher stimulation index, i.e. a larger difference between the stimulated samples and the control, are preferable. To determine, whether the observed background proliferation is a characteristic feature of the TCR, the PBMC donor or the cell batch, further experiments are warranted.

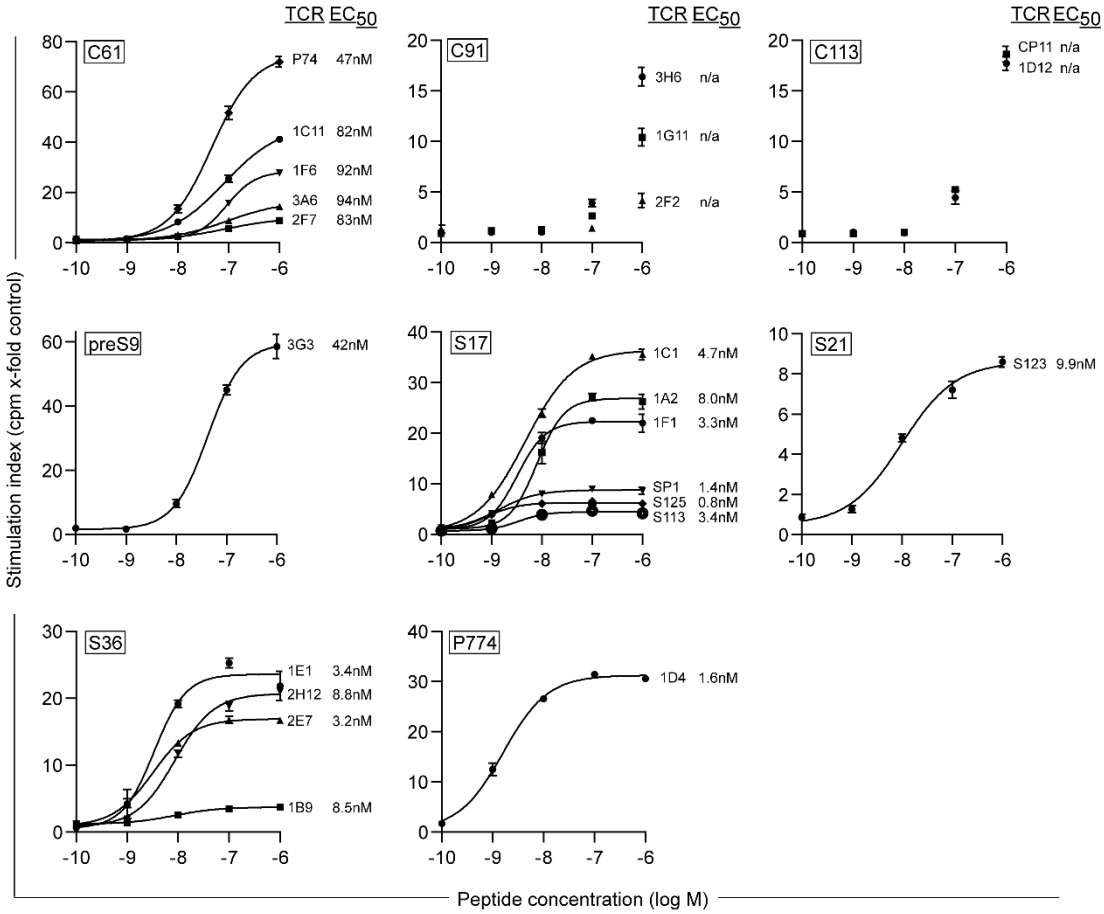

Figure 25: Proliferation assay to determine functional avidity of TCRs. TCR-transduced CD4$^+$ T cells were co-cultured at an effector to target (E:T) cell ratio of 2:1 with HLA-matched B-LCLs titrating the amount of target peptide from 1 µM to 100 pM. Proliferation was assessed through integration of ^{3}H-Thymidine after 72 hours of co-culture. Results are expressed as stimulation index, i.e. counts per minute (cpm) divided by the negative control without peptide. Data points represent mean values ± SD from triplicates. All indicated EC_{50} values were calculated with a non-linear dose-response ordinary fit. R^2 values were consistently ≥0.99 with the exception of TCR $1E1_{S36}$ (0.97). EC_{50} values for C91- and C113-specific TCRs could not be determined because they did not reach a plateau of proliferation. Square boxes at the top left of each graph indicate peptide specificities.

2.3.6 Cytokine secretion of TCR-transduced CD4$^+$ and CD8$^+$ T cells

Given the high functional avidity of the majority of MHC class II-restricted TCRs tested in this thesis, the question arouse whether TCRs were able to activate both transduced CD4$^+$ as well as CD8$^+$ T cells and which functional profile they would induce upon activation. Therefore, these two populations were compared in separate co-cultures with HLA-matched, peptide-pulsed B-LCLs and their cytokine and granzyme B (GrzB) secretion was measured via intracellular cytokine staining and flow cytometry (Figure 26). CD4$^+$ T cells (Figure 26A) generally secreted high amounts of TNF-α and IL-2, with most TCRs inducing TNF-α in >81% and IL-2 in >74% of all CD4$^+$ TCR$^+$ T cells. C91-specific TCRs showed a slightly reduced cytokine secretion, especially TCR 2F2$_{C91}$, which only caused TNF-α secretion in 66% and IL-2 secretion in 26% of all CD4$^+$ TCR$^+$ T cells. This correlates with the lower functional avidity of these TCRs, observed in section 2.3.5. C113-specific TCRs, however, showed a cytokine secretion profile comparable to that of TCRs with high functional avidity. Interestingly, most TCRs also induced GrzB secretion, a serine protease associated with cytotoxic activity, in 20-50% of all CD4$^+$ TCR$^+$ cells with the expection of C91-specific TCR-transduced T cells. IFN-γ secretion was relatively low and occurred on average in only 10% of all CD4$^+$ TCR$^+$ T cells.

CD8$^+$ T cells (Figure 26B), on the other hand, secreted vast amounts of GrzB in 65-93% of all TCR$^+$ cells for most TCRs. They also secreted IL-2 and TNF-α in approximately 35-63% of CD8$^+$ TCR$^+$ T cells, as well as lower amounts of IFN-γ. However, still more in comparison to CD4$^+$ T cells, i.e. on average 15% of all CD8$^+$ TCR$^+$ T cells. All C91-specific TCRs, especially TCR 2F2$_{C91,}$ once again induced slightly less cytokines and GrzB in CD8$^+$ T cells compared to other TCRs.

Overall, activation of T cells induced a polyfunctional profile, pointing towards a Th1 phenotype of transduced CD4$^+$ T cells. Furthermore, MHC II-restricted TCRs were able to activate CD8$^+$ T cells despite the absence of a CD4 coreceptor.

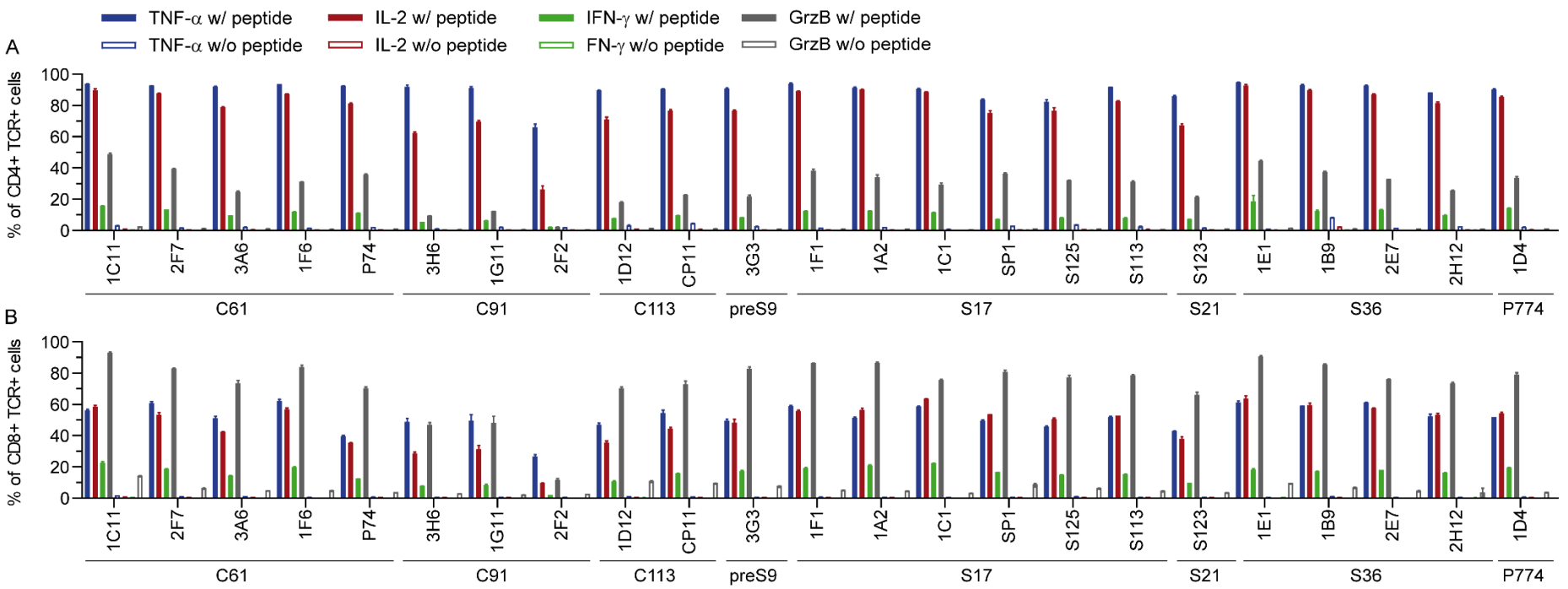

Figure 26: Cytokine and GrzB secretion of TCR-transduced CD4⁺ or CD8⁺ T cells. CD4⁺ and CD8⁺ T cells were co-transduced and then separated by positive selection through magnetic-activated cell sorting with purities ≥98%. TCR-transduced CD4⁺ (A) or CD8⁺ (B) T cells were co-cultured with HLA-matched B-LCLs, pulsed with 1 µM target peptide (w/ peptide). Brefeldin A was added one hour after co-culture start. TNF-α (blue bars), IL-2 (red bars), IFN-γ (green bars) and GrzB (grey bars) were measured via intracellular cytokine staining and flow cytometry after 14 hours of co-culture in CD4⁺TCR⁺ or CD8⁺TCR⁺ subsets, respectively. Co-cultures without peptide (w/o peptide) served as negative control (empty bars in respective colors). Data points represent mean values ± SD from triplicates. Square boxes below TCRs indicate peptide specificities.

2.3.7 Cytotoxic activity of TCR-transduced CD4$^+$ and CD8$^+$ T cells

Cytotoxic T cells can help to clear HBV infection through direct killing of target cells. However, they also bear the risk of causing severe liver damage and inflammation. In view of the strong GrzB secretion observed for most TCRs in both CD8$^+$ and to a lesser extent also in CD4$^+$ T cells, the cytotoxic capacity of both T cells subsets was analyzed. To this end, an xCELLigence killing assay was performed, which is based on the measurement of electrical impedance from viable, adherent target cell lines. Cytotoxic activity by effector cells, i.e. CD4$^+$ or CD8$^+$ T cells, leads to killing and detachment of target cells and therefore to decreased values of electrical impedance. These are translated into a cell index, normalized to the starting point of each co-culture. Considering the technical requirements of this assay, only those TCRs were compared, for which adherent single transfectant fibroblasts expressing the restricting MHC class II molecule were available. The TCRs were tested on CD4$^+$ and CD8$^+$ T cells in separate co-cultures at three different effector to target (E:T) ratios, i.e. 1:1, 0.3:1 and 0.1:1 (cytotoxicity kinetics in Figure 27, endpoint analysis after 24 hours in Figure 28). Most tested TCRs showed a very similar cytotoxic activity in CD4$^+$ and CD8$^+$ T cells. The cytotoxic effect of C61- and S36-specific TCRs was most prominent, reaching a half-maximal effect after approx. 6 hours (Figure 27). TCR-transduced CD8$^+$ T cells were generally very effective, killing on average 97% of target cells after 24 hours at an effector-to-target ratio of 1:1 for C61-, C91-, C113- and S36-specific TCRs. Only S17-specific TCRs displayed slightly less cytotoxic activity in CD8$^+$ T cells, i.e. 85% on average after 24 hours (Figure 28). CD4$^+$ T cells transduced with TCRs $3H6_{C91}$, $1G11_{C91}$ and $1F1_{S17}$ showed slower killing kinetics (Figure 27) and reduced endpoint cytotoxicity (Figure 28) in comparison to CD8$^+$ T cells. Unexpectedly, TCR $2F2_{C91}$ showed unspecific killing of the unloaded control (Figure 27). This cross-reactivity could be an artefact observed only in single MHC class II transfectant fibroblasts, due to their artificial nature. Further in-depth experiments are required to explain this observation. TCRs $SP1_{S17}$, $S125_{S17}$ and $S113_{S17}$ were also submitted to the xCELLigence killing assay; however, they did not show any specific cytotoxic activity, neither in CD8$^+$ nor CD4$^+$ T cells (data not shown). Mock-transduced T cells served as an additional negative control and no killing was observed after 24 hours of co-culture (data not shown).

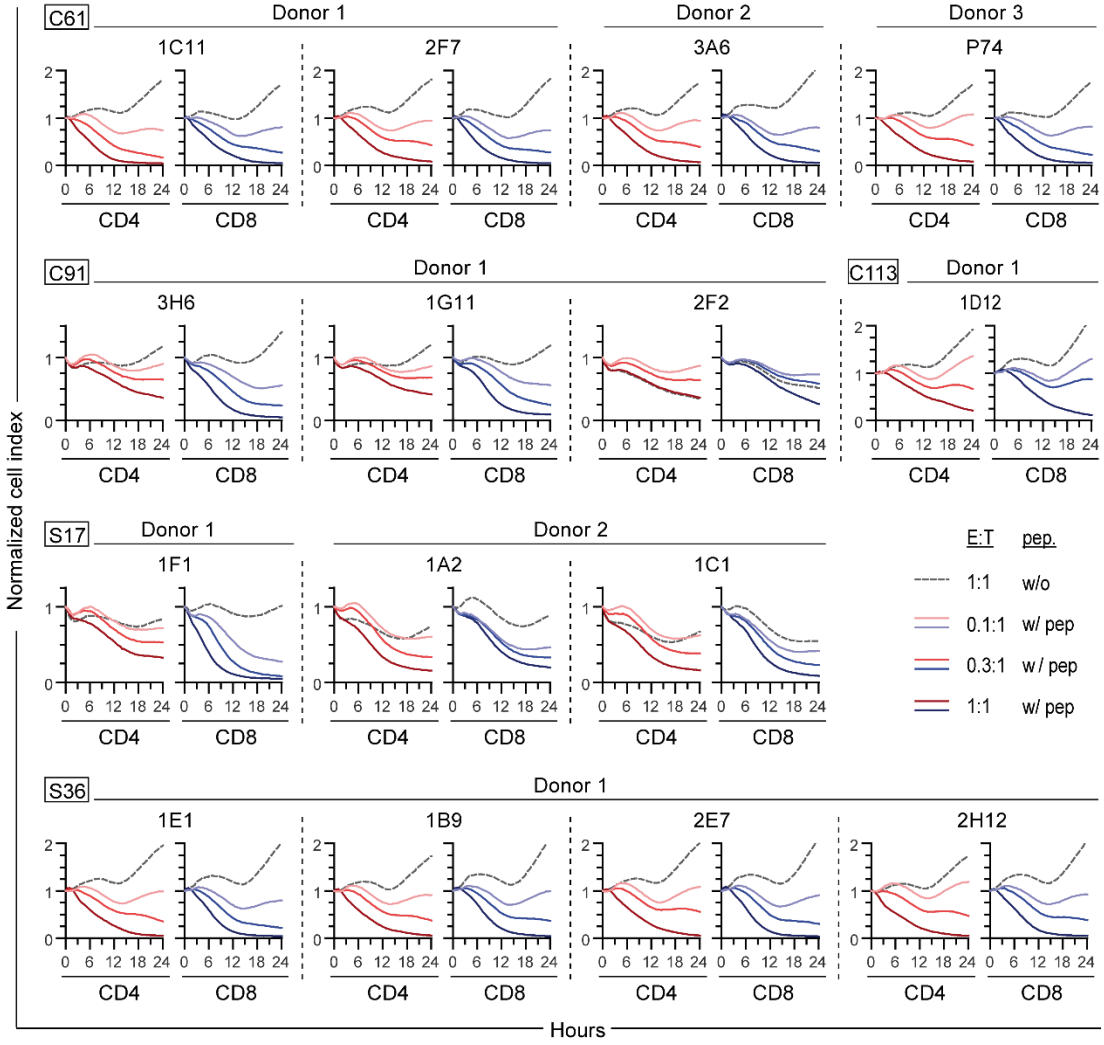

Figure 27: xCELLigence killing assay kinetics with TCR-transduced CD4⁺ or CD8⁺ T cells. CD4⁺ and CD8⁺ T cells were co-transduced and then separated by positive selection through magnetic-activated cell sorting prior to the experiment with to purities of ≥98%. TCR-transduced CD4⁺ (red) or CD8⁺ (blue) T cells were co-cultured for 24 hours with single MHC II transfectant fibroblasts pulsed with 1 µM peptide (w/ pep) at an effector to target (E:T) cell ratio ofs 1:1 (dark color), 0.3:1 (medium color), or 0.1:1 (light color) or without peptide (w/o pep) at E:T ratio 1:1 (grey). Cytotoxicity was assessed via the adherence of target cells measured through electrical impedance and is given as a cell index normalized to the starting point of each co-culture. Considering the technical requirements of this assay, only TCRs were included for which adherent single MHC II transfectant fibroblasts were available. Data points were acquired every 30 minutes and represent mean values from triplicates. Square boxes at the top left of each graph indicate peptide specificities.

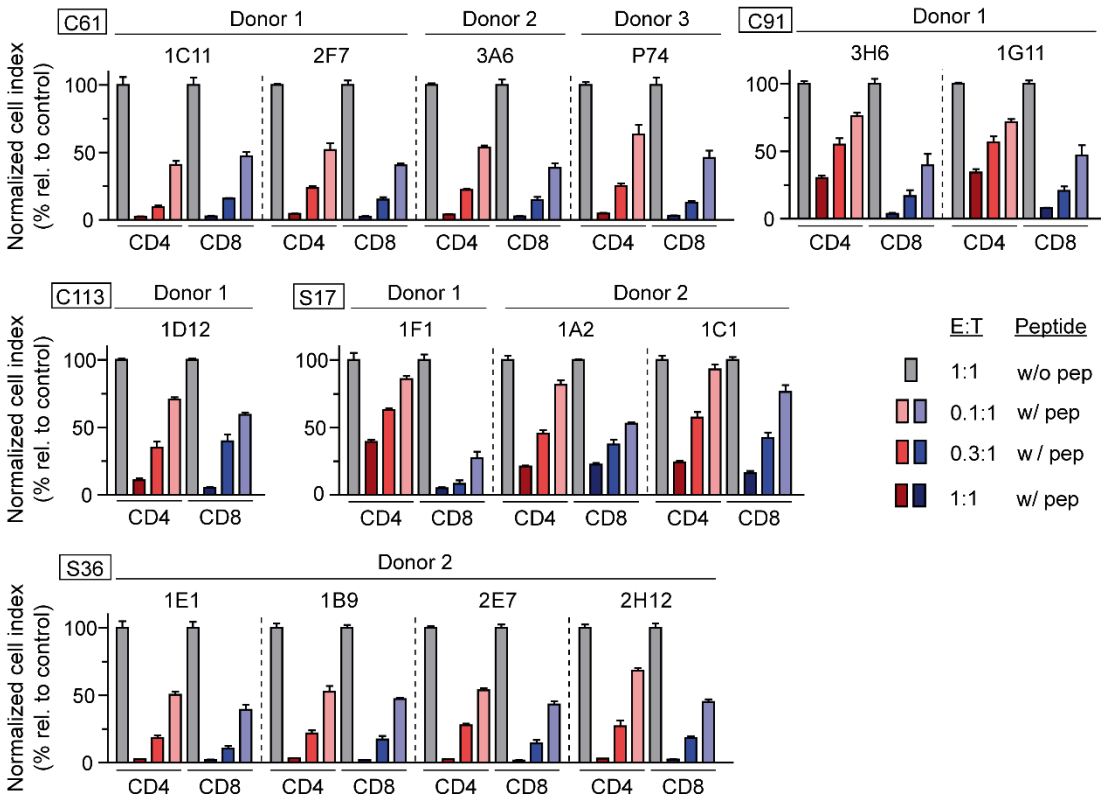

Figure 28: xCELLigence killing assay endpoint analysis with TCR-transduced CD4$^+$ or CD8$^+$ T cells. Assay conditions are described in Figure 27. Endpoint cytotoxicity after 24 hours of co-culture. The normalized cell index is given relative to killing of target cells without peptide at the highest E:T of 1:1. TCR 2F2$_{C91}$ was excluded from endpoint analysis given the unspecific killing of the unloaded control (Figure 27). Data points represent mean values ± SD from triplicates. Square boxes at the top left of each graph indicate peptide specificities.

2.3.8 Summary of TCR characterization

Table 8 shows a summary of the characteristics of all 23 TCRs analyzed during this thesis.

Table 8: Summary table of TCR characterization. Transduction (transd.) rates in % of $CD4^+$ T cells and vector copy number (VCN) as an average number of integrates per cell (avg./cell) are indicated for a representative cell batch. MFI of TCR^+ populations in flow cytometry from four independent transductions is normalized (norm.) to mean of each experiment. The recognition of processed (proc.) antigen is scored according to TNF-α secretion in co-culture with B-LCls: low (<100 pg/ml), medium (100-200 pg/ml) and high (>200 pg/ml). The number of recognized HBV genotypes (Gt) by each TCR is given as a number of four (x/4) genotypes tested: A/B/C/D. Functional avidity is specified as EC_{50} in nM calculated from proliferation assays with peptide titration. $CD4^+IL\text{-}2^+$ cells and $CD8^+GrzB^+$ in % of TCR^+ T cells are listed representative for cytokine secretion. Cytotoxicity endpoint values for $CD4^+$ and $CD8^+$ T cells after 24 hours of co-culture are indicated in % relative (rel.) to the unloaded control. EC_{50} could not be determined (n.d.) when a plateau of maximum response was not reached. Cytotoxity was not measured when matching single MHCII-transfectant adherent target cell lines were not available (n.a.). For TCRs $SP1_{S17}$, $S125_{S17}$ and $S113_{S17}$, cytotoxicity was not determinable (n.d.).

TCR	Peptide	MHC restriction b-chain	Transd. rate (%)	VCN (avg./ cell)	MFI (norm.)	Proc. antigen (score)	HBV Gt (x/4)	EC_{50} (nM)	Cytokine secretion (% of TCR^+T cells)		Cytotoxicity 24 h (% rel. to control)	
									CD4 (IL-2)	CD8 (GrzB)	CD4	CD8
1C11	C61	DRB1*01:01	87.6	4.7	0.70	low	4	82	89.3	92.6	2.4	2.8
2F7			67.3	2.0	1.24	low	4	83	87.1	82.7	4.6	2.5
3A6			70.6	1.9	0.89	low	4	94	87.0	83.5	4.0	2.7
P74			84.5	3.1	0.65	low	4	47	81.0	69.9	4.7	3.2
1F6		DQB1*06:03	76.7	1.8	1.57	low	1	92	78.5	73.2	n.a.	
3H6	C91	DRB1*13:01	73.2	2.1	1.09	high	3	n.d.	61.9	46.5	30.5	3.7
1G11			59.3	1.2	1.28	high	3	n.d.	69.2	47.7	34.3	8.0
2F2			84.6	2.8	0.89	low	4	n.d.	25.8	11.3	n.a.	
1D12	C113	DRB1*01:01	59.2	3.9	0.26	high	4	n.d.	70.6	70.0	10.9	5.3
CP11		DRB3*02:02	75.1	2.6	0.78	high	4	n.d.	76.4	72.3	n.a.	
3G3	preS9	DQB1*06:03	86.0	2.6	1.61	n.d.	3	42	76.4	82.3	n.a.	
1F1	S17	DPB1*02:01	78.0	2.6	1.06	low	3	3.3	88.8	86.1	39.3	4.9
1A2		DRB1*07:01	75.9	4.4	0.48	low	3	8	89.8	86.0	21.1	22.5
1C1			71.5	2.7	0.62	high	3	4.7	88.3	75.2	24.1	16.2
SP1		DRB1*11:04	84.9	4.1	0.76	high	4	1.4	74.7	80.2	n.d.	
S125			79.0	3.4	0.64	high	4	0.8	76.1	76.9	n.d.	
S113			67.3	2.5	0.64	medium	4	3.4	82.3	78.1	n.d.	
S123	S21	DPB1*15:01	75.7	2.6	0.71	low	4	9.9	66.8	65.7	n.a.	
1E1	S36	DRB1*01:01	65.1	2.5	0.32	high	1	3.4	92.3	90.3	2.7	2.1
1B9			75.6	2.5	0.59	high	1	8.5	89.3	84.9	3.3	2.0
2E7			72.4	1.7	1.30	med	1	3.2	86.8	75.7	2.9	1.8
2H12			85.5	2.4	2.56	med	1	8.8	81.2	73.1	3.1	2.5
1D4	P774	DPB1*04:01	82.7	2.8	1.20	n.d.	4	1.6	85.2	78.5	n.a.	

2.4 Functional studies

To further test MHC class II-restricted HBV-specific TCRs in functional studies with regards to their antiviral and therapeutic potential, suitable MHC class II-expressing target cells for *in vitro* testing as well as an animal model for *in vivo* studies are needed. To this end, a number of cell lines were evaluated regarding their HLA type as well as their MHC class II expression and a transgenic mouse model was taken into consideration. An initial *in vitro* test of functionality demonstrated $CD4^+$ help for $CD8^+$ T cells with an exemplary TCR.

2.4.1 Suitability of cell lines

To set up an *in vitro* cell culture model for testing MHC class II-restricted $CD4^+$ T cells and their benefit especially for MHC class I-restricted $CD8^+$ T cells, an MHC class II-expressing cell line is needed, ideally combining both the restricting MHC class I and II molecules for the respective transgenic TCRs. Since all TCRs generated previously by Wisskirchen et al.[193] are HLA-A*02:01-restricted, a target cell line expressing the HLA-A*02:01 in combination with one of the restricting MHC class II molecules identified during this thesis would be of particular relevance.

Table 9 shows the HLA typing results of several liver-derived cell lines as well as THP-1 cells, an immortalized monocyte-like cell line[230]. To compare these cell lines in terms of MHC class II surface expression, they were analyzed by staining HLA-DR in flow cytometry, since it is the most abundant of the classical MHC class II molecules HLA-DR, DP and DQ (Figure 29). HepG2, Huh7 and Hep3B did not express HLA-DR, even when exposed to high amounts (i.e. 100 ng/ml) of IFN-γ (Figure 29A), which typically increases MHC II expression in a number of cell types and tissues[231]. Although HepaRG did express HLA-DR to a maximum of approx. 80%, its HLA type is not ideal for *in vitro* assays since it does not match the available HLA-A*02:01-restricted TCRs. In addition, HepaRGs are bipotent progenitor cells which are able to differentiate into biliary cells or hepatocytes[232]; this may explain their mixed HLA-DR phenotype. In terms of HLA type and MHC class II expression, SK-HEP-1 and THP-1 were found to be theoretically suitable candidates for an *in vitro* cell culture model, since they were each typed positive for the HLA-A*02:01 gene as well as one or more matching MHC class II molecules, i.e. HLA-DR*11:04 or HLA-DR*01:01 and HLA-DP*02:01, respectively (Table 9). SK-HEP-1 and THP-1 both expressed HLA-DR, with SK-HEP-1 requiring longer duration and higher concentration of IFN-γ exposure than THP-1. Whereas HLA-DR-expressing SK-HEP-1 cells plateaued at only 65%, even after 48

h exposure with 100 ng/ml of IFN-γ (Figure 29B), HLA-DR-expressing THP-1 cells leveled at 95% after 24 hours of 3.1 µg/ml IFN-γ exposure (Figure 29C). Taken together, both SK-HEP-1 cells as well as THP-1 cells could theoretically be used as cell lines in an *in vitro* model to test the functionality of MHC class II-restricted TCRs in combination with MHC class I-restricted TCRs: SK-HEP-1 cells for the HLA-DR*11:04-restricted TCRs $SP1_{S17}$, $S125_{S17}$ and $S113_{S17}$ and THP-1 for the HLA-DR*01:01-restricted TCRs $1C11_{C61}$, $2F7_{C61}$, $3A6_{C61}$, $P74_{C61}$, $1D12_{C113}$, $1E1_{S36}$, $1B9_{S36}$, $2E7_{S36}$, $2H12_{S36}$ and HLA-DP*02:01-restricted TCR $1F1_{S17.}$ Nevertheless, additional factors, such as the adherent character and liver-derived background of SK-HEP-1 versus the soluble and monocyte-like nature of THP-1 cells, have to be taken into account.

Table 9: HLA type of cell line candidates for *in vitro* cell culture model to test MHC class II-restricted TCRs.

Cell line	HLA-A		HLA-B		HLA-C		HLA-DRB1		HLA-DQB1		HLA-DPB1	
HepG2	02:01	24:02	35:14	51:08	04:01	16:02	13:02	16:02	03:01	06:04	02:01	04:02
HuH7	11:01		54:01		01:02		08:03		06:01		02:01	
Hep3B	68:02	74:01	14:01	35:01	04:01	08:02	07:01	13:02	02:02	05:01	01:01	
HepaRG	23:01	29:02	44:03		04:24	16:01	07:01		02:02		04:01	06:01
SK-HEP-1	02:01	24:02	35:02	44:03	04:01		10:01	11:04	03:01	05:01	04:01	
THP-1	02:01		15:11		03:03		01:01	15:01	05:01	06:02	02:01	04:02

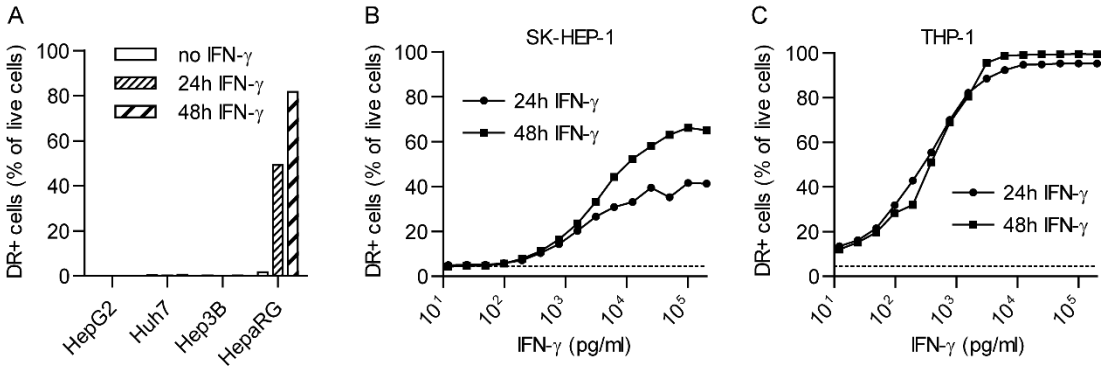

Figure 29: HLA-DR surface expression of different cell lines analyzed via flow cytometry, with or without IFN-γ stimulation for 24 h or 48 h. (A) Undifferentiated cell lines HepG2, HuH7, Hep3B and HepaRG were submitted to 100 ng/ml IFN-γ stimulation. (B) SK-HEP-1 and (C) THP-1 cells were exposed to IFN-γ ranging from 0 to 100 ng/ml.

2.4.2 Suitability of mouse model

For further *in vivo* characterization of the MHC class II-restricted TCRs generated in this thesis, a suitable animal model is needed. To this end, the previously described HLA-DR1-HHDII transgenic mouse[233] was taken into consideration. In this model, both murine MHC class I and II genes were knocked out and substituted by a chimeric HHDII molecule, a monochain consisting of the human HLA-A*0201 α1 and α2 domains, linked to the murine cytoplasmic α3 domain as well as the human β2m. In terms of MHC class II, these mice are transgenic for the human HLA-DR1 molecule. To evaluate the general suitability of this model, ten genotyped HLA-DR1$^+$-HHDII$^+$ animals were analyzed regarding their HHDII and HLA-DR expression on CD3$^+$ or CD19$^+$ splenocytes via flow cytometry (Figure 30). Indeed, all animals expressed high levels of HHDII on both cell populations when compared to wildtype mice (Figure 30A). HLA-DR expression, on the other hand, was only minor on CD3$^+$ cells, and intermediate on CD19$^+$ lymphocytes, with substantial variability between individuals (Figure 30B). These results prove the transgene surface expression in certain cell types of HLA-DR1-HHDII mice. Nevertheless, further analysis of liver-resident cells and professional antigen-presenting cells is needed to validate the suitability of this model for *in vivo* studies.

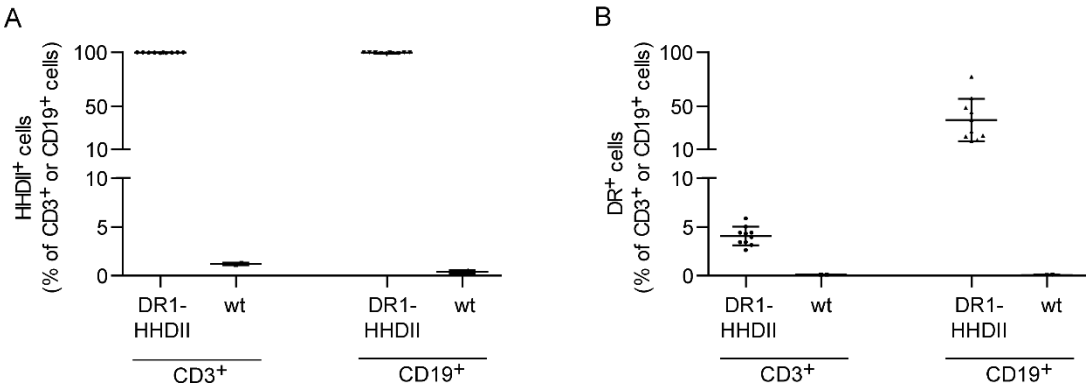

Figure 30: HHDII and HLA-DR surface expression on CD3$^+$ and CD19$^+$ lymphocytes of HLA-DR1-HHDII transgenic mice. Expression was measured via surface staining and flow cytometry on ten genotyped animals compared to wildtype mice. (A) HHDII expression. (B) HLA-DR expression. Bars represent mean values ± SD.

2.4.3 Proof-of-concept of CD4+ T-cell help

In order to conduct a first proof-of-concept experiment of CD4+ T-cell help provided to CD8+ T cells, HLA-matched peptide-pulsed monocyte-derived dendritic cells (MoDCs) were co-cultured with CD8+ T cells transduced with the MHC I-restricted TCR $WL12_{S172}$ (previously published by Wisskirchen et al.[193]) as well as with or without CD4+ T cells, transduced with the high avidity TCR $1E1_{S36}$. The target peptide concentration for the MHC class II peptide S36 was maintained at 1 µM in all assay conditions, whereas the MHC class I peptide S172 concentration varied between 10 nM and 1 µM. The help of CD4+ T cells became strikingly apparent: CD8+ T cell proliferation was increased after 3 days of co-culture when CD4+ T cells were present (Figure 31A). In addition, CD8+ T cells alone were much more sensitive to S172 peptide concentrations with only approx. 5% of $WL12_{S172}$-transduced T cells secreting IFN-γ at 10 nM of peptide versus 40% at 1 µM of peptide. Through the addition of CD4+ T cells, the number of IFN-γ-secreting CD8+ T cells was increased dramatically to approx. 69% and 79%, respectively (Figure 31A).

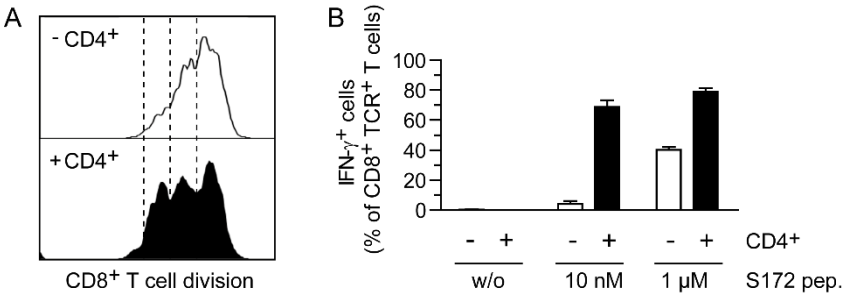

Figure 31: Proof-of-concept experiment for CD4+ T-cell help. HLA-matched MoDCs were co-cultured with $WL12_{S172}$-transduced CD8+ T cells, either without (white) or with (black) the addition of $1E1_{S36}$-transduced CD4+ helper T cells for three days at a helper to effector to target ratio of 5:5:1. MoDCs were pulsed with the respective target peptides prior to co-culture: S36 (1 µM) and S172 (10 nM or 1 µM). (A) Proliferation of CD8+ T cells was analyzed by CellTrace Violet staining. Each peak indicates a cycle of cell division. (B) IFN-γ production in CD8+ T cells was measured via intracellular cytokine staining and flow cytometry. Data points represent mean values ± SD from triplicates.

3 Discussion

Chronic HBV infection and HBV-related hepatocellular carcinoma remain a serious global health issue. As current treatment options are limited and rarely achieve viral clearance, adoptive T-cell therapy represents a promising therapeutic approach. This thesis aimed at the identification and characterization of MHC class II-restricted T-cell receptors for use in adoptive T-cell therapy of chronic HBV infection and HBV-related HCC. 23 HBV-specific T-cell receptors specific for eight epitopes from the HBV core, envelope and polymerase proteins were mainly restricted against ten different MHC molecules. Most TCRs displayed a high binding affinity, recognized several HBV genotypes, secreted various amounts of IFN-γ, TNF-α, IL-2 and GrzB, and specifically killed peptide-loaded target cells. Important aspects concerning the identification and isolation procedure, the T-cell receptor constitution and characterization as well as the clinical application of this approach will be discussed in the following section.

3.1 T-cell receptor identification and isolation

Within the T-cell receptor identification and isolation process, the *in silico* prediction of MHC class II-restricted HBV epitopes as well as the *in vitro* stimulation, cell sorting and TCR identification will be reviewed in more detail below.

3.1.1 *In silico* prediction of MHC class II-restricted HBV epitopes

The selection of HBV peptides for *in vitro* stimulation was made based on a literature review of published MHC class II-restricted HBV epitopes, as well as *in silico* peptide-MHC binding prediction using the algorithms SMM-align[208] and/or NetMHCIIpan 3.2[209]. In a recent evaluation of computational methods for MHC class II peptide binding prediction by Andreatta et al., NetMHCIIpan was rated the most accurate tool currently available[234]. Ultimately, the TCRs characterized throughout this thesis were specific for eight epitopes from the HBV core, envelope and polymerase protein: C61, C91, C113, preS9, S17, S21, S36 and P774. Of these, only C91 and preS9 had no previous literature reference. In other words, of the 21 peptides solely identified through *in silico* binding prediction, 19 peptides failed to trigger clonal growth leading to the identification of specific T-cell receptors. In addition, $3G3_{preS9}$ was shown to be DQA1*01:01/DQ*06:03-restricted, i.e. an HLA molecule other than the predicted DRB1*01:01 and DRB1*13:01. Taken together, this reflects the difficulty of accurately predicting MHC class II-restricted epitopes through *in silico* binding algorithms. While certain peptides may indeed be presented in complex with MHC class II on the surface

of antigen-presenting cells, only those recognized by T-cell receptors are referred to as T-cell epitopes. Binding algorithms can only predict the former but are unable to address the latter. In addition, *in silico* binding prediction of MHC class II molecules compared to MHC class I is further complicated by multiple factors such as the polymorphic nature of MHC class II molecules as well as peptide variations in terms of length, flanking regions and binding core[209].

Nevertheless, a strong correlation between MHC peptide binding and peptide immunogenicity has been observed. As such, MHC peptide binding assays typically yield IC_{50} values <1000 nM for about 80% of all MHC class II T-cell epitopes[210-212]. Moreover, *in silico* prediction has assisted the successful identification of immunodominant MHC class II T-cell epitopes for a variety of pathogens[235-237]. Approximately 70% of all peptide-MHC affinities determined during this thesis both through *in silico* prediction and via a radioactivitey-based peptide-inhibition assay were within the same log10 range (Table 4). Of the immunogenic peptide-MHC combinations identified during this thesis, seven of twelve qualified in this range; only two peptide-MHC combinations showed IC_{50} values >1000 nM and one was not measurable, indicating that nine of twelve immunogenic epitopes, i.e. 75%, indeed displayed IC_{50} values <1000 nM (Table 4). Despite these overall encouraging values, *in silico* prediction of MHC II epitopes at the present moment appears to be too inaccurate to replace empirical testing of peptides regarding their binding affinity and immunogenicity. Given the laborious task of identifying immunogenic T-cell epitopes, continuous efforts to improve the prediction accuracy of *in silico* binding algorithms are warranted.

3.1.2 *In vitro* stimulation, cell sorting and TCR identification

The TCRs characterized during this thesis were identified from HBV-specific T-cell clones obtained via *in vitro* stimulation of PBMCs with a selection of HBV peptides, followed by an expansion period and limited dilution cloning from a single cell level. An alternative to this approach was described by Lorenz et al. in 2017 for the isolation of a TCR against the human papillomavirus (HPV) type 16 E5 protein[238]. The authors used autologous mature monocyte-derived dendritic cells transfected with IVT mRNA of the respective antigen to stimulate PBMCs. This certainly represents a valid alternative strategy, since the number of professional antigen-presenting cells, i.e. MoDCs, is more controllable in this setting. In addition, the presentation of epitopes resulting from intracellularly processed antigen may avoid a selection bias towards clones reacting to externally loaded peptide epitopes, instead leading to the

expansion of clones specific for more naturally immunodominant epitopes. Nevertheless, relying on antigen-presenting cells within the isolated PBMC fraction and peptide-based stimulation has yielded satisfactory results throughout this thesis. It requires less starting material, which is especially relevant when donor blood is scarce. In addition, expanding antigen-specific T cells from rather low precursor frequencies requires repeated stimulation[239], which may ultimately favor PBMC stimulation, since high-avidity interactions with dendritic cells could potentially lead to activation induced cell death[240,241].

Optimizing the cell sorting procedure in terms of specificity would greatly reduce the downstream workload, given that the frequency of clones with confirmed HBV-specificity during this thesis was merely 11%. Staining additional T-cell activation signals such as CD137 may be beneficial, since the expression of CD137 is limited to T cells recently activated via TCR engagement and signaling[242]. As such, CD137 has proven a useful marker for enriching the full $CD8^+$ T-cell repertoire[239,242], virus-specific T cells[238,243,244] as well as tumor-reactive lymphocytes[245,246]. Still, regarding $CD4^+$ T cells, challenges regarding the expression level and specificity of CD137 remain[243,244].

To further improve specificity, techniques using soluble peptide-MHC (pMHC) complexes for the detection of antigen-specific T cells via flow cytometry have greatly evolved during the last two decades[247]. Tetrameric pMHC complexes, so-called tetramers, have long been shown to stably bind antigen-specific T cells[248] and have since been widely used to detect, enrich or isolate T cells even from low precursor frequencies[249-252]. However, the almost irreversible nature of the tetramer-TCR interaction has been shown to interfere with T-cell functionality[253-256] or to even cause activation-induced T-cell death[257,258]. Therefore, reversible pMHC multimers, so-called streptamers, were developed[259,260] and successfully applied to the enrichment[261-263] and isolation[193,264] of $CD8^+$ antigen-specific T cells or the determination of TCR-ligand dissociation rates[265]. In a direct comparison between the enrichment of T cells using tetramers or streptamers, the latter yielded higher numbers of T cells with superior proliferative capacity, measured up to six weeks after cell sorting[266]. Compared to the success of MHC class I-peptide multimers, the production and application for MHC class II molecules initially proved more challenging[267,268]. Nonetheless, MHC class II tetramers are now commercially available, albeit at an expensive price, and have been used for the detection and enrichment of antigen-specific $CD4^+$ T cells[269], also in the context of HBV infection[214]. Interestingly, Rius et al. recently showed that standard pMHC multimer protocols

relying on high-affinity TCR interactions may potentially lead to a bias within the detected or isolated T-cell repertoire, underestimating the amount of fully functional low-affinity TCRs[270]. This may be especially relevant given the fact that MHC class II-restricted TCRs are typically of lower affinity than MHC class I-restricted TCRs[271].

In vitro stimulation and expansion strategies tend to substantially modify or even limit the TCR repertoire composition, since not all T cells respond to the same experimental conditions and certain clones may outcompete others faced with limited stimulation and/or nutrients during *in vitro* cell culture[272-274]. Therefore, several groups have developed methods to circumvent *in vitro* expansion[264,275]. Dössinger et al. developed a sophisticated approach based on streptamer-assisted enrichment of specific T-cell clones in combination with single cell TCR sequencing, consisting of a highly efficient rapid amplification of cDNA ends (RACE)-PCR protocol[264]. While this approach allows the identification of TCRs from original precursor frequencies <0.1% of $CD3^+$ T cells, it consequently requires large amounts of starting material. Given the low *ex vivo* frequency of HBV-specific T cells in donors with resolved infection, e.g. approx. 0.01-0.001% core protein-specific $CD4^+$ T cells[135], and the limited access to suitable donors, the *in vitro* stimulation and expansion of T-cell clones appears to be a safer though more time consuming choice.

Instead of expanding and sequencing T-cell clones from a single cell level, TCR α- and β-chain analysis can also be done through bulk sequencing of T-cell lines. This was demonstrated among others by Lorenz et al. By cross-combining the most common α- and β-chains through cloning and transduction into healthy donor-derived T cells, a functional HPV-specific TCR was ultimately identified[238]. Although bulk sequencing of TCR α- and β-chains may yield adequate results under optimal stimulation conditions and increases the chance of obtaining a positive hit, it greatly diminishes the variety of TCRs since it is only feasible to test the most dominant TCR α- and β-chain combinations.

Innovative commercial technical devices now also allow the rapid identification of large T-cell repertoires with single cell resolution, such as the Chromium Single Cell Immune Profiling Solution by 10x Genomics or the Optofluidic Technology by Berkeley Lights. While these systems certainly improve workflow efficiency, they remain costly and are equally susceptible to the problem of identifying T-cell specificity as the procedures described above.

3.2 T-cell receptor constitution and epitope recognition

Regarding the structural constitution and target epitopes of the final T-cell receptor constructs generated throughout this thesis, several points of interested are elaborated below, addressing the receptor expression, their constant domains as well as the relevance of the targeted HBV epitopes.

3.2.1 "Weakly" expressing TCRs

Throughout this thesis, TCRs $1C11_{C61}$, $1D12_{C113}$ and $1A2_{S17}$ repeatedly displayed a "weak" expression pattern, e.g. concerning their cell surface expression on RD114 producer cells (see section 2.2.2) and their relatively low MFI in flow cytometry, especially in relation to their rather high number of integrates when compared to other TCRs (see section 2.3.1). In line with these findings, Thomas et al. recently distinguished between endogenous TCRs that were "dominant" and therefore able to co-express alongside a transgenic TCR, whereas others were "weak" and less stable with regards to cell surface expression[276]. Similar observations had been made previously[163,226,277,278], however, Thomas et al. were now able to link this expression pattern to the α- and β-chain variable domain framework regions outside the antigen-binding CDR loops. While the surface expression of "weak" TCRs was 3- to 5-fold lower in Jurkat cells compared to "dominant" TCRs, intracellular α- and β-chain mRNA levels were similar. By analyzing distinct clonotypes of "dominant" and "weak" origin, they were able to show an over-representation of α- and β-chains TRAV13-2, TRBV9, TRBV7-9 and TRBV2 in "weak" TCRs. In addition, they observed a significant enrichment of particular amino acids at certain positions of the "dominant" TCRs' sequence which seem to influence interchain affinities. The specific exchange of individual amino acids between "dominant" and "weak" TCRs allowed to narrow down most of the "dominant" effect to the following three residues: a hydrophobic amino acid at position 96 of the variable α-chain ($L96\alpha_V$) as well as arginine and tyrosine at positions 9 and 10 of the β-chain ($R9\beta_V$ and $Y10\beta_V$). The modification of $L96\alpha_V$, $R9\beta_V$ and $Y10\beta_V$ enhanced antigen-specific function and substantially improved T-cell avidity, as measured by peptide titration and dose response profiling. Furthermore, it reduced the level of mis-pairing between the transgenic and endogenous TCR[276].

Notably, several parallels to these observations were seen during this thesis: TCRs $1C11_{C61}$ and $1D12_{C113}$ indeed contain TRBV9 and TRBV7-9, respectively (see Table 3). Also, despite differences in TCR surface expression, intracellular staining in RD114 cells was comparable (see 2.2.2, Figure 15A). This suggests that a specific

exchange of residues L96α_V, R9β_V and Y10β_V may optimize T-cell avidity and functionality in particular for TCRs 1C11$_{C61}$, 1D12$_{C113}$ and possibly also for 1A2$_{S17}$ or other “weakly” expressing TCRs. Moreover, this engineering approach could enhance therapeutic safety as a result of reduced mis-pairing events with unknown and potentially harmful specificity.

Alongside the intrinsic nature of the TCR variable region, it seems as though CD3 may be a rate limiting factor for expression (personal communication with Hans Stauss, University College London, based on preliminary data). Along these lines, Heemskerk et al. among others have proposed the accessibility to the CD3 complex as an explanation[163,226], hypothesizing that TCRs with high interchain affinity may preferentially assemble with CD3 in particular in the presence of competing TCRs[226]. This could also explain why the transient expression of mCD3 lead to improved cell surface expression of “weakly” expressing TCRs in RD114 cell lines, attributing a stabilizing role of the CD3 complex for T-cell receptor assembly.

3.2.2 TCR α- and β-chain murine constant regions

In order to improve expression, stability and functionality of the transgenic receptor, the addition of murine constant regions with additional cysteine residues has proven successful[166,167] and was therefore also applied to the constructs generated throughout this thesis. However, this approach carries an increased risk of immunogenicity as the murine domains are susceptible to being recognized as foreign by the human immune system. In effect, early studies with adoptively transferred T cells reported T-cell mediated rejection of grafted lymphocytes in five of six HIV-infected individuals due to the introduction of a foreign antigen[279]. In a clinical trial of metastatic cancer based on autologous T cells retrovirally transduced with fully murine TCRs, approx. one in four patients developed antibodies to the transgene which in some cases lead to reduced antigen-specific cytokine release[280]. Similarly, patients receiving T cells transduced with CARs containing murine antibody sequences have been shown to develop a humoral immune response to the murine protein post-transfer[174,281]. To overcome this obstacle, Sommermeyer et al. identified nine amino acids to be mainly responsible for an improved cell surface expression and T-cell functionality. By introducing this so-called minimal murinization, a 50-85% surface expression and function compared to fully murine constant regions was achieved. The identified residues appeared to be “hidden” inside the TCR structure, therefore being less likely to cause the development of an antibody response[282].

With this in mind, one may consider changing the TCR constructs to the minimal murinization variant, maintaining a largely human, codon-optimized constant domain. While this certainly decreases the risk of immunogenicity in a therapeutic application, it comes with a potential reduction of expression and functionality. This could be compensated by additional measures to enhance the TCR α/β-chain assembly, e.g. as discussed above.

3.2.3 Target epitopes

The TCRs generated throughout this thesis are specific for HBV epitopes C61, C91, C113, preS9, S17, S21, S36 and P774. In general, HBV infection has been shown to induce $CD4^+$ and $CD8^+$ T-cell responses specific for the core[118,283-285], envelope[286,287], polymerase[285,288] and X protein[289,290]. Whereas $CD8^+$ T cells seem to recognize epitopes located in different HBV proteins, there is evidence suggesting that $CD4^+$ T-cell responses are mainly directed against core and polymerase epitopes, both in blood samples from donors with resolved infection[135] as well as in patients with chronic HBV infection[140,291-293]. What is more, Rivino et al. could show that the presence of T cells specific for the HBV core- and/or polymerase protein correlated with an absence of viral flares in patients after discontinuation of NUC treatment[292]. This could potentially indicate a status of immune control which is followed by HBsAg loss in approximately 20% of all cases[69]. Considering the relevance of $CD4^+$ T cells for the induction of a functional B-cell response, the epitope preS9 can be seen of special importance. $CD4^+$ T cells redirected with TCR $3G3_{preS9}$ would be expected to prime B cells specific for the large envelope protein, which are more likely to generate neutralizing antibodies[44,294].

Taken together, this could imply that those TCRs specific for C61, C91, C113 and P774 as well as preS9 are of particular therapeutic relevance. Nevertheless, given the initial *in vitro* stimulation to enrich and expand HBV-specific clones prior to cell sorting, it is not possible to determine whether these epitopes represent the most immunodominant targets for T-cell clones *ex vivo*. In addition, one must also keep in mind that epitopes which frequently induce T-cell clones within an individual or within the population are not always the ones with the highest antiviral efficacy[295]. And lastly, each MHC molecule presents different requirements for peptide binding and therefore potentially favors different epitopes[295]. Thus, any given epitope's significance remains to be evaluated in combination with a patient's or population's predominant HLA type.

3.3 Characterization of TCRs

To compare their potential for adoptive T-cell therapy, the TCRs generated in this thesis were subjected to in depth characterization studies. As such all TCRs were found to recognize intracellularly processed antigen, with the exception of TCRs $3G3_{preS9}$ and $1D4_{P774}$, which could not be tested due to limited availability of the respective antigen. This confirms the recognition of epitopes processed via the MHC class II pathway (see section 1.2.1) and implies the activation of TCR-transduced $CD4^+$ T cells in a physiological setting of HBV infection. Further points of interested that were experimentally addressed include the recognition of different HBV genotypes, MHC restriction, T-cell receptor functional avidity, and functionality of both $CD4^+$ and $CD8^+$ T cells transduced with MHC class II-restricted TCRs, all of which will be reviewed in more detail below.

3.3.1 Recognition of different HBV genotypes

The recognition of particular HBV genotypes is especially relevant when looking at genotype distribution in regions of high HBV endemicity. As such, TCRs recognizing genotypes B and C could be applied preferentially in Eastern Asia and the Asian Pacific States, where HBV prevalence is high (see section 1.1.2) and novel therapeutic approaches are more urgently needed. Of course, a broader recognition of HBV genotypes implies an overall wider therapeutic applicability, with those TCRs recognizing all tested genotypes A, B, C and D being of particular interest for T-cell therapy. Interestingly, S36-specific TCRs failed to recognize any other genotype than A. Changes in the epitope sequence could affect the peptide binding core and expose different residues to the CDR3 regions of the TCR. Alanine scans in combination with *in silico* modelling of the peptide:MHC-TCR interaction would give futher insight into the importance of individual amino acids. Further aspects of TCR cross-reactivity with different epitopes are discussed in the context of MHC restriction below.

3.3.2 MHC restriction

Countless studies among different populations or ethnicities have investigated single nucleotide polymorphisms (SNPs) within HLA loci and/or HLA type associations with susceptibility or resistance to HBV infection, HBV resolution and spontaneous clearance, as well as disease progression to liver cirrhosis or HCC[82]. Indeed, several of the restricting MHC class II molecules identified for the TCRs during this thesis (see section 2.3.2 Table 6) have been linked to a beneficial effect with regards to HBV infection. For example, HLA-DR1 was shown to correlate with protection against HBV

in a Romanian study with 60 CHB carriers and 100 healthy controls[296], so was HLA-DQB1*06:03 in a Chinese cohort with 256 CHB patients compared to 433 healthy individuals[297], HLA-DPB1*02:01 in an Asian study including Japanese, Korean, Hong Kong, and Thai subjects[298] and HLA-DRB1*13:01/13:02 in Gambia, Germany, Korea and China[299-302]. What is more, HLA-DR13 has repeatedly been associated with resolution of HBV infection worldwide[299,303-306]. None of the MHC restrictions identified throughout this thesis were found to be associated with a negative effect regarding HBV infection, with the exception of HLA-DR7, which has been correlated with susceptibility to infection and failure in response to HBsAg vaccination[27,307] as well as persistent HBV infection[308]. This observation is well compatible with the structural explanation of HLA-DR7 given by Doganay et al.[309]. With regards to disease progression, Doganay et al. found HLA-DR7 to be a negative indicator of liver cirrhosis, possibly explained by the polymorphic structure of the HLA-DR7 T-cell recognition site leading to an overall weakened T-cell interaction and immune response[309].

Overall, these studies indicate how different HLA alleles in their role as crucial elements of the immune system positively affect the clinical outcome of HBV infection. Whether this is due to the MHC molecule itself, the epitope it presents or the T-cell repertoire, it implies that targeting these MHC molecules may be advantageous in a therapeutic setting. Nevertheless, MHC restrictions have to be placed into the context of different populations or ethnicities. As such, it is important to analyze HLA prevalence in regions where HBV is highly endemic (see 1.1.2). Substantial differences with regards to allele frequencies e.g. in Germany and China for all MHC restrictions identified during this thesis illustrate this matter (Figure 22A). Of all 23 TCRs, the HLA-DPB1*02:01-restricted ones would have the broadest therapeutic applicability, given that this allele is most common with a frequency of 23% in China's Han population[310]. Except for HLA-DP*02:01 and DRB1*07:01, the MHC molecules correlated with a positive effect on HBV infection, i.e. HLA-DRB1*01:01, HLA-DRB1*13:01 and HLA-DQB1*06:03, are all markedly less prevalent in China compared to Germany.

One possibility to increase the therapeutic range of adoptive T-cell therapy is to use a TCR which binds promiscuously yet specifically to several MHC class II molecules, such as TCR $1C11_{C61}$ (see section 2.3.2 Figure 21). One has to distinguish different levels of promiscuity when examining the interaction between MHC molecule, peptide and T-cell receptor. Promiscuous binding of a peptide to various MHC class II

molecules is common[311-313] and was also shown during this thesis (see 2.3.2 Table 6). Given the open binding grove of the MHC class II molecule, a higher degree of structural variability within the range of bound peptides is comprehensible. However, many studies have equally observed promiscuous recognition on behalf of a T-cell receptor or T-cell clone[311,314]. This cross-reactivity can either imply a single peptide being recognized on different MHC molecules[315,316] or several peptides being detected by a TCR or T-cell clone on one or more MHC molecules [317-319]. The former indeed has the potential of broadening therapeutic applicability for a given TCR in adoptive T-cell therapy, as illustrated by the cumulative frequencies in Germany and China of all MHC molecules promiscuously bound by TCR $1C11_{C61}$ (Figure 22B). The latter, however, has to be analyzed more critically. On the one hand, TCR target cross-reactivity seems to be a biological necessity, since the calculated number of potential peptide epitopes exceeds the natural TCR repertoire diversity[317,320,321]. On the other hand, it represents an increased risk for any therapeutic application as the recognition of additional peptides, in particular self-peptides, could induce graft-versus-host disease (GvHD) and/or autoimmunity. In fact, promiscuous T-cell receptors have been associated with both protective and pathogenic roles for a range of diseases[322-325], but have also been linked to autoreactivity[316,326-330]. In one clinical trial, the use of an affinity-enhanced MAGE-A3-specific TCR for melanoma and myeloma therapy even had fatal cardiotoxic consequences, most likely due to cross-reactivity with an epitope derived of the myocardial protein titin[331]. This is why further experiments are necessary to determine whether the cross-reactive binding of TCR $1C11_{C61}$ is confined to a broader MHC repertoire or includes other peptides with a particular focus on self-peptides. A large study featuring hundreds of peptides recognized by five T-cell receptors found the promiscuous effect to be explained by a motif resemblance between the cross-reactive peptides with the original binding sequence[320]. This might be an optimistic sign for TCR $1C11_{C61}$, since viral epitopes are expected to have little sequence resemblance with self-peptides.

Interestingly, structural studies of TCR-pMHC complexes have given evidence that the T-cell receptor CDR1 and CDR2 regions primarily engage with the MHC molecule itself, while the CDR3 loop, which is conformationally more flexible, preferentially engages with the presented peptide[332-334]. This was also experimentally validated by Brawley et al., showing that the substitution of single amino acids in the α-chain CDR2 controlled whether a TCR recognized its target peptide exclusively on DR7 or on DR1, DR4, DR5 and DR7[335]. Taking a closer look at the MHC molecule's site of interaction, the promiscuous affinity of a virus-specific T-cell clone towards DRB1*04:02,

DRB1*11:02, and DRB1*13:01 was associated with a common amino acid sequence at positions 67-71 within the DR β-chain. Upon mutation of this shared motif, the cross-reactivity was lost[315]. Taken together, a thorough bioinformatical and experimental analysis of both the TCR $1C11_{C61}$ and the promiscuously recognized MHC molecules could provide a deeper insight into the observed binding behavior and may consequently allow fine-tuning of the TCR-pMHC interaction.

3.3.3 T-cell receptor affinity and functional avidity

When discussing TCR affinity, it is important to distinguish between the actual interaction of the TCR with the pMHC complex and the contact between the T cell as a whole with its respective target cell. The latter has often been termed “functional avidity”, since it is measured by functional readouts, e.g. cytokine production, proliferation or cytotoxicity, upon target peptide and is typically given as the half-maximal effective peptide concentration EC_{50}. It can be influenced by a range of factors such as the TCR expression or the presence of adhesion molecules and coreceptors[336]. Measuring actual TCR affinity is technically more challenging. It has been achieved through surface plasmon resonance[229,337,338] and peptide-MHC dissociation studies based on MHC multimers[339,340] or streptamers[265] with results usually being expressed as dissociation rates k_{off}, binding constants K_D or binding half-life $t_{1/2}$, with $K_D = \frac{k_{off}}{k_{on}}$. Both functional avidity and affinity are equally important terms to describe the T-cell interaction with its target and functional avidity was determined during this thesis, since affinity measurement techonology was not available.

The human T-cell repertoire is a result from positive and negative selection occurring in the thymus. Negative selection leads to the elimination of T cells with high affinity against self-peptides from the natural repertoire in order to prevent autoimmunity. Consequently, tumor-reactive TCRs which commonly recognize self-derived peptides have been shown to be of approximately 10-fold lower affinity when compared to virus-specific TCRs with foreign targets[229]. This is why adoptive T-cell therapy especially for tumor treatment has seen efforts to enhance TCR affinity[341-344]. While this strategy has had therapeutic success on the one hand[344], other studies have revealed the danger of increased cross-reactivity with severe adverse effects[331,345,346]. Finding the “right” affinity window for TCRs in adoptive T-cell therapy has therefore been discussed from different angles, suggesting even the use of multiple receptors with different affinities simultaneously or in a sequential approach[347].

Virus-specific TCRs, in contrast, are generally of higher affinity, since they recognize foreign antigen in a *de novo* encounter and have hence eluded the negative selection process[229]. Numerous studies in murine models and humans have gathered evidence that T cells of higher functional avidity are more efficient in clearing viral infection[336,348-351]. For example, this correlation was frequently observed in HIV infection[352-354]. What is more, evidence in mice has demonstrated that high-avidity T-cell clones are preferentially expanded upon induction of an immune response and are selected for the formation of immunological memory[339,355-360]. On the other hand, evidence emerged that TCR affinity is not necessarily a measure of T-cell functionality[361,362]. Too high affinity may even inhibit functionality as permanent target attachment could prevent a T-cell from serial engagement and killing[181]. Furthermore, potential disadvantages of high-avidity T cells include a higher risk for clonal exhaustion and the selection of viral escape mutants[354]. Indeed, high-avidity T cells in viral infection were shown to express higher levels of T-cell exhaustion markers such as PD-1[363,364]. Consequently, low-avidity T cells could benefit from longer survival rates and may be less exposed to activation-induced cell death[336]. Intermediate TCR affinity, however, has been favored by kinetic models of serial TCR engagement with the pMHC complex. Therefore, an optimal window of binding half-life $t_{1/2}$ has been proposed for T-cell activation to take place[365]. If $t_{1/2}$ is too short, intracellular signaling events are not completed and the T cell is not activated. If $t_{1/2}$ is too long, T cells are prevented from serially engaging with numerous pMHC targets[366,367].

For $CD4^+$ T cells, in particular, there is fewer conclusive data available. Some studies have indicated that MHC class II-restricted TCRs generally show weaker binder affinities in comparison with MHC class I-restricted TCRs[368,369]. Cole et al. have investigated this in more detail, showing an approx. 5-fold difference regarding the K_D of MHC class II- and MHC class I-restricted TCRs, which is mainly traced back to a slower k_{on} rate while k_{off} seems to be similar[271]. Taken together, TCRs of different affinities each have their assets and drawbacks. Both high- and low-avidity TCRs may come with their own therapeutic benefits, which have to be carefully evaluated – more ist not always better.

3.3.4 Cytokine secretion

Both $CD4^+$ and $CD8^+$ T cells transduced with MHC II-restricted TCRs were polyfunctional and produced varying amounts of cytokines such as TNF-α, IFN-γ and IL-2. There is ample evidence that $CD4^+$ T cells directly contribute to the protection against a variety of viral pathogens through cytokine production[86]. The TCR-

transduced CD4+ T cells analyzed in this thesis showed a Th1-phenotype[370] most likely induced by the anti-CD3/anti-CD28 and IL-2 stimulation mimicking antigen encounter during the transduction procedure. Th1 cells, which typically produce high amounts of IFN-γ, represent the main CD4+ T cell subset generated *in vivo* in response to viral infection[86]. In the context of HBV, promising data suggests a strong antiviral effect of cytokines. As such, IFN-γ and TNF-α were shown to impact the stability of cccDNA via the nuclear deaminases APOBEC3A and APOBEC3B, leading to subsequent cccDNA degradation[371]. This cytokine-mediated HBV inhibition was also observed upon the addition of HBV-specific redirected T cells without direct cell-cell contact[371]. In an *ex vivo* study of patients with chronic HBV infection, the presence of IFN-γ-secreting CD4+ T cells was associated with viral clearance. HBV core-specific TNF-α-producing CD4+ T cells, however, were linked to liver damage in patients with hepatitis B flares[132]. Overall, given their cytokine profile, TCR-transduced HBV-specific CD4+ T cells could contribute to the success of adoptive T cell therapy with a direct antiviral effect on infected hepatocytes upon activation by MHC II-expressing cells in the liver.

3.3.5 Cytotoxic activity of CD4+ T cells

During this thesis, CD4+ T cells transduced with MHC class II-restricted TCRs were shown to secrete varying amounts of GrzB and selectively kill MHC class II-expressing peptide-pulsed target cells (see section 2.3.7). Cytotoxic activity of both CD8+ and CD4+ T cells was observed for 15 TCRs, some of which showed nearly equal killing capacity in both subsets (e.g. DR1-restricted C61- and S36-specific TCRs), whereas others displayed a more pronounced difference in killing efficiency and kinetics (e.g. $TCR1F1_{S17}$).

The presence and characteristics of CD4+ cytotoxic T lymphocytes have frequently been described in the literature [372,373]. Initially, they were believed to be an artefact of long-term *in vitro* cell culture, however, over time, numerous studies also reported their existence *ex vivo*[374-379]. CD4+ CTLs are believed to use two effector mechanisms which are also employed by CD8+ CTLs and natural killer cells[373]: the Fas/Fas ligand-mediated pathway, which ultimately leads to caspase 3-induced apoptosis, or the direct lysis of target cells via perforin and granzymes[380], which has been investigated to a larger extent comparing both CD4+ and CD8+ CTLs. For example, in a murine model of acute lymphocytic choriomeningitis virus (LCMV) infection, Hildemann et al. demonstrated that formation of CD4+ CTLs was induced and led to comparable *in vivo* killing via perforin and granzyme in relation to CD8+ CTLs[381]. Of interest, they noted

that the kinetics of cytotoxic activity of $CD4^+$ T cells were slightly delayed compared to $CD8^+$ CTLs[381]. A different study, analyzing $CD4^+$ and $CD8^+$ memory cells from human healthy donors *ex vivo,* showed that both cell types secreted similar amounts of GrzB, however, $CD8^+$ T cells stored more GrzB intracellularly than $CD4^+$ T cells[382]. This may explain some of the *in vitro* observations made during this thesis. The percentage of $GrzB^+$ cells was consistently lower for $CD4^+$ T cells compared to $CD8^+$ T cells. Since the intracellular cytokine staining assay reflected both stored and secreted GrzB due to the use Brefeldin A (BFA) to inhibit vesicular secretion, the larger fraction of $GrzB^+$ $CD8^+$ T cells may be explained by a larger proportion of pre-existing stored granules. Similarly, the slower killing kinetic of $CD4^+$ T cells, which was especially prominent in certain TCRs, such as $1F1_{S17}$, correlated with observations made in the literature.

It is still unclear whether $CD4^+$ CTLs are a novel T-cell lineage or have evolved from other T helper cell subsets acquiring cytotoxic characteristics along the way[372,373]. Several groups have therefore investigated factors that determine the cytotoxic fate of $CD4^+$ T cells. The transcription factors T-bet and Eomes have been known for some time as regulators of $CD8^+$ T-cell fate [383,384]. This was also confirmed for $CD4^+$ CTLs: T-bet expression seems to be indeed necessary for Th1 lineage development and IFN-γ production; in addition, it can bind to promotors of GzmB and perforin both in $CD4^+$ and $CD8^+$ T cells[385,386]. Eomes has been equally implicated in GrzB expression and the induction of cytotoxicity in $CD4^+$ T cells [387,388]. Takeuchi et al. have recently linked the class I-restricted T cell-associated molecule (CRTAM) to elevated levels of Eomes and GrzB in $CD4^+$ CTLs[389]. CRTAM, which is known to play a role for $CD8^+$ T-cell maturation during an immune response in secondary lymphatic tissue[390], is expressed in a small fraction of $CD4^+$ T cells upon activation and seems to be indispensable for $CD4^+$ T cells in order to acquire cytotoxic characteristics[389]. While $CD4^+$ CTLs seem to be able to differentiate from a number of different $CD4^+$ T-cell subsets, Th1-derived $CD4^+$ CTLs producing IFN-γ, alone or in combination with TNF-α and IL-2, seem to be most common[372]. Further studies indicate that the development of $CD4^+$ CTLs is induced in response to antigen stimulation and IL-2 [391,392]. This, in turn has been linked to Eomes expression and ultimately the secretion of IFN-γ and GrzB[91,383]. In view of the transduction protocol in this thesis, which relies on IL-2 stimulation as well as anti-CD3/CD28 stimulation mimicking antigen encounter, a differentiation of MHC class II-transduced $CD4^+$ T cells into CTLs seems plausible. Further experiments are needed to clarify the involvement of T-bet, Eomes

and possibly CRTAM. A phenotypic analysis of the transduced cell population would help to establish a link to Th1 or other T-cell subsets.

$CD4^+$ T cells with cytotoxic functionality were predominantly observed in studies of murine or human viral infection[372,373]. In humans, they have been associated with a protective role in influenza [393], HIV infection[394] and cytomegalovirus (CMV) disease[395]. Similar observations were made in mouse models with murine poxvirus[396] and gammaherpesvirus infection[397]. Little is known, however, with regards to their role in HBV infection. A study comparing 76 individuals with chronic HBV, HCV or HBV/HDV (co-)infection to healthy controls showed a fluctuating, but significantly elevated number of $CD4^+$ T cells expressing perforin *ex vivo*; rates of perforin-positive $CD4^+$ T cells were particularly high in HBV/HDV co-infected patients, reaching up to 25% of all $CD4^+$ T cells in some cases[398]. Perforin expression was most pronounced in patients with advanced hepatitis and was linked to liver damage as measured by ALT levels and platelet counts[398]. This has led to the hypothesis that $CD4^+$ CTLs in chronic hepatitis may in fact contribute to immunopathology[373]. Further studies are certainly needed to elucidate the role of $CD4^+$ CTLs in chronic hepatitis in more detail.

One central question is, which cells would be primarily targeted by the cytotoxic activity of HBV-specific $CD4^+$ T cells. Since MHC class II expression is a basic requirement, professional APCs in the liver may be at risk. These include dendritic cells, Kupffer cells and monocyte-derived myeloid cells[399], though dendritic cells might be protected from cytotoxic $CD4^+$ CTL activity, given that they express the GrzB inhibitor SerpinB9[400]. Moreover, T cells upregulate CTLA-4 upon activation by dendritic cells which then competes with CD28 for interaction with CD80. This prevents the formation of an effective immunological synapse and thereby protects the antigen-presenting cell from becoming a T cell target[401]. Liver sinusoidal endothelial cells also express low levels of MHC class II, which can be enhanced through exposure to pro-inflammatory cytokines such as IFN-γ[402]. While hepatocytes do not express MHC class II under normal conditions, some upregulation has been reported during inflammation[399,403]. In a murine model, MHC class II-expressing hepatocytes have even been shown to function as antigen-presenting cells, specifically activating $CD4^+$ T cells[403]. Taken together, the outcome of using $CD4^+$ CTLs for adoptive T-cell therapy of HBV infection is still unclear and remains to be thoroughly investigated. While they may cause liver damage and inflammation in chronic infection on the one hand, targeting MHC class II-expressing hepatocytes could also contribute to tumor clearance in HBV-related hepatocellular carcinoma. In

any case, an attempt to control the desired phenotype of transduced CD4$^+$ T cells via adjustments in the expansion and transduction protocol should be made, with a subsequent analysis regarding T-cell subsets prior to transfer into the patient.

3.3.6 CD8$^+$ T cells transduced with MHC class II-restricted TCRs

During this thesis, MHC class II-restricted TCRs were shown to be functional not only in CD4$^+$ T cells, but also in CD8$^+$ T cells, i.e. in the absence of the CD4 coreceptor. CD8$^+$ T cells secreted higher levels of IFN-γ and GrzB and displayed a slightly more rapid killing kinetic compared to CD4$^+$ T cells for some TCRs, e.g. 1F1$_{S17}$.

So far, several attempts have been made to switch TCRs among CD4$^+$ and CD8$^+$ T cells, mostly focusing on the delivery of an MHC class I-restricted TCR to CD4$^+$ T cells to harvest the benefits of CD4$^+$ T cells for tumor therapy [404-408]. It was shown that the functionality of MHC class I-restricted TCRs in CD4$^+$ T cells is only preserved for high-affinity TCRs, which are independent of coreceptor CD8 binding to MHC class I[409,410]. This dilemma has been resolved alternatively through co-introduction of the CD8 molecule or CD8α chain along with the transgenic receptor[406,410]. In tumor mouse models, MHC class I-restricted CD4$^+$ T cells provided critical T-cell help[411,412] or in fact mediated an equally effective anti-tumor activity as CD8$^+$ T cells alone[408]. Engels et al. even showed superior activity of CD4$^+$ T cells: while CD4$^+$ T cells transduced with a high-affinity MHC class I-restricted TCR exerted long-term anti-tumor function *in vivo*, CD8$^+$ transduced with the same TCR failed to persist[407]. In a human *in vitro* model with melanoma-derived patient samples, comparable cytokine secretion and killing capacity between MHC class I-restricted CD4$^+$ and CD8$^+$ T cells was observed[404]. CD4$^+$ T cells transduced with several different HBV-specific MHC class I-restricted TCRs showed slightly reduced lysis in an *in vitro* model of HBV infection compared to CD8$^+$ T cells, which came along with an approximately 10-fold reduced functional avidity[193]. While clinical trials in particular for melanoma treatment with MHC class I-restricted TCRs have been performed based on the adoptive transfer of a mixed product containing both transduced CD4$^+$ and CD8$^+$ T cells[154,344,413] with some reporting good persistence of CD4$^+$ T cells[344,413], the actual *in vivo* activity of MHC class I-restricted CD4$^+$ T cells in humans remains to be characterized.

Meanwhile, the introduction of MHC class II-restricted TCRs in CD8$^+$ T cells has rarely been attempted. One group compared CD4$^+$ and CD8$^+$ T cells transduced with an HLA-DQ5-restricted TCR targeting the dead box RNA helicase Y *in vitro*. They reported similar killing capacity of both transduced CD4$^+$ and CD8$^+$ T cells, but

cytokine secretion was significantly diminished in CD8$^+$ T cells. Co-introduction of the CD4 coreceptor in CD8$^+$ T cells increased their cytolytic capacity, however, cytokine secretion remained low[414]. Others have observed rare accounts of naturally occurring MHC class II-restricted CD8$^+$ T cells in HIV infected individuals [415] as well as SIV infected macaques[416]. Evidently, ample opportunity remains to further investigate the nature and potential of MHC class II-restricted CD8$^+$ T cells based on the panel of TCRs characterized throughout this thesis.

The relationship between TCR affinity, coreceptor presence and T-cell functionality remains intriguing. As mentioned above, high-affinity TCRs can function coreceptor independent and coreceptor co-introduction seems to somewhat compensate for TCR affinity resulting in an overall increased functionality. Some studies have attempted to set an affinity threshold for CD8 coreceptor independence of MHC class I-restricted TCRs with results ranging from K_D values of 200 µM[417] to 3 µM[418]. An approximately 10-fold lower functional avidity was repeatedly observed in CD4$^+$ T cells when compared to CD8$^+$ T cells expressing the same MHC class I-restricted TCR[193,406], which may approximately quantify the contribution of coreceptor to functional avidity for a range of TCRs. Attempts to explain the significance of the coreceptor have thus far been based on two mechanisms: first, it is believed to stabilize the interaction between TCR and pMHC through direct binding of the MHC molecule; second, it is thought to promote the recruitment of essential signaling components to the cytoplasmatic side of the TCR-pMHC complex, therefore facilitating the TCR signaling process[419,420]. For CD8, the stabilizing interaction between coreceptor and MHC class I molecule has been investigated and quantified in detail[421]. For CD4, however, the binding to MHC class II has been extremely hard to measure and is of notably low affinity, suggesting only a minor if any influence on the factual TCR affinity[422,423]. Nevertheless, CD4 is regularly needed for antigen recognition *in vivo* and increases T-cell sensitivity[423-425]. Hence, this has mainly been attributed to TCR signaling enhancement via its strong intracellular association with tyrosine kinase Lck[426,427]. Lck is crucial for signaling initiation since it phosphorylates the immunoreceptor tyrosine-based activation motifs (ITAMs) within the TCR-associated CD3ζ domains, thereby starting the TCR signaling cascade[428]. Through its localization in close proximity of the TCR-pMHC complex, CD4 is thought to control the spatial accumulation of Lck in the immunological synapse[420]. A similar model has also been proposed for the CD8 coreceptor with the absence of CD8-MHC interaction leading to reduced phosphorylation of CD3-ζ[429]. In contrast to CD4, both the stabilizing effect with regards to the TCR-pMHC complex as well as T-cell signaling enhancement seem

equally important functions of CD8[420]. The minor role of CD4 regarding the actual TCR-pMHC interaction may explain why all the MHC class II-restricted TCRs characterized throughout this thesis were equally able to activate $CD8^+$ T cells, despite their different functional avidities. Further experiments with e.g. CD4 k.o. cells could help clarify and quantify the role of the CD4 coreceptor in T-cell receptor signaling.

3.4 Further aspects to consider for clinical application

Last but not least, to advance the therapeutic application towards a clinical direction, certain aspects regarding adoptive T-cell therapy should be taken into account and will be elaborated below.

3.4.1 Delivery method of the transgenic receptor

To generate TCR-redirected T cells from healthy donors during this thesis, γ-retroviral transduction was used for transgene delivery. Potent retroviral titers were produced with the help of RD114 cells[430], enabling high transduction rates of TCR-redirected T cells. For in depth characterization studies, retroviral transduction has proven convenient, since large amounts of highly transduced T cells could be produced with simple and effective techniques. However, for the clinical application of TCR-redirected T cells, viral vectors are thought to have certain drawbacks. While their production under clinical grade conditions is rather costly, they also raise safety concerns, such as the random integration into the human genome, potentially resulting in oncogene activation or tumor suppressor gene disruption. Although such cases are rare[431] and T cells engineered with viral vectors have been safely applied in several clinical studies[432,433], there have been occasional reports of transgene insertion e.g. leading to the overgrowth of a single lentivirally transduced T cell clone[434]. This is why one has to remain aware of this risk and consider alternatives.

Electroporation of IVT mRNA represent a non-viral alternative for gene transfer and is widely used in the field of adoptive T-cell therapy with numerous ongoing clinical trials[435]. Its main advantage is enhanced safety due to the limited persistence of the transgene. Given their transient nature, however, redirected T cells need to be administered repeatedly to patients in order to achieve an efficient response, which increases manufacturing complexity. Moreover, in case an immune response towards the transgene is triggered, intermittent dosing of the T cell product may possibly cause anaphylaxis, as reported during a clinical trial targeting mesothelin[436]. Most importantly, transiently acting engineered T cells have a limited capacity for the

formation of immunological memory. Stably redirected T cells, on the other hand, have the potential of self-renewal and differentiation into memory cells. Adoptively transferred stable effector T cells have reportedly lead to the formation of new memory cells in mice, primates and humans[437-440]. In fact, it was shown that the adoptive transfer of a single T cell clone with a central memory phenotype was sufficient to induce self-renewing memory cells while mounting an effective immune response via the differentiation of effector T cells[441]. For anti-CD19 CAR T cells in the treatment of leukemia, clinical data has given evidence that sustained remission was only reached if antigen-specific T cells were perceived for months or years in patients after the initial transfer[172,442,443].

For adoptive T-cell therapy of chronic HBV and HBV-HCC, both discussed delivery methods have been used to date. In a clinical proof-of-concept trial for the treatment of two HBV-HCC patients post liver-transplant, IVT mRNA-engineered T cells proved to be safe with no occurrence of treatment-related adverse advents and a moderate clinical efficacy in one patient. Nevertheless, trial patients received as many as 40 doses of T cell injections, underlining the necessity of repeated T cell administration when using an IVT RNA approach[207]. Retrovirally transduced T cells, on the other hand, largely outperformed transiently redirected T cells in a chimeric mouse model repopulated with HBV-infected human hepatocytes[204,205]. Remarkably, the combination therapy with HBV entry inhibitor myrcludex B even resulted in long-term control of HBV infection[205]. In a first-in-man proof-of-concept study in 2015, a patient with metastatic HCC following liver transplantation received a single dose of stably transduced HBsAg-specific T cells[206]. Although there was only a limited clinical effect during the period of observation, this case study underlined the feasibility and safety of transferring stably transduced T cells, since no adverse effects or additional liver inflammation were encountered[206]. Taken together, stably redirected HBV-specific T cells have so far given no cause for safety concerns[205,206] while showing a more potent and sustained anti-tumor effect in a humanized mouse model[205]. This argues for maintaining retroviral transduction as delivery method of choice for MHC II-restricted TCRs, in particular since a potent cell product was achieved, with a high percentage of transduced effector cells and a favorable safety profile given the consistently low number of transgene integrates (see section 2.3.1).

In view of the advantages of stable transgene integration, alternative methods circumventing the drawbacks of viral delivery are being investigated. The currently most sophisticated approach consists in CRISPR-Cas9-mediated site-directed

insertion of the transgenic TCR into the endogenous TCR α-chain locus while simultaneous knocking out the endogenous TCR α- and β-chains[171]. This not only enhanced the safety of the redirected T cell product as mispairing with and expression of the endogenous TCR was completely abolished, it also brought the additional benefit of the transgenic TCR being placed under the endogenous promotor, resulting in a more physiological regulation pattern compared to virally transduced T cells[171]. Of note, T cells engineered with a transgenic receptor in the endogenous TCR locus demonstrated similar or even superior anti-tumor efficacy in murine models compared to virally transduced T cells[444], possibly due to the more physiological mechanism of TCR regulation preventing T cells from premature exhaustion. A recent first-in-human clinical trial demonstrated the safety of CRISPR-Cas9-engineered T cells in patients with refractory cancer[445]. Further research is needed to give a more detailed insight into the functionality of such engineered T cells *in vivo* and in patients. Certainly, this represents an exciting and promising technology, which is relevant to consider also for the insertion of MHC class II-restricted TCRs. To increase the safety of ACT, additional safety switches that allow the depletion of engineered T cells post transfer have been devised. As such, inducible caspase 9 (iCASP9)[446] or the truncated epidermal growth factor receptor (tEGFR)[447] represent the most promosing options. The translation of these approaches to the context of HBV infection, however, remain to be shown.

3.4.2 Product composition

When applying MHC class II-restricted TCRs to adoptive T-cell therapy, one could either consider transferring only $CD4^+$ T cells or a mixture of $CD4^+$ and $CD8^+$ T cells. Hunder et al. administered NY-ESO-1-specific $CD4^+$ T-cells to a patient with metastatic melanoma and observed complete remission, conferred by an endogenous T-cell response, hinting towards a “real” helper function of the transferred T cells[187]. Ideally, a similar effect would be achieved by transferring HBV-specific $CD4^+$ T cells, however, this remains to be experimentally shown. Based on the proof-of-concept experiment performed during this thesis, it has become apparent that $CD4^+$ T cells may be especially helpful when $CD8^+$ T cell functionality is limited (see 2.4.3). To date, most clinical CAR-T cell applications rely on a mixed product composed of $CD4^+$ and $CD8^+$ T cells, either with a random composition or with a 1:1 ratio. The expert opinion in this field is that the exact product formulation is secondary, as long as a clinically effective cell clone or population is present, since preferential *in vivo* expansion can quickly change any pre-defined numbers; on the other hand, a 1:1 ratio

of $CD4^+$ and $CD8^+$ T cells makes a cell therapy product more consistent and may therefore be beneficial for quality control and clinical release.

An important aspect to consider in addition to specific ratios may be the transfer of defined T-cell subsets. Indeed, studies with $CD8^+$ T cells in mice and primates have shown that the T cell subset represents a major factor for T-cell persistence and functionality *in vivo*: CMV-specific T cells with a central memory (T_{CM}) but not effector memory (T_{EM}) phenotype induced lasting immunity for several years[440,448]. Similarly, TCR-redirected T cells with a T_{CM} or naïve (T_N) phenotype displayed a superior anti-tumor efficacy than T_{EM} cells in murine melanoma models[449,450]. Sommermeyer et al. investigated the transfer of both $CD4^+$ and $CD8^+$ anti-CD19 CAR T cells at a 1:1 ratio[185]. They found that the efficacy of $CD8^+$ T_{CM} cells was significantly increased upon the addition of $CD4^+$ T cells of various phenotypes, with the effect of $CD4^+$ T_N cells being most pronounced[185]. Klebanoff et al. have reviewed the effect of different T cell subsets in adoptive T-cell therapy and have come to the conclusion that both $CD8^+$ and $CD4^+$ T cells seem to benefit from a less differentiated state regarding engraftment, persistence and anti-tumor immunity[451]. Taken together, finding the right subset for optimal clinical efficacy in the patient may not only enhance the anti-target effect and sustained persistence of the transferred T cell product, it may also allow to lower the numbers of the infused cell product.

3.5 Outlook

Based on the characterization of 23 MHC class II-restricted T-cell receptors presented throughout this thesis, experiments to further elucidate the role of $CD4^+$ T cells for the therapy of chronic HBV infection and HBV-HCC will be performed with a selected number of T-cell receptors. The recommended TCRs for subsequent functional studies as well as an outlook into future experiments are outlined below.

3.5.1 Selection of TCRs for further studies and therapeutic application

The choice of TCRs for future experiments has to be made taking into account both functionality and practicability regarding cell culture and *in vivo* models. Given the HLA type of different cell lines for *in vitro* testing (see section 2.4.1), either SK-HEP-1 or THP-1 are suitable MHC class II-expressing cell lines which could be used in combination with HLA-DR11- and HLA-DR1-restricted TCRs, respectively. In addition, *in vitro* experiments can be conducted by using monocyte-derived dendritic cells as antigen-presenting cells, as described in section 2.4.3. While this is a more time-consuming approach, it allows higher flexibility regarding the HLA type and

represents a more physiological model to study the effect of $CD4^+$ T cells on $CD8^+$ T cells. In terms of *in vivo* models, the availability of an HLA-DR1-HHDII transgenic mouse model (see section 2.4.2) clearly favors the use of HLA-DR1-restricted TCRs.

As discussed in section 3.3.3, it is not yet clear, if TCRs of higher functional avidity are always preferential towards TCRs of lower functional avidity. While this is an important question to address in a separate manner, it seems reasonable to continue the study of MHC class II-restricted TCRs with TCRs of high functional avidity, since they are likely to result in a higher measurable readout in most assays. Of the HLA-DR1-restricted TCRs, C61-specific TCRs 1C11 and P74 in particular showed a high functional avidity, both in terms of EC_{50} as well as signal to background proliferation. Both TCRs recognized HBV genotypes A, B, C and D, which allows to potentially treat a large range of patients, especially from regions where HBV is highly endemic. TCR $1C11_{C61}$ is especially interesting considering its promiscuous binding towards several MHC molecules. While this broadens its therapeutic applicability as illustrated above (see section 3.3.2), it also remains to be evaluated thoroughly from a safety point of view. S36-specific TCRs 1E1, 2H12, 2E7 and 1B9 also showed a high functional avidity in terms of EC_{50}; however, $1B9_{S36}$ displayed a rather low signal to background ratio in terms of proliferation. Whether this is a reproducible characteristic of the T-cell receptor itself, or an artefact caused by the batch of transduced T cells, remains to be shown. With regards to different HBV genotypes, the S36-specific TCRs have clearly less therapeutic potential than the two C61-specific TCRs mentioned above. All four S36-specific TCRs recognized mostly HBV genotype A. TCR $1B9_{S36}$ and $2H12_{S36}$ additionally detected genotype B and C, respectively, albeit at a lower level than genotype A. While this still makes S36-specific TCRs interesting to study in *in vitro* and *in vivo* models, it limits their therapeutic applicability to patients infected with HBV genotype A or possible B and C, for $1B9_{S36}$ and $2H12_{S36}$, respectively.

Whereas the killing capacity of $CD4^+$ T cells has been an interesting observation, it is not necessarily needed for $CD4^+$ T cells to exert their physiological helper function. Nevertheless, all C61- and S36-specific TCRs mentioned specifically above induced comparable cytotoxic activity in transduced $CD4^+$ and $CD8^+$ T cells. With regards to cytokine secretion, T cells transduced with C61- and S36-specific TCRs all secreted high amounts in relation to the full panel of TCRs. Based on the above evaluation, future experimental validation with the aim of therapeutic application should be performed with the selection of MHC class II-restricted TCRs shown in Table 10.

Table 10: Selection of TCRs recommended for further experimental validation. TCRs are displayed with their main characteristics, which make them suitable for functional characterization *in vitro* and *in vivo*.

Peptide	TCR	Donor	MHC restriction	HBV genotypes	EC_{50}	Killing by CD4+ T cells
C61	1C11	1	HLA-DR*0101 + others	A/B/C/D	69 nM	+
	P74	3	HLA-DR*0101	A/B/C/D	47 nM	+
S36	2H12	2	HLA-DR*0101	A/C	8.8 nM	+

3.5.2 *In vitro* experiments

Based on the initial experiments with dendritic cells presented in section 2.4.3, further experiments should be performed to identify the conditions under which $CD4^+$ T cells are able to render T-cell help to $CD8^+$ T cells *in vitro* by varying target peptide concentrations and/or the amount of transduced $CD4^+$ or $CD8^+$ T cells. In addition, TCRs of different affinities may give further insight into this mechanism. To elucidate the conditions of optimal cross-priming, dendritic cells should be incubated with soluble antigen or even HBV virus instead of peptide pulsing. By titrating the amount of soluble antigen or virus, the minimum amount of antigen needed to effectively cross-prime $CD8^+$ T cells in the presence or absence of $CD4^+$ T cells could be determined. This would provide valuable insight into the physiological mechanism of T-cell activation by dendritic cells upon HBV encounter.

To identify a purely cytokine-mediated effect of $CD4^+$ T cells, a transwell assay may prove useful. This experimental setup allows for cells to be co-cultured within the same well separated by a porous membrane, which enables the exchange of cytokines but prevents cell-to-cell contact. This way, one could analyze a potentially cytokine-mediated proliferative stimulus on $CD8^+$ T cells, provided by $CD4^+$ T cells co-cultured with antigen-presenting cells in the transwell. By adding HBV-infected HLA-matched hepatoma cell lines to each setting containing transduced $CD8^+$ T cells, both cross-priming by dendritic cells and the cytokine-mediated effect of $CD4^+$ T cells on $CD8^+$ T cells could be analyzed in terms of cytotoxicity towards target cells.

$CD4^+$ T cells are also known to have a variety of “helper effects” on B cells *in vivo*, such as the induction of proliferation, differentiation and class-switching[452]. To analyze the effect of $CD4^+$ T cells on B cells, using the T_{fh} subset of $CD4^+$ T cells is advisable, since it has been shown to be directly responsible for many of the observed effects[452]. Among others, the CD40-CD40L interaction based on a direct cell-to-cell contact and the secretion of cytokines such as IL-4 and IL-21 have been implicated in B-cell help and could be investigated in a co-culture of HBV virus, transduced $CD4^+$ T cells and B cells, ideally from a donor with resolved infection. The reactivation of memory B

cells could be monitored via proliferation and detection of HBV-specific B cells by flow cytometry, which has been established in the group of Ulrike Protzer (Wolff et al., *manuscript in preparation*).

In addition to the HBV-related studies, the panel of TCRs characterized during this thesis can also be used to address immunological questions of basic science. For example, the role of the CD4 coreceptor remains to be further investigated, e.g. by studying MHC class II-restricted TCRs in CD4 k.o. T cells or by adding a transgenic CD4 coreceptor to CD8 T cells transduced with MHC class II-restricted TCRs. The latter also provide a scientific opportunity of their own, since this phenomenon has not yet been studied in detail in the literature.

3.5.3 *In vivo* experiments

As illustrated in section 2.4.2, an HLA-DR1-HHDII transgenic mouse could potentially serve as an *in vivo* model to study HLA-DR1-restricted TCRs alone or in combination with HLA-A2-restricted TCRs. To this end, the expression levels of the HLA-A2-like HHDII molecule as well as the transgenic HLA-DR1 molecule were confirmed through surface staining and flow cytometry on $CD3^+$ and $CD19^+$ lymphocytes, with high levels of HHDII being expressed on both populations and HLA-DR being expressed at intermediate levels mostly on $CD19^+$ cells. The HHDII expression can be considered physiological, since MHC class I molecules are typically present on nearly all cell types. MHC class II expression, however, is restricted to antigen-presenting cells, which also coincides with the observed results, since $CD19^+$ lymphocytes represent naturally MHC class II-expressing B cells. To further evaluate this model, a transgene expression staining of liver-resident cells such as hepatocytes, Kupffer cells and liver sinusoidal endothelial cells should be performed.

In the group of Ulrike Protzer at the Institute of Virology in Munich, AAV-HBV injection has successfully been used as a chronic HBV model in wildtype and HHDII transgenic mice (Festag et al., *manuscript in preparation*). This method could equally be applied to HLA-DR1-HHDII transgenic mice. In an initial mouse experiment, wildtype $CD4^+$ and $CD8^+$ T cells transduced with an HLA-DR1-restricted TCR and an HLA-A2-restricted TCR, respectively, could be transferred to HLA-DR1-HHDII mice with $CD4^+$ T cells only, compared to $CD8^+$ T cells or both $CD4^+$ and $CD8^+$ T cells at a 1:1 ratio. After $CD4^+$ T cell transfer, a potential readout may include antiviral parameters such as serum HBsAg levels and liver damage measured in ALT levels. In addition, the formation of HBV-specific $CD8^+$ T cells and the induction of a B cell response through

germinal center reactions and the appearance of HBV-specific antibodies may be of interest. When transferring both $CD4^+$ and $CD8^+$ T cells, the persistence and antiviral activity of $CD8^+$ T cells could be assessed in comparison to the transfer of $CD8^+$ T cells only.

Further functional studies with MHC class II-restricted TCRs are also feasible in a humanized mouse model, similar as described in Wisskirchen et al.[205]. This model consists of an immunodeficient mouse, genetically deficient of its own hepatocytes, which can thus be repopulated with human liver cells and subsequently be infected with HBV[453]. With a liver xenograft from a human HLA-A2-DR1-positive donor, assuming the transfer of both hepatocytes and antigen-presenting cells of the liver, the respective MHC class I and II-restricted TCRs could be investigated therapeutically.

3.5.4 Final comment

HBV infection remains a major health problem and current treatment methods are unable to cure the disease. Given the major differences in T-cell responses between the self-limiting course of infection and chronic disease, adoptive T-cell therapy represents a promising therapeutic approach for the treatment of chronic HBV infection and HBV-HCC. In view of the importance of $CD4^+$ T cells for the course of HBV infection, the use of MHC class II-restricted T-cell receptors may have great potential; their clinical benefit, however, remains to be shown. This thesis lays the groundwork for the further use of MHC class II-restricted T-cell receptors in T-cell therapy of chronic HBV infection and HBV-HCC through the identification and in-depth characterization of a set of 23 T-cell receptors specific for the HBV core, envelope and polymerase protein. Certain TCRs in particular, such as $1C11_{C61}$ and $P74_{C61}$, have demonstrated excellent qualities for therapeutic application with regards to their expression levels, MHC restriction, recognition of different HBV genotypes, their functional avidity and their functionality in $CD4^+$ and $CD8^+$ T cells *in vitro*. Taken together, the MHC class II-restricted T-cell receptors generated and characterized during this thesis provide a valuable tool for the study of $CD4^+$ T cells and their role in HBV infection and cure and remain to be further studied regarding their therapeutic potential for ACT *in vivo.*

4 Materials and Methods

4.1 Materials

4.1.1 Devices and technical equipment

Product	Supplier
Agarose gel electrophoresis PowerBac Basic	Bio Rad
AutoMACS	Miltenyi
Bacterial incubator	Heraeus Holding GmbH
Bacterial shaker	INFORS AG
Cell sorter FACS Aria II	BD
Cell sorter MoFlo II	Beckman Coulter
Centrifuge 5417R	Eppendorf
Centrifuge 5920R	Eppendorf
CytoFLEX S	Beckman Coulter
DynaMag™-15 Magnet	Thermo Fisher Scientific
DynaMag™-2 Magnet	Thermo Fisher Scientific
ELISA-Reader infinite F200	Tecan
Filtermat-96 Harvester for MicroBeta	PerkinElmer
Freezing device	Nalgene
Fusion Fx7	Peqlab
Incubator Heracell 150	Heraeus Holding GmbH
LightCycler® 480 II	Roche Diagnostics
MicroBeta TriLux 1450	PerkinElmer
Nalgene Mr. Frosty Freezing Container	Sigma-Aldrich
NanoDrop One	Thermo Scientific
NucleoCounter NC-250	chemometec
OctoMACS	Miltenyi
Professional TRIO Thermocycler	analytik jena
Rotator SB3	Stuart
Sterile hood HERA safe	Thermo Scientific
Thermo Mixer F1.5	Eppendorf
Water bath WNB 10	Memmert GmbH
xCELLigence RTCA	ACEA Biosciences

4.1.2 Consumables

Product	Supplier
0.2ml Thin-walled 8 Tube & Domed Cap Strips for PCR	Thermo Scientific
96-well plates for qPCR, FrameStar 480/96	4titude
Cell culture flasks and plates	TPP
Falcon® Non-Tissue Culture-Treated Plate 24-well	Corning
Falcon® Cell strainer 100 mm	Corning
Cryo vials	Greiner Bio One
Cuvettes	Implen
ELISA 96-well plates Nunc MaxiSorb	Thermo Scientific
E-Plate 96	ACEA Biosciences
FACS 96-well V-bottom plates	Roth
Falcon tubes 15 ml / 50 ml	Greiner Bio One
Falcon® 5 mL Round Bottom Polystyrene Test Tube	BD

Filcons 030-33 S	Biogenetics Steriline
Filtermat A	PerkinElmer
Filters 0.45 µm/0.2 µm	Sarstedt
MS Columns	Miltenyi
Needles	Braun
Pipette tips and filter pipette tips 10 µl - 1 ml	Biozym / Greiner Bio One / Gilson
Pipettes 2, 5, 10, 25, 50 ml	Greiner Bio One
Reaction tubes 0.5, 1.5, 2 ml	Greiner Bio One, Eppendorf
Reagent reservoirs, sterile	Corning
Surgical Disposable Scalpels	Braun
Syringes	Braun
TopSeal-A Plus	PerkinElmer

4.1.3 Chemicals, reagents and media supplements

Product	Article no.	Supplier
0.5% Trypsin-EDTA (10x)	15400-054	Thermo Fisher Scientific
2-Mercaptoethanol 50 mM	31350-010	Thermo Fisher Scientific
3H-Thymidine, spec. activity: 2 Ci/mmol, 5 mCi	Net027A005MC	PerkinElmer
BetaPlate Scint	1205-44	PerkinElmer
Biocoll Separating Solution	L6115	Merck
Blasticidine	46-1120	Thermo Fisher Scientific
Bovine Serum Albumin	A2153	Sigma-Aldrich
Brefeldin A	B5936	Sigma-Aldrich
Cyclosporin A	30024	Sigma-Aldrich
Dimethyl sulfoxide	D5879-100ML	Honeywell
Ethylene diamine tetraacetic acid (EDTA)	8043.2	Roth
Fetal Bovine Serum, Heat Inactivated	10500-064	Thermo Fisher Scientific
Geneticin / G418 50 mg/ml	10131-027	Thermo Fisher Scientific
Gentamicin	PZN 03928180	ratiopharm
Heparin-Natrium 25000	PZN 03029843	ratiopharm
HEPES Buffer Solution, 1 M	15630-056	Thermo Fisher Scientific
Human serum	-	AG Protzer
Hyclone FetalClone II	SH30066.03	GE
Hydrocortison 100mg	PZN 01877030	Pfizer
Insuman® Rapid 100 I.E./ml (Insulin human)	PZN 05961106	Sanofi-Aventis
L-Glutamine, 200 mM	25030-081	Thermo Fisher Scientific
NEAA, 100x	11140-035	Thermo Fisher Scientific
OPTI-MEM I Reduced Serum Medium	31985-062	Thermo Fisher Scientific
Pen/Strep, 10,000 U/ml	15140-122	Thermo Fisher Scientific
peqGOLD Agarose, universal	35-1020	VWR
Phorbol-12-myristate-13-acetate	P8139	Sigma-Aldrich
Phosphate buffered saline pH 7.4 (10x)	70011-036	Thermo Fisher Scientific
PROLEUKIN 18 x 106 IE, recombinant human IL-2	1-22475; PZN 1265031	Novartis
Recombinant human GM-CSF	300-03	Peprotech
Recombinant human IL-4	200-04	Peprotech
RetroNectin (r-Fibronectin CH-296)	T100A/B	TaKaRa
rh IL-15	1413-010	CellGenix
rh IL-7	1410-010	CellGenix
RPMI medium 1640 (1x)	22409-015	Thermo Fisher Scientific
S.O.C. Medium	15544034	Thermo Fisher Scientific
Sodium butyrate 98%	B5887	Sigma-Aldrich
Sodium chloride	3957.2	Roth
Sodium pyruvate, 100 mM	11360-039	Thermo Fisher Scientific

TRIzol Reagent	15596018	Thermo Fisher Scientific
Tryptone	8952.2	Roth
Williams E medium	12551-032	Thermo Fisher Scientific
Yeast extract	2363.3	Roth

4.1.4 Enzymes and proteins

Enzyme	Article no.	Supplier
FastAP Thermosensitive Alkaline Phosphatase	EF0651	Thermo Fisher Scientific
T4 DNA Ligase	EL0011	Thermo Fisher Scientific
FastDigest NotI	FD0593	Thermo Fisher Scientific
FastDigest EcoRI	FD0274	Thermo Fisher Scientific
FastDigest Bsp1407I	FD0933	Thermo Fisher Scientific
FastDigest HindIII	FD0504	Thermo Fisher Scientific
FastDigest OliI	FD1634	Thermo Fisher Scientific

Protein	Source
HBcAg 13.3.2017 0.8 mg/ml	Centro de Ingeniería Genética y Biotecnología de Cuba (CIGB)
HBsAg 13.3.2017 0.51 mg/ml	Centro de Ingeniería Genética y Biotecnología de Cuba (CIGB)

4.1.5 Kits

Kit	Article no.	Supplier
Dynabeads™ Human T-Expander CD3/CD28	11141D	Thermo Fisher Scientific
EndoFree Plasmid Maxi Kit	12362	Qiagen
First Strand cDNA Synthesis Kit for RT-PCR (AMV)	11483188001	Roche
Fixation/Permeabilization Solution Kit	554714	BD
GeneJET Gel Extraction Kit	K0692	Thermo Fisher Scientific
GeneJET Plasmid Miniprep Kit	K0503	Thermo Fisher Scientific
High Pure PCR Product Purification Kit	11732668001	Roche
Human CD4 MicroBeads	130-045-101	Miltenyi
Human CD8 MicroBeads	130-045-201	Miltenyi
Human IFN Gamma Uncoated ELISA	88-7316-88	Thermo Fisher Scientific
Human IFN-γ Secretion Assay (PE)	130-054-201	Miltenyi
Human Pan Monocyte Isolation Kit	130-096-537	Miltenyi
Human TNF alpha Uncoated ELISA	88-7346	Thermo Fisher Scientific
Human TNF ELISA Set	555212	BD
Human TNF-α Secretion Assay (PE)	130-091-269	Miltenyi
Lipofectamine 2000 Transfection Reagent	11668019	Thermo Fisher Scientific
NucleoSpin Tissue - DNA, RNA, and protein purification	740952.250	Macherey-Nagel
Phusion® Hot Start Flex 2X Master Mix	M0536	New England Biolabs
PuReTaq Ready-To-Go PCR Beads	27-9557-02	GE Healthcare
SuperScript™ III First-Strand Synthesis SuperMix for qRT-PCR	11752050	Thermo Fisher Scientific
TaqMan™ Fast Advanced Master Mix	4444964	Thermo Fisher Scientific
VersaComp Antibody Capture Bead Kit	B22804	Beckman Coulter

4.1.6 Buffers

Buffer	Component	Concentration
MACS buffer	PBS	
	EDTA	2 mM
	BSA	0.5%
FACS buffer	PBS	
	BSA	0.1%

4.1.7 Blood donors and cells

Donor	Age	Sex	HBV infection status	DRB1*	DQB1*	DPB1*	DQA1*	DPA1*	DRB3*	DRB4*	DRB5*
1	52	M	resolved	01:01, 13:01	05:01, 06:03	02:01, 04:01	01, 01	01:03	02:02	n.d.	n.d.
2	33	F	resolved	01:01, 07:01	02:02, 05:01	03:01, 11:01	01, 02:01	01:03, 02:01	n.d.	01:01	n.d.
3	63	M	acute, resolving	01:01, 03:01	02:01, 05:01	03:01, 04:01	n.a.	n.a.	n.a.	n.a.	n.a.
4	30	F	resolved	01:01, 11:04	03:01, 05:01	04:01, 04:02	01:01, 05:01	01:03	02:02	n.d.	n.d.
5	24	M	acute	13:01, 14:54	05:03, 06:03	03:01	01, 01	01:03	02:02	n.d.	n.d.
6	57	M	acute, resolving	04:03, 11:04	03:01, 03:02	04:01, 15:01	03:01, 05:05	01:03, 01:04	02:02	01:03	n.d.

All B-LCLs from healthy, HLA-typed donors (Table 5) were generated through transformation with Epstein-Barr virus (EBV) (see 4.2.2.9) and cultured in RPMI full.

Cell line	Description	Medium	Source
single HLA transfectant DAP3	single HLA transfectant adherent fibroblasts	RPMI full + G418	AG Sette, LJI
B95-8	semi-adherent cells for generation of EBV SN	RPMI full	AG Protzer
GALV	293T, stably transfected with MLV gag-pol and gibbon ape leukemia virus env	DMEM full	AG Caruso, CHU de Québec
Hep3B	human hepatoma cell line	DMEM full	AG Protzer
HepaRG	human hepatoma cell line	WilliamsE for HepaRG	AG Protzer
HepG2	human hepatoma cell line	DMEM full	AG Protzer
HuH7	human hepatoma cell line	DMEM full	AG Protzer
Jurkat	T-cell line, lacking the enodgenous TCR	hTCM	AG Protzer
JY	commercially available B-LCL	RPMI full	AG Krackhardt, TUM
OZB	commercially available B-LCL	RPMI full	AG Krackhardt, TUM
PBMC feeder cells	PBMC mix of several donors	hTCM	AG Protzer, own production
RD114	293T, stably transfected with MLV gag-pol and feline endogenous virus RD114 env	DMEM full	AG Caruso, CHU de Québec
SK-HEP-1	human hepatoma cell line	DMEM full	AG Knolle, TUM
Stbl3	chemically competent *E. coli*	LB medium	Thermo Fisher Scientific
single HLA transfectant RM3	single HLA transfectant Raji-based susp. cells	RPMI full + G418/blasti	AG Sette, LJI
THP-1	human monocyte-like cell line	RPMI full + β-mercapto	AG Protzer
TUBO	commercially available B-LCL	RPMI full	AG Krackhardt, TUM

4.1.8 Media

Medium	Component	Conc. (M) / vol. (ml)
freezing medium	FBS	90%
	Dimethyl sulfoxide	10%
human T cell medium (hTCM)	RPMI 1640	500 ml

	FBS	50 ml
	Pen/Strep, 10,000 U/ml	5.5 ml
	L-Glutamine, 200 mM	5.5 ml
	NEAA, 100x	5.5 ml
	Sodium pyruvate, 100 mM	5.5 ml
	HEPES Buffer Solution, 1M	5.5 ml
	Gentamicin	15µg/ml
hTCM + human serum (HS)	RPMI 1640	500 ml
	Human serum	50 ml
	Pen/Strep, 10,000 U/ml	5.5 ml
	L-Glutamine, 200 mM	5.5 ml
	NEAA, 100x	5.5 ml
	Sodium pyruvate, 100 mM	5.5 ml
	HEPES Buffer Solution, 1M	5.5 ml
	Gentamicin	208 µl
Lysogeny broth (LB) medium pH 7.0	Tryptone	10 g
	Yeast extract	5 g
	NaCl	5 g
	H_2O	add to 1 l
RPMI full medium	RPMI 1640	500 ml
	FBS	50 ml
	Pen/Strep, 10,000 U/ml	5.5 ml
	L-Glutamine, 200 mM	5.5 ml
	NEAA, 100x	5.5 ml
	Sodium pyruvate, 100 mM	5.5 ml
RPMI full + β-mercapto	RPMI 1640	500 ml
	FBS	50 ml
	Pen/Strep, 10,000 U/ml	5.5 ml
	L-Glutamine, 200 mM	5.5 ml
	NEAA, 100x	5.5 ml
	Sodium pyruvate, 100 mM	5.5 ml
	β-mercaptoethanol	0.05 nM
RPMI full + G418	RPMI 1640	500 ml
	FBS	50 ml
	Pen/Strep, 10,000 U/ml	5.5 ml
	L-Glutamine, 200 mM	5.5 ml
	NEAA, 100x	5.5 ml
	Sodium pyruvate, 100 mM	5.5 ml
	G418	200 µg/ml
RPMI full + G418/blasti	RPMI 1640	500 ml
	FBS	50 ml
	Pen/Strep, 10,000 U/ml	5.5 ml
	L-Glutamine, 200 mM	5.5 ml
	NEAA, 100x	5.5 ml
	Sodium pyruvate, 100 mM	5.5 ml
	G418	700 µg/ml
	Basticidine	12 µg/ml
wash medium	RPMI 1640	500 ml
	Pen/Strep, 10000 U/ml	5.5 ml
Williams E for HepaRG	Williams E medium	500 ml
	FCS Hyclone	50 ml
	Pen/Strep, 10,000 U/ml	5.5 ml
	L-Glutamine, 200 mM	5.5 ml
	Insuline, 155 nM	320 µl
	Hydrocortisone, 5.5 µg/ml	600 µl
	Gentamicin, 80 µg/ml	1 ml

4.1.9 Antibodies and stains

Antigen / stain	Fluorophore	Dilution / Conc.	Clone	Article no.	Supplier
mouse IgG	FITC	1:50	polyclonal	115-096-071	Jackson
HLA-DP	-	1:100	B7/21	origin: mouse	LJI, in house
HLA-DQ	-	1:100	SVPL3	origin: mouse	LJI, in house
HLA-DR	-	1:100	LB3.1	origin: mouse	LJI, in house
human BD Fc Block	-	1:20	-	564220	BD Pharmigen
human CD11c	PerCP	1:100	Bu15	337234	BioLegend
human CD14	BV510	1:100	M5E2	301841	BioLegend
human CD3	FITC	1:100	UCHT1	11-0038-42	Invitrogen
human CD4	APC	1:100	OKT4	17-0048-42	Invitrogen
human CD4	FITC	1:50	OKT4	11-0048-42	Invitrogen
human CD4	PerCP	1:100	SK3	344623	BioLegend
human CD8	PB	1:50	SK1	344717	BioLegend
human CD8	FITC	1:100	RPA-T8	11-0088-42	Invitrogen
human CD86	APC	1:100	IT2.2	305412	BioLegend
human Granzyme B	PB	1:100	N4TL33	48-8896-42	Invitrogen
human IFN-γ	AF700	1:100	B27	557995	BD Pharmigen
human IL-2	PE-Cy7	1:100	MQ1-17H12	25-7029-42	Invitrogen
human TNF-α	APC	1:100	MAb11	502912	BioLegend
live/dead stain	NIR	1:1000	-	L10119	Invitrogen
live/dead stain	Aqua	1:1000	-	L34965	Invitrogen
live/dead stain	PI	1-2 µg/ml	-	CN74.3	Roth
murine β constant	PE	1:200	H57-597	553172	BD Pharmigen
murine CD3	PB	1:100	17A2	48-0032-82	Invitrogen

4.1.10 Peptides

All peptides were ordered from Peptides & Elephants or JPT Peptide Technologies with >80% purity (assessed by HPLC). Lyophilized peptides were dissolved in 100% DMSO and stored at -80 °C at 5 mM stock or 1 mM working concentration.

Protein	Peptide	Sequence	Protein	Peptide	Sequence
Core	C7	KEFGATVELLSFLPSDFF	Envelope	preS9	RKGMGTNLSVPNPLGFFP
	C28	RDLLDTASALYREALESP		preS83	GILTTVSTIPPPASTNRQ
	C61	WGELMTLATWVGNNLEDP		preS116	HPQAMQWNSTAFHQALQD
	C84	LVVNYVNTNMGLKIRQLL		preS134	PRVRGLYFPAGGSSSGTV
	C91	TNMGLKIRQLLWFHISCL		S8	FLGPLLVLQAGFFLLTRI
	C113	ETVLEYLVSFGVWIRTPP		S17	AGFFLLTRILTIPQSLDS
	C119	LVSFGVWIRTPPAYRPPN		S21	LLTRILTIPQSLDSW
	C133	RPPNAPILSTLPETTVVR		S36	WTSLNFLGGSPVCLGQNS
Polymerase	P104	NEKRRLKLIMPARFYPTH		S69	CPGYRWMCLRRFIIFLFI
	P412	PNLQSLTNLLSSNLSWLS		S93	FLLVLLDYQGMLPVCPLI
	P454	SGLSRYVARLSSNSRIFN		S158	FAKYLWEWASVRFSWLSL
	P524	SPFLLAQFTSAICSVVRR		S165	WASVRFSWLSLLVPFVQW
	P573	TNFLLSLGIHLNPNKTKR		S179	FVQWFVGLSPTVWLSAIW
	P636	QRIVGLLGFAAPFTQCGY		S199	WYWGPSLYSIVSPFIPLL
	P650	QCGYPALMPLYACIQSKQ		S209	VSPFIPLLPIFFCLWVYI
	P774	LRGTSFVYVPSALNPADD			
	P827	HLPVRVHFASPLHVAWRP			

4.1.11 Plasmids

For each TCR generated throughout this thesis, three plasmids were used. The individual fully human α- and β-chain were cloned separately into the pMP71 vector[225]. In addition, codon-optimized α- and β-chain variable regions were cloned into the pMP71 vector along with murine α- and β-chain constant regions, as described in 4.2.1.9. Additional plasmids used throughout this thesis are listed below.

Plasmid	Description	Source
pcDNA_mCD3	murine CD3 δγεζ-chains seperated by 2A linkers	addgene, followed by own cloning
pMP71_c.o.+Cys_TCR_Uckert	Source for murine α and β constant	AG Uckert
pMP71_GFP	Source for pMP71 vector backbone	AG Uckert

4.1.12 Primers

To identify the TCR variable α- and β-chain by degenerate primer PCR, the forward primer VPANHUM with reverse primer CA2 and forward primers VP1 and VP2 with reverse primer CP1 were applied. Specific primers for TCR identification included 34 different α-chain (5'Vαx) and 37 different β-chain (5'Vβx) forward primers; they are described in the dissertation of Ingrid Schuster[454].

Forward primers for cloning of TCR α- or β-chains were designed based on the initial 18-20 bp of the respective variable sequence. A reference sequence for the latter was extracted from the National Center for Biotechnology Information (NCBI) sequence viewer (https://www.ncbi.nlm.nih.gov/projects/sviewer/). Forward primers were designed containing a NotI restriction site and Kozak sequence (GCCGCCACC). Reverse primers for the TCR α-chain constant region or TCR β-chain constant region 1 or 2 were used preferentially with an EcoRI restriction site. In case the amplified sequence contained an inherent EcoRI site, Bsp1407I (BsrGI) was used alternatively for the reverse primer.

Primer	Description	Purpose	Sequence
CA1	Primer for cDNA synthesis for TCR α-chain identification	cDNA synthesis	AGACCTCATGTCTAGCACAG
3'TRAC_BsrGI	Reverse primer for TCR α constant with BsrGI	Cloning of TCR chains	CTTGTACATCAGCTGGACCACAGCCGCAGC
3'TRAC_EcoRI	Reverse primer for TCR α constant with EcoRI	Cloning of TCR chains	TGGAATTCTCAGCTGGACCACAGCCGCAGC
3'TRBC1_BsrGI	Reverse primer for TCR β constant 1 with BsrGI	Cloning of TCR chains	TGTGTACATCAGAAATCCTTTCTCTTGACC
3'TRBC1_EcoRI	Reverse primer for TCR β constant 1 with EcoRI	Cloning of TCR chains	TGGAATTCTCAGAAATCCTTTCTCTTGACC
3'TRBC2_BsrGI	Reverse primer for TCR β constant 2 with BsrGI	Cloning of TCR chains	TGTGTACACTAGCCTCTGGAATCCTTTCTC
3'TRBC2_EcoRI	Reverse primer for TCR β constant 2 with EcoRI	Cloning of TCR chains	TGGAATTCCTAGCCTCTGGAATCCTTTCTC
CA2	Reverse primer for TCR α-chain constant region	Identification of TCR variable chain via degenerate primer PCR	GTGACACATTTGTTTGAGAATC
CP1	Reverse primer for TCR β-chain constant region	Identification of TCR variable chain via degenerate primer PCR	GCACCTCCTTCCCATTCAC
VP1	Degenerate forward primer for TCR β-chain variable region	Identification of TCR variable chain via degenerate primer PCR	GCIITKTIYTGGTAYMGACA
VP2	Degenerate forward primer for TCR β-chain variable region	Identification of TCR variable chain via degenerate primer PCR	CTITKTWTTGGTAYCIKCAG
VPANHUM	Degenerate forward primer for TCR α-chain variable region	Identification of TCR variable chain via degenerate primer PCR	TGAGTGTCCCRGARGGDR
3'TCα	Reverse primer for identification of TCR α-chain	Identification of TCR variable chain via specific primer PCR	GGTGAATAGGCAGACAGACTTGTCACTGGA
3'αST	Reverse primer for control sequence TCR α-chain constant region	Identification of TCR variable chain via specific primer PCR	CTT GCC TCT GCC GTG AAT GT
3'Cβll	Reverse primer for identification of TCR β-chain	Identification of TCR variable chain via specific primer PCR	GAT GGC TCA AAC ACA GCG ACC TC
3'βST	Reverse primer for control sequence TCR β-chain constant region	Identification of TCR variable chain via specific primer PCR	GAG GTA AAG CCA CAG TCT GCT
5'αST	Forward primer for control sequence TCR α-chain constant region	Identification of TCR variable chain via specific primer PCR	CTG TGC TAG ACA TGA GGT CT
5'βST	Forward primer for control sequence TCR β-chain constant region	Identification of TCR variable chain via specific primer PCR	AAG CAG AGA TCT CCC ACA C
b constant fw	Forward primer binding 5' end of murine b constant	Overlap extension PCR to create final codon-optimized construct	GAAGATCTGAGGAACGTGACC
b constant rev	Reverse primer binding 3' end of murine b constant	Overlap extension PCR to create final codon-optimized construct	CCGGGGTTCTCTTCCACGTC
b variable fw	Forward primer binding 5' end of b variable gene synthesis	Overlap extension PCR to create final codon-optimized construct	TCCCTCTCTCCAAGCTCACT
b variable rev	Reverse primer binding 3' end of b variable gene synthesis	Overlap extension PCR to create final codon-optimized construct	GCTCGAACAGGGACACCTT
α constant fw	Forward primer binding 5' end of murine a constant	Overlap extension PCR to create final codon-optimized construct	CCGCCGTGTACCAGCTGAA
α constant rev_EcoRI	Reverse primer binding 3' end of murine a constant + EcoRI	Overlap extension PCR to create final codon-optimized construct	TGGAATTCTCAGCTGGACCACAGCC
α variable fw	Forward primer binding 5' end of a variable gene synthesis	Overlap extension PCR to create final codon-optimized construct	AAGCAGGCCGGCGACG
α variable rev	Reverse primer binding 3' end of a variable gene synthesis	Overlap extension PCR to create final codon-optimized construct	TCTGGGGTCCTTCAGCTGGT
PTBP2 forward	Forward primer for PTBP2 genomic reference	Taqman qPCR to determine number of TCR integrates	TCTCCATTCCCTATGTTCATGC
PTBP2 probe	PTBP2 probe with JOE fluorophore and BHQ-1 quencher	Taqman qPCR to determine number of TCR integrates	ATGTTCCTCGGACCAACTTG
PTBP2 reverse	Reverse primer for PTBP2 genomic reference	Taqman qPCR to determine number of TCR integrates	GTTCCCGCAGAATGGTGAGGTG
WPRE forward	Forward primer for WPRE vector element	Taqman qPCR to determine number of TCR integrates	GAGGAGTTGTGGCCCGTTGT
WPRE probe	WPRE-specific probe with FAM fluorophore and BHQ-1 quencher	Taqman qPCR to determine number of TCR integrates	CTGTGTTTGCTGACGCAAC
WPRE reverse	Reverse primer for WPRE vector element	Taqman qPCR to determine number of TCR integrates	TGACAGGTGGTGGCAATGCC
pMP71_fw	Forward primer for sequencing of pMP71 vector-based constructs	Sequencing	GCAGCATCGTTCTGTGTTGT
pMP71_rev	Reverse primer for sequencing of pMP71 vector-based constructs	Sequencing	TTGTCTTGTGGCAATACACC

4.1.13 Software

Software	Description	Supplier
FlowJo v10	Analysis of flow cytometry data	BD
Prism 6.07	Data analysis and statistics program	GraphPad
RTCA 2.0	Measurement and analysis of xCELLigence data	ACEA Biosciences
MicroBeta Software	Measurement of scintillation counts per minute	PerkinElmer
Microsoft Excel	Analysis of ELISA data	Microsoft

4.2 Methods

4.2.1 Molecular biology and cloning

4.2.1.1 *RNA extraction*

To isolate RNA from specific T cell clones, 2 ml cell suspension of expanded T-cell clones in a 12-well-format (as described in 4.2.3.2) were centrifuged for 5 min at 400 x g, RT. The pellet was then resuspended in 1 ml TRIzol reagent (Thermo Fisher Scientific) and incubated for 5 min at RT to lyse the cells. At this point, samples could be stored at -80 °C for up to 6 months. After addition of 200 µl 1-Bromo-3-chloropropane and 15 sec of thorough vortexing, the sample was incubated for 10 min at RT, followed by centrifugation for 15 min at 12'000 x g and 4 °C. The upper aqueous phase was transferred to a new reaction tube, carefully avoiding contamination with the intermediate phase. 500 µl of isopropanol was added and thoroughly mixed by vortexing. Once again, the sample was incubated for 10 min at RT, followed by centrifugation for 10 min at 12'000 x g and 4 °C. The SN was removed and 1 ml 75% ethanol was added to wash the pellet. After vortexing, the sample was centrifuged for 5 min at 7'500 x g, 4 °C. Then, the SN was carefully removed as thoroughly as possibly without touching the pellet. The reaction tube was placed up-side-down on a paper towel to dry the pellet. After approximately 30 min, when the remaining liquid was completely dried out, the pellet was resuspended in 100 µl H_2O and incubated for 10 min at 60 °C. RNA concentration was measured via the Nano Drop One spectral photometer (Thermo Fisher Scientific) and RNA samples were stored at -80 °C.

4.2.1.2 *cDNA synthesis*

cDNA synthesis from RNA of T-cell clones was performed using the SuperScript™ III First-Strand Synthesis kit (Invitrogen) according to manufacturer's instructions. Volumes were downscaled to a total reaction volume of 10 µl, using ≤500 ng of RNA.

For degenerate TCR α-chain PCR, cDNA was additionally synthesized with the First Strand cDNA Synthesis kit (Roche) according to manufacturer's instructions. Volumes were downscaled to a total reaction volume of 10 µl, using ≤500 ng of RNA and the sequence-specific CA1 primer at 1 pmol/µl.

4.2.1.3 *Polymerase chain reaction*

To identify the TCR β-chain by degenerate primer PCR, PuReTaq Ready-To-Go PCR Beads (GE Healthcare) were used with a total reaction volume of 25 µl. The degenerate forward primer VP1 (binding within the variable region) was added at 3.2 pmol/µl final concentration, the reverse primer CP1 (binding in the constant region) was added at 0.32 pmol/µl, with 1.5 µl of cDNA per TCR clone from a 10 µl reaction volume of reverse transcription with the SuperScript™ III First-Strand Synthesis kit (Invitrogen). Whenever VP1 did not yield a PCR product, VP2 was used as an alternative degenerate forward primer, covering an additional, less common group of TCR β-chain variable regions. The expected PCR product measured 400-500 bp in length. The following PCR program was used:

Step	Temp (°C)	Time (min:sec)	Repeat
1	95	02:00	
2	95	00:30	40x
3	50	00:30	
4	72	00:30	
5	72	10:00	
6	4	Pause	

To identify the TCR α-chain by degenerate primer PCR, PuReTaq Ready-To-Go PCR Beads (GE Healthcare) were used with a total reaction volume of 25 µl. The degenerate forward primer VPANHUM (binding within the variable region) and the reverse primer CA2 (binding within the constant region) were added at 1.6 pmol/µl final concentration, with 3 µl of cDNA per TCR clone from a 10 µl reaction volume of reverse transcription with either the SuperScript™ III First-Strand Synthesis kit (Invitrogen) or the First Strand cDNA Synthesis kit (Roche). The expected PCR product measured 400-500 bp in length. The following PCR program was used:

Step	Temp (°C)	Time (min:sec)	Repeat
1	95	10:00	
2	95	01:00	2x
3	50	02:00	
4	72	02:00	
5	95	01:00	40x
6	55	02:00	
7	72	02:00	
8	72	10:00	
9	4	Pause	

To identify the TCR α- or β-chain with a large set of specific primers covering the most common variable chains, PuReTaq Ready-To-Go PCR Beads (GE Healthcare) were used with a total reaction volume of 25 µl. For α-chain identification, the primers were used at the following final concentrations: 5'Vαx (1.2 pmol/µl), 3'TCα (0.8 pmol/µl), 5'αST and 3'αST (0.28 pmol/µl each). For β-chain identification, the primers were used at the following final concentrations: 5'Vβx (1.2 pmol/µl), 3'CβII, 5'βST and 3'βST (0.8 pmol/µl each). "x" stands for a large set of specific forward primers and primer combinations containing "ST" are used to amplify a control sequence within the constant regions of each TCR chain. In each case, 1 µl of cDNA per TCR clone from a 10 µl reaction volume of reverse transcription with the SuperScript™ III First-Strand Synthesis kit (Invitrogen) and the following PCR program were used:

Step	Temp (°C)	Time (min:sec)	Repeat
1	95	02:00	
2	95	00:30	40x
3	56	00:30	
4	72	01:00	
5	72	10:00	
6	4	Pause	

To amplify the TCR α- or β-chain for cloning, Phusion® Hot Start Flex 2X Master Mix (New England Biolabs) was used due to the inherent proof-reading function with a total reaction volume of 50 µl. The forward primer (specific for the respective variable region) and the constant reverse primer were added at 0.5 pmol/µl final concentration, with 2 µl of cDNA per TCR clone from a 10 µl reaction volume of reverse transcription with the SuperScript™ III First-Strand Synthesis kit (Invitrogen). The expected PCR product measured 800-950 bp in length. The following PCR program was used, where x stands for the specific annealing temperature for each primer combination, as derived from the New England Biolabs online calculator (https://tmcalculator.neb.com/):

Step	Temp (°C)	Time (min:sec)	Repeat
1	98	00:30	
2	98	00:10	6x
3	x	00:20	
4	72	00:20	
5	98	00:10	28x
6	72	00:30	
7	72	10:00	
8	4	Pause	

4.2.1.4 *DNA digestion analysis with restriction enzymes*

All restriction enzymes were fast digest variants from Thermo Fisher Scientific. The digestion was performed according to manufacturer's instructions, using 1 µl of enzyme for a maximum of 1 µg of plasmid DNA or 200 ng of PCR product with an incubation time of 30 min at 37 °C. In case of plasmid backbone digestion, 1 µl of alkaline phosphatase (Thermo Fisher Scientific) was added for an additional 10 min at 37 °C, to dephosphorylate the backbone and prevent recircularization. This was followed by heat inactivation of the alkaline phosphatase for 5 min at 75 °C. The digested DNA was analyzed in a 1% agarose gel for subsequent preparation with the objective of further cloning or for analytical purposes in case of a control digestion after plasmid DNA preparation.

4.2.1.5 *DNA ligation*

DNA ligation was performed using the T4 DNA Ligase (Thermo Fisher Scientific) according to manufacturer's instructions for 1 h at RT with a total reaction volume of 20 µl, 100 ng of vector backbone and a 3:1 molar ratio of insert. This was followed by heat inactivation of the T4 DNA ligase for 5 min at 70 °C.

4.2.1.6 *Transformation of chemically competent bacteria*

The transformation and amplification of the retroviral vector pMP71 was conducted in chemically competent Stbl3 (Invitrogen), since they feature reduced recombination of cloned DNA and are thus recommended for plasmids containing repeat elements. Stbl3 cells were thawed on ice. 2 µl DNA ligation product or 50-100 pg plasmid DNA were added per tube of Stbl3 and incubated for 30 min on ice. The sample was then submitted to heat shock for 45 sec at 42 °C in a heating block, followed by 2 min on ice. After adding 500 µl of S.O.C. medium (Thermo Fisher Scientific), cells were allowed to recover for 1 h at 37 °C, shaking slowly. The cells were centrifuged for approx. 1 min at 6000 x g and the supernatant was decanted. The pellet was

resuspended in the remaining liquid and plated on antibiotic-containing agar plates, i.e. 100 µg/ml ampicillin for vector pMP71.

4.2.1.7 *DNA isolation and purification*

Plasmid DNA was isolated from bacterial suspensions according to manufacturer's instructions using the respective kits: GeneJET Plasmid Miniprep Kit (Thermo Fisher Scientific) for 2-4 ml cell suspension; EndoFree Plasmid Maxi Kit (Qiagen) for a maximum cell suspension volume "x" in ml, calculated with the formula OD*x = 80. Importantly, the OD of bacterial suspensions for a midi preparation of the retroviral plasmid pMP71 should not exceed 1.2, since higher values have resulted in reduced DNA yield. The resulting DNA concentration and quality were measured via the Nano Drop One spectral photometer (Thermo Fisher Scientific). Purified plasmid DNA was assessed by control digestion with 1 U/µg fast digest restriction enzymes (Thermo Fisher Scientific) for 30 min at 37 °C and 1% agarose gel electrophoresis. Plasmids showing the correct digestion pattern were sent to Eurofins Genomics for sequencing.

Genomic DNA for HLA typing and integrate quatification was extracted from cell suspensions (PBMCs or B-LCLs) according to manufacturer's instructions using the NucleoSpin Tissue kit (Macherey-Nagel).

PCR products were purified according to manufacturer's instructions using the High Pure PCR Product Purification Kit (Roche), in case a distinct band was visible in a 1% agarose gel prepared for analytical reasons. If several products of different sizes were amplified during PCR, the whole PCR product was loaded on a 1% agarose gel and the right size band was extracted using the GeneJET Gel Extraction Kit (Thermo Fisher Scientific) according to manufacturer's instructions.

All DNA samples were stored at -20 °C.

4.2.1.8 *Sequencing of DNA*

Sanger sequencing reactions were ordered at Eurofins Genomics. Constructs based on the pMP71 vector were sequenced using the primers pMP71_fw and pMP71_rev.

4.2.1.9 *Codon optimization and overlap extension PCR*

The sequences of the TCR α- and β-chain variable region were both codon-optimized *in silico* and subsequently synthesized via Thermo Fisher Scientific, using the online tool Invitrogen GeneArt Gene Synthesis with the integrated GeneArt GeneOptimizer.

To enable the subsequent overlap extension PCR, all sequences were ordered with the following additional 5' and 3' nucleotide sequences:

TCR chain	5'/3' end	nucleotide sequence
α variable	5'	aagcaggccggcgacgtggaagagaaccccgggccc
α variable	3'	atccagaaccccgagcccgccgtgtaccagctgaaggaccccaga
β variable	5'	tccctctctccaagctcacttacaggcggccgccacc
β variable	3'	gaagatctgaggaacgtgacccccccccaaggtgtccctgttcgagc

An overlap extension PCR was conducted to create a construct containing the following elements in the indicated order: β variable region, murine β constant region, P2A site, α variable region, murine α constant region. All PCRs were performed with the Phusion® Hot Start Flex 2X Master Mix (New England Biolabs) and a total reaction volume of 50 µl. Primers were added at 0.5 pmol/µl final concentration each.

For the first step of amplification, 10 ng of each gene synthesis product was used to amplify the α and β variable regions and 10 ng of the plasmid pMP71_c.o.+Cys_TCR_Uckert was used to amplify the α and β murine constant regions. The following PCR program was used, where "x" stands for the specific annealing temperature for each primer combination: α-chain variable region (68 °C), β-chain variable region (65 °C), murine α-chain constant region (65 °C), murine β-chain constant region (63 °C).

Step	Temp (°C)	Time (min:sec)	Repeat
1	98	00:30	
2	98	00:10	30x
3	x	00:20	
4	72	00:20	
5	72	10:00	
6	4	Pause	

The PCR products measuring 300-500 bp in length were purified by gel excision and served as templates for the next step, the amplification of the full α- or β-chain as a combination of human variable and murine constant region. To this end, 100 ng of each variable and constant PCR product were submitted to an initial stepwise cooling phase prior to the addition of primers, allowing the annealing of the overlapping templates. After adding primers to a final concentration of 0.5 pg/µl, the PCR amplification of the full α- or β-chain was then completed. The following PCR program was used, where "x" stands for the specific annealing temperature for each primer combination: α-chain (65 °C), β-chain (68 °C).

Step	Temp (°C)	Time (min:sec)	Repeat
1	98	01:00	5x
2	93	00:30	
3	88	00:30	
4	83	00:30	
5	78	00:30	
6	72	00:30	
7	4	Pause	
Add primer at 0.5 pg/µl			
8	98	01:00	
9	98	00:10	30x
10	x	00:20	
11	72	00:45	
12	72	10:00	
13	4	Pause	

The PCR products measuring 800-1000 bp in length were purified by gel excision and served as templates for the next step, the amplification of the full construct, containing both the β- and α-chain combined by a P2A site. To this end, 100 ng of each β- and α-chain PCR product were submitted to an initial stepwise cooling phase prior to the addition of primers, similar to the above. After adding primers to a final concentration of 0.5 pg/µl, the PCR amplification of the full construct was completed. The following PCR program was used:

Step	Temp (°C)	Time (min:sec)	Repeat
1	98	01:00	
2	93	00:30	
3	88	00:30	
4	83	00:30	
5	78	00:30	
6	72	00:30	
7	4	Pause	
Add primer at 0.5 pg/µl			
8	98	01:00	
9	98	00:10	30x
10	65	00:20	
11	72	01:00	
12	72	10:00	
13	4	Pause	

The resulting PCR product measuring approx. 1700-1800 bp in length was cloned into the vector backbone of the pMP71 plasmid using the restriction enzymes NotI and EcoRI.

4.2.1.10 *Quantitative PCR*

The number of TCR integrates in a transduced cell population was determined in a quantitative polymerase chain reaction of viral woodchuck hepatitis virus

postregulatory element (WPRE), which is located downstream of the TCR coding sequence in the 3' end untranslated region of the retroviral vector pMP71, relative to the genomic PTBP2, as described elsewhere[455]. The protocol and plasmid standard were kindly provided by the Hannover Medical School, Institute of Experimental Hematology.

4.2.1.11 *HLA typing*

HLA typing was realized by cooperation partner Dr. Klaus Witter, Labor für Immungenetik und molekulare Diagnostik in Munich, based on PCR identification from genomic DNA samples.

4.2.2 Cell culture methods

4.2.2.1 *Culturing conditions for adherent and suspension cells*

For maintenance, all adherent cells were split 1:10 every 3-4 days depending on their confluency. Their respective media and media compositions are listed under 4.1.7 and 0. B-LCLs were cultured preferentially at a density of 0.2-0.5x10^6 cells/ml in RPMI full. Primary human T cells were cultured in hTCM + 50 U/ml IL-2 for maintenance or 180 U/ml IL-2 for expansion with an optimal density of 0.5-1x10^6, as described in 4.2.2.6. THP-1 cells were cultured in RPMI full + 0.05 nM β-mercaptoethanol. Single HLA transfectant cell lines were kindly provided by Dr. Alessandro Sette, La Jolla Institute of Immunology, and are described elsewhere[456]. They were cultured in RPMI full + 200 µg/ml G418 (DAP3-based fibroblasts) or 700 µg/ml G418 + 12 µg/ml blasticidine (RM3-based Raji cells).

4.2.2.2 *Isolation of peripheral blood mononuclear cells*

Fresh blood mixed approx. 1:1000 with heparin to prevent clotting was diluted 1:1 with wash medium. 25 ml of blood-medium mixture was carefully added on top of 12.5 ml of Biocoll separating solution in a 50 ml reaction tube, followed by 20 min of centrifugation at 1200 x g, RT, setting the centrifuge break to zero. From the resulting gradient, the intermediate lymphocyte-containing ring-shaped phase was pipetted out with caution into a new 50 ml reaction tube, making sure not to disturb the lower phase with erythrocytes and granulocytes. The 50 ml reaction tube was filled up with wash medium and centrifuged for 10 min at 700 x g, RT, with the centrifuge break set back to standard settings. The wash step was repeated, with centrifugation for 20 min at 75 x g, RT, with the centrifuge break set to an intermediate level, in order to remove

most thrombocytes from the preparation. The supernatant was finally discarded, and the remaining PBMCs were resuspended in hTCM for counting. On average $1x10^6$ PBMCs per ml blood were to be expected; however, this number could vary depending on donor age, sex, immune status etc.

4.2.2.3 *Freezing and thawing cells*

Cells were pelleted for 5 min at 350 x g, RT, resuspended in 1 ml/vial FBS + 10% DMSO and placed into a Nalgene Mr. Frosty Freezing Container (Sigma-Aldrich) overnight (ON) at -80 °C. For long-term storage, cells were then transferred to a liquid nitrogen tank.

Cells were thawed by swiftly placing the cryo vial into a 37 °C waterbath for approximately 1 min until cells had barely liquefied. The cells were then transferred into 10 ml of pre-warmed wash medium, centrifuged for 5 min at 350 x g, RT, and resuspended in the corresponding culture medium.

4.2.2.4 *Magnetic activated cell sorting of $CD4^+$ and $CD8^+$ T cells*

To sort $>5x10^7$ $CD4^+$ T cells from approx. $5x10^8$ fresh PBMCs, human CD4 MicroBeads (Miltenyi) were used on an autoMACS® Pro Separator (Miltenyi) according to manufacturer's instructions.

$1\text{-}5x10^7$ transduced T cells were sorted for $CD4^+$ or $CD8^+$ T cells by positive selection with the human CD4 MicroBeads or human CD8 MicroBeads (Miltenyi) using MS columns (Miltenyi) on a manual OctoMACS Separator (Miltenyi) according to manufacturer's instructions. Sorted cells were maintained in hTCM for 1 d at 37 °C, frozen and stored in liquid nitrogen until further use. According to the manufacturer, the magnetic beads are estimated to detach after approximately 3 days at 37 °C.

4.2.2.5 *Transient transfection of adherent cells*

Transient transfection of adherent cells was typically performed at 70-80% confluency in 6-well cell culture plates using Lipofectamine 2000 transfection reagent (Thermo Fisher Scientific). 5 µg of DNA and 5 µl of Lipofectamine reagent were each mixed with 125 µl of OPTI-MEM reduced serum medium (Thermo Fisher Scientific) each and preincubated for 5 min at RT. The two solutions were then mixed and incubated for further 20 min at RT. After a change of 2 ml fresh medium per 6-well, the mixture was uniformly applied to each well by careful dripping. Cells were further processed

after 48 h at 37 °C, e.g. for retroviral transduction as described in section 4.2.2.6. Volumes for transfection of T75 flasks were upscaled according to the surface area.

4.2.2.6 *Retroviral transduction of primary human T cells*

PBMCs isolated from healthy human donors were stimulated with Dynabeads Human T-Expander CD3/CD28 (Thermo Fisher Scientific) according to manufacturer's instructions, estimating the number of T cells at 60% of all PBMCs. After stimulation, $5x10^6$ cells were seeded per 6-well in 5 ml hTCM + 300 U/ml IL-2.

The transduction protocol was conducted after 48 h, using either supernatant from transient transfection of RD114 producer cells with TCR-containing pMP71 plasmid, or supernatant from stable retroviral producer cell lines (as described in 4.2.2.7). 24-well non-tissue-culture plates (Corning) were coated with 250 µl/well of RetroNectin 20 µg/ml PBS for 2 h at RT. The plate was then blocked with 250 µl/well 2% BSA in PBS for 30 min at 37 °C and subsequently washed 2x with 1ml/well of PBS. 1 ml of viral supernatant, either undiluted or diluted according to titration in section 4.2.2.8, pre-filtered with 0.45 µm sterile filters, was added to each well, followed by centrifugation for 2 h at 2000 x g, 32 °C. Next, $1x10^6$ stimulated T cells were added to each well, based on the numbers calculated during initial stimulation 48 h prior to transduction, since bead-adhering cells could not be adequately counted. Centrifugation for 10 min at 1000 x g, 32 °C completed the transduction. The procedure was performed 1x for supernatant from stable producer cell lines or 2x (repeated after 24 h) for supernatant from transient transfection. The magnetic beads were removed 48 h after transduction with the help of a DynaMag-2 Magnet (Thermo Fisher Scientific). After thorough resuspension, samples were placed in a 2 ml reaction tube in the magnet for 1 min at RT to allow the separation of beads and cells. The cells were then transferred to a new cell culture plate and cultured at $0.5\text{-}1x10^6$ cells/ml in hTCM + 180 U/ml IL-2, adjusting the cell concentration and flask size every 3-4 days. Earliest transduction analysis via staining of the TCR murine β constant and flow cytometry was performed at 48 h after transduction. Transduced cells were used for co-culture experiments at days 5-9 after transduction. Cells were expanded latest until day 9 after transduction, frozen and stored in liquid nitrogen until further use.

4.2.2.7 *Generation of stable retroviral producer cell lines and supernatant*

To generate stable cell lines for the production of TCR-encoding retrovirus, regular RD114 producer cells had to be transduced with retrovirus containing the TCR RNA, in order for the latter to stably integrate into the host cell genome after infection and

retroviral transcription. GALV cells have been known to produce retroviral supernatant which is highly infective for RD114 cells. Therefore, GALV producer cells were transfected with pMP71 plasmid containing the respective TCR genes. After 48 hours, supernatant was harvested and GALV cells were replenished with 2 ml of fresh medium. The supernatant was filtered with a 0.45 µM sterile filter and applied undiluted to RD114 cells in a 12-well-format. This procedure was repeated two more times after 24 h each. When RD114 cells reached confluency, they were transferred to a 6-well-format in order to maintain growth capacity during transduction. The transduced RD114 cells were subsequently expanded to a T75 cell culture flask. By staining the TCR with an anti-mTRBC-PE antibody (1:200), TCR^+ RD114 cells were enriched via FACS. Samples, for which surface staining of the TCR was unsuccessful, were transfected with a vector containing the murine CD3 δγεζ-chains 24-48 hours prior to cell sorting to increase surface localization of the TCR. To gather highly potent retroviral supernatant for T cell transduction, stable producer cells were cultured in a T75 cell culture flask until 70% confluency. They were washed 1x with PBS and 12 ml of fresh medium was added. After 24 h, the supernatant was collected, passed through a 0.45 µm sterile filter, aliquoted and stored at -80 °C until further use.

4.2.2.8 *Titration of retroviral supernatant from stable producer cell lines*

The retroviral supernatant harvested from stable producer cell lines was titrated on Jurkat cells in order to estimate its potency of infection. The transduction protocol was performed as in 4.2.2.6 with minor changes. In contrast to primary human T cells, Jurkat cells were transduced during their exponential growth phase without the need of additional stimulation. A single round of transduction of $1x10^6$ Jurkat cells per well in a 24-well-format was performed, either with undiluted supernatant or in dilutions ranging from 1:10 to 1:80. 48 h after transduction, cells were analyzed by flow cytometry regarding their transduction rate. The observed transduction rates were plotted against the supernatant dilution factor for each TCR. From this curve, the dilution factor to achieve a 70% transduction rate in primary human T cells was estimated, based on the protocol described in 4.2.2.6.

4.2.2.9 *Generation of B-lymphoblastoid cell lines*

B-LCLs were generated via infection and transformation of B cells with potent EBV supernatant. To generate the latter, semi-adherent B95-8 cells were stimulated at $1x10^6$ cells/ml in RPMI full + 20 ng/ml phorbol-12-myristate-13-acetate for 1 h at 37 °C. They were subsequently washed 3x by centrifugation for 5 min at 350 x g, RT,

and taken into culture at $1x10^6$ cells/ml. After 3 d at 37° C, the supernatant was collected and passed through a 0.45 µm sterile filter. It was either used directly for generation of B-LCLs or after storage at -80 °C for up to one year.

Up to $5x10^6$ preferably freshly isolated PBMCs were incubated in 1 ml RPMI full plus 1 ml EBV supernatant for 2 h at 37 °C. 1 ml of RPMI full was then added containing Cyclosporin A to a final concentration of 1 µg/ml to inhibit T cell growth. The cell suspension was transferred to a T25 cell culture flask and incubated at 37 °C, standing and gently tipped on edge. When first clusters of lymphoblastoid cells became macroscopically visible, typically after 2-3 weeks, B-LCLs were expanded by adding RPMI full, taking into account an optimal culturing density of $0.2\text{-}0.5x10^6$ cells/ml.

4.2.2.10 *Differentiation of monocyte-derived dendritic cells*

Monocyte-derived dendritic cells were differentiated from $CD14^+$ monocytes, isolated from freshly prepped PBMCs by magnetic activated cell sorting using the Human Pan Monocyte Isolation Kit (Miltenyi) according to manufacturer's instructions. A maximum of $8x10^6$ cells were seeded in a 10 cm cell culture dish in 20 ml RPMI full + 20 ng/ml GM-CSF + 20 ng/ml IL-4. On day 1, 20 ng/ml GM-CSF + 20 ng/ml IL-4 were again added directly to the medium. On day 3, the medium was replenished with 5 ml; in addition, 20 ng/ml GM-CSF + 20 ng/ml IL-4 were added, calculated to a final volume of 20 ml. MoDCs were ready to use for co-culture at day 6. They were analyzed in flow cytometry, using an Fc receptor block (1:20) followed by antibodies anti-CD11c-PerCP (1:100), anti-CD14-BV510 (1:100) and anti-CD86-APC (1:100). MoDCs were identified as $CD11c^+$ $CD14^-$ $CD86^-$. Immature MoDCs remained largely in suspension, whereas pre-activated MoDCs tend to adhere to the cell culture dish and become $CD86^+$. Careful handling during the differentiation protocol was required to prevent pre-activation and early maturation of MoDCs.

4.2.3 T-cell assays

4.2.3.1 *Stimulation and expansion of T cells with viral peptides*

Donor PBMCs were preferentially used fresh or thawed, washed by centrifugation for 5 min at 350 x g, RT, resuspended in hTCM + HS at $1x10^6$ cells/ml and rested ON at 37 °C. $1x10^6$ cells/well were then stimulated in a 24-well cell culture plate in 1 ml hTCM + 1 µM of the respective peptide + 10 ng/ml IL-15 + 10 ng/ml IL-7. At day 1 after stimulation, 500 µl/well of hTCM + HS + 50 U/ml IL-2 was added. At day 7 and 14

after stimulation, 150 µl cells/well were restimulated with the respective peptide and an intracellular cytokine staining was performed (see 4.2.5.2). Based on these results, samples were either sorted via a cytokine capture assay and fluorescence activated cell sorting (see 4.2.5.3 and 4.2.5.4) or discarded on day 15-18.

4.2.3.2 *Clonal expansion with feeder cells*

Sorted cells were seeded into round-bottom 96-well-plates, at an estimated dilution factor of 0.3-0.5 cells/well. Pooled PBMCs from different donors or B-LCL, preferentially from several lines, were used as feeder cells to support clonal survival and expansion. PBMCs and B-LCLs were irradiated with 35 Gy and 50 Gy, respectively, and were added as follows: $1x10^6$ B-LCLs and $7.5x10^6$ PBMCs per 96-well-plate; $6x10^4$ B-LCLs and $4.5x10^5$ PBMCs per 24-well. Cells were seeded in hTCM + HS + 50 U/ml IL-2 + 30 ng/ml anti-CD3 OKT3 antibody. Approx. 3-5 96-well-plates were seeded per sample, the remaining cells were seeded as lines in a 24-well format.

After 12-14 days, plates were analyzed via microscopy and outgrown clones were identified based on their round and viable-looking morphology. Screening for HBV-specificity was performed by co-culture, similar to 4.2.3.3 with the following modifications: 5-10% of the culture volume per clone was co-cultured at 37 °C ON with $1x10^4$ donor-derived or HLA-matched B-LCLs loaded with 1 µM of the respective peptide. HBV-specific clones were identified by increased IFN-γ or TNF-α secretion compared to the control sample without peptide, measured via ELISA as described in 4.2.4.1. They were subsequently expanded to a 12-well-format with irradiated feeder cells as described above, using $1x10^6$ B-LCLs and $5x10^6$ PBMCs per 12-well in hTCM + HS + 50 U/ml IL-2 + 30 ng/ml anti-CD3 OKT3 antibody. After approx. 14 days, clones were rescreened by co-culture as described above. HBV-specific clones were submitted to RNA extraction as described in 4.2.1.1.

4.2.3.3 *Co-culture of T cells with peptide-pulsed B-LCLs*

Co-cultures were typically performed in a 96-well round-bottom plate at an effector to target ratio of 5:1 ($5x10^4$ transduced T cells and $1x10^4$ B-LCLs) or 2:1 ($1x10^5$ transduced T cells and $5x10^4$ B-LCLs) per well. TCR-transduced T cells were thawed and preferentially rested ON in hTCM at an approx. density of $1x10^6$ cells/ml. B-LCLs were irradiated with 50 Gy and loaded with 1 µM of the respective peptide or DMSO as a negative control for 2 h at 37°C, either in 15 ml reaction tubes or in V-bottom plates. B-LCLs were then washed 2x with wash medium and seeded in a 96-well round-bottom plate together with transduced T cells in 200 µl hTCM/well. Co-cultures

were incubated ON (approximately 16 hours) at 37 °C. Supernatants were transferred to a new plate with 150 µl/well and stored at -20 °C until further use. IFN-γ or TNF-α secretion was measured via ELISA as described in 4.2.4.1.

4.2.3.4 *Co-culture of T cells with single HLA transfectant target cells*

Co-culture experiments with single HLA transfectant target cells were mostly performed during my TUM International Graduate School of Science and Engineering (IGSSE) exchange at the La Jolla Institute for Immunology in the lab of Dr. Alessandro Sette. To increase MHC expression prior to co-culture, single HLA transfectants were stimulated with 100 µg/ml sodium butyrate ON at 37 °C in their respective culture medium. MHC expression was then confirmed by flow cytometry using in house produced mouse antibodies anti-HLA-DR (1:100), anti-HLA-DQ (1:100) or anti-HLA-DP (1:100) in combination with a secondary goat anti-mouse IgG-FITC antibody (1:50). The expression was assessed as a ratio of mean fluorescence intensity of positively stained populations compared to the negative control with secondary antibody only; a minimal ratio of 20 was considered acceptable.

Prestimulated single HLA transfectant fibroblasts were detached with 1 ml of 1x Trypsin in PBS per T75 cell culture flask for approx. 1 min until cells visually detached and seeded with $5x10^4$ cells/well in flat-bottom 96-well plates and loaded with 1 µM peptide for 4 h at 37 °C, followed by 2x washing. Single HLA transfectant RM3 suspension cells were loaded in V-bottom plates with 1 µM peptide for 4 h at 37 °C followed by 2x washing, and subsequently seeded into round-bottom 96-well plates with $5x10^4$ cells/well. Transduced T cells were added with $1x10^5$ cells/well to fibroblasts or RM3 suspension cells and incubated ON at 37 °C. Supernatants were transferred to a new plate with 150 µl/well and stored at -20 °C until further use. TNF-α secretion was measured with the human TNF alpha uncoated ELISA (Invitrogen), similar as described in 4.2.4.1.

4.2.3.5 *Proliferation assay with peptide titration*

For proliferation assays, co-cultures were set up similar as described in 4.2.3.3 with minor changes: B-LCLs were pulsed with peptide concentrations ranging from 100 µM to 1 pM. Co-cultures were incubated for 72 h with 200 µl/well. 20 µl of hTCM with 1 µl radioactive ^{3}H-Thymidine was added per well, which is approx. equivalent to 1 µCi (depending on stock decay). Samples were incubated for 14-16 h at 37 °C and 96-well-plates were placed at -80 °C for a maximum of 1 month until further analysis.

The transfer of samples to a membrane and readout of radioactive labeling was done with the help of a Filtermat-96 Harvester for MicroBeta (PerkinElmer) in combination with a MicroBeta TriLux 1450 Counter (PerkinElmer). 96-well-plates were thawed at RT. A filtermat A membrane and a 96-well wash plate were positioned in the Filtermat-96 Harvester and moisturized by 2x cold-wash, i.e. water which was disposed in the non-radioactive waste. The wash plate was then replaced by the 96-well sample plate and the cells were transferred from the plate to the membrane by 1x hot-wash, i.e. water which was disposed in the radioactive waste. The wash plate was placed back into the Filtermat-96 Harvester and the membrane was washed with 3x hot-wash and 3x cold-wash. The membrane was carefully removed, pinned loosely onto a styrofoam dish and placed into a 37 °C incubator to dry for approx. 6 h.

The dried membrane was placed into a transparent plastic pouch. Approx. 1 ml of BetaPlate Scint was distributed within the pouch, making sure to moisturize all parts of the membrane evenly. After having removed all excess liquid, the sleeve was sealed on all edges, placed into a plastic cassette and positioned into the MicroBeta TriLux 1450 Counter (PerkinElmer). The measurement was started via the MicroBeta Software and radioactive labeling of each well was captured as counts per minute. Results were expressed as stimulation index, representing the ratio between the mean cpm obtained in the presence and absence of antigen.

4.2.3.6 *xCELLigence killing assay*

Killing assays were performed with the xCELLigence device in compatible E-Plate 96 plates (ACEA Biosciences) with a total volume of 180 µl/well. Plates were blanked with 90 µl/well RPMI full + G418. Single HLA transfectant fibroblasts, which had been prestimulated ON with sodium butyrate to a final concentration of 100 µg/ml, were seeded with $5x10^4$ cells/well in 90 µl/well RPMI full + G418 with peptide to a final concentration of 1 µM or without peptide as a negative control. After 4 h at 37 °C, the complete medium was removed, the plates were washed 1x in wash medium and transduced T cells were added in 180 µl/well hTCM at different E:T ratios. Killing assays were incubated for approx. 24 h after the addition of transduced T cells and measurements were recorded via the RTCA 2.0 software. The cell index was normalized to the starting point of each co-culture, as defined by the addition of transduced T cells.

4.2.3.7 *Co-culture with monocyte-derived dendritic cells*

MoDCs were differentiated from monocytes as described in 4.2.2.10. They were harvested and loaded with 1 µM of the MHC class II peptide S36 as well as 1 µM or 10 nM of the respective MHC class I peptide S20 or S172 for 2 h at 37 °C. They were then washed 2x with wash medium and seeded into a 96-well round-bottom format at $5x10^4$ MoDCs/well. $CD8^+$ T cells previously transduced with MHC class I-restricted TCRs $4G_{S20}$ or $WL12_{S172}$ were added at $1x10^5$ transduced cells/well. $CD4^+$ T cells previously transduced with TCR $1E1_{S36}$ were optionally added at $1x10^5$ transduced cells/well. The co-culture was incubated for 48 h at 37 °C. 2.5 µg/ml BFA was added to all samples, followed by incubation ON at 37 °C. Cytokine-secreting cells were subsequently detected by intracellular cytokine staining and flow cytometry.

4.2.4 Immunosorbent assays and peptide chemistry

4.2.4.1 *Enzyme-linked immunosorbent assay*

Human TNF-α (BD) and human IFN-γ (Thermo Fisher Scientific) ELISAs were performed according to manufacturer's instructions in 96-well Nunc MaxiSorb plates (Thermo Fisher Scientific). Samples were typically diluted 1:20 for IFN-γ ELISA and 1:4 for TNF-α ELISA. The OD was measured on an ELISA-Reader infinite F200 (Tecan) at 450 nm with a reference measurement at 560 nm. The background value (i.e. of a well containing only assay diluent) was substracted from all samples. The standard curve was then calculated using a logarithmic regression in Microsoft Excel.

4.2.4.2 *MHC peptide binding assay*

MHC peptide binding assays were performed during a visit at the La Jolla Institute for Immunology in the lab of Dr. Alessandro Sette based on the protocol, i.e. material and methods published by Sidney et al. in 2013[457]. The assay principle is based on the ability of the peptide of interest to competitively inhibit the binding of a radiolabeled standard reference peptide to a purified MHC molecule. Monoclonal antibody capture of the peptide-MHC complex on an absorbent plate allows subsequent assessment of radioactivity in a scintillation counter. The inhibitory capacity of the peptide of interest is calculated based on a dilution serious of the standard reference peptide and given as half maximal inhibitory concentration, i.e. IC_{50}.

4.2.5 Flow cytometry and cell sorting

4.2.5.1 *Staining of surface expression*

Extracellular staining of surface expression was performed on ice. Wash and centrifugation steps were conducted with 200 µl/well for 2 min at 450 x g, 4 °C. Approx. 1-5x10^5 cells/well were transferred to FACS 96-well V-bottom plates and washed 1.5x with FACS buffer. They were stained for 30 min on ice with the respective antibodies/stains in 50 µl FACS buffer/well, most commonly anti-mTRBC-PE (1:200), anti-CD4-APC (1:100), anti-CD8-PB (1:50), live/dead NIR stain (1:1000). Samples were then washed 2.5x, resuspended in 180 µl FACS buffer/well and measured on a CytoFLEX S (Beckman Coulter), typically recording 50.000 events. Single color compensation controls were preferentially stained with cells or alternatively with VersaComp Antibody Capture beads (Beckman Coulter).

4.2.5.2 *Intracellular cytokine staining*

Co-cultures prior to intracellular cytokine staining were typically performed as described in 4.2.3.3 with minor changes, i.e. 2.5x10^4 B-LCLs/well and 5x10^4 transduced T cells/well. 2.5 µg/ml BFA was added 1 h after the start of the co-culture, followed by incubation for 14h/ON at 37 °C.

Intracellular cytokine staining was performed with a Fixation/Permeabilization Solution kit (BD) working on ice. All wash and centrifugation steps were conducted with 200 µl/well for 2 min at 450 x g, 4 °C. Samples were entirely transferred to FACS 96-well V-bottom plates and washed 1.5x with FACS buffer. They were stained extracellularly for 30 min on ice with the following antibodies/stains in 50 µl FACS buffer/well: live/dead Aqua stain (1:1000), anti-CD4-PerCP (1:100) and anti-CD8-FITC (1:100). Cells were subsequently washed 2.5x with FACS buffer and permeabilized with 100 µl cytofix/well for 15 min on ice. Samples were then washed 2.5x with cytowash and stained intracellularly for 30 min on ice with the following antibodies in 50 µl cytowash/well: anti-mTRBC-PE (1:200), anti-hIFN-γ-AF700 (1:100), anti-hTNF-α-APC (1:100), anti-hIL-2-PE/Cy7 (1:100), anti-hGrzB-PB (1:100). Cells were again washed 2.5x with cytowash and resuspended in 180 µl cytowash for flow cytometry. The samples were measured on a CytoFLEX S (Beckman Coulter), recording a maximum of 100’000 cells/well. Single color compensation controls were stained with VersaComp Antibody Capture beads (Beckman Coulter) as well a mixture of $CD4^+$ and $CD8^+$ T cells.

4.2.5.3 *Cytokine capture assay*

Stimulated PBMCs that had been chosen for cell sorting were restimulated in vitro with 1 µM of the respective peptide for 3 h at 37 °C, maintaining the sample in the original well. They were then stained with the Human IFN-γ and/or TNF-α Secretion Assay kit (Miltenyi) according to manufacturer's instructions. During the addition of cytokine detection antibody, samples were also stained with antibodies anti-CD8-PB (1:50) and anti-CD4-APC (1:100). Single color controls were stained in parallel. Cells were then passed through a filcon filter and submitted to cell sorting on a FACS Aria II (BD) or MoFlo II (Beckman Coulter) with a stringent gating strategy in order to lower the number of false positive cells. PI (approx. 1-2 µg/ml) was added for live/dead staining to each sample prior to cell sorting.

4.2.5.4 *Cell sorting*

All staining steps for fluorescence activated cell sorting were performed on ice. Wash and centrifugation steps were conducted with 200 µl/well for 2 min at 450 x g, 4 °C. Samples were washed 1.5x with MACS buffer and stained for 30 min on ice with the respective antibodies in approx. 1 ml MACS buffer for $1x10^7$ cells. Cells were then washed 2.5x with MACS buffer, thoroughly resuspended in 500 µl MACS buffer and passed through a filcon filter to remove clumps. PI (approx. 1-2 µg/ml) was added for live/dead staining to each sample prior to cell sorting on a FACS Aria II (BD) or MoFlo II (Beckman Coulter).

4.2.6 *In silico* methods

4.2.6.1 *Peptide-MHC binding prediction*

The prediction of HBV epitopes was made based on donor 1's dominant MHC class II molecules, i.e. HLA-DR*1301 and HLA-DR*0101, as well as the protein sequence from HBV genotype A, since this was donor 1's originally diagnosed genotype. Prediction algorithms NetMHCIIpan 3.2[209] (www.cbs.dtu.dk/services/NetMHCIIpan) and SMM-align[208] (http://tools.iedb.org/mhcii) were used for *in silico* prediction of the binding affinity between overlapping 18-mers spanning the HBV envelope, core and polymerase proteins and the respective MHC class II molecule. In general terms, peptides are considered strong binders for IC_{50} values below 50 nM and weak binders for IC_{50} values below 500 nM.

4.2.6.2 *Identification of TCR α- or β-chains*

PCR products that were amplified from T-cell clones by PCR with degenerate or specific primers were sent for sequencing to Eurofins Genomics with the respective reverse primer, CP1 for β-chains and CA2 for α-chains. Sequencing results were then submitted to IMGT (http://www.imgt.org/IMGT_vquest/) in fasta format. The output generally contained the identified V-GENE, D-GENE and J-GENE based on sequence alignment as well as the amino acid sequence of the CDR for each TCR chain.

4.2.6.3 *EC_{50} calculations via non-linear log(dose) vs. response modeling*

The EC_{50} affinity values for each TCR were calculated from cpm values divided by the negative control obtained from proliferation assays with peptide titration. Calculations were based on a non-linear log(dose) vs. response fit using Prism 6.07 (GraphPad). R^2 is a measure of the fit quality with a maximum value of 1.

5 List of Figures and Tables

5.1 List of Figures

5.2 List of Tables

6 Acknowledgements

First of all, I would like to thank my first supervisor Prof. Ulrike Protzer for her continuous support during my PhD studies as well as her encouraging and supportive stance towards my wish to pursue a clinical career. Her trust in my abilities has allowed me to engage in medical studies while still making scientific research a priority on my own schedule.

Moreover, I am thankful to Prof. Iris Antes, who acted as my second supervisor until her sudden passing in August 2021. She always gave valuable insights and discussions during thesis committee meetings and beyond and she will be missed as a valuable cooperation partner and colleague. Prof. Aphrodite Kapurniotu kindly assumed the position as my second supervisor from September 2021 onwards. For her spontaneous help and commitment, I am extremely thankful.

Most importantly, I would like to express my deep gratitude to my mentor Dr. Karin Wisskirchen, who has greatly impacted my work as a scientist and shaped my way of thinking since my time as a bachelor student in 2013 at the Institute of Virology. Her thoughtful input and supervision have been crucial to this thesis. In addition, she has become a dear friend.

Many thanks go to Alessandro Sette and his lab members at the La Jolla Institute of Immunology. They provided me with the infrastructure and guidance to successfully perform the experiments involving single MHC class II transfectants during my IGSSE exchange in San Diego, USA. Thanks to the IGSSE graduate school, I was able to gain valuable experience during my stay abroad, attend national and international conferences and engage in specialized and interdisciplinary training to broaden my scientific horizion.

I would also like to thank my parents for their unwavering support regarding my career choices and Iván Nájera, who was by my side during most of my dissertational journey, encouraging me to give my best at all times. Last but certainly not least, my colleagues at the Institute of Virology were always a source of cheerfulness and distraction and I am happy and grateful for their friendship.

7 Publications and Meetings

Schreiber, S., Honz, M., Mamozai, W., Kurktschiev, P., Schiemann, M., Witter, K., Moore, E., Zielinski, C., Sette, A., Protzer, U., Wisskirchen, K. Characterization of a library of twenty HBV-specific MHC class II-restricted T cell receptors. Mol Ther Methods Clin Dev 23:476-489 (October 2021).

Tan, A., **Schreiber, S.** Adoptive T-cell Therapy for HBV-associated HCC and HBV Infection. Antiviral Research 76:104748 (April 2020).

Schreiber, S., Honz, M., Schiemann, M., Sette, A., Zielinski, C., Protzer, U., Wisskirchen, K. Characterization of MHC class II-restricted T-cell receptors for T-cell therapy of HBV infection. Poster presented at the 23rd Annual Meeting of the American Society for Gene and Cell Therapy, virtual conference (May 2020).

Schreiber, S., Honz, M., Schiemann, M., Sette, A., Zielinski, C., Protzer, U., Wisskirchen, K. Characterization of MHC class II-restricted T-cell receptors for T-cell therapy of HBV infection. Oral presentation at the Theme day „CAR-T cells and beyond“ of the Deutsche Gesellschaft für Gentherapie, Leipzig, Germany (September 2019).

Schreiber, S., Honz, M., Schiemann, M., Sette, A., Zielinski, C., Protzer, U., Wisskirchen, K. Characterization of MHC class II-restricted T-cell receptors for T-cell therapy of HBV infection. Poster presented at the 2nd International Conference on Lymphocyte Engineering, London, United Kingdom (September 2019).

Festag, M. M., Festag, J., Fräßle, S. P., Asen, T., Sacherl, J., **Schreiber, S.**, Mück-Häusl, M. A., Busch, D. H., Wisskirchen, K., Protzer, U. Evaluation of a Fully Human, Hepatitis B Virus-Specific Chimeric Antigen Receptor in an Immunocompetent Mouse Model. Molecular Therapy 27, 947-959 (May 2019).

Schreiber, S., Honz, M., Schiemann, M., Zielinski, C., Protzer, U., Wisskirchen, K. Characterization of MHC class II-restricted T-cell receptors for T-cell therapy of HBV infection. Oral presentation at the Annual Meeting of the International Society for Cell and Gene Therapy, Melbourne, Australia (May 2019).

Schreiber, S., Honz, M., Schiemann, M., Protzer, U., Wisskirchen, K. Generating $CD4^+$ T cells for the T-cell therapy of HBV infection. Poster presented at the 16th International Symposium on Viral Hepatitis and Liver Disease – Global Hepatitis Summit, Toronto, Canada (June 2018).

Wisskirchen, K., Metzger, K., **Schreiber, S.**, Asen, T., Weigand, L., Dargel, C., Witter, K., Kieback, E., Sprinzl, M. F., Uckert, W., Schiemann, M., Busch, D. H., Krackhardt, A. M., Protzer, U. Isolation and functional characterization of hepatitis B virus-specific T-cell receptors as new tools for experimental and clinical use. PLoS One 12, e0182936 (August 2017).

8 References

1 McMahon, B. J. *et al.* Acute hepatitis B virus infection: relation of age to the clinical expression of disease and subsequent development of the carrier state. *J Infect Dis* **151**, 599-603, doi:10.1093/infdis/151.4.599 (1985).

2 World Health Organization. *Hepatitis B Fact Sheet*, <https://www.who.int/news-room/fact-sheets/detail/hepatitis-b> (2019).

3 Thomas, D. L. Global Elimination of Chronic Hepatitis. *N Engl J Med* **380**, 2041-2050, doi:10.1056/NEJMra1810477 (2019).

4 Foreman, K. J. *et al.* Forecasting life expectancy, years of life lost, and all-cause and cause-specific mortality for 250 causes of death: reference and alternative scenarios for 2016-40 for 195 countries and territories. *Lancet* **392**, 2052-2090, doi:10.1016/s0140-6736(18)31694-5 (2018).

5 Dane, D. S., Cameron, C. H. & Briggs, M. Virus-like particles in serum of patients with Australia-antigen-associated hepatitis. *Lancet* **1**, 695-698, doi:10.1016/s0140-6736(70)90926-8 (1970).

6 Seeger, C. & Mason, W. S. Molecular biology of hepatitis B virus infection. *Virology* **479-480**, 672-686, doi:10.1016/j.virol.2015.02.031 (2015).

7 Robinson, W. S. & Lutwick, L. I. The virus of hepatitis, type B (first of two parts). *N Engl J Med* **295**, 1168-1175, doi:10.1056/nejm197611182952105 (1976).

8 Ganem, D. & Prince, A. M. Hepatitis B virus infection--natural history and clinical consequences. *N Engl J Med* **350**, 1118-1129, doi:10.1056/NEJMra031087 (2004).

9 Wynne, S. A., Crowther, R. A. & Leslie, A. G. The crystal structure of the human hepatitis B virus capsid. *Mol Cell* **3**, 771-780, doi:10.1016/s1097-2765(01)80009-5 (1999).

10 Chen, M. T. *et al.* A function of the hepatitis B virus precore protein is to regulate the immune response to the core antigen. *Proc Natl Acad Sci U S A* **101**, 14913-14918, doi:10.1073/pnas.0406282101 (2004).

11 Lucifora, J. *et al.* Hepatitis B virus X protein is essential to initiate and maintain virus replication after infection. *J Hepatol* **55**, 996-1003, doi:10.1016/j.jhep.2011.02.015 (2011).

12 Decorsiere, A. *et al.* Hepatitis B virus X protein identifies the Smc5/6 complex as a host restriction factor. *Nature* **531**, 386-389, doi:10.1038/nature17170 (2016).

13 Liu, S., Koh, S. S. & Lee, C. G. Hepatitis B Virus X Protein and Hepatocarcinogenesis. *Int J Mol Sci* **17**, doi:10.3390/ijms17060940 (2016).

14 Schulze, A., Gripon, P. & Urban, S. Hepatitis B virus infection initiates with a large surface protein-dependent binding to heparan sulfate proteoglycans. *Hepatology* **46**, 1759-1768, doi:10.1002/hep.21896 (2007).

15 Sureau, C. & Salisse, J. A conformational heparan sulfate binding site essential to infectivity overlaps with the conserved hepatitis B virus a-determinant. *Hepatology* **57**, 985-994, doi:10.1002/hep.26125 (2013).

16 Yan, H. *et al.* Sodium taurocholate cotransporting polypeptide is a functional receptor for human hepatitis B and D virus. *Elife* **1**, e00049, doi:10.7554/eLife.00049 (2012).

17 Huang, H. C., Chen, C. C., Chang, W. C., Tao, M. H. & Huang, C. Entry of hepatitis B virus into immortalized human primary hepatocytes by clathrin-dependent endocytosis. *J Virol* **86**, 9443-9453, doi:10.1128/jvi.00873-12 (2012).

18 Nassal, M. HBV cccDNA: viral persistence reservoir and key obstacle for a cure of chronic hepatitis B. *Gut* **64**, 1972-1984, doi:10.1136/gutjnl-2015-309809 (2015).

19 Ko, C., Michler, T. & Protzer, U. Novel viral and host targets to cure hepatitis B. *Curr Opin Virol* **24**, 38-45, doi:10.1016/j.coviro.2017.03.019 (2017).

20 Urban, S., Schulze, A., Dandri, M. & Petersen, J. The replication cycle of hepatitis B virus. *J Hepatol* **52**, 282-284, doi:10.1016/j.jhep.2009.10.031 (2010).

21 MacLachlan, J. H. & Cowie, B. C. Hepatitis B virus epidemiology. *Cold Spring Harb Perspect Med* **5**, a021410, doi:10.1101/cshperspect.a021410 (2015).

22 Velkov, S., Ott, J. J., Protzer, U. & Michler, T. The Global Hepatitis B Virus Genotype Distribution Approximated from Available Genotyping Data. *Genes (Basel)* **9**, doi:10.3390/genes9100495 (2018).

23 Lin, C. L. & Kao, J. H. Hepatitis B virus genotypes and variants. *Cold Spring Harb Perspect Med* **5**, a021436, doi:10.1101/cshperspect.a021436 (2015).

24 Le Bouvier, G. L. *et al.* Subtypes of Australia antigen and hepatitis-B virus. *Jama* **222**, 928-930, doi:10.1001/jama.222.8.928 (1972).

25 Bhatnagar, P. K. *et al.* Immune response to synthetic peptide analogues of hepatitis B surface antigen specific for the a determinant. *Proc Natl Acad Sci U S A* **79**, 4400-4404, doi:10.1073/pnas.79.14.4400 (1982).

26 Du, X. *et al.* Virological and serological features of acute hepatitis B in adults. *Medicine (Baltimore)* **96**, e6088, doi:10.1097/md.0000000000006088 (2017).

27 Peeridogaheh, H. *et al.* Current concepts on immunopathogenesis of hepatitis B virus infection. *Virus Res* **245**, 29-43, doi:10.1016/j.virusres.2017.12.007 (2018).

28 Bertoletti, A. & Le Bert, N. Immunotherapy for Chronic Hepatitis B Virus Infection. *Gut Liver* **12**, 497-507, doi:10.5009/gnl17233 (2018).

29 Rehermann, B., Ferrari, C., Pasquinelli, C. & Chisari, F. V. The hepatitis B virus persists for decades after patients' recovery from acute viral hepatitis despite active maintenance of a cytotoxic T-lymphocyte response. *Nat Med* **2**, 1104-1108, doi:10.1038/nm1096-1104 (1996).

30 Organization, W. H. *Guidelines for the prevention, care and treatment of persons with chronic hepatitis B infection*. (World Health Organization, 2015).

31 Malani, P. N. Mandell, Douglas, and Bennett's Principles and Practice of Infectious Diseases. *JAMA* **304**, 2067-2071, doi:10.1001/jama.2010.1643 (2010).

32 Balogh, J. *et al.* Hepatocellular carcinoma: a review. *J Hepatocell Carcinoma* **3**, 41-53, doi:10.2147/jhc.S61146 (2016).

33 Ghouri, Y. A., Mian, I. & Rowe, J. H. Review of hepatocellular carcinoma: Epidemiology, etiology, and carcinogenesis. *J Carcinog* **16**, 1, doi:10.4103/jcar.JCar_9_16 (2017).

34 Ma, N. F. *et al.* COOH-terminal truncated HBV X protein plays key role in hepatocarcinogenesis. *Clin Cancer Res* **14**, 5061-5068, doi:10.1158/1078-0432.Ccr-07-5082 (2008).

35 Toh, S. T. *et al.* Deep sequencing of the hepatitis B virus in hepatocellular carcinoma patients reveals enriched integration events, structural alterations and sequence variations. *Carcinogenesis* **34**, 787-798, doi:10.1093/carcin/bgs406 (2013).

36 Furuta, M. *et al.* Characterization of HBV integration patterns and timing in liver cancer and HBV-infected livers. *Oncotarget* **9**, 25075-25088, doi:10.18632/oncotarget.25308 (2018).

37 Minami, M. *et al.* Hepatitis B virus-related insertional mutagenesis in chronic hepatitis B patients as an early drastic genetic change leading to hepatocarcinogenesis. *Oncogene* **24**, 4340-4348, doi:10.1038/sj.onc.1208628 (2005).

38 Jiang, Z. *et al.* The effects of hepatitis B virus integration into the genomes of hepatocellular carcinoma patients. *Genome Res* **22**, 593-601, doi:10.1101/gr.133926.111 (2012).

39 Schlüter, V., Meyer, M., Hofschneider, P. H., Koshy, R. & Caselmann, W. H. Integrated hepatitis B virus X and 3' truncated preS/S sequences derived from human hepatomas encode functionally active transactivators. *Oncogene* **9**, 3335-3344 (1994).

40 Gramantieri, L. *et al.* MicroRNA-221 targets Bmf in hepatocellular carcinoma and correlates with tumor multifocality. *Clin Cancer Res* **15**, 5073-5081, doi:10.1158/1078-0432.Ccr-09-0092 (2009).

41 Li, Y. *et al.* Role of the miR-106b-25 microRNA cluster in hepatocellular carcinoma. *Cancer Sci* **100**, 1234-1242, doi:10.1111/j.1349-7006.2009.01164.x (2009).

42 Byam, J., Renz, J. & Millis, J. M. Liver transplantation for hepatocellular carcinoma. *Hepatobiliary Surg Nutr* **2**, 22-30, doi:10.3978/j.issn.2304-3881.2012.11.03 (2013).

43 Bray, F. *et al.* Global cancer statistics 2018: GLOBOCAN estimates of incidence and mortality worldwide for 36 cancers in 185 countries. *CA Cancer J Clin* **68**, 394-424, doi:10.3322/caac.21492 (2018).

44 Gerlich, W. H. Prophylactic vaccination against hepatitis B: achievements, challenges and perspectives. *Med Microbiol Immunol* **204**, 39-55, doi:10.1007/s00430-014-0373-y (2015).

45 World Health, O. Hepatitis B vaccines: WHO position paper, July 2017 - Recommendations. *Vaccine* **37**, 223-225, doi:10.1016/j.vaccine.2017.07.046 (2019).

46 Jack, A. D., Hall, A. J., Maine, N., Mendy, M. & Whittle, H. C. What level of hepatitis B antibody is protective? *J Infect Dis* **179**, 489-492, doi:10.1086/314578 (1999).

47 Iwarson, S. *et al.* Neutralization of hepatitis B virus infectivity by a murine monoclonal antibody: an experimental study in the chimpanzee. *J Med Virol* **16**, 89-96, doi:10.1002/jmv.1890160112 (1985).

48 Cassidy, A., Mossman, S., Olivieri, A., De Ridder, M. & Leroux-Roels, G. Hepatitis B vaccine effectiveness in the face of global HBV genotype diversity. *Expert Rev Vaccines* **10**, 1709-1715, doi:10.1586/erv.11.151 (2011).

49 Hamada-Tsutsumi, S. *et al.* Validation of cross-genotype neutralization by hepatitis B virus-specific monoclonal antibodies by in vitro and in vivo infection. *PLoS One* **10**, e0118062, doi:10.1371/journal.pone.0118062 (2015).

50 Wen, W. H. *et al.* Secular trend of the viral genotype distribution in children with chronic hepatitis B virus infection after universal infant immunization. *Hepatology* **53**, 429-436, doi:10.1002/hep.24061 (2011).

51 Ye, H., Teng, J., Lin, Z., Wang, Y. & Fu, X. Analysis of HBsAg mutations in the 25 years after the implementation of the hepatitis B vaccination plan in China. *Virus Genes* **56**, 546-556, doi:10.1007/s11262-020-01773-1 (2020).

52 Chiang, C. J., Yang, Y. W., You, S. L., Lai, M. S. & Chen, C. J. Thirty-year outcomes of the national hepatitis B immunization program in Taiwan. *Jama* **310**, 974-976, doi:10.1001/jama.2013.276701 (2013).

53 Wiesen, E., Diorditsa, S. & Li, X. Progress towards hepatitis B prevention through vaccination in the Western Pacific, 1990-2014. *Vaccine* **34**, 2855-2862, doi:10.1016/j.vaccine.2016.03.060 (2016).

54 Organization, W. H. Hepatitis B vaccines: WHO position paper - July 2017. *Wkly Epidemiol Rec* **92**, 369-392 (2017).

55 Tang, L. S. Y., Covert, E., Wilson, E. & Kottilil, S. Chronic Hepatitis B Infection: A Review. *Jama* **319**, 1802-1813, doi:10.1001/jama.2018.3795 (2018).

56 Belloni, L. *et al.* IFN-alpha inhibits HBV transcription and replication in cell culture and in humanized mice by targeting the epigenetic regulation of the nuclear cccDNA minichromosome. *J Clin Invest* **122**, 529-537, doi:10.1172/jci58847 (2012).

57 Pasquetto, V., Wieland, S. F., Uprichard, S. L., Tripodi, M. & Chisari, F. V. Cytokine-sensitive replication of hepatitis B virus in immortalized mouse hepatocyte cultures. *J Virol* **76**, 5646-5653, doi:10.1128/jvi.76.11.5646-5653.2002 (2002).

58 Wieland, S. F., Guidotti, L. G. & Chisari, F. V. Intrahepatic induction of alpha/beta interferon eliminates viral RNA-containing capsids in hepatitis B virus transgenic mice. *J Virol* **74**, 4165-4173, doi:10.1128/jvi.74.9.4165-4173.2000 (2000).

59 Rang, A., Gunther, S. & Will, H. Effect of interferon alpha on hepatitis B virus replication and gene expression in transiently transfected human hepatoma cells. *J Hepatol* **31**, 791-799, doi:10.1016/s0168-8278(99)80279-7 (1999).

60 Uprichard, S. L., Wieland, S. F., Althage, A. & Chisari, F. V. Transcriptional and posttranscriptional control of hepatitis B virus gene expression. *Proc Natl Acad Sci U S A* **100**, 1310-1315, doi:10.1073/pnas.252773599 (2003).

61 Lucifora, J. *et al.* Specific and nonhepatotoxic degradation of nuclear hepatitis B virus cccDNA. *Science* **343**, 1221-1228, doi:10.1126/science.1243462 (2014).

62 Micco, L. *et al.* Differential boosting of innate and adaptive antiviral responses during pegylated-interferon-alpha therapy of chronic hepatitis B. *J Hepatol* **58**, 225-233, doi:10.1016/j.jhep.2012.09.029 (2013).

63 Zoulim, F., Lebosse, F. & Levrero, M. Current treatments for chronic hepatitis B virus infections. *Curr Opin Virol* **18**, 109-116, doi:10.1016/j.coviro.2016.06.004 (2016).

64 Buster, E. H. *et al.* Sustained HBeAg and HBsAg loss after long-term follow-up of HBeAg-positive patients treated with peginterferon alpha-2b. *Gastroenterology* **135**, 459-467, doi:10.1053/j.gastro.2008.05.031 (2008).

65 Lau, G. K. *et al.* Peginterferon Alfa-2a, lamivudine, and the combination for HBeAg-positive chronic hepatitis B. *N Engl J Med* **352**, 2682-2695, doi:10.1056/NEJMoa043470 (2005).

66 Marcellin, P. *et al.* Peginterferon alfa-2a alone, lamivudine alone, and the two in combination in patients with HBeAg-negative chronic hepatitis B. *N Engl J Med* **351**, 1206-1217, doi:10.1056/NEJMoa040431 (2004).

67 Janssen, H. L. *et al.* Pegylated interferon alfa-2b alone or in combination with lamivudine for HBeAg-positive chronic hepatitis B: a randomised trial. *Lancet* **365**, 123-129, doi:10.1016/s0140-6736(05)17701-0 (2005).

68 Buti, M. *et al.* Seven-Year Efficacy and Safety of Treatment with Tenofovir Disoproxil Fumarate for Chronic Hepatitis B Virus Infection. *Digestive Diseases and Sciences* **60**, 1457-1464, doi:10.1007/s10620-014-3486-7 (2015).

69 van Bömmel, F. & Berg, T. Stopping long-term treatment with nucleos(t)ide analogues is a favourable option for selected patients with HBeAg-negative chronic hepatitis B. *Liver Int* **38 Suppl 1**, 90-96, doi:10.1111/liv.13654 (2018).

70 Villanueva, A. Hepatocellular Carcinoma. *N Engl J Med* **380**, 1450-1462, doi:10.1056/NEJMra1713263 (2019).

71 Llovet, J. M. *et al.* Sorafenib in advanced hepatocellular carcinoma. *N Engl J Med* **359**, 378-390, doi:10.1056/NEJMoa0708857 (2008).

72 Iavarone, M. *et al.* Field-practice study of sorafenib therapy for hepatocellular carcinoma: a prospective multicenter study in Italy. *Hepatology* **54**, 2055-2063, doi:10.1002/hep.24644 (2011).

73 Al-Salama, Z. T., Syed, Y. Y. & Scott, L. J. Lenvatinib: A Review in Hepatocellular Carcinoma. *Drugs* **79**, 665-674, doi:10.1007/s40265-019-01116-x (2019).

74 Llovet, J. M., Montal, R., Sia, D. & Finn, R. S. Molecular therapies and precision medicine for hepatocellular carcinoma. *Nat Rev Clin Oncol* **15**, 599-616, doi:10.1038/s41571-018-0073-4 (2018).

75 El-Khoueiry, A. B. *et al.* Nivolumab in patients with advanced hepatocellular carcinoma (CheckMate 040): an open-label, non-comparative, phase 1/2 dose escalation and expansion trial. *Lancet* **389**, 2492-2502, doi:10.1016/s0140-6736(17)31046-2 (2017).

76 Murphy, K. & Weaver, C. *Janeway's Immunobiology*. (W.W. Norton, 2016).

77 Blum, J. S., Wearsch, P. A. & Cresswell, P. Pathways of antigen processing. *Annu Rev Immunol* **31**, 443-473, doi:10.1146/annurev-immunol-032712-095910 (2013).

78 Chicz, R. M. *et al.* Predominant naturally processed peptides bound to HLA-DR1 are derived from MHC-related molecules and are heterogeneous in size. *Nature* **358**, 764-768, doi:10.1038/358764a0 (1992).

79 Zhang, L., Udaka, K., Mamitsuka, H. & Zhu, S. Toward more accurate pan-specific MHC-peptide binding prediction: a review of current methods and tools. *Briefings in bioinformatics* **13**, 350-364, doi:10.1093/bib/bbr060 (2012).

80 Holland, C. J., Cole, D. K. & Godkin, A. Re-Directing CD4(+) T Cell Responses with the Flanking Residues of MHC Class II-Bound Peptides: The Core is Not Enough. *Front Immunol* **4**, 172, doi:10.3389/fimmu.2013.00172 (2013).

81 Marsh, S. G. *et al.* Nomenclature for factors of the HLA system, 2010. *Tissue antigens* **75**, 291-455, doi:10.1111/j.1399-0039.2010.01466.x (2010).

82 Wang, L., Zou, Z. Q. & Wang, K. Clinical Relevance of HLA Gene Variants in HBV Infection. *Journal of immunology research* **2016**, 9069375, doi:10.1155/2016/9069375 (2016).

83 Crotty, S., Kersh, E. N., Cannons, J., Schwartzberg, P. L. & Ahmed, R. SAP is required for generating long-term humoral immunity. *Nature* **421**, 282-287, doi:10.1038/nature01318 (2003).

84 McCausland, M. M. *et al.* SAP regulation of follicular helper CD4 T cell development and humoral immunity is independent of SLAM and Fyn kinase. *J Immunol* **178**, 817-828, doi:10.4049/jimmunol.178.2.817 (2007).

85 Kuchen, S. *et al.* Essential role of IL-21 in B cell activation, expansion, and plasma cell generation during CD4+ T cell-B cell collaboration. *J Immunol* **179**, 5886-5896, doi:10.4049/jimmunol.179.9.5886 (2007).

86 Swain, S. L., McKinstry, K. K. & Strutt, T. M. Expanding roles for $CD4^+$ T cells in immunity to viruses. *Nat Rev Immunol* **12**, 136-148, doi:10.1038/nri3152 (2012).

87 Borst, J., Ahrends, T., Bąbała, N., Melief, C. J. M. & Kastenmüller, W. CD4(+) T cell help in cancer immunology and immunotherapy. *Nat Rev Immunol* **18**, 635-647, doi:10.1038/s41577-018-0044-0 (2018).

88 van de Ven, K. & Borst, J. Targeting the T-cell co-stimulatory CD27/CD70 pathway in cancer immunotherapy: rationale and potential. *Immunotherapy* **7**, 655-667, doi:10.2217/imt.15.32 (2015).

89 Janssen, E. M. *et al.* CD4+ T cells are required for secondary expansion and memory in CD8+ T lymphocytes. *Nature* **421**, 852-856, doi:10.1038/nature01441 (2003).

90 Janssen, E. M. *et al.* CD4+ T-cell help controls CD8+ T-cell memory via TRAIL-mediated activation-induced cell death. *Nature* **434**, 88-93, doi:10.1038/nature03337 (2005).

91 Pipkin, M. E. *et al.* Interleukin-2 and inflammation induce distinct transcriptional programs that promote the differentiation of effector cytolytic T cells. *Immunity* **32**, 79-90, doi:10.1016/j.immuni.2009.11.012 (2010).

92 Curtsinger, J. M., Agarwal, P., Lins, D. C. & Mescher, M. F. Autocrine IFN-γ promotes naive CD8 T cell differentiation and synergizes with IFN-α to stimulate strong function. *J Immunol* **189**, 659-668, doi:10.4049/jimmunol.1102727 (2012).

93 Elsaesser, H., Sauer, K. & Brooks, D. G. IL-21 is required to control chronic viral infection. *Science* **324**, 1569-1572, doi:10.1126/science.1174182 (2009).

94 Tan, A., Koh, S. & Bertoletti, A. Immune Response in Hepatitis B Virus Infection. *Cold Spring Harb Perspect Med* **5**, a021428, doi:10.1101/cshperspect.a021428 (2015).

95 Alberti, A., Diana, S., Sculard, G. H., Eddleston, A. L. & Williams, R. Detection of a new antibody system reacting with Dane particles in hepatitis B virus infection. *Br Med J* **2**, 1056-1058, doi:10.1136/bmj.2.6144.1056 (1978).

96 Dunn, C. *et al.* Temporal analysis of early immune responses in patients with acute hepatitis B virus infection. *Gastroenterology* **137**, 1289-1300, doi:10.1053/j.gastro.2009.06.054 (2009).

97 Stacey, A. R. *et al.* Induction of a striking systemic cytokine cascade prior to peak viremia in acute human immunodeficiency virus type 1 infection, in contrast to more modest and delayed responses in acute hepatitis B and C virus infections. *J Virol* **83**, 3719-3733, doi:10.1128/jvi.01844-08 (2009).

98 Wieland, S., Thimme, R., Purcell, R. H. & Chisari, F. V. Genomic analysis of the host response to hepatitis B virus infection. *Proc Natl Acad Sci U S A* **101**, 6669-6674, doi:10.1073/pnas.0401771101 (2004).

99 Fletcher, S. P. *et al.* Transcriptomic analysis of the woodchuck model of chronic hepatitis B. *Hepatology* **56**, 820-830, doi:10.1002/hep.25730 (2012).

100 Wieland, S. F. & Chisari, F. V. Stealth and cunning: hepatitis B and hepatitis C viruses. *J Virol* **79**, 9369-9380, doi:10.1128/jvi.79.15.9369-9380.2005 (2005).

101 Biron, C. A. & Brossay, L. NK cells and NKT cells in innate defense against viral infections. *Curr Opin Immunol* **13**, 458-464, doi:10.1016/s0952-7915(00)00241-7 (2001).

102 Webster, G. J. *et al.* Incubation phase of acute hepatitis B in man: dynamic of cellular immune mechanisms. *Hepatology* **32**, 1117-1124, doi:10.1053/jhep.2000.19324 (2000).

103 Fisicaro, P. *et al.* Early kinetics of innate and adaptive immune responses during hepatitis B virus infection. *Gut* **58**, 974-982, doi:10.1136/gut.2008.163600 (2009).

104 Peppa, D. *et al.* Blockade of immunosuppressive cytokines restores NK cell antiviral function in chronic hepatitis B virus infection. *PLoS Pathog* **6**, e1001227, doi:10.1371/journal.ppat.1001227 (2010).

105 Zhang, Z. *et al.* Hypercytolytic activity of hepatic natural killer cells correlates with liver injury in chronic hepatitis B patients. *Hepatology* **53**, 73-85, doi:10.1002/hep.23977 (2011).

106 Tan, A. T. *et al.* Reduction of HBV replication prolongs the early immunological response to IFNalpha therapy. *J Hepatol* **60**, 54-61, doi:10.1016/j.jhep.2013.08.020 (2014).

107 Loomba, R. & Liang, T. J. Hepatitis B Reactivation Associated With Immune Suppressive and Biological Modifier Therapies: Current Concepts, Management Strategies, and Future Directions. *Gastroenterology* **152**, 1297-1309, doi:10.1053/j.gastro.2017.02.009 (2017).

108 Lindemann, M. *et al.* Control of hepatitis B virus infection in hematopoietic stem cell recipients after receiving grafts from vaccinated donors. *Bone Marrow Transplant* **51**, 428-431, doi:10.1038/bmt.2015.253 (2016).

109 Zhang, S., Zhao, J. & Zhang, Z. Humoral immunity, the underestimated player in hepatitis B. *Cell Mol Immunol* **15**, 645-648, doi:10.1038/cmi.2017.132 (2018).

110 Das, A. *et al.* IL-10-producing regulatory B cells in the pathogenesis of chronic hepatitis B virus infection. *J Immunol* **189**, 3925-3935, doi:10.4049/jimmunol.1103139 (2012).

111 Burton, A. R. *et al.* Circulating and intrahepatic antiviral B cells are defective in hepatitis B. *J Clin Invest* **128**, 4588-4603, doi:10.1172/jci121960 (2018).

112 Beasley, R. P. *et al.* Prevention of perinatally transmitted hepatitis B virus infections with hepatitis B immune globulin and hepatitis B vaccine. *Lancet* **2**, 1099-1102, doi:10.1016/s0140-6736(83)90624-4 (1983).

113 Galun, E. *et al.* Clinical evaluation (phase I) of a combination of two human monoclonal antibodies to HBV: safety and antiviral properties. *Hepatology* **35**, 673-679, doi:10.1053/jhep.2002.31867 (2002).

114 Kang, C. *et al.* A novel therapeutic anti-HBV antibody with increased binding to human FcRn improves in vivo PK in mice and monkeys. *Protein Cell* **9**, 130-134, doi:10.1007/s13238-017-0438-y (2018).

115 Thimme, R. *et al.* CD8(+) T cells mediate viral clearance and disease pathogenesis during acute hepatitis B virus infection. *J Virol* **77**, 68-76, doi:10.1128/jvi.77.1.68-76.2003 (2003).

116 Maini, M. K. *et al.* Direct ex vivo analysis of hepatitis B virus-specific CD8(+) T cells associated with the control of infection. *Gastroenterology* **117**, 1386-1396, doi:10.1016/s0016-5085(99)70289-1 (1999).

117 Stelma, F. *et al.* Dynamics of the Immune Response in Acute Hepatitis B Infection. *Open Forum Infect Dis* **4**, ofx231, doi:10.1093/ofid/ofx231 (2017).

118 Bertoletti, A. *et al.* HLA class I-restricted human cytotoxic T cells recognize endogenously synthesized hepatitis B virus nucleocapsid antigen. *Proc Natl Acad Sci U S A* **88**, 10445-10449, doi:10.1073/pnas.88.23.10445 (1991).

119 Guidotti, L. G. *et al.* Intracellular inactivation of the hepatitis B virus by cytotoxic T lymphocytes. *Immunity* **4**, 25-36, doi:10.1016/s1074-7613(00)80295-2 (1996).

120 Guidotti, L. G. *et al.* Viral clearance without destruction of infected cells during acute HBV infection. *Science* **284**, 825-829, doi:10.1126/science.284.5415.825 (1999).

121 Guidotti, L. G. & Chisari, F. V. Immunobiology and pathogenesis of viral hepatitis. *Annu Rev Pathol* **1**, 23-61, doi:10.1146/annurev.pathol.1.110304.100230 (2006).

122 Iannacone, M. *et al.* Platelets mediate cytotoxic T lymphocyte-induced liver damage. *Nat Med* **11**, 1167-1169, doi:10.1038/nm1317 (2005).

123 Iannacone, M., Sitia, G., Ruggeri, Z. M. & Guidotti, L. G. HBV pathogenesis in animal models: recent advances on the role of platelets. *J Hepatol* **46**, 719-726, doi:10.1016/j.jhep.2007.01.007 (2007).

124 Sitia, G., Iannacone, M., Muller, S., Bianchi, M. E. & Guidotti, L. G. Treatment with HMGB1 inhibitors diminishes CTL-induced liver disease in HBV transgenic mice. *J Leukoc Biol* **81**, 100-107, doi:10.1189/jlb.0306173 (2007).

125 Sitia, G. *et al.* MMPs are required for recruitment of antigen-nonspecific mononuclear cells into the liver by CTLs. *J Clin Invest* **113**, 1158-1167, doi:10.1172/jci21087 (2004).

126 Sandalova, E. *et al.* Increased levels of arginase in patients with acute hepatitis B suppress antiviral T cells. *Gastroenterology* **143**, 78-87.e73, doi:10.1053/j.gastro.2012.03.041 (2012).

127 Chisari, F. V. Regulation of human lymphocyte function by a soluble extract from normal human liver. *J Immunol* **121**, 1279-1286 (1978).

128 Asabe, S. *et al.* The size of the viral inoculum contributes to the outcome of hepatitis B virus infection. *J Virol* **83**, 9652-9662, doi:10.1128/jvi.00867-09 (2009).

129 Yang, P. L. *et al.* Immune effectors required for hepatitis B virus clearance. *Proc Natl Acad Sci U S A* **107**, 798-802, doi:10.1073/pnas.0913498107 (2010).

130 Penna, A. *et al.* Predominant T-helper 1 cytokine profile of hepatitis B virus nucleocapsid-specific T cells in acute self-limited hepatitis B. *Hepatology* **25**, 1022-1027, doi:10.1002/hep.510250438 (1997).

131 Bertoletti, A. & Ferrari, C. Kinetics of the immune response during HBV and HCV infection. *Hepatology* **38**, 4-13, doi:10.1053/jhep.2003.50310 (2003).

132 Wang, H. *et al.* TNF-α/IFN-γ profile of HBV-specific CD4 T cells is associated with liver damage and viral clearance in chronic HBV infection. *J Hepatol* **72**, 45-56, doi:10.1016/j.jhep.2019.08.024 (2020).

133 Wherry, E. J. & Ahmed, R. Memory CD8 T-cell differentiation during viral infection. *J Virol* **78**, 5535-5545, doi:10.1128/jvi.78.11.5535-5545.2004 (2004).

134 Wherry, E. J., Barber, D. L., Kaech, S. M., Blattman, J. N. & Ahmed, R. Antigen-independent memory CD8 T cells do not develop during chronic viral infection. *Proc Natl Acad Sci U S A* **101**, 16004-16009, doi:10.1073/pnas.0407192101 (2004).

135 Penna, A. *et al.* Long-lasting memory T cell responses following self-limited acute hepatitis B. *J Clin Invest* **98**, 1185-1194, doi:10.1172/jci118902 (1996).

136 Takaki, A. *et al.* Cellular immune responses persist and humoral responses decrease two decades after recovery from a single-source outbreak of hepatitis C. *Nat Med* **6**, 578-582, doi:10.1038/75063 (2000).

137 Ferrari, C. *et al.* Cellular immune response to hepatitis B virus-encoded antigens in acute and chronic hepatitis B virus infection. *J Immunol* **145**, 3442-3449 (1990).

138 Webster, G. J. *et al.* Longitudinal analysis of CD8+ T cells specific for structural and nonstructural hepatitis B virus proteins in patients with chronic hepatitis B: implications for immunotherapy. *J Virol* **78**, 5707-5719, doi:10.1128/jvi.78.11.5707-5719.2004 (2004).

139 Rehermann, B. Pathogenesis of chronic viral hepatitis: differential roles of T cells and NK cells. *Nat Med* **19**, 859-868, doi:10.1038/nm.3251 (2013).

140 Boni, C. *et al.* Characterization of hepatitis B virus (HBV)-specific T-cell dysfunction in chronic HBV infection. *J Virol* **81**, 4215-4225, doi:10.1128/jvi.02844-06 (2007).

141 Maini, M. K. *et al.* The role of virus-specific CD8(+) cells in liver damage and viral control during persistent hepatitis B virus infection. *J Exp Med* **191**, 1269-1280, doi:10.1084/jem.191.8.1269 (2000).

142 Schurich, A. *et al.* Role of the coinhibitory receptor cytotoxic T lymphocyte antigen-4 on apoptosis-Prone CD8 T cells in persistent hepatitis B virus infection. *Hepatology* **53**, 1494-1503, doi:10.1002/hep.24249 (2011).

143 Nebbia, G. *et al.* Upregulation of the Tim-3/galectin-9 pathway of T cell exhaustion in chronic hepatitis B virus infection. *PLoS One* **7**, e47648, doi:10.1371/journal.pone.0047648 (2012).

144 Kurktschiev, P. D. *et al.* Dysfunctional CD8+ T cells in hepatitis B and C are characterized by a lack of antigen-specific T-bet induction. *J Exp Med* **211**, 2047-2059, doi:10.1084/jem.20131333 (2014).

145 Wu, W. *et al.* Blockade of Tim-3 signaling restores the virus-specific CD8(+) T-cell response in patients with chronic hepatitis B. *Eur J Immunol* **42**, 1180-1191, doi:10.1002/eji.201141852 (2012).

146 Bengsch, B., Martin, B. & Thimme, R. Restoration of HBV-specific CD8+ T cell function by PD-1 blockade in inactive carrier patients is linked to T cell differentiation. *J Hepatol* **61**, 1212-1219, doi:10.1016/j.jhep.2014.07.005 (2014).

147 Fisicaro, P. *et al.* Antiviral intrahepatic T-cell responses can be restored by blocking programmed death-1 pathway in chronic hepatitis B. *Gastroenterology* **138**, 682-693, 693.e681-684, doi:10.1053/j.gastro.2009.09.052 (2010).

148 Raziorrouh, B. *et al.* The immunoregulatory role of CD244 in chronic hepatitis B infection and its inhibitory potential on virus-specific CD8+ T-cell function. *Hepatology* **52**, 1934-1947, doi:10.1002/hep.23936 (2010).

149 Schurich, A. *et al.* Distinct Metabolic Requirements of Exhausted and Functional Virus-Specific CD8 T Cells in the Same Host. *Cell Rep* **16**, 1243-1252, doi:10.1016/j.celrep.2016.06.078 (2016).

150 Fisicaro, P. *et al.* Targeting mitochondrial dysfunction can restore antiviral activity of exhausted HBV-specific CD8 T cells in chronic hepatitis B. *Nat Med* **23**, 327-336, doi:10.1038/nm.4275 (2017).

151 Rosenberg, S. A. *et al.* Use of tumor-infiltrating lymphocytes and interleukin-2 in the immunotherapy of patients with metastatic melanoma. A preliminary report. *N Engl J Med* **319**, 1676-1680, doi:10.1056/nejm198812223192527 (1988).

152 Dudley, M. E. *et al.* Cancer regression and autoimmunity in patients after clonal repopulation with antitumor lymphocytes. *Science* **298**, 850-854, doi:10.1126/science.1076514 (2002).

153 Rohaan, M. W., van den Berg, J. H., Kvistborg, P. & Haanen, J. Adoptive transfer of tumor-infiltrating lymphocytes in melanoma: a viable treatment option. *J Immunother Cancer* **6**, 102, doi:10.1186/s40425-018-0391-1 (2018).

154 Morgan, R. A. *et al.* Cancer regression in patients after transfer of genetically engineered lymphocytes. *Science* **314**, 126-129, doi:10.1126/science.1129003 (2006).

155 Gross, G., Waks, T. & Eshhar, Z. Expression of immunoglobulin-T-cell receptor chimeric molecules as functional receptors with antibody-type specificity. *Proc Natl Acad Sci U S A* **86**, 10024-10028, doi:10.1073/pnas.86.24.10024 (1989).

156 Holzinger, A. & Abken, H. Advances and Challenges of CAR T Cells in Clinical Trials. *Recent Results Cancer Res* **214**, 93-128, doi:10.1007/978-3-030-23765-3_3 (2020).

157 Garrido, F. & Algarra, I. MHC antigens and tumor escape from immune surveillance. *Adv Cancer Res* **83**, 117-158, doi:10.1016/s0065-230x(01)83005-0 (2001).

158 Garrido, F. *et al.* Implications for immunosurveillance of altered HLA class I phenotypes in human tumours. *Immunol Today* **18**, 89-95, doi:10.1016/s0167-5699(96)10075-x (1997).

159 Seliger, B., Cabrera, T., Garrido, F. & Ferrone, S. HLA class I antigen abnormalities and immune escape by malignant cells. *Semin Cancer Biol* **12**, 3-13, doi:10.1006/scbi.2001.0404 (2002).

160 Marincola, F. M., Jaffee, E. M., Hicklin, D. J. & Ferrone, S. Escape of human solid tumors from T-cell recognition: molecular mechanisms and functional significance. *Adv Immunol* **74**, 181-273, doi:10.1016/s0065-2776(08)60911-6 (2000).

161 Cole, D. J. *et al.* Characterization of the functional specificity of a cloned T-cell receptor heterodimer recognizing the MART-1 melanoma antigen. *Cancer Res* **55**, 748-752 (1995).

162 van Loenen, M. M. *et al.* Mixed T cell receptor dimers harbor potentially harmful neoreactivity. *Proc Natl Acad Sci U S A* **107**, 10972-10977, doi:10.1073/pnas.1005802107 (2010).

163 Sommermeyer, D. *et al.* Designer T cells by T cell receptor replacement. *Eur J Immunol* **36**, 3052-3059, doi:10.1002/eji.200636539 (2006).

164 Bendle, G. M. *et al.* Lethal graft-versus-host disease in mouse models of T cell receptor gene therapy. *Nat Med* **16**, 565-570, 561p following 570, doi:10.1038/nm.2128 (2010).

165 Rosenberg, S. A. Of mice, not men: no evidence for graft-versus-host disease in humans receiving T-cell receptor-transduced autologous T cells. *Mol Ther* **18**, 1744-1745, doi:10.1038/mt.2010.195 (2010).

166 Cohen, C. J., Zhao, Y., Zheng, Z., Rosenberg, S. A. & Morgan, R. A. Enhanced antitumor activity of murine-human hybrid T-cell receptor (TCR) in human lymphocytes is associated with improved pairing and TCR/CD3 stability. *Cancer Res* **66**, 8878-8886, doi:10.1158/0008-5472.Can-06-1450 (2006).

167 Cohen, C. J. *et al.* Enhanced antitumor activity of T cells engineered to express T-cell receptors with a second disulfide bond. *Cancer Res* **67**, 3898-3903, doi:10.1158/0008-5472.Can-06-3986 (2007).

168 Scholten, K. B. *et al.* Codon modification of T cell receptors allows enhanced functional expression in transgenic human T cells. *Clin Immunol* **119**, 135-145, doi:10.1016/j.clim.2005.12.009 (2006).

169 Jorritsma, A. *et al.* Selecting highly affine and well-expressed TCRs for gene therapy of melanoma. *Blood* **110**, 3564-3572, doi:10.1182/blood-2007-02-075010 (2007).

170 Leisegang, M. *et al.* T-cell receptor gene-modified T cells with shared renal cell carcinoma specificity for adoptive T-cell therapy. *Clin Cancer Res* **16**, 2333-2343, doi:10.1158/1078-0432.Ccr-09-2897 (2010).

171 Schober, K. *et al.* Orthotopic replacement of T-cell receptor alpha- and beta-chains with preservation of near-physiological T-cell function. *Nat Biomed Eng* **3**, 974-984, doi:10.1038/s41551-019-0409-0 (2019).

172 Maude, S. L. *et al.* Tisagenlecleucel in Children and Young Adults with B-Cell Lymphoblastic Leukemia. *N Engl J Med* **378**, 439-448, doi:10.1056/NEJMoa1709866 (2018).

173 Watanabe, K., Kuramitsu, S., Posey, A. D., Jr. & June, C. H. Expanding the Therapeutic Window for CAR T Cell Therapy in Solid Tumors: The Knowns and Unknowns of CAR T Cell Biology. *Front Immunol* **9**, 2486, doi:10.3389/fimmu.2018.02486 (2018).

174 Lamers, C. H. *et al.* Treatment of metastatic renal cell carcinoma with autologous T-lymphocytes genetically retargeted against carbonic anhydrase IX: first clinical experience. *J Clin Oncol* **24**, e20-22, doi:10.1200/jco.2006.05.9964 (2006).

175 Parkhurst, M. R. *et al.* T cells targeting carcinoembryonic antigen can mediate regression of metastatic colorectal cancer but induce severe transient colitis. *Mol Ther* **19**, 620-626, doi:10.1038/mt.2010.272 (2011).

176 Morgan, R. A. *et al.* Case report of a serious adverse event following the administration of T cells transduced with a chimeric antigen receptor recognizing ERBB2. *Mol Ther* **18**, 843-851, doi:10.1038/mt.2010.24 (2010).

177 Yang, J. D., Nakamura, I. & Roberts, L. R. The tumor microenvironment in hepatocellular carcinoma: current status and therapeutic targets. *Semin Cancer Biol* **21**, 35-43, doi:10.1016/j.semcancer.2010.10.007 (2011).

178 Knolle, P. A. & Thimme, R. Hepatic immune regulation and its involvement in viral hepatitis infection. *Gastroenterology* **146**, 1193-1207, doi:10.1053/j.gastro.2013.12.036 (2014).

179 Protzer, U., Maini, M. K. & Knolle, P. A. Living in the liver: hepatic infections. *Nat Rev Immunol* **12**, 201-213, doi:10.1038/nri3169 (2012).

180 Kamphorst, A. O. & Ahmed, R. CD4 T-cell immunotherapy for chronic viral infections and cancer. *Immunotherapy* **5**, 975-987, doi:10.2217/imt.13.91 (2013).

181 Garber, K. Driving T-cell immunotherapy to solid tumors. *Nat Biotechnol* **36**, 215-219, doi:10.1038/nbt.4090 (2018).

182 Greenberg, P. D., Cheever, M. A. & Fefer, A. Eradication of disseminated murine leukemia by chemoimmunotherapy with cyclophosphamide and adoptively transferred immune syngeneic Lyt-1+2- lymphocytes. *J Exp Med* **154**, 952-963, doi:10.1084/jem.154.3.952 (1981).

183 Kahn, M. *et al.* CD4+ T cell clones specific for the human p97 melanoma-associated antigen can eradicate pulmonary metastases from a murine tumor expressing the p97 antigen. *J Immunol* **146**, 3235-3241 (1991).

184 Perez-Diez, A. *et al.* CD4 cells can be more efficient at tumor rejection than CD8 cells. *Blood* **109**, 5346-5354, doi:10.1182/blood-2006-10-051318 (2007).

185 Sommermeyer, D. *et al.* Chimeric antigen receptor-modified T cells derived from defined CD8+ and CD4+ subsets confer superior antitumor reactivity in vivo. *Leukemia* **30**, 492-500, doi:10.1038/leu.2015.247 (2016).

186 Alspach, E. *et al.* MHC-II neoantigens shape tumour immunity and response to immunotherapy. *Nature* **574**, 696-701, doi:10.1038/s41586-019-1671-8 (2019).

187 Hunder, N. N. *et al.* Treatment of metastatic melanoma with autologous CD4+ T cells against NY-ESO-1. *N Engl J Med* **358**, 2698-2703, doi:10.1056/NEJMoa0800251 (2008).

188 Kyte, J. A. *et al.* T-helper cell receptors from long-term survivors after telomerase cancer vaccination for use in adoptive cell therapy. *Oncoimmunology* **5**, e1249090, doi:10.1080/2162402x.2016.1249090 (2016).

189 Yao, X. *et al.* Isolation and Characterization of an HLA-DPB1*04: 01-restricted MAGE-A3 T-Cell Receptor for Cancer Immunotherapy. *J Immunother* **39**, 191-201, doi:10.1097/cji.0000000000000123 (2016).

190 Mercier-Letondal, P. *et al.* Isolation and Characterization of an HLA-DRB1*04-Restricted HPV16-E7 T Cell Receptor for Cancer Immunotherapy. *Hum Gene Ther* **29**, 1202-1212, doi:10.1089/hum.2018.091 (2018).

191 Dillard, P. *et al.* Targeting Telomerase with an HLA Class II-Restricted TCR for Cancer Immunotherapy. *Mol Ther* **29**, 1199-1213, doi:10.1016/j.ymthe.2020.11.019 (2021).

192 Straetemans, T. *et al.* TCR gene transfer: MAGE-C2/HLA-A2 and MAGE-A3/HLA-DP4 epitopes as melanoma-specific immune targets. *Clinical & developmental immunology* **2012**, 586314, doi:10.1155/2012/586314 (2012).

193 Wisskirchen, K. *et al.* Isolation and functional characterization of hepatitis B virus-specific T-cell receptors as new tools for experimental and clinical use. *PLoS One* **12**, e0182936, doi:10.1371/journal.pone.0182936 (2017).

194 Poncette, L., Chen, X., Lorenz, F. K. & Blankenstein, T. Effective NY-ESO-1-specific MHC II-restricted T cell receptors from antigen-negative hosts enhance tumor regression. *J Clin Invest* **129**, 324-335, doi:10.1172/jci120391 (2019).

195 Lu, Y. C. *et al.* Treatment of Patients With Metastatic Cancer Using a Major Histocompatibility Complex Class II-Restricted T-Cell Receptor Targeting the Cancer Germline Antigen MAGE-A3. *J Clin Oncol* **35**, 3322-3329, doi:10.1200/jco.2017.74.5463 (2017).

196 Ilan, Y. *et al.* Adoptive transfer of immunity to hepatitis B virus after T cell-depleted allogeneic bone marrow transplantation. *Hepatology* **18**, 246-252 (1993).

197 Lau, G. K. *et al.* Clearance of hepatitis B surface antigen after bone marrow transplantation: role of adoptive immunity transfer. *Hepatology* **25**, 1497-1501, doi:10.1002/hep.510250631 (1997).

198 Bohne, F. *et al.* T cells redirected against hepatitis B virus surface proteins eliminate infected hepatocytes. *Gastroenterology* **134**, 239-247, doi:10.1053/j.gastro.2007.11.002 (2008).
199 Krebs, K. *et al.* T cells expressing a chimeric antigen receptor that binds hepatitis B virus envelope proteins control virus replication in mice. *Gastroenterology* **145**, 456-465, doi:10.1053/j.gastro.2013.04.047 (2013).
200 Festag, M. M. *et al.* Evaluation of a Fully Human, Hepatitis B Virus-Specific Chimeric Antigen Receptor in an Immunocompetent Mouse Model. *Mol Ther* **27**, 947-959, doi:10.1016/j.ymthe.2019.02.001 (2019).
201 Gehring, A. J. *et al.* Engineering virus-specific T cells that target HBV infected hepatocytes and hepatocellular carcinoma cell lines. *J Hepatol* **55**, 103-110, doi:10.1016/j.jhep.2010.10.025 (2011).
202 Banu, N. *et al.* Building and optimizing a virus-specific T cell receptor library for targeted immunotherapy in viral infections. *Sci Rep* **4**, 4166, doi:10.1038/srep04166 (2014).
203 Koh, S. *et al.* A practical approach to immunotherapy of hepatocellular carcinoma using T cells redirected against hepatitis B virus. *Mol Ther Nucleic Acids* **2**, e114, doi:10.1038/mtna.2013.43 (2013).
204 Kah, J. *et al.* Lymphocytes transiently expressing virus-specific T cell receptors reduce hepatitis B virus infection. *J Clin Invest* **127**, 3177-3188, doi:10.1172/jci93024 (2017).
205 Wisskirchen, K. *et al.* T cell receptor grafting allows virological control of Hepatitis B virus infection. *J Clin Invest* **129**, 2932-2945, doi:10.1172/jci120228 (2019).
206 Qasim, W. *et al.* Immunotherapy of HCC metastases with autologous T cell receptor redirected T cells, targeting HBsAg in a liver transplant patient. *J Hepatol* **62**, 486-491, doi:10.1016/j.jhep.2014.10.001 (2015).
207 Tan, A. T. *et al.* Use of Expression Profiles of HBV-DNA Integrated Into Genomes of Hepatocellular Carcinoma Cells to Select T Cells for Immunotherapy. *Gastroenterology* **156**, 1862-1876.e1869, doi:10.1053/j.gastro.2019.01.251 (2019).
208 Nielsen, M., Lundegaard, C. & Lund, O. Prediction of MHC class II binding affinity using SMM-align, a novel stabilization matrix alignment method. *BMC Bioinformatics* **8**, 238, doi:10.1186/1471-2105-8-238 (2007).
209 Jensen, K. K. *et al.* Improved methods for predicting peptide binding affinity to MHC class II molecules. *Immunology* **154**, 394-406, doi:10.1111/imm.12889 (2018).
210 Sidney, J. *et al.* Divergent motifs but overlapping binding repertoires of six HLA-DQ molecules frequently expressed in the worldwide human population. *J Immunol* **185**, 4189-4198, doi:10.4049/jimmunol.1001006 (2010).
211 Sidney, J. *et al.* Five HLA-DP molecules frequently expressed in the worldwide human population share a common HLA supertypic binding specificity. *J Immunol* **184**, 2492-2503, doi:10.4049/jimmunol.0903655 (2010).
212 Southwood, S. *et al.* Several common HLA-DR types share largely overlapping peptide binding repertoires. *J Immunol* **160**, 3363-3373 (1998).
213 Ferrari, C. *et al.* Identification of immunodominant T cell epitopes of the hepatitis B virus nucleocapsid antigen. *J Clin Invest* **88**, 214-222, doi:10.1172/jci115280 (1991).
214 Raziorrouh, B. *et al.* Inhibitory phenotype of HBV-specific CD4+ T-cells is characterized by high PD-1 expression but absent coregulation of multiple inhibitory molecules. *PLoS One* **9**, e105703, doi:10.1371/journal.pone.0105703 (2014).
215 Chisari, F. V. & Ferrari, C. Hepatitis B virus immunopathogenesis. *Annu Rev Immunol* **13**, 29-60, doi:10.1146/annurev.iy.13.040195.000333 (1995).
216 Barnaba, V. *et al.* Recognition of hepatitis B virus envelope proteins by liver-infiltrating T lymphocytes in chronic HBV infection. *J Immunol* **143**, 2650-2655 (1989).
217 Pajot, A. *et al.* Identification of novel HLA-DR1-restricted epitopes from the hepatitis B virus envelope protein in mice expressing HLA-DR1 and vaccinated human subjects. *Microbes Infect* **8**, 2783-2790, doi:10.1016/j.micinf.2006.08.009 (2006).
218 Barnaba, V. *et al.* Selective expansion of cytotoxic T lymphocytes with a CD4+CD56+ surface phenotype and a T helper type 1 profile of cytokine secretion in the liver of patients chronically infected with Hepatitis B virus. *J Immunol* **152**, 3074-3087 (1994).
219 Desombere, I., Gijbels, Y., Verwulgen, A. & Leroux-Roels, G. Characterization of the T cell recognition of hepatitis B surface antigen (HBsAg) by good and poor responders to hepatitis B vaccines. *Clin Exp Immunol* **122**, 390-399, doi:10.1046/j.1365-2249.2000.01383.x (2000).

220 Ru, Z. *et al.* Development of a humanized HLA-A2.1/DP4 transgenic mouse model and the use of this model to map HLA-DP4-restricted epitopes of HBV envelope protein. *PLoS One* **7**, e32247, doi:10.1371/journal.pone.0032247 (2012).

221 Honorati, M. C. *et al.* Epitope specificity of Th0/Th2 CD4+ T-lymphocyte clones induced by vaccination with rHBsAg vaccine. *Gastroenterology* **112**, 2017-2027, doi:10.1053/gast.1997.v112.pm9178695 (1997).

222 Mizukoshi, E. *et al.* Cellular immune responses to the hepatitis B virus polymerase. *J Immunol* **173**, 5863-5871, doi:10.4049/jimmunol.173.9.5863 (2004).

223 Lefranc, M.-P. & Lefranc, G. e. *The immunoglobulin factsbook*. (Academic Press, 2001).

224 Arden, B., Clark, S. P., Kabelitz, D. & Mak, T. W. Human T-cell receptor variable gene segment families. *Immunogenetics* **42**, 455-500, doi:10.1007/bf00172176 (1995).

225 Engels, B. *et al.* Retroviral vectors for high-level transgene expression in T lymphocytes. *Hum Gene Ther* **14**, 1155-1168, doi:10.1089/104303403322167993 (2003).

226 Heemskerk, M. H. *et al.* Efficiency of T-cell receptor expression in dual-specific T cells is controlled by the intrinsic qualities of the TCR chains within the TCR-CD3 complex. *Blood* **109**, 235-243, doi:10.1182/blood-2006-03-013318 (2007).

227 Gonzalez-Galarza, F. F. *et al.* Allele frequency net 2015 update: new features for HLA epitopes, KIR and disease and HLA adverse drug reaction associations. *Nucleic acids research* **43**, D784-788, doi:10.1093/nar/gku1166 (2015).

228 Graffelman, J. & Weir, B. S. On the testing of Hardy-Weinberg proportions and equality of allele frequencies in males and females at biallelic genetic markers. *Genetic epidemiology* **42**, 34-48, doi:10.1002/gepi.22079 (2018).

229 Aleksic, M. *et al.* Different affinity windows for virus and cancer-specific T-cell receptors: implications for therapeutic strategies. *Eur J Immunol* **42**, 3174-3179, doi:10.1002/eji.201242606 (2012).

230 Bosshart, H. & Heinzelmann, M. THP-1 cells as a model for human monocytes. *Annals of translational medicine* **4**, 438, doi:10.21037/atm.2016.08.53 (2016).

231 Reith, W. & Mach, B. The bare lymphocyte syndrome and the regulation of MHC expression. *Annu Rev Immunol* **19**, 331-373, doi:10.1146/annurev.immunol.19.1.331 (2001).

232 Marion, M. J., Hantz, O. & Durantel, D. The HepaRG cell line: biological properties and relevance as a tool for cell biology, drug metabolism, and virology studies. *Methods Mol Biol* **640**, 261-272, doi:10.1007/978-1-60761-688-7_13 (2010).

233 Pajot, A. *et al.* A mouse model of human adaptive immune functions: HLA-A2.1-/HLA-DR1-transgenic H-2 class I-/class II-knockout mice. *Eur J Immunol* **34**, 3060-3069, doi:10.1002/eji.200425463 (2004).

234 Andreatta, M. *et al.* An automated benchmarking platform for MHC class II binding prediction methods. *Bioinformatics* **34**, 1522-1528, doi:10.1093/bioinformatics/btx820 (2018).

235 Iwai, L. K. *et al.* In silico prediction of peptides binding to multiple HLA-DR molecules accurately identifies immunodominant epitopes from gp43 of Paracoccidioides brasiliensis frequently recognized in primary peripheral blood mononuclear cell responses from sensitized individuals. *Molecular medicine (Cambridge, Mass.)* **9**, 209-219 (2003).

236 Mustafa, A. S. & Shaban, F. A. ProPred analysis and experimental evaluation of promiscuous T-cell epitopes of three major secreted antigens of Mycobacterium tuberculosis. *Tuberculosis (Edinburgh, Scotland)* **86**, 115-124, doi:10.1016/j.tube.2005.05.001 (2006).

237 Al-Attiyah, R. & Mustafa, A. S. Computer-assisted prediction of HLA-DR binding and experimental analysis for human promiscuous Th1-cell peptides in the 24 kDa secreted lipoprotein (LppX) of Mycobacterium tuberculosis. *Scandinavian journal of immunology* **59**, 16-24, doi:10.1111/j.0300-9475.2004.01349.x (2004).

238 Lorenz, F. K. M. *et al.* Unbiased Identification of T-Cell Receptors Targeting Immunodominant Peptide-MHC Complexes for T-Cell Receptor Immunotherapy. *Hum Gene Ther* **28**, 1158-1168, doi:10.1089/hum.2017.122 (2017).

239 Wolfl, M., Kuball, J., Eyrich, M., Schlegel, P. G. & Greenberg, P. D. Use of CD137 to study the full repertoire of CD8+ T cells without the need to know epitope specificities.

Cytometry. Part A : the journal of the International Society for Analytical Cytology **73**, 1043-1049, doi:10.1002/cyto.a.20594 (2008).

240 Ho, W. Y., Nguyen, H. N., Wolfl, M., Kuball, J. & Greenberg, P. D. In vitro methods for generating CD8+ T-cell clones for immunotherapy from the naive repertoire. *Journal of immunological methods* **310**, 40-52, doi:10.1016/j.jim.2005.11.023 (2006).

241 Mehrotra, S. *et al.* Regulation of melanoma epitope-specific cytolytic T lymphocyte response by immature and activated dendritic cells, in vitro. *Cancer Res* **63**, 5607-5614 (2003).

242 Wolfl, M. *et al.* Activation-induced expression of CD137 permits detection, isolation, and expansion of the full repertoire of CD8+ T cells responding to antigen without requiring knowledge of epitope specificities. *Blood* **110**, 201-210, doi:10.1182/blood-2006-11-056168 (2007).

243 Zandvliet, M. L. *et al.* Simultaneous isolation of CD8(+) and CD4(+) T cells specific for multiple viruses for broad antiviral immune reconstitution after allogeneic stem cell transplantation. *J Immunother* **34**, 307-319, doi:10.1097/CJI.0b013e318213cb90 (2011).

244 Watanabe, K. *et al.* CD137-guided isolation and expansion of antigen-specific CD8 cells for potential use in adoptive immunotherapy. *International journal of hematology* **88**, 311-320, doi:10.1007/s12185-008-0134-z (2008).

245 Parkhurst, M. *et al.* Isolation of T-Cell Receptors Specifically Reactive with Mutated Tumor-Associated Antigens from Tumor-Infiltrating Lymphocytes Based on CD137 Expression. *Clin Cancer Res* **23**, 2491-2505, doi:10.1158/1078-0432.Ccr-16-2680 (2017).

246 Ye, Q. *et al.* CD137 accurately identifies and enriches for naturally occurring tumor-reactive T cells in tumor. *Clin Cancer Res* **20**, 44-55, doi:10.1158/1078-0432.Ccr-13-0945 (2014).

247 Schmidt, J., Dojcinovic, D., Guillaume, P. & Luescher, I. Analysis, Isolation, and Activation of Antigen-Specific CD4(+) and CD8(+) T Cells by Soluble MHC-Peptide Complexes. *Front Immunol* **4**, 218, doi:10.3389/fimmu.2013.00218 (2013).

248 Altman, J. D. *et al.* Phenotypic analysis of antigen-specific T lymphocytes. *Science* **274**, 94-96, doi:10.1126/science.274.5284.94 (1996).

249 Busch, D. H., Pilip, I. M., Vijh, S. & Pamer, E. G. Coordinate regulation of complex T cell populations responding to bacterial infection. *Immunity* **8**, 353-362, doi:10.1016/s1074-7613(00)80540-3 (1998).

250 Keenan, R. D. *et al.* Purification of cytomegalovirus-specific CD8 T cells from peripheral blood using HLA-peptide tetramers. *British journal of haematology* **115**, 428-434, doi:10.1046/j.1365-2141.2001.03106.x (2001).

251 Subbramanian, R. A. *et al.* Engineered T-cell receptor tetramers bind MHC-peptide complexes with high affinity. *Nat Biotechnol* **22**, 1429-1434, doi:10.1038/nbt1024 (2004).

252 Krueger, L. A., Nugent, C. T. & Hampl, J. Identification of human antigen-specific T cells using MHC class I and class II tetramers. *Current protocols in cytometry* **Chapter 6**, Unit 6.18, doi:10.1002/0471142956.cy0618s30 (2004).

253 Whelan, J. A. *et al.* Specificity of CTL interactions with peptide-MHC class I tetrameric complexes is temperature dependent. *J Immunol* **163**, 4342-4348 (1999).

254 Daniels, M. A. & Jameson, S. C. Critical role for CD8 in T cell receptor binding and activation by peptide/major histocompatibility complex multimers. *J Exp Med* **191**, 335-346, doi:10.1084/jem.191.2.335 (2000).

255 Maile, R. *et al.* Antigen-specific modulation of an immune response by in vivo administration of soluble MHC class I tetramers. *J Immunol* **167**, 3708-3714, doi:10.4049/jimmunol.167.7.3708 (2001).

256 O'Herrin, S. M. *et al.* Antigen-specific blockade of T cells in vivo using dimeric MHC peptide. *J Immunol* **167**, 2555-2560, doi:10.4049/jimmunol.167.5.2555 (2001).

257 Cebecauer, M. *et al.* CD8+ cytotoxic T lymphocyte activation by soluble major histocompatibility complex-peptide dimers. *The Journal of biological chemistry* **280**, 23820-23828, doi:10.1074/jbc.M500654200 (2005).

258 Xu, X. N. *et al.* A novel approach to antigen-specific deletion of CTL with minimal cellular activation using alpha3 domain mutants of MHC class I/peptide complex. *Immunity* **14**, 591-602, doi:10.1016/s1074-7613(01)00133-9 (2001).

259 Knabel, M. *et al.* Reversible MHC multimer staining for functional isolation of T-cell populations and effective adoptive transfer. *Nat Med* **8**, 631-637, doi:10.1038/nm0602-631 (2002).

260 Neudorfer, J. *et al.* Reversible HLA multimers (Streptamers) for the isolation of human cytotoxic T lymphocytes functionally active against tumor- and virus-derived antigens. *Journal of immunological methods* **320**, 119-131, doi:10.1016/j.jim.2007.01.001 (2007).

261 Schmitt, A. *et al.* Adoptive transfer and selective reconstitution of streptamer-selected cytomegalovirus-specific CD8+ T cells leads to virus clearance in patients after allogeneic peripheral blood stem cell transplantation. *Transfusion* **51**, 591-599, doi:10.1111/j.1537-2995.2010.02940.x (2011).

262 Wang, X. *et al.* Streptamer-based selection of WT1-specific CD8+ T cells for specific donor lymphocyte infusions. *Experimental hematology* **38**, 1066-1073, doi:10.1016/j.exphem.2010.07.002 (2010).

263 van Loenen, M. M. *et al.* A Good Manufacturing Practice procedure to engineer donor virus-specific T cells into potent anti-leukemic effector cells. *Haematologica* **99**, 759-768, doi:10.3324/haematol.2013.093690 (2014).

264 Dossinger, G. *et al.* MHC multimer-guided and cell culture-independent isolation of functional T cell receptors from single cells facilitates TCR identification for immunotherapy. *PLoS One* **8**, e61384, doi:10.1371/journal.pone.0061384 (2013).

265 Nauerth, M. *et al.* TCR-ligand koff rate correlates with the protective capacity of antigen-specific CD8+ T cells for adoptive transfer. *Sci Transl Med* **5**, 192ra187, doi:10.1126/scitranslmed.3005958 (2013).

266 Govers, C., Berrevoets, C., Treffers-Westerlaken, E., Broertjes, M. & Debets, R. Magnetic-activated cell sorting of TCR-engineered T cells, using tCD34 as a gene marker, but not peptide-MHC multimers, results in significant numbers of functional CD4+ and CD8+ T cells. *Human gene therapy methods* **23**, 213-224, doi:10.1089/hgtb.2012.074 (2012).

267 Vollers, S. S. & Stern, L. J. Class II major histocompatibility complex tetramer staining: progress, problems, and prospects. *Immunology* **123**, 305-313, doi:10.1111/j.1365-2567.2007.02801.x (2008).

268 Nepom, G. T. MHC class II tetramers. *J Immunol* **188**, 2477-2482, doi:10.4049/jimmunol.1102398 (2012).

269 Kong, Y. Y. & Kwok, W. W. Identification of Human Antigen-Specific CD4(+) T-Cells with Peptide-MHC Multimer Technologies. *Methods Mol Biol* **1988**, 375-386, doi:10.1007/978-1-4939-9450-2_26 (2019).

270 Rius, C. *et al.* Peptide-MHC Class I Tetramers Can Fail To Detect Relevant Functional T Cell Clonotypes and Underestimate Antigen-Reactive T Cell Populations. *J Immunol* **200**, 2263-2279, doi:10.4049/jimmunol.1700242 (2018).

271 Cole, D. K. *et al.* Human TCR-binding affinity is governed by MHC class restriction. *J Immunol* **178**, 5727-5734, doi:10.4049/jimmunol.178.9.5727 (2007).

272 Dietrich, P. Y. *et al.* TCR analysis reveals significant repertoire selection during in vitro lymphocyte culture. *International immunology* **9**, 1073-1083, doi:10.1093/intimm/9.8.1073 (1997).

273 Pilch, H. *et al.* Antigen-driven T-cell selection in patients with cervical cancer as evidenced by T-cell receptor analysis and recognition of autologous tumor. *Clinical and diagnostic laboratory immunology* **9**, 267-278, doi:10.1128/cdli.9.2.267-278.2002 (2002).

274 Kim, M., Moon, H. B., Kim, K. & Lee, K. Y. Antigen dose governs the shaping of CTL repertoires in vitro and in vivo. *International immunology* **18**, 435-444, doi:10.1093/intimm/dxh383 (2006).

275 Neller, M. A. *et al.* High efficiency ex vivo cloning of antigen-specific human effector T cells. *PLoS One* **9**, e110741, doi:10.1371/journal.pone.0110741 (2014).

276 Thomas, S. *et al.* Framework engineering to produce dominant T cell receptors with enhanced antigen-specific function. *Nat Commun* **10**, 4451, doi:10.1038/s41467-019-12441-w (2019).

277 Aggen, D. H. *et al.* Single-chain ValphaVbeta T-cell receptors function without mispairing with endogenous TCR chains. *Gene therapy* **19**, 365-374, doi:10.1038/gt.2011.104 (2012).

278 Hart, D. P. *et al.* Retroviral transfer of a dominant TCR prevents surface expression of a large proportion of the endogenous TCR repertoire in human T cells. *Gene therapy* **15**, 625-631, doi:10.1038/sj.gt.3303078 (2008).

279 Riddell, S. R. *et al.* T-cell mediated rejection of gene-modified HIV-specific cytotoxic T lymphocytes in HIV-infected patients. *Nat Med* **2**, 216-223, doi:10.1038/nm0296-216 (1996).

280 Davis, J. L. *et al.* Development of human anti-murine T-cell receptor antibodies in both responding and nonresponding patients enrolled in TCR gene therapy trials. *Clin Cancer Res* **16**, 5852-5861, doi:10.1158/1078-0432.Ccr-10-1280 (2010).

281 Kershaw, M. H. *et al.* A phase I study on adoptive immunotherapy using gene-modified T cells for ovarian cancer. *Clin Cancer Res* **12**, 6106-6115, doi:10.1158/1078-0432.Ccr-06-1183 (2006).

282 Sommermeyer, D. & Uckert, W. Minimal amino acid exchange in human TCR constant regions fosters improved function of TCR gene-modified T cells. *J Immunol* **184**, 6223-6231, doi:10.4049/jimmunol.0902055 (2010).

283 Penna, A. *et al.* Cytotoxic T lymphocytes recognize an HLA-A2-restricted epitope within the hepatitis B virus nucleocapsid antigen. *J Exp Med* **174**, 1565-1570, doi:10.1084/jem.174.6.1565 (1991).

284 Jung, M. C. *et al.* Hepatitis B virus antigen-specific T-cell activation in patients with acute and chronic hepatitis B. *J Hepatol* **13**, 310-317, doi:10.1016/0168-8278(91)90074-l (1991).

285 Sobao, Y. *et al.* Identification of hepatitis B virus-specific CTL epitopes presented by HLA-A*2402, the most common HLA class I allele in East Asia. *J Hepatol* **34**, 922-929, doi:10.1016/s0168-8278(01)00048-4 (2001).

286 Nayersina, R. *et al.* HLA A2 restricted cytotoxic T lymphocyte responses to multiple hepatitis B surface antigen epitopes during hepatitis B virus infection. *J Immunol* **150**, 4659-4671 (1993).

287 Abbott, W. G. *et al.* Associations between HLA class I alleles and escape mutations in the hepatitis B virus core gene in New Zealand-resident Tongans. *J Virol* **84**, 621-629, doi:10.1128/jvi.01471-09 (2010).

288 Rehermann, B. *et al.* The cytotoxic T lymphocyte response to multiple hepatitis B virus polymerase epitopes during and after acute viral hepatitis. *J Exp Med* **181**, 1047-1058, doi:10.1084/jem.181.3.1047 (1995).

289 Jung, M. C. *et al.* Immune response of peripheral blood mononuclear cells to HBx-antigen of hepatitis B virus. *Hepatology* **13**, 637-643 (1991).

290 Boni, C. *et al.* Restored function of HBV-specific T cells after long-term effective therapy with nucleos(t)ide analogues. *Gastroenterology* **143**, 963-973.e969, doi:10.1053/j.gastro.2012.07.014 (2012).

291 Lohr, H. F. *et al.* Proliferative response of CD4+ T cells and hepatitis B virus clearance in chronic hepatitis with or without hepatitis B e-minus hepatitis B virus mutants. *Hepatology* **22**, 61-68, doi:10.1002/hep.1840220110 (1995).

292 Rivino, L. *et al.* Hepatitis B virus-specific T cells associate with viral control upon nucleos(t)ide-analogue therapy discontinuation. *J Clin Invest* **128**, 668-681, doi:10.1172/jci92812 (2018).

293 Jacobi, F. J. *et al.* OX40 stimulation and PD-L1 blockade synergistically augment HBV-specific CD4 T cells in patients with HBeAg-negative infection. *J Hepatol* **70**, 1103-1113, doi:10.1016/j.jhep.2019.02.016 (2019).

294 Neurath, A. R., Seto, B. & Strick, N. Antibodies to synthetic peptides from the preS1 region of the hepatitis B virus (HBV) envelope (env) protein are virus-neutralizing and protective. *Vaccine* **7**, 234-236, doi:10.1016/0264-410x(89)90235-1 (1989).

295 Yewdell, J. W. Confronting complexity: real-world immunodominance in antiviral CD8+ T cell responses. *Immunity* **25**, 533-543, doi:10.1016/j.immuni.2006.09.005 (2006).

296 Matei, H. V., Vica, M. L. & Siserman, C. V. Association between HLA class II alleles and hepatitis B virus infection in Transylvania, Romania. *Immunological investigations* **47**, 735-744, doi:10.1080/08820139.2018.1489832 (2018).

297 Ou, G. *et al.* The roles of HLA-DQB1 gene polymorphisms in hepatitis B virus infection. *Journal of translational medicine* **16**, 362, doi:10.1186/s12967-018-1716-z (2018).

298 Nishida, N. *et al.* New susceptibility and resistance HLA-DP alleles to HBV-related diseases identified by a trans-ethnic association study in Asia. *PLoS One* **9**, e86449, doi:10.1371/journal.pone.0086449 (2014).

299 Thursz, M. R. *et al.* Association between an MHC class II allele and clearance of hepatitis B virus in the Gambia. *N Engl J Med* **332**, 1065-1069, doi:10.1056/nejm199504203321604 (1995).

300 Hohler, T. *et al.* HLA-DRB1*1301 and *1302 protect against chronic hepatitis B. *J Hepatol* **26**, 503-507, doi:10.1016/s0168-8278(97)80414-x (1997).

301 Ahn, S. H. *et al.* Association between hepatitis B virus infection and HLA-DR type in Korea. *Hepatology* **31**, 1371-1373, doi:10.1053/jhep.2000.7988 (2000).

302 Li, X. *et al.* The influence of HLA alleles and HBV subgenotyes on the outcomes of HBV infections in Northeast China. *Virus Res* **163**, 328-333, doi:10.1016/j.virusres.2011.10.020 (2012).

303 Cotrina, M. *et al.* [Study of HLA-II antigens in chronic hepatitis C and B and in acute hepatitis B]. *Gastroenterologia y hepatologia* **20**, 115-118 (1997).

304 Singh, R., Kaul, R., Kaul, A. & Khan, K. A comparative review of HLA associations with hepatitis B and C viral infections across global populations. *World journal of gastroenterology* **13**, 1770-1787, doi:10.3748/wjg.v13.i12.1770 (2007).

305 Kummee, P., Tangkijvanich, P., Poovorawan, Y. & Hirankarn, N. Association of HLA-DRB1*13 and TNF-alpha gene polymorphisms with clearance of chronic hepatitis B infection and risk of hepatocellular carcinoma in Thai population. *J Viral Hepat* **14**, 841-848, doi:10.1111/j.1365-2893.2007.00880.x (2007).

306 Yan, Z. H. *et al.* Relationship between HLA-DR gene polymorphisms and outcomes of hepatitis B viral infections: a meta-analysis. *World journal of gastroenterology* **18**, 3119-3128, doi:10.3748/wjg.v18.i24.3119 (2012).

307 Xu, Y. Y. *et al.* Association between the frequency of class II HLA antigens and the susceptibility to intrauterine infection of hepatitis B virus. *International journal of biological sciences* **4**, 111-115, doi:10.7150/ijbs.4.111 (2008).

308 Almarri, A. & Batchelor, J. R. HLA and hepatitis B infection. *Lancet* **344**, 1194-1195, doi:10.1016/s0140-6736(94)90510-x (1994).

309 Doganay, L. *et al.* Association of human leukocyte antigen DQB1 and DRB1 alleles with chronic hepatitis B. *World journal of gastroenterology* **20**, 8179-8186, doi:10.3748/wjg.v20.i25.8179 (2014).

310 Lv, N., Dang, A., Wang, Z., Zheng, D. & Liu, G. Association of susceptibility to Takayasu arteritis in Chinese Han patients with HLA-DPB1. *Hum Immunol* **72**, 893-896, doi:10.1016/j.humimm.2011.05.001 (2011).

311 Panina-Bordignon, P. *et al.* Universally immunogenic T cell epitopes: promiscuous binding to human MHC class II and promiscuous recognition by T cells. *Eur J Immunol* **19**, 2237-2242, doi:10.1002/eji.1830191209 (1989).

312 Hu, Y. *et al.* Immunologic hierarchy, class II MHC promiscuity, and epitope spreading of a melanoma helper peptide vaccine. *Cancer Immunol Immunother* **63**, 779-786, doi:10.1007/s00262-014-1551-x (2014).

313 Kobayashi, H., Wood, M., Song, Y., Appella, E. & Celis, E. Defining promiscuous MHC class II helper T-cell epitopes for the HER2/neu tumor antigen. *Cancer Res* **60**, 5228-5236 (2000).

314 Tsai, S. & Santamaria, P. MHC Class II Polymorphisms, Autoreactive T-Cells, and Autoimmunity. *Front Immunol* **4**, 321, doi:10.3389/fimmu.2013.00321 (2013).

315 Doherty, D. G. *et al.* Structural basis of specificity and degeneracy of T cell recognition: pluriallelic restriction of T cell responses to a peptide antigen involves both specific and promiscuous interactions between the T cell receptor, peptide, and HLA-DR. *J Immunol* **161**, 3527-3535 (1998).

316 Shi, Y. *et al.* Promiscuous presentation and recognition of nucleosomal autoepitopes in lupus: role of autoimmune T cell receptor alpha chain. *J Exp Med* **187**, 367-378, doi:10.1084/jem.187.3.367 (1998).

317 Wooldridge, L. *et al.* A single autoimmune T cell receptor recognizes more than a million different peptides. *The Journal of biological chemistry* **287**, 1168-1177, doi:10.1074/jbc.M111.289488 (2012).

318 Joshi, S. K., Suresh, P. R. & Chauhan, V. S. Flexibility in MHC and TCR recognition: degenerate specificity at the T cell level in the recognition of promiscuous Th epitopes exhibiting no primary sequence homology. *J Immunol* **166**, 6693-6703, doi:10.4049/jimmunol.166.11.6693 (2001).

319 Geluk, A., van Meijgaarden, K. E. & Ottenhoff, T. H. Flexibility in T-cell receptor ligand repertoires depends on MHC and T-cell receptor clonotype. *Immunology* **90**, 370-375, doi:10.1111/j.1365-2567.1997.00370.x (1997).

320 Birnbaum, M. E. *et al.* Deconstructing the peptide-MHC specificity of T cell recognition. *Cell* **157**, 1073-1087, doi:10.1016/j.cell.2014.03.047 (2014).

321 Mason, D. A very high level of crossreactivity is an essential feature of the T-cell receptor. *Immunol Today* **19**, 395-404, doi:10.1016/s0167-5699(98)01299-7 (1998).

322 Benoist, C. & Mathis, D. Autoimmunity provoked by infection: how good is the case for T cell epitope mimicry? *Nature immunology* **2**, 797-801, doi:10.1038/ni0901-797 (2001).

323 Shann, F., Nohynek, H., Scott, J. A., Hesseling, A. & Flanagan, K. L. Randomized trials to study the nonspecific effects of vaccines in children in low-income countries. *The Pediatric infectious disease journal* **29**, 457-461, doi:10.1097/INF.0b013e3181c91361 (2010).

324 Welsh, R. M., Che, J. W., Brehm, M. A. & Selin, L. K. Heterologous immunity between viruses. *Immunol Rev* **235**, 244-266, doi:10.1111/j.0105-2896.2010.00897.x (2010).

325 Wucherpfennig, K. W. & Strominger, J. L. Molecular mimicry in T cell-mediated autoimmunity: viral peptides activate human T cell clones specific for myelin basic protein. *Cell* **80**, 695-705, doi:10.1016/0092-8674(95)90348-8 (1995).

326 Schmidt, D., Verdaguer, J., Averill, N. & Santamaria, P. A mechanism for the major histocompatibility complex-linked resistance to autoimmunity. *J Exp Med* **186**, 1059-1075, doi:10.1084/jem.186.7.1059 (1997).

327 Ranheim, E. A. *et al.* Selection of aberrant class II restricted CD8+ T cells in NOD mice expressing a glutamic acid decarboxylase (GAD)65-specific T cell receptor transgene. *Autoimmunity* **37**, 555-567, doi:10.1080/08916930400020545 (2004).

328 Serreze, D. V. *et al.* MHC class II molecules play a role in the selection of autoreactive class I-restricted CD8 T cells that are essential contributors to type 1 diabetes development in nonobese diabetic mice. *J Immunol* **172**, 871-879, doi:10.4049/jimmunol.172.2.871 (2004).

329 Logunova, N. N. *et al.* Restricted MHC-peptide repertoire predisposes to autoimmunity. *J Exp Med* **202**, 73-84, doi:10.1084/jem.20050198 (2005).

330 Sundberg, E. J., Deng, L. & Mariuzza, R. A. TCR recognition of peptide/MHC class II complexes and superantigens. *Seminars in immunology* **19**, 262-271, doi:10.1016/j.smim.2007.04.006 (2007).

331 Linette, G. P. *et al.* Cardiovascular toxicity and titin cross-reactivity of affinity-enhanced T cells in myeloma and melanoma. *Blood* **122**, 863-871, doi:10.1182/blood-2013-03-490565 (2013).

332 Davis, M. M. & Bjorkman, P. J. T-cell antigen receptor genes and T-cell recognition. *Nature* **334**, 395-402, doi:10.1038/334395a0 (1988).

333 Garcia, K. C. & Adams, E. J. How the T cell receptor sees antigen--a structural view. *Cell* **122**, 333-336, doi:10.1016/j.cell.2005.07.015 (2005).

334 Rudolph, M. G., Stanfield, R. L. & Wilson, I. A. How TCRs bind MHCs, peptides, and coreceptors. *Annu Rev Immunol* **24**, 419-466, doi:10.1146/annurev.immunol.23.021704.115658 (2006).

335 Brawley, J. V. & Concannon, P. Modulation of promiscuous T cell receptor recognition by mutagenesis of CDR2 residues. *J Exp Med* **183**, 2043-2051, doi:10.1084/jem.183.5.2043 (1996).

336 Vigano, S. *et al.* Functional avidity: a measure to predict the efficacy of effector T cells? *Clinical & developmental immunology* **2012**, 153863, doi:10.1155/2012/153863 (2012).

337 Corr, M. *et al.* T cell receptor-MHC class I peptide interactions: affinity, kinetics, and specificity. *Science* **265**, 946-949, doi:10.1126/science.8052850 (1994).

338 Matsui, K., Boniface, J. J., Steffner, P., Reay, P. A. & Davis, M. M. Kinetics of T-cell receptor binding to peptide/I-Ek complexes: correlation of the dissociation rate with T-cell responsiveness. *Proc Natl Acad Sci U S A* **91**, 12862-12866, doi:10.1073/pnas.91.26.12862 (1994).

339 Busch, D. H. & Pamer, E. G. T cell affinity maturation by selective expansion during infection. *J Exp Med* **189**, 701-710, doi:10.1084/jem.189.4.701 (1999).

340 Lyons, D. S. *et al.* A TCR binds to antagonist ligands with lower affinities and faster dissociation rates than to agonists. *Immunity* **5**, 53-61, doi:10.1016/s1074-7613(00)80309-x (1996).
341 Border, E. C., Sanderson, J. P., Weissensteiner, T., Gerry, A. B. & Pumphrey, N. J. Affinity-enhanced T-cell receptors for adoptive T-cell therapy targeting MAGE-A10: strategy for selection of an optimal candidate. *Oncoimmunology* **8**, e1532759, doi:10.1080/2162402x.2018.1532759 (2019).
342 Schmitt, T. M. *et al.* Generation of higher affinity T cell receptors by antigen-driven differentiation of progenitor T cells in vitro. *Nat Biotechnol* **35**, 1188-1195, doi:10.1038/nbt.4004 (2017).
343 Thomas, S. *et al.* Human T cells expressing affinity-matured TCR display accelerated responses but fail to recognize low density of MHC-peptide antigen. *Blood* **118**, 319-329, doi:10.1182/blood-2010-12-326736 (2011).
344 Robbins, P. F. *et al.* Tumor regression in patients with metastatic synovial cell sarcoma and melanoma using genetically engineered lymphocytes reactive with NY-ESO-1. *J Clin Oncol* **29**, 917-924, doi:10.1200/jco.2010.32.2537 (2011).
345 Morgan, R. A. *et al.* Cancer regression and neurological toxicity following anti-MAGE-A3 TCR gene therapy. *J Immunother* **36**, 133-151, doi:10.1097/CJI.0b013e3182829903 (2013).
346 Cameron, B. J. *et al.* Identification of a Titin-derived HLA-A1-presented peptide as a cross-reactive target for engineered MAGE A3-directed T cells. *Sci Transl Med* **5**, 197ra103, doi:10.1126/scitranslmed.3006034 (2013).
347 D'Ippolito, E., Schober, K., Nauerth, M. & Busch, D. H. T cell engineering for adoptive T cell therapy: safety and receptor avidity. *Cancer Immunol Immunother* **68**, 1701-1712, doi:10.1007/s00262-019-02395-9 (2019).
348 Alexander-Miller, M. A. Differential expansion and survival of high and low avidity cytotoxic T cell populations during the immune response to a viral infection. *Cellular immunology* **201**, 58-62, doi:10.1006/cimm.1999.1632 (2000).
349 Derby, M., Alexander-Miller, M., Tse, R. & Berzofsky, J. High-avidity CTL exploit two complementary mechanisms to provide better protection against viral infection than low-avidity CTL. *J Immunol* **166**, 1690-1697, doi:10.4049/jimmunol.166.3.1690 (2001).
350 Almeida, J. R. *et al.* Superior control of HIV-1 replication by CD8+ T cells is reflected by their avidity, polyfunctionality, and clonal turnover. *J Exp Med* **204**, 2473-2485, doi:10.1084/jem.20070784 (2007).
351 Yerly, D. *et al.* Increased cytotoxic T-lymphocyte epitope variant cross-recognition and functional avidity are associated with hepatitis C virus clearance. *J Virol* **82**, 3147-3153, doi:10.1128/jvi.02252-07 (2008).
352 Snyder, J. T., Alexander-Miller, M. A., Berzofskyl, J. A. & Belyakov, I. M. Molecular mechanisms and biological significance of CTL avidity. *Current HIV research* **1**, 287-294, doi:10.2174/1570162033485230 (2003).
353 Berger, C. T. *et al.* High-functional-avidity cytotoxic T lymphocyte responses to HLA-B-restricted Gag-derived epitopes associated with relative HIV control. *J Virol* **85**, 9334-9345, doi:10.1128/jvi.00460-11 (2011).
354 Appay, V. & Iglesias, M. C. Antigen sensitivity and T-cell receptor avidity as critical determinants of HIV control. *Current opinion in HIV and AIDS* **6**, 157-162, doi:10.1097/COH.0b013e3283453dfd (2011).
355 Savage, P. A., Boniface, J. J. & Davis, M. M. A kinetic basis for T cell receptor repertoire selection during an immune response. *Immunity* **10**, 485-492, doi:10.1016/s1074-7613(00)80048-5 (1999).
356 Malherbe, L., Hausl, C., Teyton, L. & McHeyzer-Williams, M. G. Clonal selection of helper T cells is determined by an affinity threshold with no further skewing of TCR binding properties. *Immunity* **21**, 669-679, doi:10.1016/j.immuni.2004.09.008 (2004).
357 Whitmire, J. K., Benning, N. & Whitton, J. L. Precursor frequency, nonlinear proliferation, and functional maturation of virus-specific CD4+ T cells. *J Immunol* **176**, 3028-3036, doi:10.4049/jimmunol.176.5.3028 (2006).
358 Williams, M. A., Ravkov, E. V. & Bevan, M. J. Rapid culling of the CD4+ T cell repertoire in the transition from effector to memory. *Immunity* **28**, 533-545, doi:10.1016/j.immuni.2008.02.014 (2008).

359 Cukalac, T. *et al.* Reproducible selection of high avidity CD8+ T-cell clones following secondary acute virus infection. *Proc Natl Acad Sci U S A* **111**, 1485-1490, doi:10.1073/pnas.1323736111 (2014).

360 Day, E. K. *et al.* Rapid CD8+ T cell repertoire focusing and selection of high-affinity clones into memory following primary infection with a persistent human virus: human cytomegalovirus. *J Immunol* **179**, 3203-3213, doi:10.4049/jimmunol.179.5.3203 (2007).

361 Roszkowski, J. J. *et al.* Simultaneous generation of CD8+ and CD4+ melanoma-reactive T cells by retroviral-mediated transfer of a single T-cell receptor. *Cancer Res* **65**, 1570-1576, doi:10.1158/0008-5472.Can-04-2076 (2005).

362 Moore, T. V. *et al.* Relationship between CD8-dependent antigen recognition, T cell functional avidity, and tumor cell recognition. *Cancer Immunol Immunother* **58**, 719-728, doi:10.1007/s00262-008-0594-2 (2009).

363 Harari, A. *et al.* Skewed association of polyfunctional antigen-specific CD8 T cell populations with HLA-B genotype. *Proc Natl Acad Sci U S A* **104**, 16233-16238, doi:10.1073/pnas.0707570104 (2007).

364 Conrad, J. A. *et al.* Dominant clonotypes within HIV-specific T cell responses are programmed death-1high and CD127low and display reduced variant cross-reactivity. *J Immunol* **186**, 6871-6885, doi:10.4049/jimmunol.1004234 (2011).

365 Walker, L. J., Sewell, A. K. & Klenerman, P. T cell sensitivity and the outcome of viral infection. *Clin Exp Immunol* **159**, 245-255, doi:10.1111/j.1365-2249.2009.04047.x (2010).

366 Valitutti, S. & Lanzavecchia, A. Serial triggering of TCRs: a basis for the sensitivity and specificity of antigen recognition. *Immunol Today* **18**, 299-304 (1997).

367 Coombs, D., Kalergis, A. M., Nathenson, S. G., Wofsy, C. & Goldstein, B. Activated TCRs remain marked for internalization after dissociation from pMHC. *Nature immunology* **3**, 926-931, doi:10.1038/ni838 (2002).

368 van der Merwe, P. A. & Davis, S. J. Molecular interactions mediating T cell antigen recognition. *Annu Rev Immunol* **21**, 659-684, doi:10.1146/annurev.immunol.21.120601.141036 (2003).

369 Nakatsugawa, M. *et al.* CD4(+) and CD8(+) TCRbeta repertoires possess different potentials to generate extraordinarily high-avidity T cells. *Sci Rep* **6**, 23821, doi:10.1038/srep23821 (2016).

370 Raphael, I., Nalawade, S., Eagar, T. N. & Forsthuber, T. G. T cell subsets and their signature cytokines in autoimmune and inflammatory diseases. *Cytokine* **74**, 5-17, doi:10.1016/j.cyto.2014.09.011 (2015).

371 Xia, Y. *et al.* Interferon-γ and Tumor Necrosis Factor-α Produced by T Cells Reduce the HBV Persistence Form, cccDNA, Without Cytolysis. *Gastroenterology* **150**, 194-205, doi:10.1053/j.gastro.2015.09.026 (2016).

372 Takeuchi, A. & Saito, T. CD4 CTL, a Cytotoxic Subset of CD4(+) T Cells, Their Differentiation and Function. *Front Immunol* **8**, 194, doi:10.3389/fimmu.2017.00194 (2017).

373 Juno, J. A. *et al.* Cytotoxic CD4 T Cells-Friend or Foe during Viral Infection? *Front Immunol* **8**, 19, doi:10.3389/fimmu.2017.00019 (2017).

374 Suni, M. A. *et al.* CD4(+)CD8(dim) T lymphocytes exhibit enhanced cytokine expression, proliferation and cytotoxic activity in response to HCMV and HIV-1 antigens. *Eur J Immunol* **31**, 2512-2520, doi:10.1002/1521-4141(200108)31:8<2512::aid-immu2512>3.0.co;2-m (2001).

375 Appay, V. *et al.* Characterization of CD4(+) CTLs ex vivo. *J Immunol* **168**, 5954-5958, doi:10.4049/jimmunol.168.11.5954 (2002).

376 Zaunders, J. J. *et al.* Identification of circulating antigen-specific CD4+ T lymphocytes with a CCR5+, cytotoxic phenotype in an HIV-1 long-term nonprogressor and in CMV infection. *Blood* **103**, 2238-2247, doi:10.1182/blood-2003-08-2765 (2004).

377 Norris, P. J. *et al.* Beyond help: direct effector functions of human immunodeficiency virus type 1-specific CD4(+) T cells. *J Virol* **78**, 8844-8851, doi:10.1128/jvi.78.16.8844-8851.2004 (2004).

378 van Leeuwen, E. M. *et al.* Emergence of a CD4+CD28- granzyme B+, cytomegalovirus-specific T cell subset after recovery of primary cytomegalovirus infection. *J Immunol* **173**, 1834-1841, doi:10.4049/jimmunol.173.3.1834 (2004).

379 Brown, D. M. Cytolytic CD4 cells: Direct mediators in infectious disease and malignancy. *Cellular immunology* **262**, 89-95, doi:10.1016/j.cellimm.2010.02.008 (2010).

380 Trapani, J. A. & Smyth, M. J. Functional significance of the perforin/granzyme cell death pathway. *Nat Rev Immunol* **2**, 735-747, doi:10.1038/nri911 (2002).

381 Hildemann, S. K. *et al.* High efficiency of antiviral CD4(+) killer T cells. *PLoS One* **8**, e60420, doi:10.1371/journal.pone.0060420 (2013).

382 Lin, L. *et al.* Granzyme B secretion by human memory CD4 T cells is less strictly regulated compared to memory CD8 T cells. *BMC immunology* **15**, 36, doi:10.1186/s12865-014-0036-1 (2014).

383 Pearce, E. L. *et al.* Control of effector CD8+ T cell function by the transcription factor Eomesodermin. *Science* **302**, 1041-1043, doi:10.1126/science.1090148 (2003).

384 Intlekofer, A. M. *et al.* Anomalous type 17 response to viral infection by CD8+ T cells lacking T-bet and eomesodermin. *Science* **321**, 408-411, doi:10.1126/science.1159806 (2008).

385 Hua, L. *et al.* Cytokine-dependent induction of CD4+ T cells with cytotoxic potential during influenza virus infection. *J Virol* **87**, 11884-11893, doi:10.1128/jvi.01461-13 (2013).

386 Glimcher, L. H., Townsend, M. J., Sullivan, B. M. & Lord, G. M. Recent developments in the transcriptional regulation of cytolytic effector cells. *Nat Rev Immunol* **4**, 900-911, doi:10.1038/nri1490 (2004).

387 Qui, H. Z. *et al.* CD134 plus CD137 dual costimulation induces Eomesodermin in CD4 T cells to program cytotoxic Th1 differentiation. *J Immunol* **187**, 3555-3564, doi:10.4049/jimmunol.1101244 (2011).

388 Eshima, K. *et al.* Ectopic expression of a T-box transcription factor, eomesodermin, renders CD4(+) Th cells cytotoxic by activating both perforin- and FasL-pathways. *Immunol Lett* **144**, 7-15, doi:10.1016/j.imlet.2012.02.013 (2012).

389 Takeuchi, A. *et al.* CRTAM determines the CD4+ cytotoxic T lymphocyte lineage. *J Exp Med* **213**, 123-138, doi:10.1084/jem.20150519 (2016).

390 Takeuchi, A. *et al.* CRTAM confers late-stage activation of CD8+ T cells to regulate retention within lymph node. *J Immunol* **183**, 4220-4228, doi:10.4049/jimmunol.0901248 (2009).

391 Brown, D. M., Kamperschroer, C., Dilzer, A. M., Roberts, D. M. & Swain, S. L. IL-2 and antigen dose differentially regulate perforin- and FasL-mediated cytolytic activity in antigen specific CD4+ T cells. *Cellular immunology* **257**, 69-79, doi:10.1016/j.cellimm.2009.03.002 (2009).

392 Workman, A. M., Jacobs, A. K., Vogel, A. J., Condon, S. & Brown, D. M. Inflammation enhances IL-2 driven differentiation of cytolytic CD4 T cells. *PLoS One* **9**, e89010, doi:10.1371/journal.pone.0089010 (2014).

393 Brown, D. M., Lee, S., Garcia-Hernandez Mde, L. & Swain, S. L. Multifunctional CD4 cells expressing gamma interferon and perforin mediate protection against lethal influenza virus infection. *J Virol* **86**, 6792-6803, doi:10.1128/jvi.07172-11 (2012).

394 Soghoian, D. Z. *et al.* HIV-specific cytolytic CD4 T cell responses during acute HIV infection predict disease outcome. *Sci Transl Med* **4**, 123ra125, doi:10.1126/scitranslmed.3003165 (2012).

395 Gamadia, L. E. *et al.* Primary immune responses to human CMV: a critical role for IFN-gamma-producing CD4+ T cells in protection against CMV disease. *Blood* **101**, 2686-2692, doi:10.1182/blood-2002-08-2502 (2003).

396 Fang, M. *et al.* Perforin-dependent CD4+ T-cell cytotoxicity contributes to control a murine poxvirus infection. *Proc Natl Acad Sci U S A* **109**, 9983-9988, doi:10.1073/pnas.1202143109 (2012).

397 Stuller, K. A. & Flano, E. CD4 T cells mediate killing during persistent gammaherpesvirus 68 infection. *J Virol* **83**, 4700-4703, doi:10.1128/jvi.02240-08 (2009).

398 Aslan, N. *et al.* Cytotoxic CD4 T cells in viral hepatitis. *J Viral Hepat* **13**, 505-514, doi:10.1111/j.1365-2893.2006.00723.x (2006).

399 Knolle, P. A. Staying local-antigen presentation in the liver. *Curr Opin Immunol* **40**, 36-42, doi:10.1016/j.coi.2016.02.009 (2016).

400 Law, R. H. *et al.* An overview of the serpin superfamily. *Genome biology* **7**, 216, doi:10.1186/gb-2006-7-5-216 (2006).

401 Wei, S. C., Duffy, C. R. & Allison, J. P. Fundamental Mechanisms of Immune Checkpoint Blockade Therapy. *Cancer Discov* **8**, 1069-1086, doi:10.1158/2159-8290.Cd-18-0367 (2018).
402 Lohse, A. W. *et al.* Antigen-presenting function and B7 expression of murine sinusoidal endothelial cells and Kupffer cells. *Gastroenterology* **110**, 1175-1181, doi:10.1053/gast.1996.v110.pm8613007 (1996).
403 Herkel, J. *et al.* MHC class II-expressing hepatocytes function as antigen-presenting cells and activate specific CD4 T lymphocyutes. *Hepatology* **37**, 1079-1085, doi:10.1053/jhep.2003.50191 (2003).
404 Chhabra, A. *et al.* CD4+CD25- T cells transduced to express MHC class I-restricted epitope-specific TCR synthesize Th1 cytokines and exhibit MHC class I-restricted cytolytic effector function in a human melanoma model. *J Immunol* **181**, 1063-1070, doi:10.4049/jimmunol.181.2.1063 (2008).
405 Soto, C. M. *et al.* MHC-class I-restricted CD4 T cells: a nanomolar affinity TCR has improved anti-tumor efficacy in vivo compared to the micromolar wild-type TCR. *Cancer Immunol Immunother* **62**, 359-369, doi:10.1007/s00262-012-1336-z (2013).
406 Xue, S. A. *et al.* Human MHC Class I-restricted high avidity CD4(+) T cells generated by co-transfer of TCR and CD8 mediate efficient tumor rejection in vivo. *Oncoimmunology* **2**, e22590, doi:10.4161/onci.22590 (2013).
407 Engels, B., Chervin, A. S., Sant, A. J., Kranz, D. M. & Schreiber, H. Long-term persistence of CD4(+) but rapid disappearance of CD8(+) T cells expressing an MHC class I-restricted TCR of nanomolar affinity. *Mol Ther* **20**, 652-660, doi:10.1038/mt.2011.286 (2012).
408 Frankel, T. L. *et al.* Both CD4 and CD8 T cells mediate equally effective in vivo tumor treatment when engineered with a highly avid TCR targeting tyrosinase. *J Immunol* **184**, 5988-5998, doi:10.4049/jimmunol.1000189 (2010).
409 Roszkowski, J. J. *et al.* CD8-independent tumor cell recognition is a property of the T cell receptor and not the T cell. *J Immunol* **170**, 2582-2589, doi:10.4049/jimmunol.170.5.2582 (2003).
410 Willemsen, R., Ronteltap, C., Heuveling, M., Debets, R. & Bolhuis, R. Redirecting human CD4+ T lymphocytes to the MHC class I-restricted melanoma antigen MAGE-A1 by TCR alphabeta gene transfer requires CD8alpha. *Gene therapy* **12**, 140-146, doi:10.1038/sj.gt.3302388 (2005).
411 Kessels, H. W., Schepers, K., van den Boom, M. D., Topham, D. J. & Schumacher, T. N. Generation of T cell help through a MHC class I-restricted TCR. *J Immunol* **177**, 976-982, doi:10.4049/jimmunol.177.2.976 (2006).
412 Morris, E. C., Tsallios, A., Bendle, G. M., Xue, S. A. & Stauss, H. J. A critical role of T cell antigen receptor-transduced MHC class I-restricted helper T cells in tumor protection. *Proc Natl Acad Sci U S A* **102**, 7934-7939, doi:10.1073/pnas.0500357102 (2005).
413 Johnson, L. A. *et al.* Gene therapy with human and mouse T-cell receptors mediates cancer regression and targets normal tissues expressing cognate antigen. *Blood* **114**, 535-546, doi:10.1182/blood-2009-03-211714 (2009).
414 van der Veken, L. T. *et al.* HLA class II restricted T-cell receptor gene transfer generates CD4+ T cells with helper activity as well as cytotoxic capacity. *Gene therapy* **12**, 1686-1695, doi:10.1038/sj.gt.3302586 (2005).
415 Ranasinghe, S. *et al.* Antiviral CD8(+) T Cells Restricted by Human Leukocyte Antigen Class II Exist during Natural HIV Infection and Exhibit Clonal Expansion. *Immunity* **45**, 917-930, doi:10.1016/j.immuni.2016.09.015 (2016).
416 Hansen, S. G. *et al.* Broadly targeted CD8(+) T cell responses restricted by major histocompatibility complex E. *Science* **351**, 714-720, doi:10.1126/science.aac9475 (2016).
417 Laugel, B. *et al.* Different T cell receptor affinity thresholds and CD8 coreceptor dependence govern cytotoxic T lymphocyte activation and tetramer binding properties. *The Journal of biological chemistry* **282**, 23799-23810, doi:10.1074/jbc.M700976200 (2007).
418 Holler, P. D. & Kranz, D. M. Quantitative analysis of the contribution of TCR/pepMHC affinity and CD8 to T cell activation. *Immunity* **18**, 255-264, doi:10.1016/s1074-7613(03)00019-0 (2003).

419 Janeway, C. A., Jr. The T cell receptor as a multicomponent signalling machine: CD4/CD8 coreceptors and CD45 in T cell activation. *Annu Rev Immunol* **10**, 645-674, doi:10.1146/annurev.iy.10.040192.003241 (1992).

420 Artyomov, M. N., Lis, M., Devadas, S., Davis, M. M. & Chakraborty, A. K. CD4 and CD8 binding to MHC molecules primarily acts to enhance Lck delivery. *Proc Natl Acad Sci U S A* **107**, 16916-16921, doi:10.1073/pnas.1010568107 (2010).

421 Wooldridge, L. *et al.* Interaction between the CD8 coreceptor and major histocompatibility complex class I stabilizes T cell receptor-antigen complexes at the cell surface. *The Journal of biological chemistry* **280**, 27491-27501, doi:10.1074/jbc.M500555200 (2005).

422 Jonsson, P. *et al.* Remarkably low affinity of CD4/peptide-major histocompatibility complex class II protein interactions. *Proc Natl Acad Sci U S A* **113**, 5682-5687, doi:10.1073/pnas.1513918113 (2016).

423 Huppa, J. B. *et al.* TCR-peptide-MHC interactions in situ show accelerated kinetics and increased affinity. *Nature* **463**, 963-967, doi:10.1038/nature08746 (2010).

424 Harding, S., Lipp, P. & Alexander, D. R. A therapeutic CD4 monoclonal antibody inhibits TCR-zeta chain phosphorylation, zeta-associated protein of 70-kDa Tyr319 phosphorylation, and TCR internalization in primary human T cells. *J Immunol* **169**, 230-238, doi:10.4049/jimmunol.169.1.230 (2002).

425 Li, Q. J. *et al.* CD4 enhances T cell sensitivity to antigen by coordinating Lck accumulation at the immunological synapse. *Nature immunology* **5**, 791-799, doi:10.1038/ni1095 (2004).

426 Ballek, O., Valecka, J., Manning, J. & Filipp, D. The pool of preactivated Lck in the initiation of T-cell signaling: a critical re-evaluation of the Lck standby model. *Immunology and cell biology* **93**, 384-395, doi:10.1038/icb.2014.100 (2015).

427 Veillette, A., Bookman, M. A., Horak, E. M. & Bolen, J. B. The CD4 and CD8 T cell surface antigens are associated with the internal membrane tyrosine-protein kinase p56lck. *Cell* **55**, 301-308, doi:10.1016/0092-8674(88)90053-0 (1988).

428 Chakraborty, A. K. & Weiss, A. Insights into the initiation of TCR signaling. *Nature immunology* **15**, 798-807, doi:10.1038/ni.2940 (2014).

429 Purbhoo, M. A. *et al.* The human CD8 coreceptor effects cytotoxic T cell activation and antigen sensitivity primarily by mediating complete phosphorylation of the T cell receptor zeta chain. *The Journal of biological chemistry* **276**, 32786-32792, doi:10.1074/jbc.M102498200 (2001).

430 Ghani, K. *et al.* Efficient human hematopoietic cell transduction using RD114- and GALV-pseudotyped retroviral vectors produced in suspension and serum-free media. *Hum Gene Ther* **20**, 966-974, doi:10.1089/hum.2009.001 (2009).

431 Marcucci, K. T. *et al.* Retroviral and Lentiviral Safety Analysis of Gene-Modified T Cell Products and Infused HIV and Oncology Patients. *Mol Ther* **26**, 269-279, doi:10.1016/j.ymthe.2017.10.012 (2018).

432 June, C. H., Blazar, B. R. & Riley, J. L. Engineering lymphocyte subsets: tools, trials and tribulations. *Nat Rev Immunol* **9**, 704-716, doi:10.1038/nri2635 (2009).

433 Milone, M. C. & O'Doherty, U. Clinical use of lentiviral vectors. *Leukemia* **32**, 1529-1541, doi:10.1038/s41375-018-0106-0 (2018).

434 Fraietta, J. A. *et al.* Disruption of TET2 promotes the therapeutic efficacy of CD19-targeted T cells. *Nature* **558**, 307-312, doi:10.1038/s41586-018-0178-z (2018).

435 Foster, J. B., Barrett, D. M. & Kariko, K. The Emerging Role of In Vitro-Transcribed mRNA in Adoptive T Cell Immunotherapy. *Mol Ther* **27**, 747-756, doi:10.1016/j.ymthe.2019.01.018 (2019).

436 Maus, M. V. *et al.* T cells expressing chimeric antigen receptors can cause anaphylaxis in humans. *Cancer immunology research* **1**, 26-31, doi:10.1158/2326-6066.Cir-13-0006 (2013).

437 Chandran, S. S. *et al.* Tumor-Specific Effector CD8+ T Cells That Can Establish Immunological Memory in Humans after Adoptive Transfer Are Marked by Expression of IL7 Receptor and c-myc. *Cancer Res* **75**, 3216-3226, doi:10.1158/0008-5472.Can-15-0584 (2015).

438 Powell, D. J., Jr., Dudley, M. E., Robbins, P. F. & Rosenberg, S. A. Transition of late-stage effector T cells to CD27+ CD28+ tumor-reactive effector memory T cells in humans after adoptive cell transfer therapy. *Blood* **105**, 241-250, doi:10.1182/blood-2004-06-2482 (2005).

439 Kaech, S. M. *et al.* Selective expression of the interleukin 7 receptor identifies effector CD8 T cells that give rise to long-lived memory cells. *Nature immunology* **4**, 1191-1198, doi:10.1038/ni1009 (2003).

440 Berger, C. *et al.* Adoptive transfer of effector CD8+ T cells derived from central memory cells establishes persistent T cell memory in primates. *J Clin Invest* **118**, 294-305, doi:10.1172/jci32103 (2008).

441 Graef, P. *et al.* Serial transfer of single-cell-derived immunocompetence reveals stemness of CD8(+) central memory T cells. *Immunity* **41**, 116-126, doi:10.1016/j.immuni.2014.05.018 (2014).

442 Lee, D. W. *et al.* T cells expressing CD19 chimeric antigen receptors for acute lymphoblastic leukaemia in children and young adults: a phase 1 dose-escalation trial. *Lancet* **385**, 517-528, doi:10.1016/s0140-6736(14)61403-3 (2015).

443 Gardner, R. A. *et al.* Intent-to-treat leukemia remission by CD19 CAR T cells of defined formulation and dose in children and young adults. *Blood* **129**, 3322-3331, doi:10.1182/blood-2017-02-769208 (2017).

444 Eyquem, J. *et al.* Targeting a CAR to the TRAC locus with CRISPR/Cas9 enhances tumour rejection. *Nature* **543**, 113-117, doi:10.1038/nature21405 (2017).

445 Stadtmauer, E. A. *et al.* CRISPR-engineered T cells in patients with refractory cancer. *Science* **367**, doi:10.1126/science.aba7365 (2020).

446 Straathof, K. C. *et al.* An inducible caspase 9 safety switch for T-cell therapy. *Blood* **105**, 4247-4254, doi:10.1182/blood-2004-11-4564 (2005).

447 Wang, X. *et al.* A transgene-encoded cell surface polypeptide for selection, in vivo tracking, and ablation of engineered cells. *Blood* **118**, 1255-1263, doi:10.1182/blood-2011-02-337360 (2011).

448 Berger, C., Berger, M., Anderson, D. & Riddell, S. R. A non-human primate model for analysis of safety, persistence, and function of adoptively transferred T cells. *Journal of medical primatology* **40**, 88-103, doi:10.1111/j.1600-0684.2010.00451.x (2011).

449 Klebanoff, C. A. *et al.* Central memory self/tumor-reactive CD8+ T cells confer superior antitumor immunity compared with effector memory T cells. *Proc Natl Acad Sci U S A* **102**, 9571-9576, doi:10.1073/pnas.0503726102 (2005).

450 Hinrichs, C. S. *et al.* Adoptively transferred effector cells derived from naive rather than central memory CD8+ T cells mediate superior antitumor immunity. *Proc Natl Acad Sci U S A* **106**, 17469-17474, doi:10.1073/pnas.0907448106 (2009).

451 Klebanoff, C. A., Gattinoni, L. & Restifo, N. P. Sorting through subsets: which T-cell populations mediate highly effective adoptive immunotherapy? *J Immunother* **35**, 651-660, doi:10.1097/CJI.0b013e31827806e6 (2012).

452 Crotty, S. A brief history of T cell help to B cells. *Nat Rev Immunol* **15**, 185-189, doi:10.1038/nri3803 (2015).

453 Dandri, M. *et al.* Repopulation of mouse liver with human hepatocytes and in vivo infection with hepatitis B virus. *Hepatology* **33**, 981-988, doi:10.1053/jhep.2001.23314 (2001).

454 Schuster, I. *Identifikation, Klonierung und retroviraler Transfer allorestringierter FMNL1-peptidspezifischer T-Zellrezeptoren für die Entwicklung adoptiver Immuntherapien gegen B-Zell-Non-Hodgkin-Lymphome.* PhD thesis, Ludwigs-Maximilians-University Munich, (2008).

455 Heinz, N. *et al.* Retroviral and transposon-based tet-regulated all-in-one vectors with reduced background expression and improved dynamic range. *Hum Gene Ther* **22**, 166-176, doi:10.1089/hum.2010.099 (2011).

456 McKinney, D. M. *et al.* A strategy to determine HLA class II restriction broadly covering the DR, DP, and DQ allelic variants most commonly expressed in the general population. *Immunogenetics* **65**, 357-370, doi:10.1007/s00251-013-0684-y (2013).

457 Sidney, J. *et al.* Measurement of MHC/peptide interactions by gel filtration or monoclonal antibody capture. *Curr Protoc Immunol* **Chapter 18**, Unit 18.13., doi:10.1002/0471142735.im1803s100 (2013).